

PHOTOCHROMISM IN THE BI-IMIDAZOLYL SYSTEM

BY

M. W. LITOBARSKI, B.Sc.

Thesis submitted to the University of Nottingham, for the degree of
Doctor of Philosophy, October 1973.

M. W. LITOBARSKI, B.Sc. (Mattiw Wołan)

"~~Ph.D.~~" Photochromism in the bi-imidazolyl system".
Ph.D., 1974.

Photochromism in the Bi-Imidazolyl System

ABSTRACT

The work, which is reported in this thesis, is concerned with the photochromic processes, or light induced changes of colour displayed by the hexaaryl bi-imidazolyl system.

The thesis includes a study of the solid state photochromic decay reaction, in which the colour change is brought about by the dimerisation of triphenyl imidazolyl radicals. Equipment, used in conjunction with a U.V./visible spectrophotometer, was assembled to allow the process to be followed at various temperatures and from the data accrued a kinetic scheme, based upon a diffusion controlled reaction involving a radical-dimer complex species, has been suggested.

Investigations were also carried out into the photochromic processes of the bi-imidazolyl system in benzene solution. Based on earlier observations, the work included the study of the effect of variation of the parent dimer concentration upon the generation and decay kinetics of the triphenyl imidazolyl radicals and the related radicals fluorinated on the 2 phenyl ring. Kinetic schemes, most of which have necessarily involved a postulation of radical-dimer complexes of some sort, have been formulated for each radical system at each dimer concentration used. Rate constants for the reactions have been given.

The electron spin resonance spectra for the three fluorinated derivatives of the triphenyl imidazolyl radical have been reported. Assignment of the splitting constants was attempted by use of simple Hückel molecular orbital calculations but this proved largely unsuccessful. Accurate theoretical reproduction of the experimental spectra

was thus not achieved. It was decided, that Hückel was in too many ways unsatisfactory for the system, and work on an alternative, more complete molecular orbital approach (that of Pople, Pariser and Parr) was initiated. A computer program was obtained to permit such calculations to be made, and although not all problems had been overcome by the end of the time allowed for this thesis much headway had been made, and guide lines for further work have been suggested.

	Page
Chapter 1	
INTRODUCTION	
Summary	1
1.1 Photochromism	3
1.1.1 Nature of colour change	4
1.1.2 Examples of photochromism	4
1.1.3 Photodissociation	6
1.1.4 Hexaphenyl bi-imidazolyl system	9
1.2 Electron Spin Resonance	14
1.2.1 Theoretical aspects of electron spin resonance	14
1.2.2 Hyperfine splitting	16
1.3 Molecular Orbital Theory	19
1.3.1 Hückel Molecular Orbital Theory	19
1.3.2 The McLachlan Perturbation Theory	24
1.3.3 Self consistent field molecular orbital equations	27
1.3.4 Pariser Pople and Parr Self Consistent Field Molecular Orbital Theory	31
1.3.5 Parameterization of the P.P.P method	34
1.3.6 Open shell calculations	36
1.4 α Protons in Organic Radicals	41
1.4.1 Interpretation of the E.S.R. spectrum of 2,4,5 triphenyl imidazolyl radicals	42
Chapter 2	
EXPERIMENTAL	
2.1 Measurement of Reaction Kinetics	44
2.1.1 For the solid state recombination process of triphenyl imidazolyl radicals	44
2.1.2 For the recombination and generation process of the fluorinated imidazolyl radicals in solution	46

	Page	
2.2	Practical Aspects of Electron Spin Resonance	48
2.3	Recording E.S.R. Spectra	50
2.4	Measurement of Spin Concentration in Solution	51
2.5	Determination of Extinction Coefficient	55
2.6	Preparation of Materials	57
2.7	Purification of Benzene	58
Chapter 3	RESULTS	
3.1	Photochromic Decay Reaction	59
3.1.1	Methods of analysis of results	59
3.1.2	Decay kinetics of solid 2,4,5 triphenyl imidazolyl radicals	60
3.1.3	Decay kinetics of fluorinated imidazolyl radicals in solution	62
3.2	Calculation of Rate Constants	65
3.3	Calibration of Spin Content of the Carbon Sample	65
3.4	Calculation of the Extinction Coefficients for the radicals	66
3.5	Kinetics of the Generation of Radicals in solution	69
Chapter 4	DISCUSSION	
4.1	Electron Spin Resonance Spectra and Interpretation	71
4.1.1	Experimental spectra	71
4.1.2	E.S.R. simulation program	71
4.1.3	Hückel molecular orbital program	74
4.2	Pariser, Pople and Parr Molecular Orbital Program	77
4.3	The Photochromic Process in the Solid	86
4.4	The Photochromic Processes in Solution	91
4.4.1	Decay of 2 metafluorophenyl 4,5 diphenyl imidazolyl radicals	91
4.4.2	Decay of 2 parafluorophenyl 4,5 diphenyl imidazolyl radicals	95

4.4.4	The nature of the radical-dimer complex	96
4.4.5	Generation kinetics in solution	98
4.5	Suggestions for Further Work	100
	References	

Acknowledgements

I would like to express my gratitude, to Professor D.D.Eley, for the interest he has shown in my work and for the provision of Departmental facilities; to the Science Research Council for the allocation of a grant; to Mr. Lemunier and his technical staff for their continuous assistance; to Mr. A. Hands for his constructions of the constant temperature device used in studying the solid state kinetics; to Dr. D. Brailsford for his help in setting up the computer program for the semi-empirical molecular orbital calculations used in this thesis, and to Mr. D. F. Monk and Mr. J. A. Phillipson for many useful discussions. Finally, I would especially like to thank Dr. M. R. Willis for his help, advice and encouragement he has given throughout my work on this thesis.

As non S.I. units have been used from time to time throughout this thesis, factors for their conversion to the S.I. equivalent are given in the table below.

Unit	S.I. Equivalent
Angstrom (\AA)	10^{-10} metre (m)
Centimetre (cm)	10^{-2} m.
Gramme (g.)	10^{-3} kilogramme (kg)
Centigrade ($^{\circ}\text{C}$)	$(^{\circ}\text{C} + 273.2)$ kelvin (K)
Electron Volt (eV.)	1.602×10^{-19} Joules (J)
Kilocalorie (kcal)	4.187 kilo Joules (kJ)
Gauss (G)	10^{-4} Tesla (T)
Cycles/second (c/s)	1 Hertz (Hz)
Degree (angle, $^{\circ}$)	$\pi/180$ radian (rad.)
Oersted (Oe)	$10 \frac{3}{4} \pi$ Ampere metre $^{-1}$ (Am^{-1})
Bohr magneton	9.2732×10^{-24} AM^2

CHAPTER 1

INTRODUCTION

SUMMARY

Much work has been done in studying compounds which exhibit light induced changes of colour, in one form or another. Some of the work concerned with this process, known as photochromism, has been devoted to the hexaaryl bi-imidazolyl system (in which a dissociation from dimer to radicals or alternatively an association of the radicals, is responsible for the colour change), but as yet a complete picture of the system has not been attained. The original purpose of the thesis, therefore, was to add fresh information to that already possessed in the field and to obtain if possible an insight into the problems posed by previous work.

The initial investigations concerned the solid state photochromism brought about by association of triphenyl imidazolyl radicals. Equipment for use in conjunction with a U.V./visible spectrophotometer was assembled to allow the process to be followed at various temperatures, and although the system proved complex, data was accumulated which permitted a kinetic scheme for the solid state radical decay to be subsequently suggested.

Following the work on the solid state, investigations were carried out into the photochromic process of the bi-imidazolyl system in benzene solution. Based on earlier observations, the work included the study of the effect of variation of the parent dimer concentration upon the generation and decay kinetics of the triphenyl imidazolyl radicals and the related radicals fluorinated on the 2 phenyl ring. Kinetic schemes have been formulated for each system and comparisons have been made between the various reactions at the different dimer concentrations used. **Rate constants for the reactions** have been given.

The electron spin resonance spectra for the three fluorinated derivatives of the triphenyl imidazolyl radical have been reported. Assignment of the splitting constants was attempted by use of simple Hückel molecular orbital calculations but this proved largely unsuccessful. Accurate theoretical reproduction of the experimental spectra was thus not achieved. It was decided, that Hückel was in too many ways unsatisfactory for the system, and work on an alternative, more complete molecular orbital approach (that of Pople, Pariser and Parr) was initiated. A computer program was obtained to permit such calculations to be made, and although not all problems had been overcome by the end of the time allowed for this thesis much headway had been made, and guide lines for further work have been suggested.

1.1 Photochromism

Under the influence of light, certain substances undergo a change of colour, this reaction being reversible in that removal of the light results in a return to the original state. The process is known as photochromism,¹ which literally means colouration by light, and substances undergoing such a reaction are called photochromics. A typical example of the response of a photochromic system to illumination Figure 1.1, shows how the optical density at the particular wavelength of the colour change, alters with the irradiation. Before illumination is initiated at T_1 , there is a finite optical density, due either to absorption by the parent material or to thermochromism (a process identical to photochromism except that it is brought about by thermal energy), but on illumination, the optical density of the system increases and continues to increase until the rate of the reverse photochromic reaction becomes equal to that of the forward reaction. The position of this photostationary state will then depend upon:-

- (i) the intensity of the light source used
- (ii) the quantity of photochromic material present
- (iii) the quantum efficiency of the process

When the light is removed at T_2 , the optical density slowly decreases until the system is back to the original state.

The picture may well be complicated by the fact that most systems are not reversible indefinitely and the excited species formed by absorption of quanta of light may well undergo side reaction with perhaps oxygen or solvent, leading to degradation of the parent material. Loss of colour in this way may appear, as indicated by Dessauer and Paris², to be part of the back photochromic reaction, and as such will lead to erroneous observations of photochromism. It may thus be necessary to check for this with continuous illumination experiments.

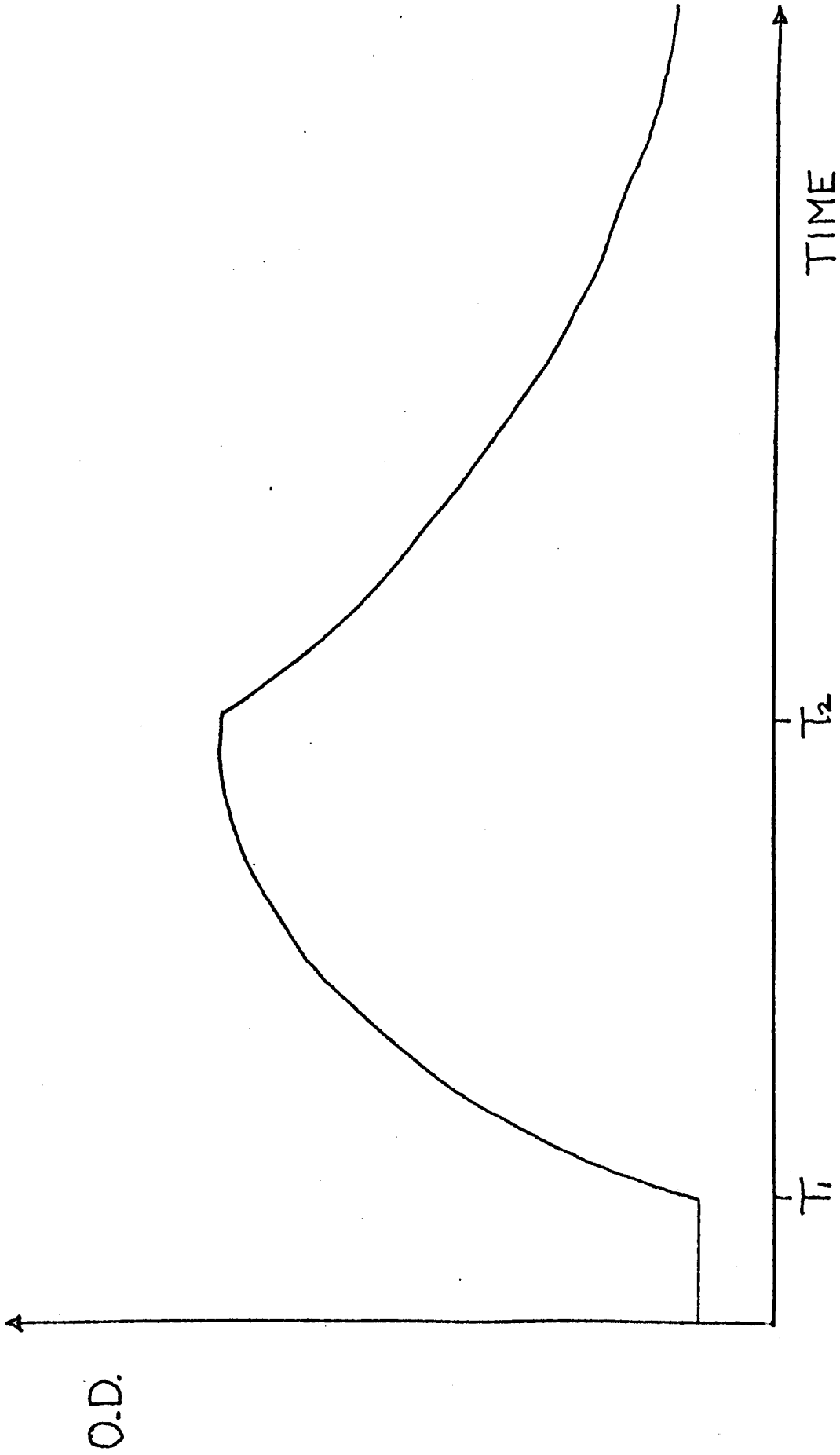


FIGURE 1.1

1.1.1 Nature of the colour change

Absorption of light by the molecule to give the colour, leads to an electron transition from a lower energy level to a higher one, and the energy required to bring about such a transition is given by:

$$E = h\nu$$

where E is the energy difference between the two levels, ν is the frequency of light absorbed, and h is Planck's constant.

Provided then that some simple assumptions are made it is possible to obtain a reasonable picture of what the transition involves. Hückel molecular orbital theory, which is described later, gives one method of obtaining some insight into the energy levels within the molecule, and a pictorial representation of such is shown in Figure 1.2.

By considering a linear combination of the various atomic orbitals of the molecule, a set of molecular bonding, non bonding and anti-bonding orbitals are obtained. The transition of the electron caused by visible light absorption will then be, in general, from the highest occupied level, normally either the highest bonding orbital or the non-bonding orbital, to the lowest unoccupied level, which is usually an antibonding π^* orbital. The intensity of the transition will be governed by the symmetry properties and will only be allowed when the electronic spin angular momentum remains unchanged (i.e. $\Delta S=0$).

Hückel molecular orbital methods are in some ways, however, unsatisfactory and a more rigorous method is described later.

1.1.2 Examples of photochromism

Photochromic processes have been studied now for nearly one hundred years, the first reported case being by ter Meer³ in 1876 who showed that the potassium salt of dinitromethane changed colour when exposed to exciting radiation. Since then, a large number of photochromic systems have been discovered and have been found to fall mainly into five categories.

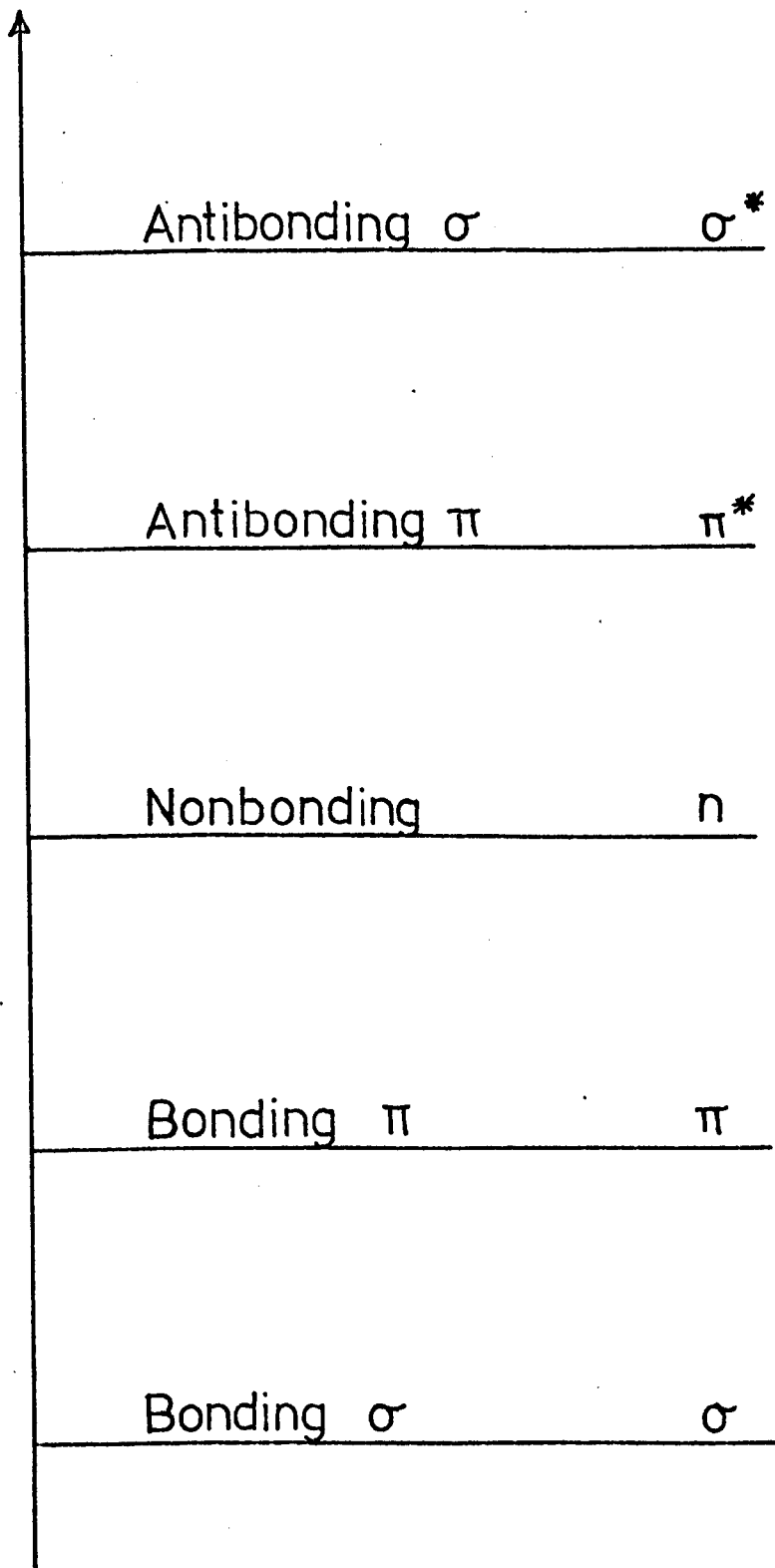


FIGURE 1.2

(i) Heterolytic cleavage

The most studied group of compounds within this category are the spiropyrans, a term used to denote very generally, a molecule containing a 2H pyran ring in which the 2 carbon atom of the ring is involved in a spiro linkage.

These compounds undergo the photochromic change by the heterolytic cleavage of the 1,2 single bond of the pyran ring and the charges of the resulting zwitterion are stabilised by resonance⁴. This increase of resonance energy leads to a colour change of the compound. Figure 1.3 shows a typical structural change on exposure to light of a spiropyran, in this case 6 nitro 1',3',3' trimethyl spiro - 2H-1 benzopyran - 2,2' indoline .

In general, spiropyrans only undergo photochromism when in solution and upon exposure to ultra violet light. The coloured solutions obtained may then either fade thermally, according to first order kinetics, or in many cases undergo bleaching with visible light.

(ii) Isomerization

A prime example of compounds undergoing photochromism by CIS-TRANS isomerization are the aromatic azo compounds⁵.

Azobenzene and nearly all its mono substituted derivatives have their principal absorption bands ($\pi \rightarrow \pi^*$) in the ultra violet region, and a weaker $n \rightarrow \pi^*$ transition near 450 nm. which gives the compounds their characteristic yellow appearance. When exposed to light, photoisomerization from the trans to the cis form of the compounds occurs (Figure 1.4A), the $\pi \rightarrow \pi^*$ bonds shift to shorter wavelengths and the $n \rightarrow \pi^*$ absorption is strengthened (Figure 1.4B). This has the overall effect of deepening the colour. The reverse reaction, i.e. the thermal dark reaction, is first order with an activation energy of about 21 K cal.

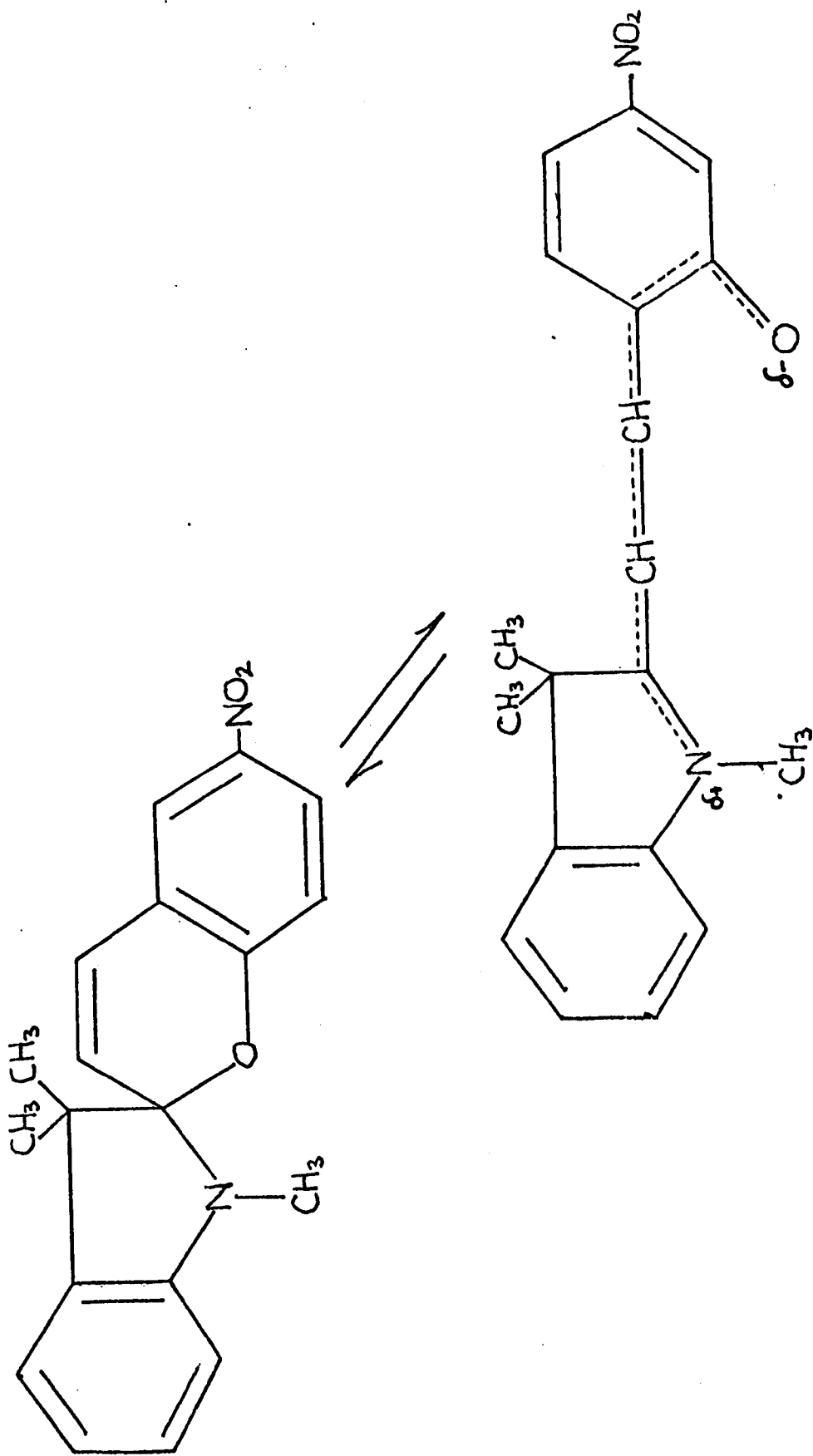


FIGURE 1.3.

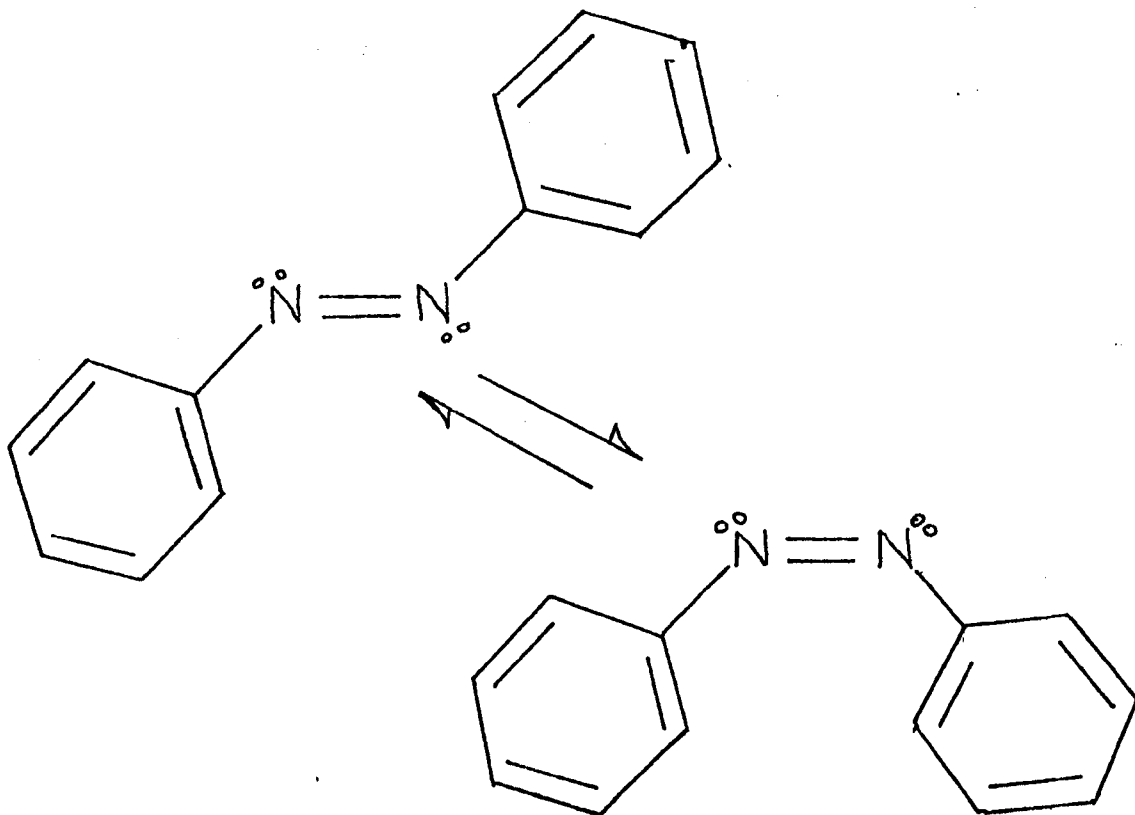


FIGURE 1.4A.

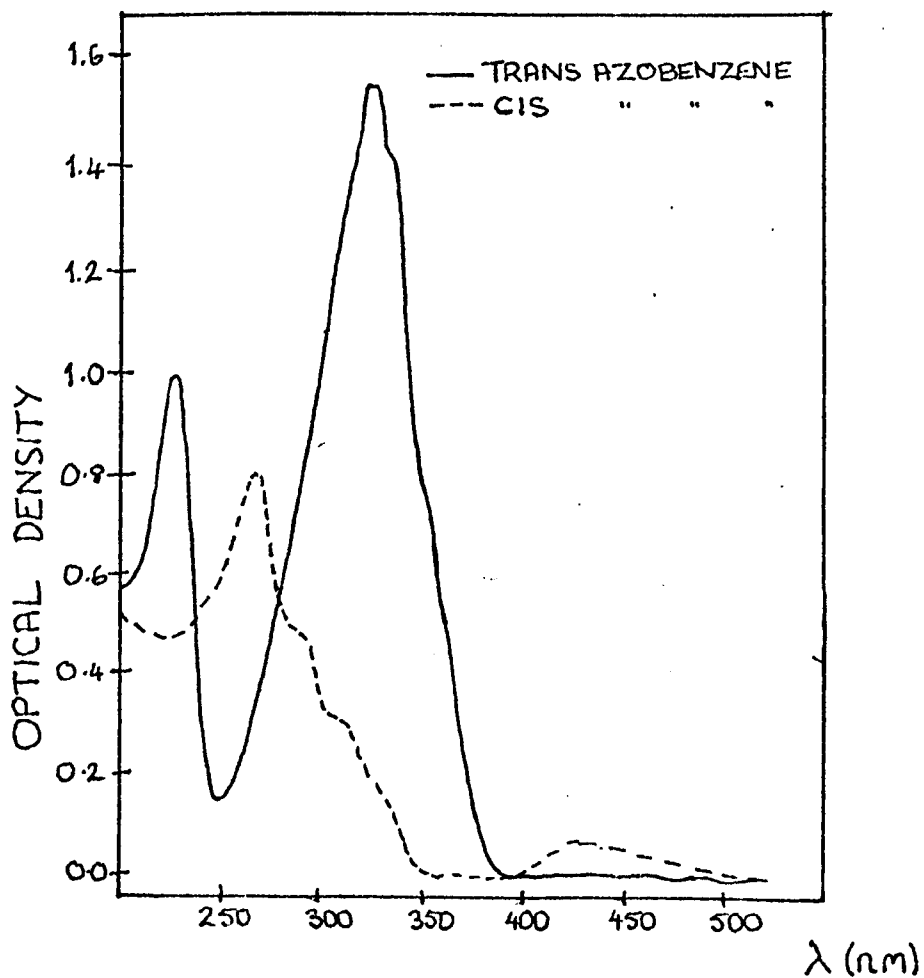


FIGURE 1.4B

(iii) Oxidation-reduction systems

This process involves a reversible transfer of an electron under the influence of light, meaning that the species involved must have two stable oxidation states. For example, illumination of phenylenediamine tetracetic acid⁶ on Vicor glass gives a blue cation radical (Figure 1.5) which in ambient light disappears according to first order kinetics. Colour centres in alkali halides are also included in this group, as the trapping of an electron at a crystal defect may be considered to be a change in oxidation state.

(iv) Triplet - triplet absorption

A long lived triplet - triplet transition may also result in a colour change. For example a number of hydrocarbons in a solid matrix at low temperatures or in a plastic matrix, undergo certain colour changes. When exposed to an ultra violet flash, the lowest triplet states of the hydrocarbon are populated and these states then have an intense absorption in the visible region. The triplet states will usually decay back to the ground state in a time of the order of one second. It is because of the speed of this reaction that Windsor and co-workers at T.R.W. Inc. have thoroughly examined hydrocarbons for use in eye protective devices.⁷

(v) Homolytic cleavage of a σ bond or dissociation

It is into this category that the hexaaryl bi-imidazolyl system falls and it is thus this type of photochromic change which is of most interest to us.

1.1.3 Photodissociation ^{B1}

Dissociation of a bond, in general, will take place when energy is absorbed by the molecule and somehow localised in the bond being ruptured. Thermal dissociation for instance is brought about by an increase in vibrational, translational

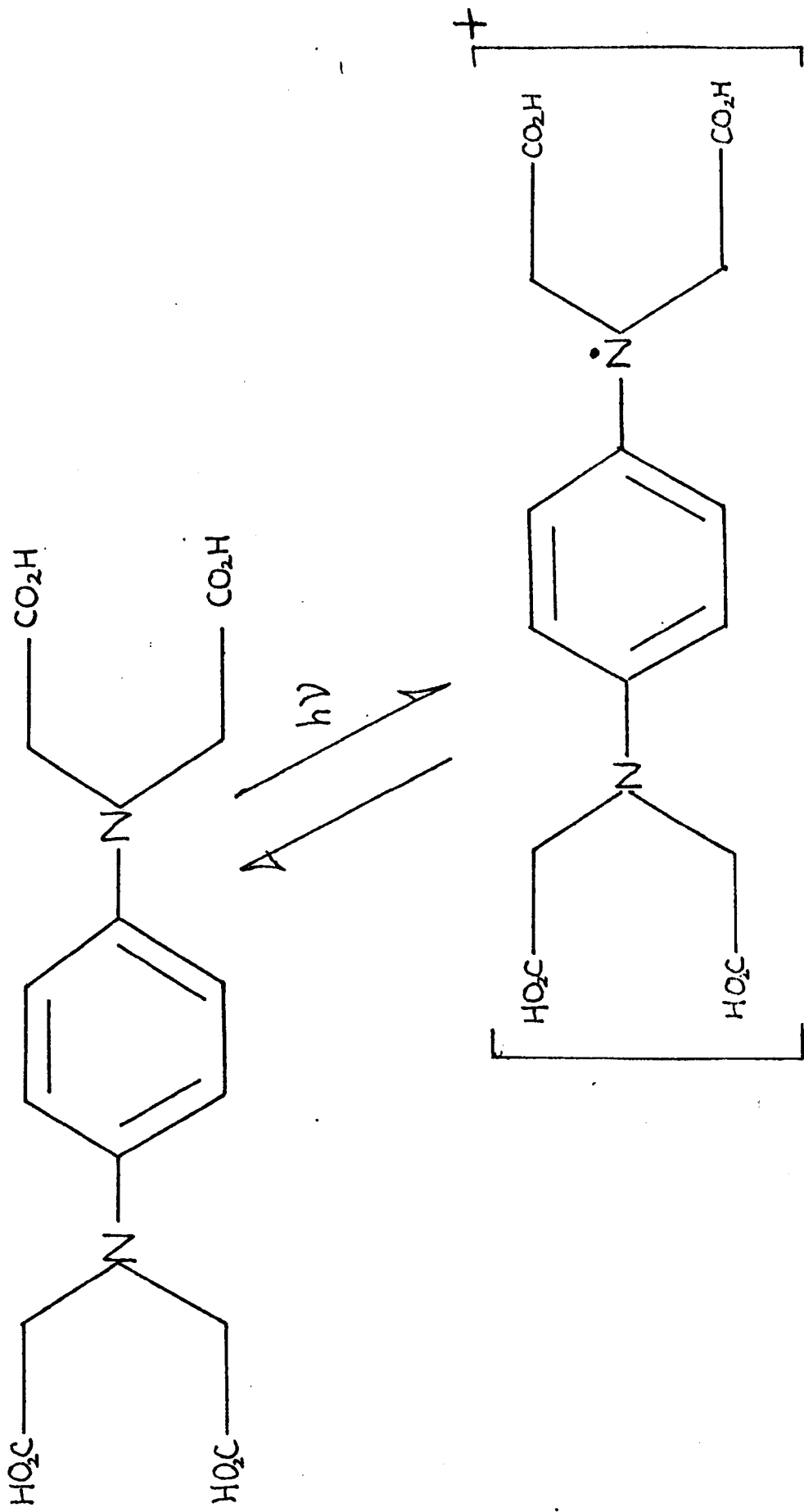


FIGURE 1.5

and rotational energies. Photodissociation, dissociation caused by the absorption of light energy, however, occurs when the molecule is promoted from its ground state to an excited molecular state in which one electron usually occupies an antibonding orbital. As molecular orbitals are generally quantized, the energy difference between these states will be quantized. Associated with each of these discrete energy levels will be certain vibrational levels, also quantized.

Excitation to an excited state

A potential energy diagram of a molecule undergoing a normal excitation is shown in Figure 1.6A. If the molecule absorbs energy, not large enough to cause dissociation (e.g. \mathcal{E}_A in Figure 1.6A), it will gradually lose this by both radiative and radiation-less processes to arrive back at the ground state, at, however, a higher vibrational level than that at which it started. (A very small fraction of the molecules, will have an internuclear distance such that the energy absorbed will give the molecule sufficient energy to dissociate). Absorption of any energy greater than \mathcal{E}_B will be continuous (the vibrational states above the dissociation energy E being non quantized) and will lead to dissociation. Quantum yields for photodissociation will thus be negligible for energies absorbed below \mathcal{E}_B but will approach unity for those above.

The picture is somewhat different, if the molecule possesses only a purely dissociative excited state (Figure 1.6B). In this case the excited state has no discrete vibrational levels and absorption of light as a result will be continuous. Quantum yields of this type of process will thus be independent of wavelength and approximate to unity.

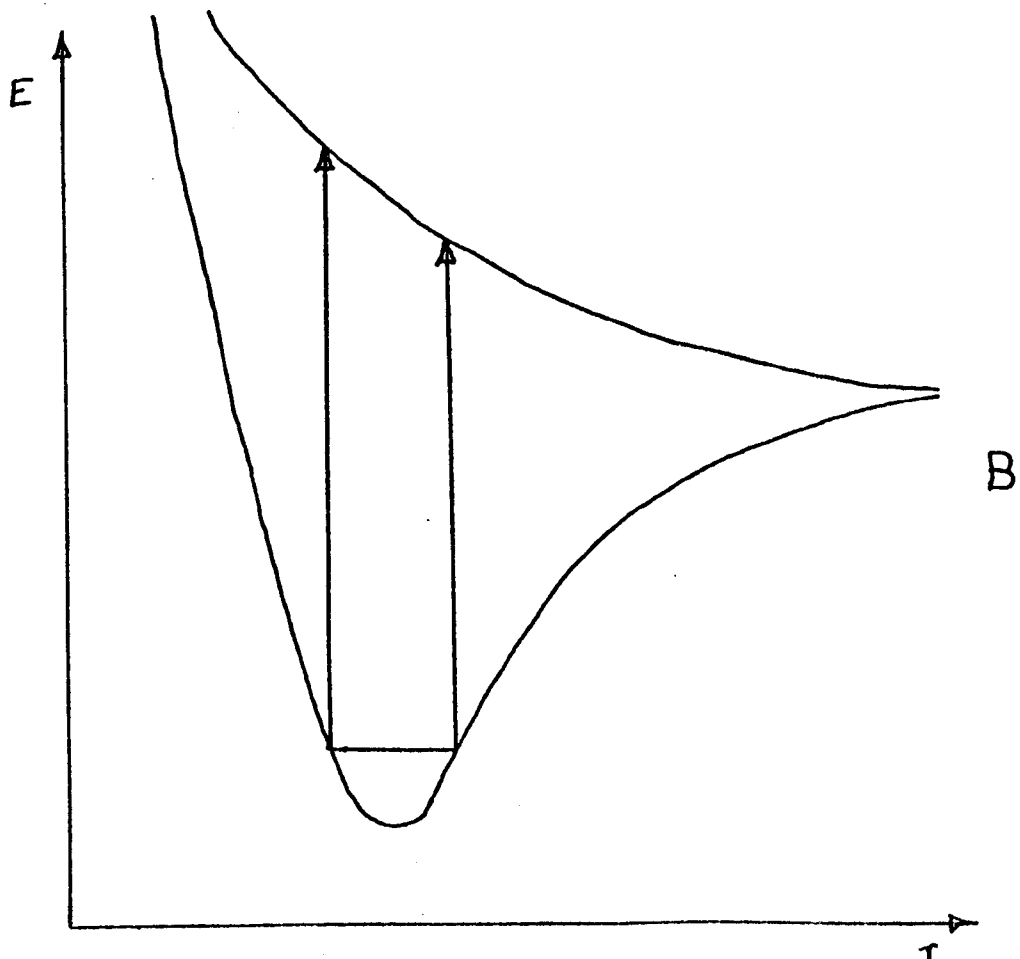
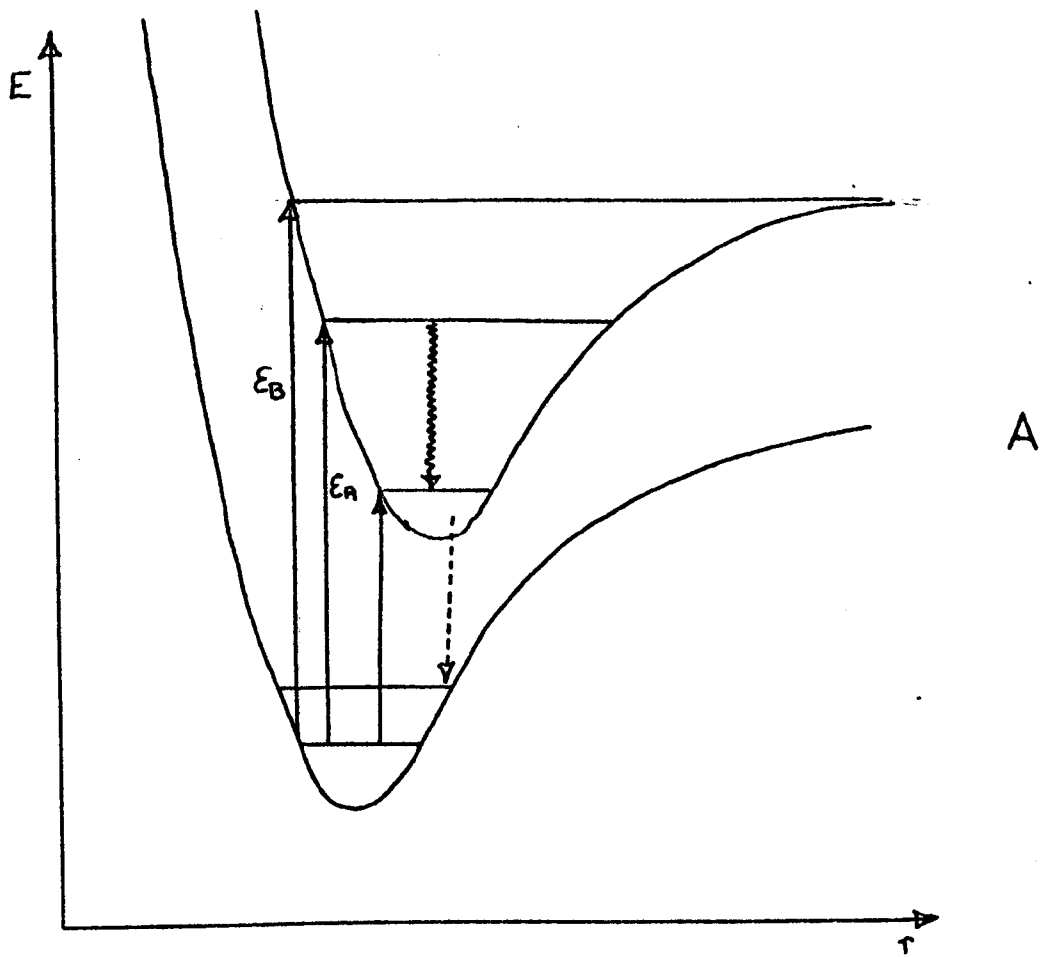


FIGURE 1.6

The Photochromic change due to photodissociation

When photodissociation causes a homolytic cleavage of an intra molecular bond, a pair of radicals will result. These radicals, normally extremely short lived, may be stabilised by the delocalisation of the single electron usually in either the highest bonding orbital or in a non bonding orbital. It follows from this, therefore, that the more strongly aromatic the radical is, the more stable will it be.

Such a process could well lead to a photochromic change, for a molecule with a certain molecular orbital structure and thus a certain light absorption, may be susceptible to photodissociation. The radicals which result then from exposure of the molecule to light will have a different molecular orbital make up, meaning that absorption of light by the single electron in the highest occupied orbital, would occur at a different wavelength to that of the original molecule.

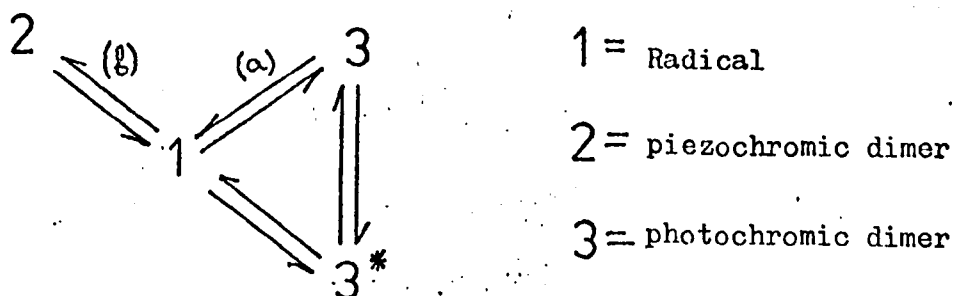
However as well as photodissociation going on, the radicals produced no matter how well stabilised, will as a rule tend to recombine so that two competing reactions will be taking place. This results in a photostationary state being established at a certain radical concentration. If the light source is then removed, the system will return to equilibrium and the predominant reaction will be recombination, the system reverting to its original colour before illumination. The rate of this recombination will of course depend upon the stability of the radicals.

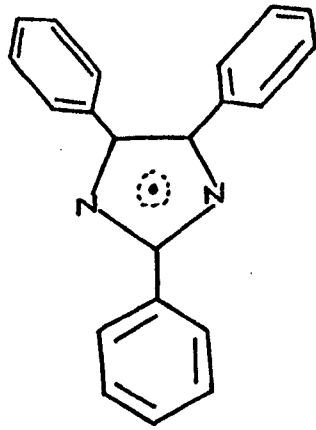
1.1.4 The Hexaphenyl bi-imidazolyl system

A light induced change of colour of this class of compound was first discovered in 1960 by Hayashi and Maeda⁸, who noticed that oxidation of 2,4,5 triphenyl imidazole yielded a pale violet precipitate which exhibited piezochromism (a change of colour caused by the exertion of pressure on the molecule) and which when dissolved in benzene gave a deep red-violet solution. On evaporation of the solvent, a pale yellow crystalline solid was obtained which was markedly photochromic and thermochromic in both the solid state and in solution. The substance was also found to have an E.S.R. absorption.

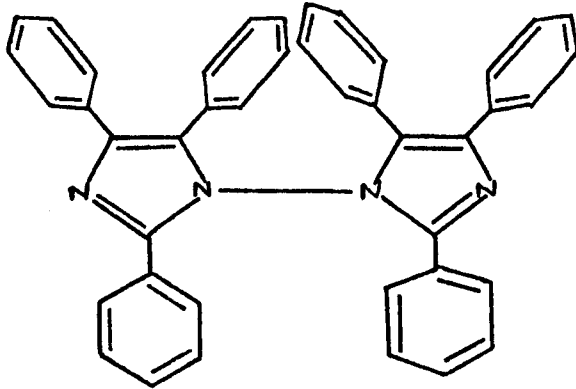
From their results, Hayashi and Maeda concluded that the red species obtained by illumination was the triphenyl imidazolyl radical (Figure 1.7A), while the yellow form was a labile meso-ionic form of the radical⁹.

It was later in 1964 that Hayashi and Maeda¹⁰ realized that the non coloured form of the compound was some kind of dimer of the triphenyl imidazolyl radical, and they assumed the structure of this was as shown in Figure 1.7B. White and Sonnenberg¹¹ however, using I.R. techniques, elucidated the structures of both the piezochromic and photochromic dimers (Figures 1.7C and 1.7D respectively) and showed these to be in equilibrium with the radical in the following way:

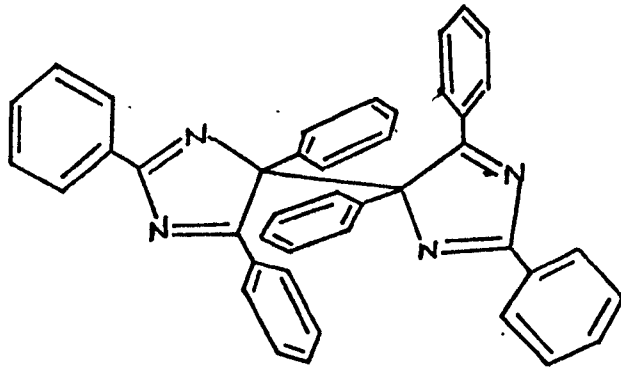




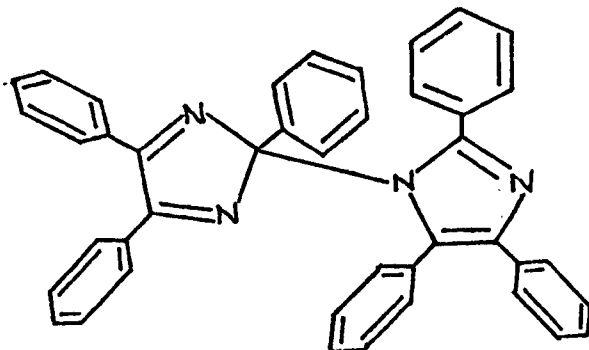
A



B



C



D

FIGURE 1.7

They postulated that in solution at room temperature, 3, the photochromic dimer, is the more stable form, evidence of which they gave as the thermolysis of the piezochromic dimer to the radical and the subsequent formation of 3. The photochromic reaction of 3 in both solid and solution, will then be represented by the formation of an excited dimeric species 3* which will dissociate to the radical 1.

This scheme has also been used to explain the phenomenon of light storage which has been reported for the system ¹² and ¹³. When a solution of the photochromic dimer is cooled to -20°C in benzene and irradiated, no photochromic colour change takes place and no E.S.R. signal of the radical is obtained. Furthermore, if a benzene solution of the radical obtained at room temperature is cooled under irradiation, the radical colour disappears, again at -20°C , and does not appear until around -150°C , at which temperature it reappears but is a bluish purple rather than red. On warming under irradiation, the reverse occurs and no colour or E.S.R. signal may be observed between -150°C and -20°C .

This behaviour has been interpreted by considering the equilibria (shown above) postulated by White and Sonnenberg.

The equilibrium (b), lies far over to the radical side at room temperature and only shifts towards the piezochromic dimer at temperatures lower than -20°C . Equilibrium (a) on the other hand, favours the existence of the photodimer at room temperature and will shift even further towards that dimer at lower temperatures.

However, upon irradiation of the system, the equilibrium (a) will be moved towards the side of the radical. If the solution is then cooled, the radical quickly dimerizes to the piezochromic dimer due to the low activation energy of the process (Figure 1.8), resulting in the loss of colour and E.S.R. signal between -20°C and -150°C .

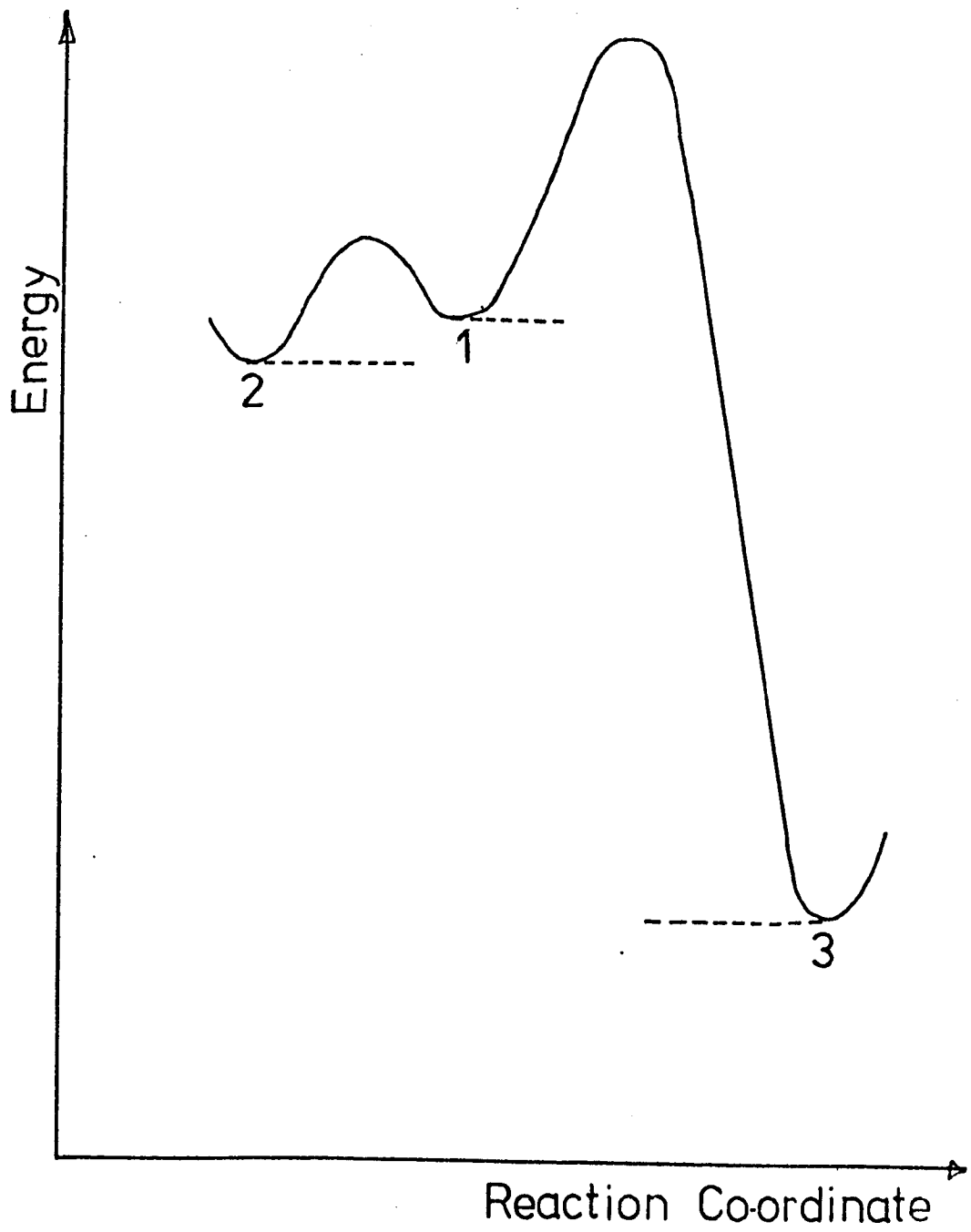


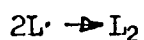
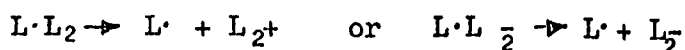
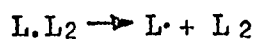
FIGURE 1.8

Warming the solid solution back up to room temperature, with the source of irradiation removed, results in the radicals being reformed, as the piezochromic form, being the less stable dimer at room temperatures, rearranges to the photodimer by way of the radical.

The reappearance of the colour at lower temperatures still, has been interpreted ¹³ to be due to the fact that the radicals produced by the photochromic process have insufficient energy at these temperatures to surmount the barrier of the activation energy of dimerization. The bluish purple appearance of the frozen solution at - 196°C has been attributed to a different conformation of the triphenyl imidazolyl radical than that at room temperatures.

Kinetics of the photochromic decay reaction

The kinetics of the photochromic decay reaction of the hexaaryl bi-imidazolyl system in solution have been for many years under discussion. Hayashi⁸ in 1960 and Ueda¹⁴ in 1964 found the order of the decay for 2,2',4,4',5,5' hexaphenyl bi-imidazole to be first order. Later Hayashi^{10a} showed the reaction to be second order using ultra-violet/visible spectrophotometry and confirmed this work with electron spin resonance techniques.^{10b} To explain this order, he stipulated that the reaction had to be a simple dimerization of the radical (Figure 1.7B). Wilks and Willis¹⁵, however, in 1969, showed that the reaction was much more complicated than this, and they found that the decay of the photochromic colour to be 3/2 order in the early stages falling later to first order. To explain this they postulated the following mechanism:-



where $L\cdot$ is the radical (Figure 1.7A) and L_2 is the photochromic dimer. The $L\cdot L_2$ radical-dimer complex, they suggested was responsible for the colour and E.S.R. signal and showed that if one applied a steady state treatment to the series of reactions one obtained:-

$$\frac{d(L\cdot)}{dt} = \frac{d(L\cdot L_2)}{dt} = 0$$

$$-\frac{d(L\cdot L_2)}{dt} = K_1(L\cdot L_2) + K_2 \left(\frac{K_1}{K_4}\right)^{\frac{1}{2}} (L\cdot L_2)^{3/2}$$

This explained the fall of order from $3/2$ to unity with time, as when the concentration of $L\cdot L_2$ is very small the term $(L\cdot L_2)$ will be more important than $(L\cdot L_2)^{3/2}$.

They supported the plausibility of this theory by pointing out that the existence of the species L^- was known (indeed the sodium salt of lophine has been prepared¹⁶) and attempted to show their presence in the reaction by measuring the change in free energy of the system resulting from a change of dielectric constant of the medium. Kirkwood¹⁷ has calculated the change in free energy resulting from transfer of a dipole from a medium of dielectric constant unity to a medium of dielectric constant D , assuming that only electrostatic interactions are involved, to be:-

$$\Delta G_{elec} = -\frac{\mu^2}{r^3} \frac{(D-1)}{(2D+1)}$$

where μ is the dipole moment and r is the radius of the molecule. Assuming then that this electrostatic term is the only important one, a plot of \ln (equilibrium constant) against $(D-1)/(2D+1)$ should yield a straight line. This was found to be true in one case (namely with benzene - pyridine mixture as the solvent) while in dioxan - water mixture the behaviour was not obeyed. The deviation was explained in terms of solubility effects.

Prochoda and Krongauz¹⁸ later investigating the effect of concentration on the reaction, confirmed the results of Wilks and Willis at a dimer concentration of 10^{-3} M, but at lower concentrations, below 10^{-4} M, they obtained a second order kinetic scheme. This they have interpreted as being due to the fact that the small dimer concentration precluded the existence of the radical-dimer complex and the reaction would appear to be a straight dimerization of the radical.

The piezochromic decay reaction and the photochromic decay reaction in the solid have been studied by Hayashi and Maeda¹⁹⁻²⁰ who found both to be third order. They suggested that this was indicative of diffusion controlled processes.

Ueda¹⁴ has observed the generation of radicals by following the intensity (Y_t) of the central line of the E.S.R. spectrum of 2, 4, 5, triphenyl imidazolyl radical with time (t) of illumination, and has found that the two are related by the expression:-

$$Y_t = A(1 - e^{-kt})$$

where A is decided as $\lim_{(t \rightarrow \infty)} Y_t$.

Finally, some studies have been carried out into the photochromic processes of a number of substituted bi-imidazoles in solution. The earlier references to the work in this field^{10b,19}, suggested that the recombination kinetics of all substituted radicals considered, followed second order only. Later investigations by Wilks,^{15c} however, indicate that this is not necessarily so and he attempted to show that for at least four of the substituted radicals (i.e. the 2 ortho, 2 parafluorophenyl, 2 parachlorophenyl and the 2 paramethoxyphenyl 4,5 diphenyl imidazolyl radicals), the kinetics followed the reaction scheme given above for the triphenyl imidazolyl radical combination.

1.2 Electron Spin Resonance

1.2.1 Theoretical aspects of electron spin resonance

An electron has an intrinsic angular momentum (spin) which according to the principles of quantum mechanics can only be measured in one direction, normally assigned as the Z direction. The component of the spin in this direction is then characterised by the quantum number M_s , which for an electron may have the value $+\frac{1}{2}$ or $-\frac{1}{2}$, the sign depending upon whether the spin is 'up' or 'down'. By convention $M_s = +\frac{1}{2}$ is used to describe the 'up spin' (α), and $M_s = -\frac{1}{2}$ is used for the 'down spin' (β). Because of this spin, a magnetic moment μ_E will be set up, and its component in the Z direction μ_E^z may be derived from the following relationship;

$$\mu_E^z = -M_s g_E \beta_E \quad 1.1$$

where g_E is a dimensionless constant whose value for a free electron is 2.0023 and β_E is the Bohr magneton for the electron given by $eh/4\pi mc$ (e being the charge of the electron, h Planck's constant, m the mass of the electron and c the velocity of light).

In the absence of a magnetic field, the two spin states are degenerate but application of a magnetic field along the z axis results in an interaction of this field with the magnetic moment of the electron and the degeneracy is removed (Figure 1.9A). This is known as the Zeeman effect, and the energy of interaction between magnetic field, H , and the electron is given by the formula,

$$\begin{aligned} E &= -\mu_E^z \cdot H \\ &= +(M_s g_E \beta_E H) \end{aligned} \quad 1.2$$

This means that when $M_s = -\frac{1}{2}$ the spin state will be stabilised due to a decrease in energy. A spin state given by $M_s = +\frac{1}{2}$ on the other hand, will be destabilised owing to a positive energy of interaction. The energy difference between the two Zeeman

$$\Delta E = g_e \beta_e H \quad 1.3$$

Transition from one Zeeman level to the other occurs when the system is exposed to an electromagnetic radiation perpendicular to the magnetic field with a resonance frequency such that

$$h\nu = g_e \beta_e H \quad 1.4$$

To satisfy the resonance condition, normally ν is kept constant at a frequency of around 9500 MHz and the field strength H is varied. For a free electron a field of around 3400 gauss is required. Figure 1.9B shows that the signal obtained from the transition is recorded as a derivative of the intensity A of the absorption with respect to the field strength H and as a function of H . The line width of the signal obtained is generally taken as the abscissa distance between the maximum and minimum of the derivative curve.

Relaxation

When the resonance condition is fulfilled, transitions from both energy levels can occur in that the probabilities of emission and absorption of energy are the same. Whether emission (transition from the higher energy level E_2 to the lower level E_1) or absorption (E_1 to E_2) will take place, depends upon the relative populations of the two Zeeman levels n_1 and n_2 , the relationship between these being given by Boltzmann distribution law:

$$\begin{aligned} \frac{n_1}{n_2} &= \exp(-\Delta E/kT) \\ &= \exp(-g_e \beta_e H/kT) \end{aligned} \quad 1.5$$

Where k is the Boltzmann constant. This means that there must be a slight excess of spins at the lower level in a magnetic field (for $H = 3400$ gauss and at room temperature, $n_2/n_1 = 0.9984$). However, since the populations of both levels are equal in the absence of a magnetic field, application of the field must result in $(n_1 - n_2)/2$ electrons transferring from E_2 to E_1 by a process of

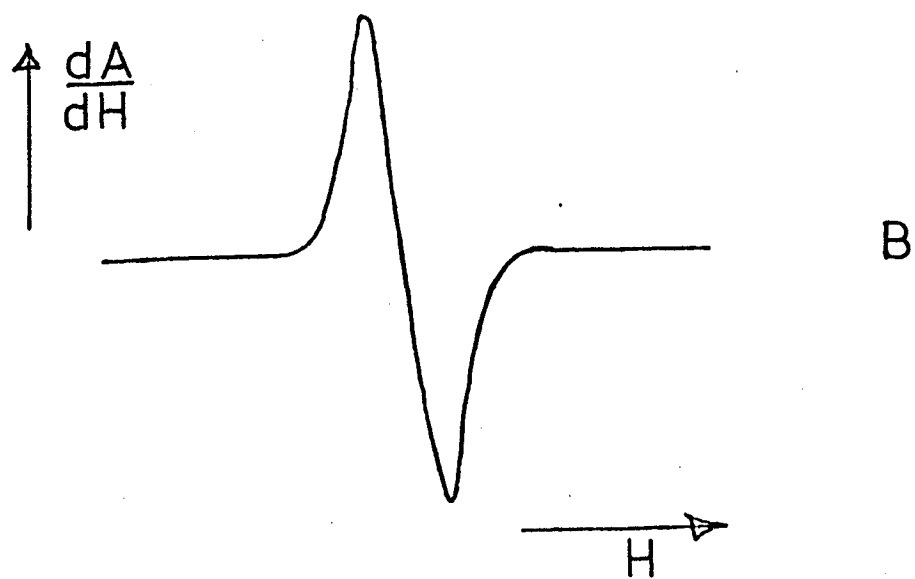
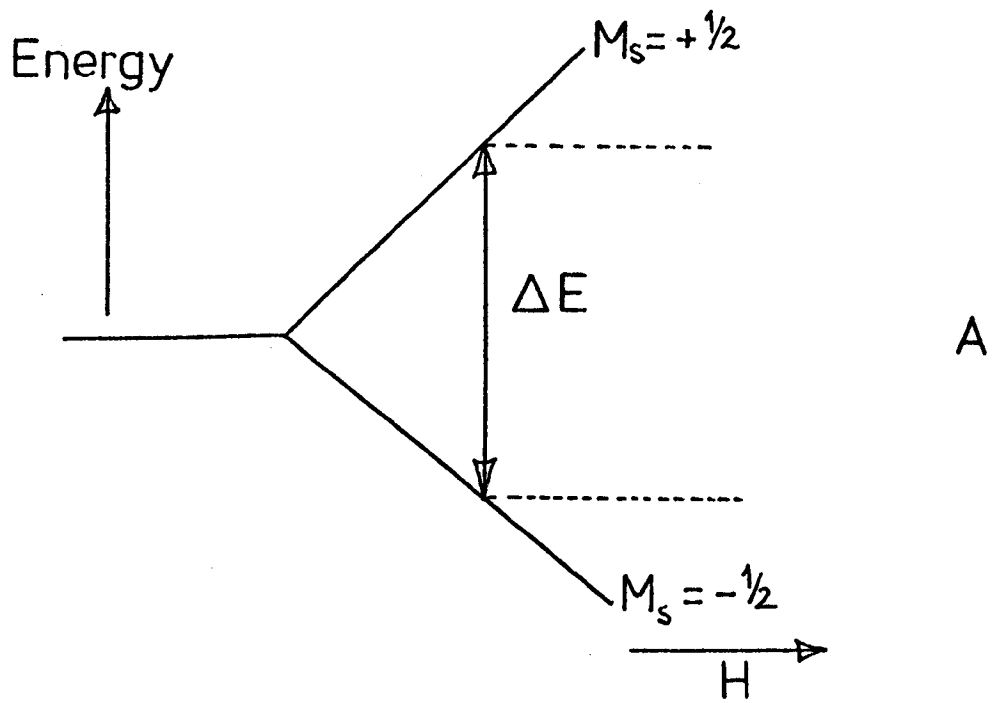


FIGURE 1.9

of energy exchange with the surroundings. This non-radiative process is called spin lattice relaxation, and is responsible for the prevention of the disappearance of the field induced population excess ($n_1 - n_2$) during irradiation. Without spin lattice relaxation the population of the states would slowly become equal and saturation would occur, with the resulting loss of the absorption signal. Saturation may well occur also, despite the relaxation process, if the incident electromagnetic radiation used is too strong.

The time in which the number of excess spins is decreased by $1/e$ is called the spin lattice relaxation time T_1 , and as this time determines the life time, Δt , of a spin state, it is related to the uncertainty δE of the Zeeman levels by Heisenberg's uncertainty principle:

$$\delta E \cdot \Delta t = h/2\pi \quad 1.6$$

T_1 will thus affect the line width of the E.S.R. signal.

1.2.2 Hyperfine splitting

In general, because of the spin pairing of electrons, most organic molecules are diamagnetic in that their total spin quantum number in the Z direction, M_s^{tot} , will be zero. There are certain molecules, however, known as radicals in which one electron remains unpaired, ($M_s^{\text{tot}} = \pm \frac{1}{2}$). These compounds because of the unpaired electron will be paramagnetic and will thus have an E.S.R. signal, composed not only of one line but made up of many. The number of lines obtained is determined by the interaction of the electron with the magnetic nuclei in the molecule.

The component of the magnetic moment of a nucleus (of spin quantum number, I) in the Z direction is given by the relationship,

$$\mu_N^z = +M_I g_N \beta_N \quad 1.7$$

where M_I is the spin quantum number in the Z direction = $-I, (-I+1), (-I+2) \dots +I$, g_N is, like g_E , a dimensionless quantity and β_N is the nuclear magneton.

In a strong magnetic field H, interaction between electron and magnetic nucleus occurs and appears as a perturbation δE to the Zeeman levels of the electron:

$$\delta E = (\delta E)_{\text{aniso.}} + (\delta E)_{\text{iso.}} \quad 1.8$$

$(\delta E)_{\text{aniso.}}$ represents the dipole-dipole interaction between the magnetic moments and is dependent upon the relative positions of μ_E and μ_N . In liquids, molecular motion results in the averaging out of the $(\delta E)_{\text{aniso.}}$ term, apart from a small residue due to viscosity of the medium, and this will contribute only to the line width, not to δE .

$(\delta E)_{\text{iso.}}$ is known as the direction independent Fermi contact term. In a strong magnetic field in the Z direction it is given by the relationship,

$$(\delta E)_{\text{iso.}} = - \frac{8\pi}{3} (\mu_E^z \cdot \mu_N^z) \rho'(0) \quad 1.9$$

where $\rho'(0)$ is the spin density at the nucleus. Bearing in mind the earlier definitions of the two magnetic moments one obtains:

$$(\delta E)_{\text{iso.}} = + \frac{8\pi}{3} (g_E \beta_E g_N \beta_N (M_S M_I) \rho'(0)) \quad 1.10$$

This relationship shows that for positive g_N and $\rho'(0)$ the Zeeman levels of the electron are stabilised when M_S and M_I have opposite signs, and are destabilised for M_S and M_I of similar signs. The number of sub levels produced for each level will obviously depend on I, and for hydrogen in which $I = \frac{1}{2}$, M_I can either $+\frac{1}{2}$ or $-\frac{1}{2}$ and each level will be split into two. For nitrogen on the other hand M_I may take three different values $+1, 0$ or -1 resulting in each Zeeman level having three sub levels.

Transactions between levels, as described earlier will now only take place if the change in the electron spin quantum number,

M_s is ± 1 and there is no change in the nuclear spin quantum number M_I . A diagrammatic representation of the transitions for hydrogen and nitrogen and the resulting spectra are shown in Figures 1.10. A and B respectively. It can be seen, that the number of lines resulting from the hyperfine splitting by a nucleus of spin quantum number, I , will be given by $2I + 1$, and that these lines will have the same intensity, due to the small value of $(\delta E)_{iso}$, and therefore the very small difference between the populations of the sub levels.

The separation between adjacent lines is given by the coupling constants of the nuclei, (a_x for nucleus X), and like the corresponding interactions $(\delta E)_{iso}$, they are dependent only on the electron spin density $\rho'(0)$ at the nucleus.

$$\text{i.e. } a_x = K_x \rho'(0) \quad 1.11$$

$$\text{where } K_x = \frac{4}{g_E \beta_E} \left| \frac{(\delta E)_{iso}}{\rho'(0)} \right| = \frac{4 \times 8\pi}{3} g_N \beta_N |M_s M_I|$$

Diagrams similar to those of Figure 1.10 A and B. can also be drawn up for radicals containing more than one magnetic nucleus, each nucleus splitting the Zeeman levels successively according to their interactions with the unpaired electron. When some of the nuclei are equivalent, certain spin configurations of the nuclei will be degenerate e.g. 2 protons A and B have two spin configurations which are of identical energy.

$$\text{i.e. } M_I(A) = +\frac{1}{2} \quad M_I(B) = -\frac{1}{2}$$

$$M_I(A) = -\frac{1}{2} \quad M_I(B) = +\frac{1}{2}$$

This results in an increase of intensity of certain lines.

In general, for n equivalent nuclei with spin quantum number I there will be $(2nI + 1)$ lines and the distribution of intensity will be binomial.

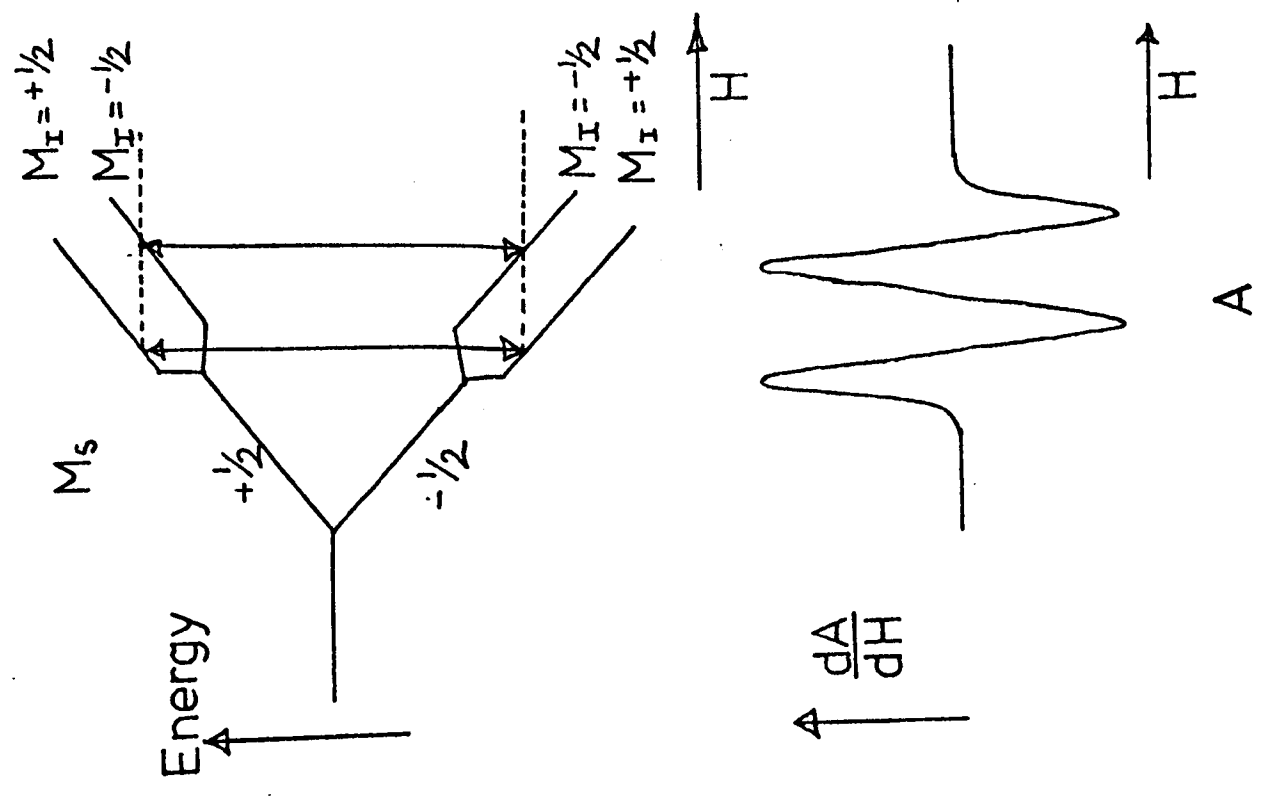
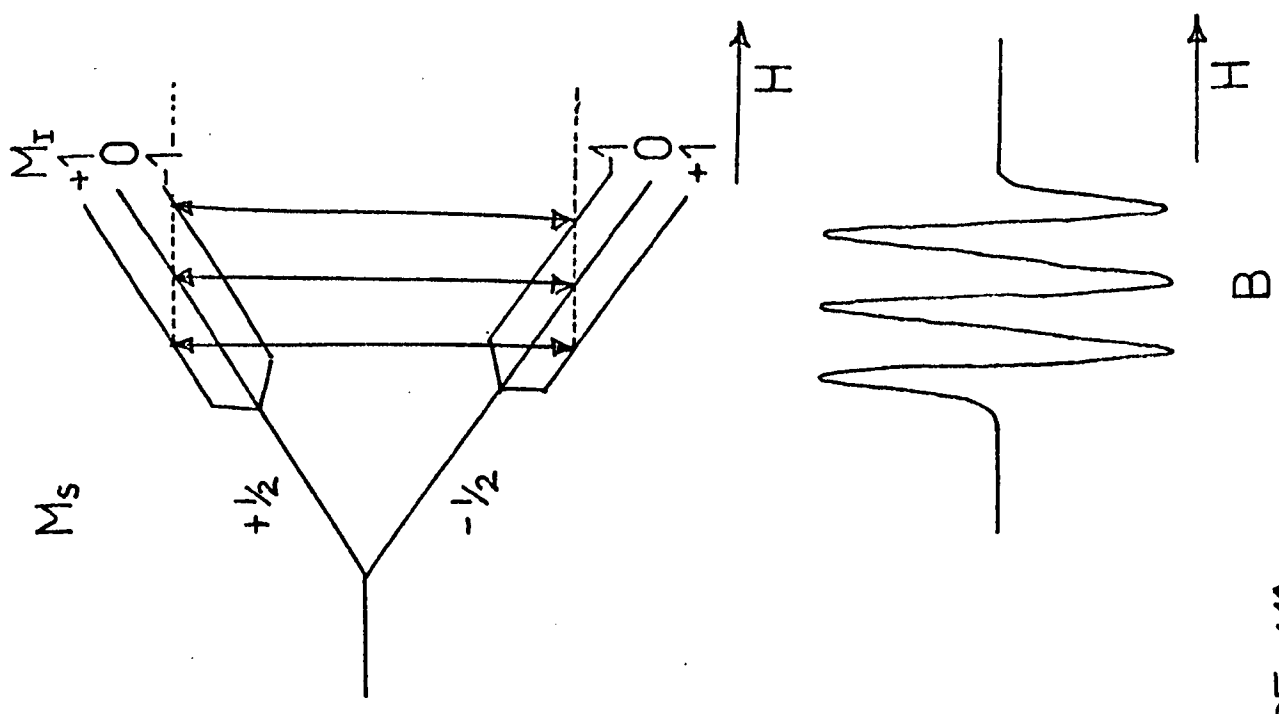


FIGURE 1.10

1.3 Molecular Orbital Theory

1.3.1 Hückel M.O. Theory

The calculation of electronic energies by the H.M.O. method is relatively simple and straight forward, providing a number of assumptions are made. The first basic assumption is defined as the L.C.A.O. (linear combination of atomic orbitals) approximation and this states that the π molecular wavefunctions or orbitals may be taken as linear combinations of the atomic orbitals of the atoms in the molecule. This will mean that the molecular orbitals for a molecule will be in the general form,

$$\psi_j = c_{j1} \phi_1 + c_{j2} \phi_2 + \dots + c_{jn} \phi_n \quad 1.12$$

$$\text{or } \psi_j = \sum_{r=1}^n c_{jr} \phi_r$$

where ψ_j is the j^{th} molecular orbital, ϕ_r is the atomic orbital for the r^{th} atom, and c_{jr} is the coefficient of the r^{th} atomic orbital in the j^{th} molecular orbital. From the combination of n atomic orbitals, there must result n molecular orbitals.

The Schrödinger equation shows that

$$H\psi = E\psi$$

H being the Hamiltonian operator and E the energy of the ψ orbital

Now if both sides of that equation are multiplied by the complex conjugate of ψ , assumed here also to be ψ , and if the equation so obtained is integrated over space, it can be seen

$$\int \psi H \psi d\tau = \int \psi E \psi d\tau \quad 1.13$$

or as E is scalar,

$$E = \frac{\int \psi H \psi d\tau}{\int \psi^2 d\tau} \quad 1.14$$

The best set of values for the coefficients of equation 1.12 may now be found by applying the variation principle which states that

$$\epsilon = \frac{\int \psi H \psi d\tau}{\int \psi^2 d\tau} > E_0 \quad 1.15$$

This means, that any function other than the correct one will yield a value for the ground state energy which is higher than the true value. The problem is thus reduced to finding the set of coefficients that yields the lowest energy when put into equation 1.15.

$$\text{i.e.} \quad \frac{d\varepsilon}{dc_r} = 0 \quad 1.16$$

Substituting 1.12 into 1.15 and omitting the molecular orbital indices for the present,

$$\varepsilon = \frac{\int (\sum_r c_r \phi_r) H (\sum_r c_r \phi_r) d\tau}{\int \sum_r (c_r \phi_r)^2 d\tau} \quad 1.17$$

$$= \frac{\sum_r \sum_s c_r c_s \int \phi_r H \phi_s d\tau}{\sum_r \sum_s c_r c_s \int \phi_r \phi_s d\tau} \quad 1.18$$

For convenience the following notations are used

$$H_{rs} \equiv \int \phi_r H \phi_s d\tau \quad 1.19$$

$$\text{and } S_{rs} = \int \phi_r \phi_s d\tau \quad 1.20$$

$$\therefore \varepsilon = \frac{\sum_r \sum_s c_r c_s H_{rs}}{\sum_r \sum_s c_r c_s S_{rs}} \quad 1.21$$

The denominator then consists of a series of overlap integrals whose sum cannot vanish so equation 1.21 becomes

$$\varepsilon \sum_r \sum_s c_r c_s S_{rs} = \sum_r \sum_s c_r c_s H_{rs} \quad 1.22$$

which on differentiation with respect to a particular coefficient c_t , bearing in mind the relationship given by equation 1.16, yields

$$\varepsilon \sum_s c_s S_{ts} + \varepsilon \sum_r c_r S_{rt} = \sum_s c_s H_{ts} + \sum_r c_r H_{rt} \quad 1.23$$

but as $S_{rs} = S_{sr}$ and $H_{rs} = H_{sr}$,

$$\varepsilon \sum_r c_r S_{rt} = \sum_r c_r H_{rt} \quad 1.24$$

$$\text{or} \quad \sum_r c_r (H_{rt} - \varepsilon S_{rt}) = 0 \quad 1.25$$

This minimization procedure may be carried out with each coefficient so that n equations of this type are obtained.

$$\begin{array}{l}
 c_1 (H_{11} - S_{11}\epsilon) + c_2 (H_{12} - S_{12}\epsilon) + \dots + c_n (H_{1n} - S_{1n}\epsilon) = 0 \\
 c_1 (H_{21} - S_{21}\epsilon) + c_2 (H_{22} - S_{22}\epsilon) + \dots + c_n (H_{2n} - S_{2n}\epsilon) = 0 \\
 \vdots \\
 c_1 (H_{n1} - S_{n1}\epsilon) + c_2 (H_{n2} - S_{n2}\epsilon) + \dots + c_n (H_{nn} - S_{nn}\epsilon) = 0
 \end{array} \quad 1.26$$

$$\text{or } \sum_{r=1}^n c_r (H_{rt} - S_{rt}\epsilon) = 0 \quad 1.27$$

The solution of these equations may be obtained by putting the value of the corresponding secular determinant equal to zero.

i.e.

$$\begin{vmatrix}
 H_{11} - S_{11}\epsilon & H_{12} - S_{12}\epsilon & \dots & H_{1n} - S_{1n}\epsilon \\
 H_{21} - S_{21}\epsilon & H_{22} - S_{22}\epsilon & \dots & H_{2n} - S_{2n}\epsilon \\
 \vdots & \vdots & \ddots & \vdots \\
 H_{n1} - S_{n1}\epsilon & H_{n2} - S_{n2}\epsilon & \dots & H_{nn} - S_{nn}\epsilon
 \end{vmatrix} = 0 \quad 1.28$$

Further approximations are now introduced.

The H_{rr} terms are called Coulomb Integrals, and represent approximately the energy of an electron in an atomic orbital (being contributed to the molecular orbital). For molecules consisting entirely of carbon atoms such integrals are assumed equal and are denoted by the term α .

The terms H_{rs} for $r \neq s$ are known as resonance integrals and from the definition $H_{rs} = \int \phi_r H \phi_s d\tau$ it can be seen that they represent the interaction of two atomic orbitals. If the two atoms r and s are not classically bonded, these terms are assumed to be 0. For bonded atoms however (again only when the lattice consists solely of carbons), the H_{rs} values are considered to be equal and are represented by β . Relative to the energy of an electron at infinity both α and β are negative energy quantities.

The overlap integrals S_{rs} , for atomic orbitals which are normalized, are put equal to 1 for $r=s$ but set to 0 for $r \neq s$. This latter assumption is partly justified in that it can be shown that S_{rs} vanishes rapidly as the distance between r and s increases.

Thus the secular determinant, equation 18, will now become

$$\begin{vmatrix} \alpha - \epsilon & \beta_{12} & \beta_{13} & \dots & \beta_{1n} \\ \beta_{21} & \alpha - \epsilon & \beta_{23} & \dots & \beta_{2n} \\ \vdots & \vdots & \vdots & \ddots & \vdots \\ \beta_{n1} & \beta_{n2} & \beta_{n3} & \dots & \alpha - \epsilon \end{vmatrix} = 0 \quad 1.29$$

with $\beta_{rs} = \beta$ or 0 depending on whether r and s are bonded.

Expansion of this determinant is then possible leading to a polynomial which has n real roots of the general form:

$$\frac{(\alpha - \epsilon)}{\beta} = -a_j \quad j=1, \dots, n \quad 1.30$$

Thus as required one obtains n possible values for the energy of the molecular orbitals, the energy of the j th molecular orbital being given by

$$\epsilon_j = \alpha + a_j \beta \quad 1.31$$

It remains then, only to find the coefficients c_{jr} . This may be done, by feeding the values of the energies back into the series of equations 1.27, to give the ratios $c_2/c_1, c_3/c_1, \dots, c_n/c_1$, for each molecular orbital, and by using the relationship $\sum c_r^2 = 1$ (for normalized orbitals) to obtain their actual values.

The conclusions arrived at above are based on the assumption that the individual atomic orbitals are identical i.e. the atoms involved must be all carbon. So if molecules containing atoms other than carbon are considered, certain modifications are needed to make allowance for the differing pull these atoms exert on the electron as compared to carbon. In Hückel theory, allowance for this is made by introducing changes for the α and β factors for the

heteroatoms. For a heteroatom X,

$$\alpha_x = \alpha_0 + h_x \beta_0 \quad 1.32$$

$$\beta_{cx} = K_{cx} \beta_0 \quad 1.33$$

where α_0 and β_0 are the values for carbon in benzene and α_x and β_{cx} are those for the heteroatom bonded to carbon. The more electronegative is the atom X the more positive will h_x be.

A carbon adjacent to the heteroatom will also tend to have a different affinity for the electron to that of a benzene carbon, and to account for this a further parameter, the auxiliary inductive parameter, is needed. This is defined by

$$\delta_x = fh_x \quad 1.34$$

where f is necessarily less than 1, and the coulomb integral will now be given by the relationship

$$\alpha_c = \alpha_0 + \delta_x \beta_0 \quad 1.35$$

Finally, although the Hückel molecular orbital theory may be sufficient at predicting unpaired electron density in some radicals, it will not by itself give spin densities necessary to predict most E.S.R. spectra. For instance Hückel predicts that an odd alternate radical (one in which there is an odd number of atoms and one in which alternate atoms may be starred without two starred atoms being adjacent e.g. in the simple allyl radical $\begin{matrix} * & * \\ \text{C}-\text{C}-\text{C} \end{matrix}$), will have zero unpaired electron density at every other atom due to the distribution of the electron in the non bonding orbital. This does not mean, however, that the spin density will be zero at these atoms or that hydrogen atoms attached to these will not contribute to the hyperfine splitting. It remains, therefore, to find some method of converting Hückel results for the wavefunctions to spin densities on the atoms in the molecular orbital framework. A reasonable method for this has been shown to be the McLachlan perturbation method²².

He began with the reasonable assumption that in a radical, the single determinant wavefunction with one unpaired electron and $2n$ other electrons, is not as useful as it is for a closed shell model, in which all the electrons are paired, due to the fact that the α and β spins are affected to a different degree by the unpaired electron. To allow for this, McLachlan employed the self consistent wave function proposed by Pople and Nesbet²³.

$$\bar{\Phi} = \sqrt{\frac{1}{(2n+1)!}} \begin{vmatrix} \psi_1^\alpha & \psi_1^\beta & \dots & \psi_n^\alpha & \psi_n^\beta & \psi_0(l) \\ \vdots & \vdots & & \vdots & \vdots & \vdots \\ \psi_1^\alpha(2n+1) & \psi_1^\beta(2n+1) & \dots & \psi_n^\alpha(2n+1) & \psi_n^\beta(2n+1) & \psi_0(2n+1) \end{vmatrix} \quad 1.36$$

in which the α and β spin electrons are in different sets of orbitals ψ^α and ψ^β and the odd electron is in the ψ_0 orbital. In the overall wavefunction $\bar{\Phi}$, the effective field produced by the other electrons is different for the different spins owing to the exchange term in the energy.

The effect of this exchange potential of the odd electron, is to alter the spin densities on the atoms by an alteration of α_r , the Coulomb integrals, and β_{rs} the resonance integrals, for electrons with α spin. This perturbation has been discussed by McLachlan in terms of the wavefunction, and he has shown that, providing the molecule is alternant and assuming the Coulomb repulsion integrals γ_{rr} are the same for all electrons,

$$p_r = c_{or}^2 - \frac{1}{2} \gamma \sum \pi_{rs} c_{os}^2 \quad 1.37$$

where p_r is the spin density on atom r , c_{or} is the coefficient of the atomic orbital of the r^{th} atom in the non bonding orbital, and π_{rs} is given by

$$\pi_{rs} = -4 \sum_i \sum_j \frac{c_{ri} c_{sj} c_{si} c_{rj}}{E_j - E_i} \quad 1.38$$

where i are the occupied and j are the vacant orbitals. The

E_i and E_j values are the energies of the occupied and unoccupied Hückel orbitals respectively.

Then by putting $\frac{1}{2} \gamma / \beta = -\lambda = -1.2$, where β is the average β_{rs} of all the bonds in the molecule, McLachlan's final equation for the spin density becomes

$$\rho_r = C_{or}^2 - \lambda \sum_s \pi_{rs} C_{os}^2 \quad 1.39$$

One of the main drawbacks of Hückel is that it is essentially a one electron method, and tends to ignore any influence of the electrons on each other. This fact is reflected in that to predict certain different experimental results for one set of compounds, different values of α and β may be needed. For instance, the first ionization potentials of aromatic hydrocarbons correlate closely with the energy of the highest Hückel orbital if $\beta = -40$ eV. but for the same compounds, is found to be -2.4 eV for good agreement with the energy of the first allowed electronic transition. Finally, a β of 0.7 eV is needed to explain the resonance energy of the compounds.

It has been concluded from these results that the β 's used in the three different calculations must represent different combinations of one electron energies (nuclear attraction and kinetic energy only) and two electron repulsion energies, which are not accounted for in the theory.

The fact that electron-electron repulsion is ignored, is also indicated by the fact that Hückel theory is not very useful for molecules with rather polar bonds or for non-alternate molecules in which there is a non-uniform distribution of charge. This is especially so for molecules containing heteroatoms, because if due to the unavailability of experimental data one uses atomic spectral data to calculate the Coulomb integrals, the bond polarities obtained are unreasonably large, as no allowance for interelectron interactions are made.

It would thus appear, that Hückel has shortcomings which may make it an unacceptable method of determining the wavefunctions of a molecule. In fact, its failure to explain spectroscopic data played a large part in the development of somewhat more rigorous methods, known as self consistent field or SCF theories. These methods lie between the two extremes of Hückel and ab initio molecular orbital calculations, which are inapplicable to all but the smallest molecules, and have a varying degree of approximation. Within the group, for instance, lies the non-empirical method known as the Hartree-Fock wave functions, while at the other end, lie the semi-empirical π -electron theories such as that developed by Pople²⁴. The method employed for the purpose of this thesis was a semi-empirical one due to Pariser, Pople and Parr (the P.P.P. method).

1.3.3 SCF molecular orbital equations

As in Hückel, the first assumption is that each molecular orbital wave function may be expressed as a series expansion of a set of orthonormal basis functions. The set is arbitrarily chosen, but for simplicity the LCAO approximation is usually invoked and the number of basis functions limited to one per atomic π centre. The wavefunction of the i^{th} molecular orbital may be thus given by:-

$$\Psi_i = \sum_{\mu} c_{i\mu} \phi_{\mu} \quad 1.40$$

where $c_{i\mu}$ is the coefficient of the atom μ in the i^{th} molecular orbital and ϕ_{μ} is the basis function for atom μ .

Now, according to the Pauli principle, the only valid form for the total wavefunction is an antisymmetric one i.e. one in which the wavefunction changes sign with an exchange of two electrons. This condition will be fulfilled if the total wavefunction is represented by a Slater determinant as follows:

$$\Phi = \frac{1}{\sqrt{N!}} \begin{vmatrix} \psi_1(1) & \psi_1(2) & \dots & \psi_1(n) \\ \psi_2(1) & \psi_2(2) & \dots & \psi_2(n) \\ \vdots & \vdots & & \vdots \\ \psi_n(1) & \psi_n(2) & & \psi_n(n) \end{vmatrix} \quad 1.41$$

It can be seen by examination of this determinant that interchange of columns (or electron exchange) leads to a change of sign for Φ , and further that if two columns are identical, Φ must be zero. This condition is also necessary if no two electrons are to be identical.

In fact, the derivation for the entire antisymmetrized product wave function need not be carried out, and only one orbital at a time may be treated. This is done by making use of the Hartree-Fock equation for a single electron,

$$F\psi_i = \epsilon \psi_i \quad 1.42$$

Where F is the new operator in place of the Hamiltonian H .

In a similar way to the Hückel treatment, application of the LCAO expansion leads to the equations:

$$\sum c_\nu (F_{\mu\nu} - E S_{\mu\nu}) = 0 \quad 1.43$$

$$\text{and} \quad |F_{\mu\nu} - E S_{\mu\nu}| = 0 \quad 1.44$$

$$\text{where} \quad F_{\mu\nu} = \int \phi_\mu F \phi_\nu d\tau \quad 1.45$$

The difference between these equations above and the corresponding ones in Hückel (equations 127, 128) lies in the difference between F and H . Lennard-Jones²⁵, Hall²⁶ and Roothan²⁷, have all shown that $F_{\mu\nu}$ for a closed shell model may be given by the expression;

$$F_{\mu\nu} = H_{\mu\nu}^c + \sum_p \sum_q P_{pq} [(\mu\nu | pq) - \frac{1}{2} (\mu p | \nu q)] \quad 1.46$$

Where H^c is the core Hamiltonian for an electron and consists of the kinetic energy term for the electron and the potential energy between an electron and all the atomic cores of the molecule.

Goeppert-Mayer and Sklar²⁸, have postulated an approximation to this core potential,

$$H^c = -\frac{\hbar^2}{2m} \nabla^2 + \sum_\alpha V_\alpha \quad 1.47$$

$$\text{where} \quad \nabla^2 = \frac{\partial^2}{\partial x^2} + \frac{\partial^2}{\partial y^2} + \frac{\partial^2}{\partial z^2}$$

If Z_α is the nuclear charge on atom α and R_α is the distance of the electron from this nucleus, then the nuclear-electron potential V_α will be given by;

$$V_\alpha = -\frac{Z_\alpha e^2}{R_\alpha} \quad 1.48$$

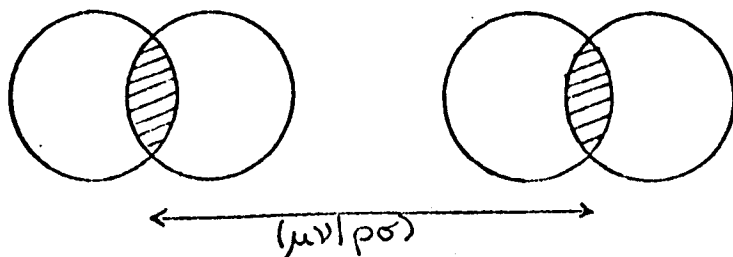
The core Hamiltonian can thus be represented in atomic units (in which the charge and mass of an electron and \hbar all become equal to unity) by the relationship:

$$H^c = -\frac{1}{2} \nabla^2 + \sum_{\alpha} -\frac{Z_{\alpha}}{R_{\alpha}} \quad 1.49$$

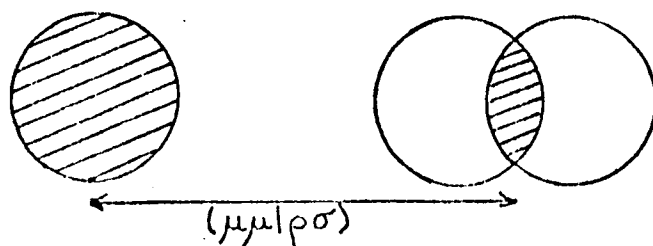
The remaining terms in the equations above, account for the effect of electron interaction. Defining $(\mu\nu|\rho\sigma)$ by

$$(\mu\nu|\rho\sigma) = \iint \phi_{\mu}(1)\phi_{\nu}(1)\left(\frac{e^2}{r_{12}}\right)\phi_{\rho}(2)\phi_{\sigma}(2)\delta\tau_1\delta\tau_2 \quad 1.50$$

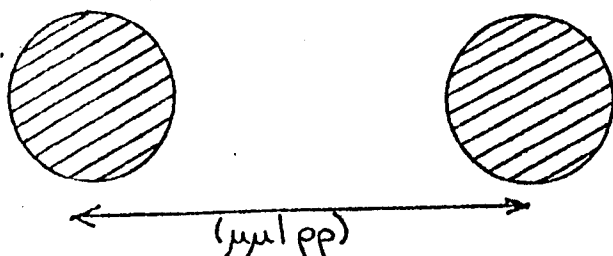
it can be seen, that this term may be physically interpreted as being due to the repulsion between an electron distributed in space according to the function $\phi_{\mu}\phi_{\nu}(1)$ and a second electron having the distribution $\phi_{\rho}\phi_{\sigma}(2)$ i.e. it represents the Coulombic interaction between the electron concentration in the overlap of two atomic orbitals μ and ν and that in the overlap between ρ and σ . This interaction may be demonstrated pictorially as follows:



$(\mu\nu|\rho\sigma)$ is thus known as a four centred integral. When $\mu=\nu$ a three centred integral is obtained, in that the repulsion becomes that between the electron in the atomic orbital μ and the second electron having the distribution $\phi_{\rho}\phi_{\sigma}$.



A two centred integral simply describes the repulsion between electrons in two atomic orbitals.



Similarly $(\mu\rho|\nu\sigma)$ is defined by:

$$(\mu\rho|\nu\sigma) = \iint \phi_\mu(1)\phi_\rho(1)\left(\frac{e^2}{r_{12}}\right)\phi_\nu(2)\phi_\sigma(2) d\tau_1 d\tau_2 \quad 1.51$$

This term is introduced to take into account the spin of the electron, and the fact that two electrons of the same spin cannot according to the Pauli principle occupy the same position in space is known as the exchange integral.

Finally, the term $P_{\rho\sigma}$ in equation 1.46 is defined as the bond order and is given by:

$$P_{\rho\sigma} = 2 \sum_k c_{k\rho} c_{k\sigma} \quad 1.52$$

the summation extending over all the occupied molecular orbitals ψ_k .

It would thus appear, that there is now a contradiction, in that to find $F_{\mu\nu}$, the equation for $P_{\rho\sigma}$ must be first solved, but in order to do this, values for $c_{k\rho}$ and $c_{k\sigma}$ are needed. These however can not be solved unless the orbitals (and hence $F_{\mu\nu}$) are known. This problem is overcome, by solving equation 1.46 iteratively. That is, estimates for the coefficients of the orbitals are made (usually by application of Hückel theory to the molecule) and these are put into the equations 1.52 and 1.46 to give values for $F_{\mu\nu}$. Using these values obtained for $F_{\mu\nu}$ then, the secular equations 1.43 and 1.44 are solved to give new values for the coefficients which are again used to find F . The process is repeated until the input and output of the coefficients are self consistent.

Choice of atomic basis functions

Basically, for a non empirical SCF calculation, two types of basis sets are commonly used in conjunction with the LCAO approximation, these being generally a compromise between functions that adequately describe the behaviour of the electrons and functions for which the calculations are not too difficult. The first are known as Slater type orbitals (STO) in which ϕ_r varies as $\exp(-kr)$, while the other type are Gaussian functions which although have little resemblance to any atomic orbital will, if a number are taken in a linear expansion, represent the atomic orbital sufficiently well. Gaussian functions have a radial dependence on distance i.e. $\exp(-kr^2)$

However, there is a drawback in using a non empirical method, and that is, that the size of molecule on which it may be used is limited by the fact that for n orbitals, the number of two electron integrals needed to be evaluated for the solution of the n secular equations is n^4 . This takes up a lot of time and at the present moment, only medium sized molecules may be treated in this way.

For larger molecules, there exists another way of approaching the problem of evaluating the integrals, and that is to ignore the form of basis functions and empirically evaluate the integrals. This is indeed the method used for the P.P.P. type calculations.

1.3.4 P.P.P. Self consistent molecular orbitals ²⁹

The major assumption in the P.P.P. calculations is, as in Hückel, that the zero differential or ZDO approximation may be adopted. This approximation means that the overlap between all atomic orbitals (whether adjacent or not) is considered to be non existent and that the overlap integrals $(\mu\nu|\rho\sigma)$ must reduce

to zero when $\nu \neq \mu$ and $\rho \neq \sigma$. The effect of this neglect of overlap is to cut the number of two electron integrals needing to be evaluated quite considerably. Examination of equation 1.46, for instance, shows that summation over ρ and σ results in only one non zero electron repulsion integral, when $\rho = \mu$ and $\sigma = \nu$ i.e. equation 1.46 becomes on application of the ZDO approximation.

$$F_{\mu\nu} = H_{\mu\nu}^c - \frac{1}{2} P_{\mu\nu} \gamma_{\mu\nu} \quad 1.53$$

where $\gamma_{\mu\nu} = (\mu\mu|\nu\nu)$

From equation 1.47 the core potential may be defined by

$$H_{\mu\nu}^c = \int \phi_{\mu} \left(-\frac{1}{2} \nabla^2 + V_M + V_N + \sum_{A(\neq M,N)} V_A \right) \phi_{\nu} d\tau \quad 1.54$$

Where V_M and V_N are the core potentials of atoms M and N, the nuclear centres of μ and ν respectively. If it is then assumed that there is sufficient overlap of μ and ν to give enough attraction between the positive charge cores M and N and the overlap cloud of orbitals μ, ν to bring about bonding, the integrals for the M and N cores will be non zero. Furthermore, if the contribution of the distant cores ($A \neq M, N$) is considered to be negligible, $H_{\mu\nu}^c$ can be written as:

$$H_{\mu\nu}^c = \int \phi_{\mu} \left(-\frac{1}{2} \nabla^2 + V_M + V_N \right) \phi_{\nu} d\tau \quad 1.55$$

This term is normally defined as the resonance integral.

Thus, the off diagonal elements for the F matrix may be defined as

$$F_{\mu\nu} = \beta_{\mu\nu} - \frac{1}{2} P_{\mu\nu} \gamma_{\mu\nu} \quad 1.56$$

Similar treatment for the diagonal elements give the following equations:

$$F_{\mu\mu} = H_{\mu\mu}^c + \sum_{\rho} P_{\rho\rho} (\mu\mu|\rho\rho) - \frac{1}{2} P_{\mu\mu} (\mu\mu|\mu\mu) \quad 1.57$$

where $H_{\mu\mu}^c = \int \phi_{\mu} \left(-\frac{1}{2} \nabla^2 + V_M + \sum_{A(\neq M)} V_A \right) \phi_{\mu} d\tau \quad 1.58$

$$= U_{\mu\mu} + \sum_{A(\neq M)} \int \phi_{\mu} V_A \phi_{\mu} d\tau \quad 1.59$$

and $U_{\mu\mu} = \int \phi_{\mu} \left(-\frac{1}{2} \nabla^2 + V_M \right) \phi_{\mu} d\tau \quad 1.60$

$U_{\mu\mu}$ may be physically interpreted as being the energy of the orbital ϕ_μ for the appropriate state of the atom M. (This is further discussed in the section on parameterization).

Now if atoms A and M are far apart,

$$\int \phi_\mu V_A \phi_\mu d\tau = - \frac{Z_A e^2}{R_{AM}} \quad 1.61$$

where $Z_A e$ is the charge on atom A and R_{AM} is the distance separating it from the orbital μ . Also, if ρ is the orbital on atom A, the two centre two electron repulsion integral $(\mu\mu|\rho\rho)$ is given by:

$$(\mu\mu|\rho\rho) = \frac{e^2}{R_{AM}} = \gamma_{\mu\rho} \quad 1.62$$

Thus combining equations 1.61 and 1.62,

$$\int \phi_\mu V_A \phi_\mu d\tau = -f(R) Z_A \gamma_{\mu\rho} \quad 1.63$$

The term $f(R)$ is known as the penetration function, and it allows for deviations of the two integrals above from their relationships (given by equations 1.61 and 1.62) at low values for R. Satisfactory results are however obtained if the value for $f(R)$ is always assumed to be unity.

Combining the above equations 1.57, 1.59 and 1.63 therefore, the diagonal elements of F will be given by

$$F_{\mu\mu} = U_{\mu\mu} + \frac{1}{2} P_{\mu\mu} \gamma_{\mu\mu} + \sum_{\rho \neq \mu} (P_{\rho\rho} - Z_A) \gamma_{\mu\rho} \quad 1.64$$

Equations 1.56 and 1.64 give the elements of the Pople SCF equations for Π electrons.

At first sight, the ZDO approximation would appear to be very severe. However, it has been shown that neglect of overlap has a real basis, in that making the assumption the results obtained are not unduly jeopardised. Also any errors which are introduced can be partially compensated for by a judicious choice of parameters.

1.3.5 Parameterization of the P.P.P. method

As has been mentioned earlier, PPP is a semi empirical molecular orbital method. The definitions of the elements of the SCF equation for the π electrons have been given above, but it remains to be stated what form do the empirical parameters needed to replace the integrals take.

There are three parameters used to construct the F matrix, and these replace

- (i) $U_{\mu\mu}$ - Energy of the orbital ϕ_{μ} (Goeppart-Mayer - Sklar potential)
- (ii) $\beta_{\mu\nu}$ - Resonance integrals
- (iii) $\gamma_{\mu\nu}$ - Two electron integrals.

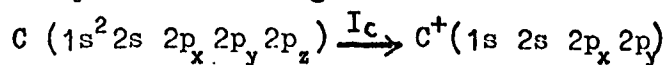
- (i) Energy of the orbital ϕ_{μ}
31

Koopman's theorem states that an orbital energy may be equated to minus the ionization potential for the removal of an electron from that orbital.

$$\text{i.e. } U_{\mu\mu} = -I_{\mu} \quad 1.65$$

where I_{μ} is the valence state ionization potential (V.S.I.P.).

The concept of valence state ionization potential is best illustrated by considering the example of a carbon atom. The process of ionization from the valence state can be represented by the following scheme:



in which $C(1s^2 2s^2 2p_x 2p_y 2p_z)$ denotes the electron configuration of the valence state of a neutral carbon atom. The value of I may then be calculated using the following relationships:

$$(i) C(1s^2 2s^2 2p_x 2p_y 2p_z) \xrightarrow{E_1} C^+(1s^2 2s^2 2p_x 2p_y)$$

$$(ii) C^+(1s^2 2s^2 2p_x 2p_y) \xrightarrow{E_2} C^+(1s^2 2s^2 2p_x 2p_y 2p_z)$$

$$(iii) C(1s^2 2s^2 2p_x 2p_y 2p_z) \xrightarrow{E_3} C(1s^2 2s^2 2p_x 2p_y 2p_z)$$

(i) represents the ground state ionization potential, and the resulting change in electronic configuration, (ii) represents the energy corresponding to an electron in the 2s orbital of the C^+ species being promoted to the 2p orbital, and (iii) represents that of a 2s electron of a carbon atom being promoted to a 2p orbital. All three of these energy terms may be determined experimentally and Hinze and Jaffe³² have tabulated various values for a number of atoms. It can be seen, therefore, that the valence state ionization potential will be given by:

$$I_C = E_1 + E_2 - E_3$$

(ii) The core resonance integrals $\beta_{\mu\nu}$

$$\beta_{\mu\nu} = \int \phi_\mu (-\frac{1}{2}\nabla^2 + V_M + V_N) \phi_\nu d\tau$$

Normally β is varied to give the best "fit" of the data to experiment, for a given set of $U_{\mu\mu}$ and $\gamma_{\mu\nu}$, but Flurry, Stout and Bell³³ give an empirical equation which is useful in obtaining a reasonable starting value for the resonance integral.

$$\beta_{\mu\nu} = -2524 \exp[-5.047((\frac{Z_\mu + Z_\nu}{Z_c} - 2)^2 - 5r_{\mu\nu})] \quad 1.66$$

where Z_c is the effective nuclear charge for carbon and Z_μ , and Z_ν are the effective nuclear charges of the atoms of which μ and ν are the orbitals (separated by a distance of $r_{\mu\nu} \text{ \AA}$). If the atoms μ and ν are carbon then equation 66 reduces to:

$$\beta_{\mu\nu} = -2524 \exp(-5r_{\mu\nu}) \quad 1.67$$

However, for a bond between atoms which are not solely carbon, the effective nuclear charges exerted upon the molecular bonding electrons are needed. Slater³⁴ has defined these charges as:

$$Z_{\text{off}} = Z - s \quad 1.68$$

where Z is the atomic number or actual nuclear charge of the atom, and s is the shielding constant which accounts for the shielding effect of the other electrons on the atom. According to Slater, these shielding constants should have the following contributions

- (1) Zero from any electron having a principal quantum number greater than that of the electron under consideration.
- (2) 0.35 from each electron with the same principal quantum number (n).
- (3) For s or p electrons a contribution of 0.85 for each electron with a principal quantum number of $n-1$, and 1.0 for those with a principal quantum number of $n-2$ or less. For d electrons with a principal quantum number of $n-1$ or less, a contribution of 1.0.

Thus for a neutral carbon atom, apart from the electron in the $2p_z$ orbital which is considered to be contributing to the π molecular orbital framework, there are three other electrons with a principal quantum number of 2 and two others with a principal quantum number of 1 (1s electrons).

$$\begin{aligned} \therefore Z_{\text{eff}} &= 6.0 - (3 \times 0.35 + 2 \times 0.85) \\ &= 3.25 \end{aligned}$$

For two non bonded atoms p and q , β_{pq} is taken as zero.

Flurry, Stout and Bells' method described above, is just one way of determining β_{pq} ; there are many others. For the purpose of this thesis however, this method was used to give an approximate value for β_{pq} and further adjustments were made in order to try to get a good fit of the calculated values to experimental data.

(3) Two electron Coulombic integrals $\gamma_{\mu\nu}$

Pariser³⁵, in defining $\gamma_{\mu\mu}$, the one centre two electron integral, reasoned that the repulsion of two electrons in the Π orbital μ should be given by the difference between the valence state ionization potential (I_{μ}) and the valence state electron affinity (E_{μ}).

$$\text{i.e. } \gamma_{\mu\mu} = I_{\mu} - E_{\mu} \quad 1.69$$

If one defines the one centre Coulombic integral empirically then an appropriate method must be found for defining $\gamma_{\mu\nu}$. Various approximations have been used for $\gamma_{\mu\nu}$, but calculations show that the results obtained are usually insensitive to whichever method is employed. A well used method (and indeed the one which is employed for the calculations in this thesis) is that due to Mataga and Nishimoto.³⁶

$$\gamma_{\mu\nu} = \frac{14.40}{R_{\mu\nu} + r} \quad 1.70$$

where R is the distance in Angstroms between orbital μ and ν ,

$$\text{and } r = \frac{14.40}{\frac{1}{2} [(I_{\mu} - E_{\mu}) + (I_{\nu} - E_{\nu})]} \quad 1.71$$

When $R_{\mu\nu} = 0$, $\gamma_{\mu\nu} = \gamma_{\mu\mu}$

1.3.6 Open shell calculations

The above treatment constitutes a restricted Hartree Fock method, in that only closed shell states are considered. In the unrestricted Hartree Fock (UHF) method, however, the wavefunction is again written as a single determinant, but different orbitals are taken for the α and β spin electrons. Thus the wave function has the form:

$$\Psi = | \Psi_{1\alpha} \Psi_{2\alpha} \dots \Psi_{n\alpha} \Psi_{1\beta}' \dots \Psi_{m\beta}' | \quad 1.72$$

The LCAO-SCF equations for this wavefunction were first given by Pople and Nesbet³⁷ and their ZDO form was derived by Brickstock and Pople³⁸. They are similar to the equations for the closed shell system, the coefficients of the α set, for example, being given by:

$$\sum_{\kappa\mu} c_{\kappa\mu}^{\alpha} (F_{\mu\nu}^{\alpha} - ES_{\mu\nu}) = 0 \quad 1.73$$

$$\text{and} \quad |F_{\mu\nu}^{\alpha} - ES_{\mu\nu}| = 0 \quad 1.74$$

Where, in the same way as for the closed shell treatment, one obtains:

$$F_{\mu\nu}^{\alpha} = H_{\mu\nu}^c + \sum_{\rho} \sum_{\sigma} \{ P_{\rho\sigma}^{\alpha} [(\mu\nu | \rho\sigma) - (\mu\rho | \nu\sigma)] + P_{\rho\sigma} (\mu\nu | \rho\sigma) \} \quad 1.75$$

$P_{\rho\sigma}^{\alpha}$ and $P_{\rho\sigma}^{\beta}$ are the separate bond orders for the α and β spin electrons and are given by

$$P_{\rho\sigma}^{\alpha} = \sum_{\kappa(\alpha)} c_{\kappa\rho} c_{\kappa\sigma} \quad 1.76$$

$$P_{\rho\sigma} = P_{\rho\sigma}^{\alpha} + P_{\rho\sigma}^{\beta} \quad 1.77$$

There will of course be a corresponding set of equations to determine the β orbitals.

To enable full consistency to be achieved in the U.H.F. method, both the α and β matrices, being linked in having common bond orders, must be diagonalized simultaneously. Thus, the iterative cycle will involve assuming a set of coefficients in order to solve one set of secular equations (e.g. the α set) and from these, to obtain an improved set of α coefficients which in turn will be used with the assumed β coefficients to construct the secular equations for the β set. In this way, the α and β sets are treated alternatively until self consistency is reached.

Subsequent combination of both states, does not only lead to the wavefunction for the state with the required multiplicity, for a radical this should be a doublet, but,

for a molecule with $2n-1$ electrons, a mixture of higher states up to those of multiplicity $2n$ will also be obtained. Removal of the unwanted components from the wavefunction may be achieved however by using a projection operator, as proposed by Löwdin³⁹, which acts upon the total UHF wavefunction Ψ . For annihilation of the state of multiplicity $2s + 1$, for example, the operator is:

$$A_s = S^2 - s(s+1) \quad 1.78$$

where S^2 is the total spin operator, given by:-

$$S^2 \Psi = s(s+1) \Psi \quad 1.79$$

Further application of such operators, may then be used to remove higher energy components. In fact, to leave only the spin eigenfunction $2s + 1$, it has been shown that the full projection operator is given by

$$\Theta_s = \prod_{l+s} \frac{S^2 - l(l+1)}{s(s+1) - l(l+1)} \quad 1.80$$

In some circumstances, a full projection of the wavefunction is unnecessary, and Amos and Hall⁴⁰ have postulated that the major contaminant in the UHF wavefunction is due to the state with the next highest multiplicity to that required. The use of a single annihilator

$$A_s = S^2 - (s+1)(s+2)$$

is thus usually sufficient to give a much improved wavefunction for the state of multiplicity $2s+1$. In either case, the new wavefunction will be given by

$$\Phi' = A_s \cdot \Phi$$

Thus one may now calculate the spin projected results for the bond orders, total π energies etc. for the open shell state.

An important inherent advantage in this, the spin polarized method, is that because the electron spin pairing constraint has

easily⁴¹. The spin densities are, in fact, directly obtained from the diagonal elements of the α and β electron bond order matrices P^α and P^β before projection, or K^α and K^β after projection, in the following way:

$$\sigma_i = (P_{ii}^\alpha - P_{ii}^\beta) \frac{1}{2} \langle S_z \rangle \quad 1.81$$

$$\text{and } f_i = (K_{ii}^\alpha - K_{ii}^\beta) \frac{1}{2} \langle S_z \rangle \quad 1.82$$

where σ_i represents the unprojected spin density results, and f_i are the projected results. S_z is the total z axis spin projection of the state. $S_z = \frac{1}{2}$ for a doublet state.

1.4 Protons in Organic Radicals

It has been shown, that a number of ways exist by which the spin densities on each carbon atom throughout the molecular framework may be found, but the connection between these and the isotropic hyperfine splittings of the protons has yet to be illustrated.

If one considers a \dot{C} -H fragment, the ground state configuration ϕ_1 is given by two electrons in the bonding σ orbital and one in the carbon π orbital., Carrington⁴² has shown that this state may be represented as

$$\phi_1 = \frac{1}{\sqrt{6}} \|\sigma_B(1)\sigma_B(2)\pi(3)\| \alpha\beta\alpha$$

in which α , β and α are the spins of the $\sigma_B(1)\sigma_B(2)$ and $\pi(3)$ electrons respectively. Now, if one of the electrons in the σ_B orbital is promoted to the σ_A or σ^- antibonding orbital, the excited state so produced, will have three component orbitals (σ_B) (π) (σ_A) in which the electrons may have either α or β spin; Admixture of these orbitals with the ground state may result in unpaired electron density being produced in the σ bond, but on spin conservation grounds, only configurations with one unpaired electron spin will mix with the ground state. The three configurations which will obey this condition are:

$$D_1 = \frac{1}{\sqrt{6}} \|\sigma_B(1)\sigma_A(2)\pi(3)\| \alpha\alpha\beta$$

$$D_2 = \frac{1}{\sqrt{6}} \|\sigma_B(1)\sigma_A(2)\pi(3)\| \alpha\beta\alpha$$

$$D_3 = \frac{1}{\sqrt{6}} \|\sigma_B(1)\sigma_A(2)\pi(3)\| \alpha\beta\beta$$

The combinations of these, which leads to a doublet then are given by:

$$\phi_2 = \frac{1}{\sqrt{6}} (2D_1 - D_2 - D_3)$$

$$\phi_3 = \frac{1}{\sqrt{6}} (D_2 - D_3)$$

of which only ϕ_2 gives unpaired spin in the σ orbital. Thus the total wavefunction for the fragment becomes:

$$\Psi = \phi_1 + \lambda \phi_2$$

where λ , the fraction of the excited orbital participating in the total wavefunction, is proportional to the spin density in the $2p_z$ orbital of the carbon. Also, as the hyperfine splitting constant a_H is proportional to the unpaired spin density $\rho'(0)$ at the proton nucleus, (equation 1.11), then a_H in turn must be linearly related to λ . Thus one may write:

$$a_H = Q_{cH}^H \rho_c \quad 1.83$$

where ρ_c is the spin density at the carbon atom, and Q_{cH}^H is a constant, of negative sign due to the fact that the unpaired spin in the $1s$ orbital is as a consequence of the Pauli principle, of opposite sign to that of the unpaired spin in the system. Equation 1.83 is often called McConnell's relationship.

1.4.1 Interpretation of the E.S.R. spectrum of 2,4,5-triphenyl imidazolyl radical.

Ueda⁴³ first reported the E.S.R. spectrum of the triphenyl imidazolyl radical as consisting of 47 lines, each having a line width of 0.3 gauss, and proposed an interpretation based on the splittings from the ortho, meta, para and ortho' protons only (Figure 1.11). Wilks⁴⁴ however in 1969, pointed out that this postulate seemed unreasonable, in that some splitting from the nitrogen should be observed. Using spectra simulated by computer from the splitting constants given by Ueda, Wilks showed that the result, did not fit the experimental observations. In fact from a spectrum of the completely deuterated radical, he ascertained the value of the nitrogen splitting constant to be 1.44 gauss.

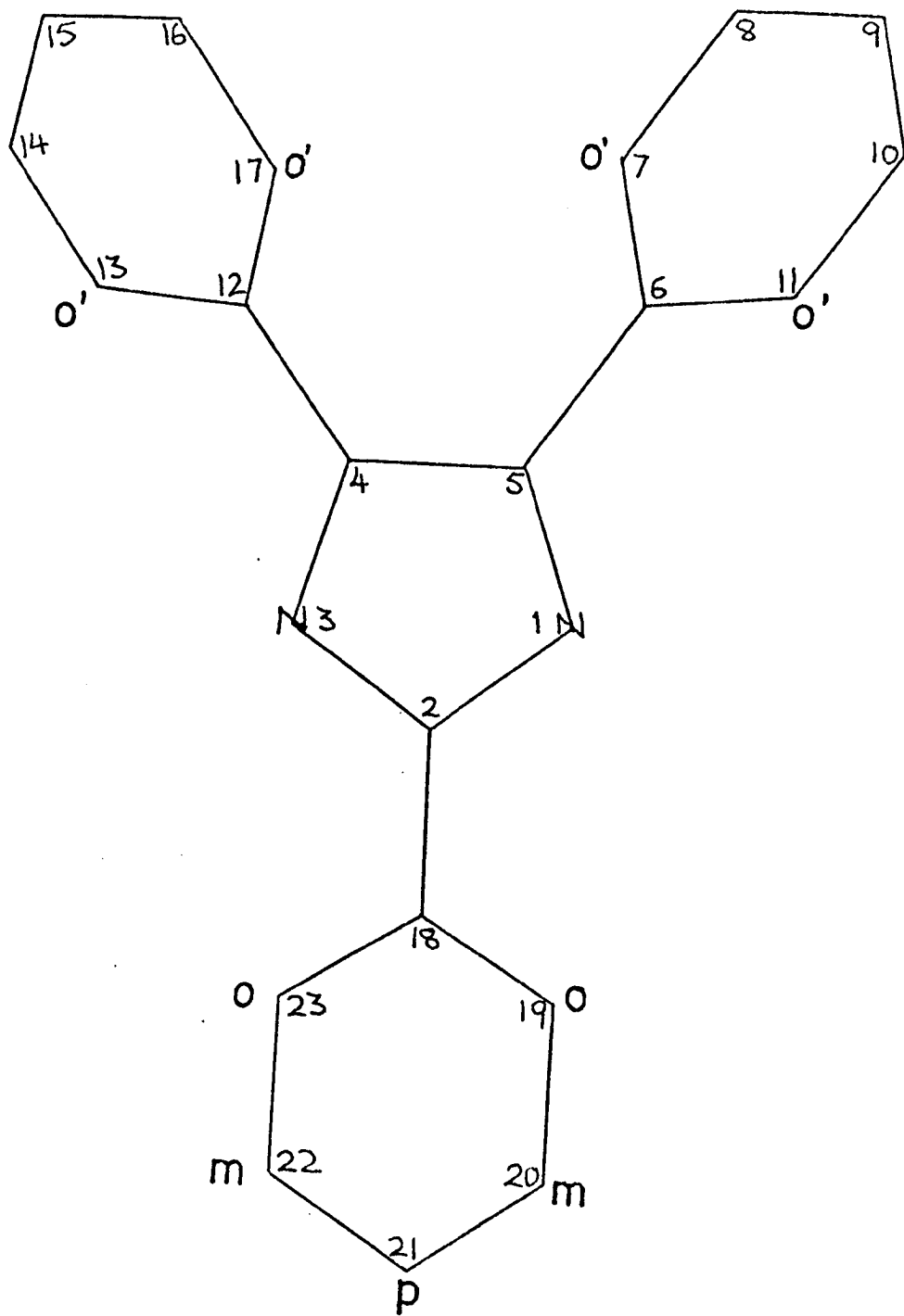


FIGURE 1.11

Cyr, Wilks and Willis⁴⁵ have further resolved the spectrum, from the 47 lines given by Ueda into well over a hundred lines, and, using again computer simulation techniques, have interpreted the splitting constants to be as follows:

Position	N	o	m	p	o'	m'	p'
Splitting constant (gauss)	1.44	1.37	0.53	1.51	2.40	0.89	2.88

Also, to aid the interpretation of the E.S.R. spectrum of substituted imidazolyl radicals, they have calculated the experimental spin densities on the various carbon atoms from the splitting constants, using McConnell's relationship with $Q=30$ gauss, and have attempted to match these values, with spin densities calculated using the McLachlan method. They obtained best agreement with $\lambda = 1.2$ and the following set of parameters for the Hückel Matrix.

$$\begin{aligned} \alpha_N &= \alpha_0 + 0.3\beta_0 \\ \alpha_{c_2} &= \alpha_0 + 0.09\beta_0 \\ \alpha_{c_{4,5}} &= \alpha_0 + 0.03\beta_0 \\ \beta_{1-5}, \beta_{3-4} &= \alpha_0 + \beta_0 \\ \beta_{4-12}, \beta_{5-6} &= + 0.9\beta_0 \\ \beta_{1-2}, \beta_{2-3} &= + 0.9\beta_0 \end{aligned}$$

Because of the drawbacks already mentioned for Hückel Type methods, however, these parameters are only reasonable for agreement between theory and experiment for the parent triphenyl imidazolyl radical, and spin densities for related radical can not be predicted with any certainty using the same values.

CHAPTER 2

EXPERIMENTAL

2.1. Measurement of Reaction Kinetics.

All kinetic measurements were made using a Unicam SP800 double beam U.V/Visible spectrophotometer coupled by means of an expansion head to a servoscribe with which the optical density of the sample could be monitored with time at a fixed wavelength, i.e. the wavelength at which the radical species absorbed.

2.1.1 Kinetic measurements of the photochromic decay process of solid 22', 44', 55' hexaphenyl bi-imidazole.

The problem of how to study the decay process for the solid, was overcome by making use of an SP 890 Diffuse Reflectance Unit. The general theory of diffuse reflectance is given in a comprehensive book by Wendlant and Hecht^{B5}, but it is of little value here, as a measure of the relative optical densities with time was needed rather than an absolute value of diffuse reflectance. The SP 890 unit is shown diagrammatically in Figure 2.1.

Light from the SP 800 source at a fixed wavelength is, by means of the lenses and mirrors shown, brought incident onto the powdered sample of the photochromic material which has been previously pressed into the shallow dish of the sample holder. Light then which is not absorbed, is reflected diffusely from the powder surface onto the parabolic mirror encircling the sample, and hence made to impinge on the photomultiplier. The light from the reference beam, on the other hand, is passed straight from the source to the photomultiplier by means of the two mirrors shown. The difference between the values of these two light intensities received, will give the amount absorbed by the sample and will be therefore, assuming Beers Law is obeyed

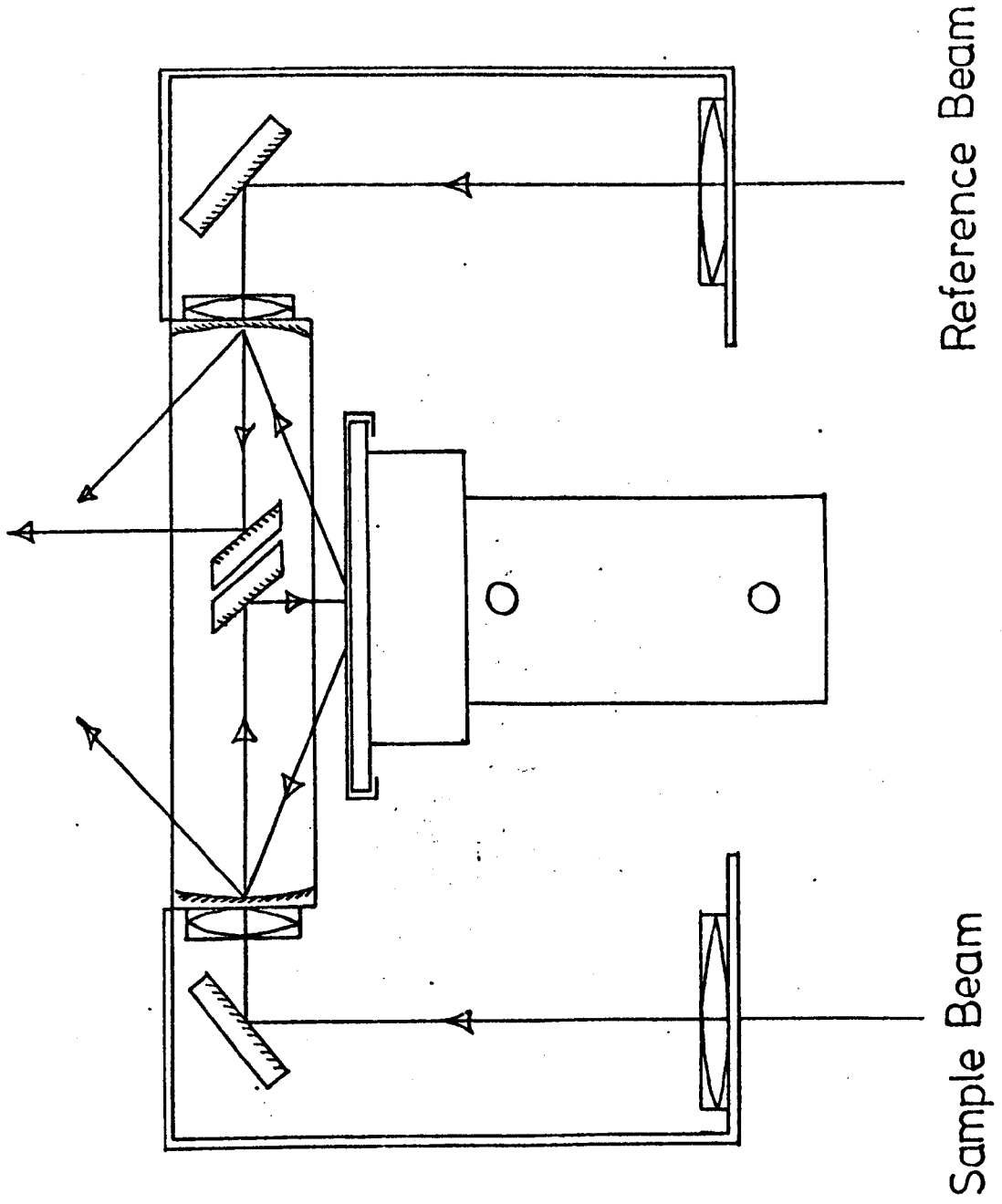


FIGURE 2.1

as it is for a solution of the dimer in benzene¹⁵⁰, a measure of the radical concentration on the surface of the sample. Monitoring the change in optical density thus, provides a way of observing the kinetics of solid 22', 44', 55', hexaphenyl bi-imidazole.

However, the SP 890 unit as supplied by Pyc-Unicam has a serious limitation in that no provision is made for temperature variation and all measurements must be made at room temperature. This was overcome by fitting the unit with a constant temperature device⁴⁵ as shown in Figure 2.2. This consisted of a small copper block through which water from a thermostatted tank was circulated, and which was fitted onto the back of the metal sample holder by means of a threaded brass collar. This collar in turn was attached to the back of the sample holder by using an epoxyresin. Finally, to thermally insulate the surface of the powder sample, ensuring uniform temperature, an optically flat silica disc was fitted over the top of the sample, and in this way it was found that the temperature of the sample, determined using a thermocouple embedded in the back of the powder sample, could be maintained constant to within $\pm 1^{\circ}\text{C}$.

Thus to monitor the decay process, powdered hexaphenyl bi-imidazole was pressed into the sample holder, which was then attached to the constant temperature block and placed into its position in the SP 890 diffuse reflectance unit. The temperature of the sample was set to the required value and the optical density due to the radical was observed (having first scanned all wavelengths to find the appropriate absorption peak) until the thermochromic process had come to equilibrium. The wavelength of this absorption was at 18,000 wavenumbers. Having then obtained

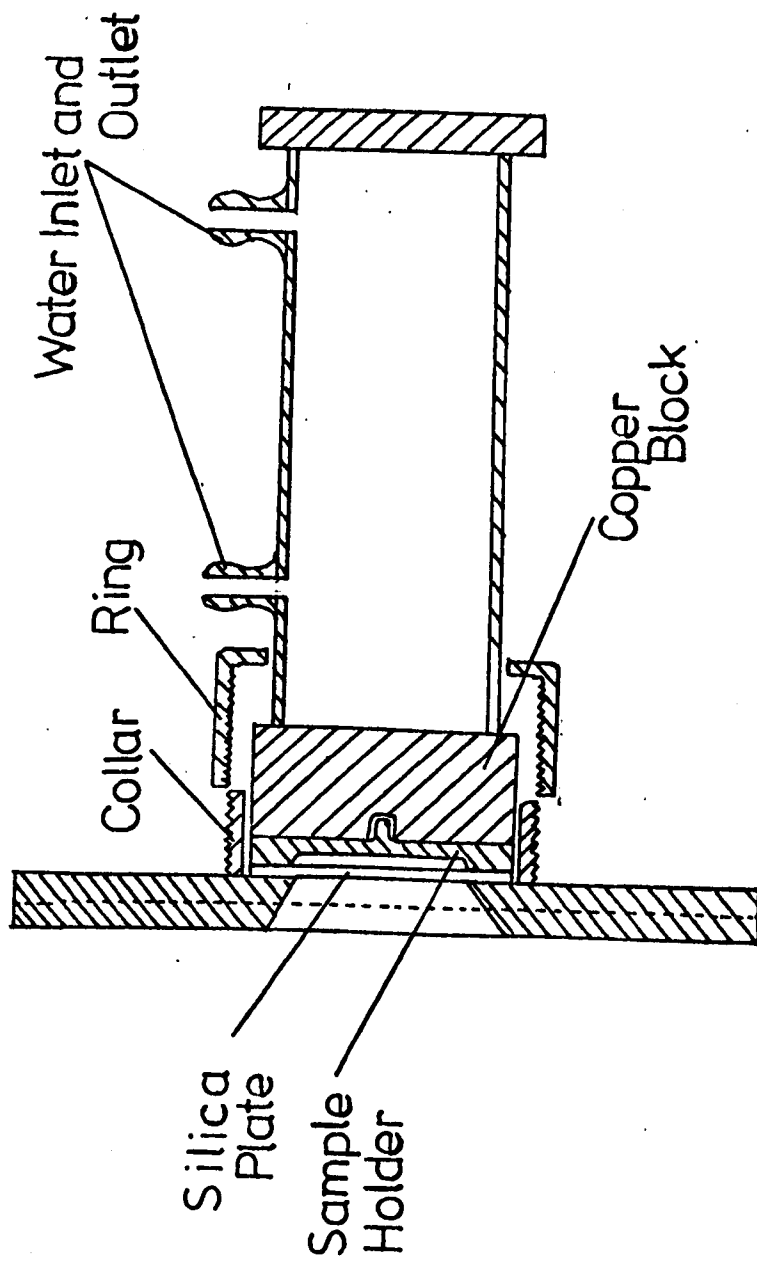


FIGURE 2.2

a constant value for the absorbance, the sample holder, together with the constant temperature block, was taken out of the SP 890 unit and the sample surface was exposed to the quartz iodine lamp being used for illumination. After about forty five minutes (the period estimated to be sufficient to obtain the maximum radical concentration), the sample along with its holder and temperature unit, was replaced into the SP 890 unit. The decrease in optical density with time was observed, as the radicals recombined to form the dimer. The final concentration of radicals (i.e. when no further recombination was taking place) was taken as that when the optical density remained constant for several hours. This is known as the infinity value.

2.1.2 Kinetic measurements in solution.

As in the case of the solid, an SP 800 spectrophotometer was employed, but in this case, adequate means of maintaining the temperature at a required value were provided by Pye-Unicam, in the form of a water thermostatted cell block positioned in such a way that the cell containing the solution of photochromic material and the blank cell, containing benzene solvent, were in the sample and reference beams respectively. The temperature was determined by means of a thermocouple placed in the blank cell.

It was possible in this case, to illuminate the sample in situ by using a hole which had been bored through the front of the spectrometer and the cell block in such a way that the light could fall upon the sample while in position in the spectrometer. The hole in the block, was lined with copper tubing to prevent any leakage of water, and a metal shutter

was placed over the end. As a source of illumination, an SP 200 high pressure mercury lamp fitted with a diffraction grating monochromator was used, and to produce the best radical concentration the wavelength of light used was set to 27,400 wave numbers.

To maintain a homogeneous distribution of radicals, stirring of the solution was necessary and to prevent evaporation of solvent during the runs, especially at the higher temperatures, a closed system of stirring as in Figure 2.3 was essential. In this, a magnet driven by a motor outside the spectrometer, caused the glass encased metal bar attached to the stirrer blade to rotate, thus providing adequate stirring without having evaporation take place. To ensure that no extraneous light was allowed to enter the spectrometer, the hole for the rod driving the magnet was made to be as tight a fit as possible.

Using these modifications, it was possible to carry out the kinetic runs of solutions of the photochromic materials for both the generation and decay processes.

The solution of the dimer (hexaaryl bi-imidazole), was placed in the appropriate position in the spectrometer and was allowed to come to thermal equilibrium. The complete spectrum was subsequently scanned to find the radical absorption band, and the spectrometer was set to monitor this wavelength. The solution was then exposed to the light source, and a reading of the optical density was taken every thirty seconds, by closing the shutter briefly, until the maximum reading had been obtained. The illumination port was closed, and the decay process was followed as before with the solid. It was found in this case,

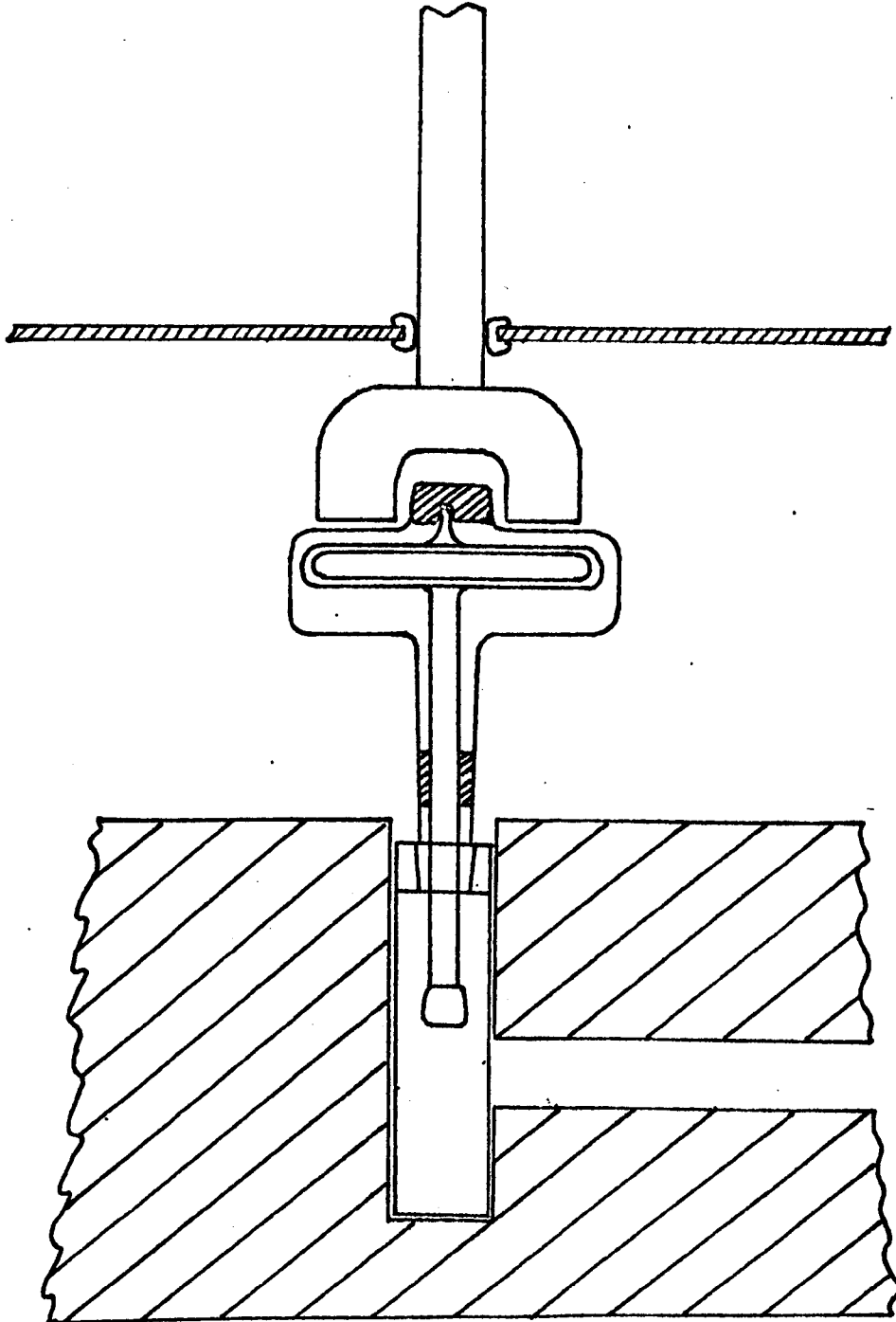


FIGURE 2.3

that the infinity value for the optical density was the same as that for the thermal equilibrium before illumination and so this pre-illumination value was used as the infinity value.

2.2 Practical Aspects of a Decca E.S.R. Spectrometer.

The essential features of an E.S.R. spectrometer are (i) a source of microwave radiation (ii) a means of applying the microwave power to the paramagnetic sample (iii) a means of detection of the power absorbed from the field and (iv) a homogeneous magnetic field.

As has previously been mentioned, most spectrometers employ radiation of a fixed frequency (9500 MHz) and use a variable magnetic field to achieve the resonance condition. The usual source of radiation is a klystron oscillator and the energy generated by it is transmitted by means of a waveguide of appropriate dimensions to the cavity in which the sample is positioned. The purpose of the cavity is to concentrate energy on to the sample by means of multiple reflections of the microwave from the walls, and to ensure the maximum concentration, the cavity is provided with tuning screws so that its geometry and size may be adjusted to match the waveguide.

The efficiency of a cavity for storing microwave energy is expressed by its Q factor given by

$$Q_0 = \frac{\omega \times \text{energy stored}}{\text{rate of energy loss.}}$$

where ω is the resonant frequency. The higher the Q therefore the more efficient the cavity.

When a magnetic field is applied perpendicularly to the microwave and varied slowly through the point at which resonance occurs, absorption of microwave power by the sample causes a change in the reflection from the cavity. Detection of this change, in a simple spectrometer, is performed by a semi conducting crystal diode rectifier which converts all microwave power into direct current. However in a highly sensitive E.S.R. spectrometer, where one observes signals small enough to be obscured by noise, detection is carried out using phase sensitive detection. This is a common electronic procedure in which an alternating signal is compared to a reference signal having the same frequency, in such a way that the output signal obtained, is rectified and is sensitive to both the magnitude and phase of the input signal.

To achieve this with E.S.R., a 100kHz modulating magnetic field is also applied to the sample giving an output signal approximately proportional to the slope of the absorption curve (Figure 2.4(a)). This signal then undergoes amplification and is mixed in the phase sensitive (p.s.d) circuit with a reference signal of the same frequency and constant amplitude, but of variable phase, to ensure that the detector crystals are always biased to give optimum conversion. The result of this process is to produce a D.C. output signal which may be recorded as shown in Figure 2.4(b). The shape and resolution of the signal largely depend on the amplitude of the 100kHz modulating field, and distortion will inevitably take place if the amplitude is not kept well below the line width for the sample. Empirically one may say that distortion is negligible and resolution is at an optimum if the modulation amplitude is less than one tenth of the line width, but

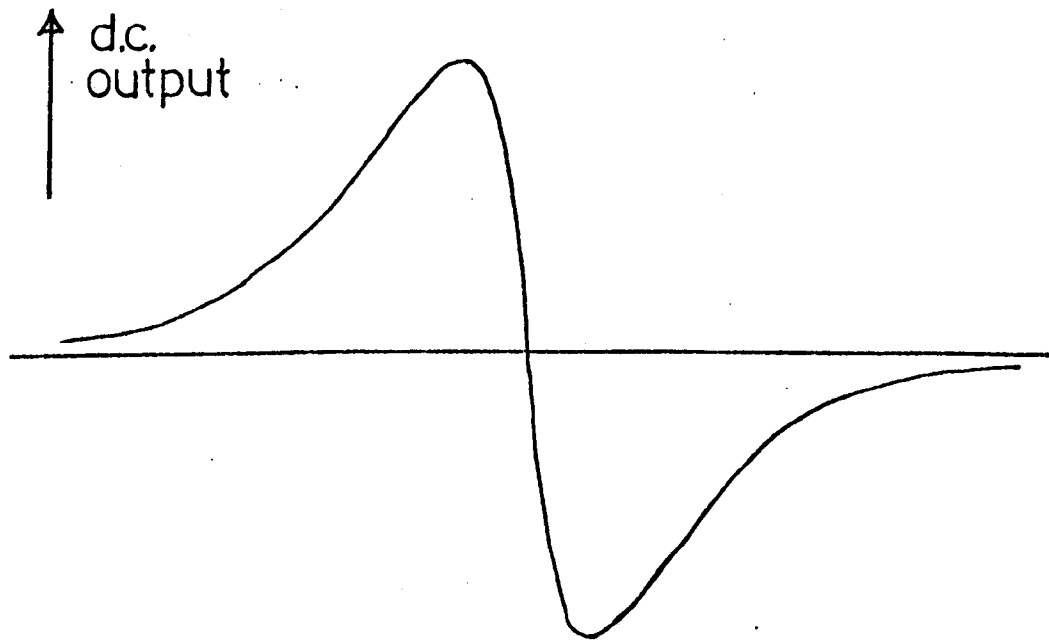
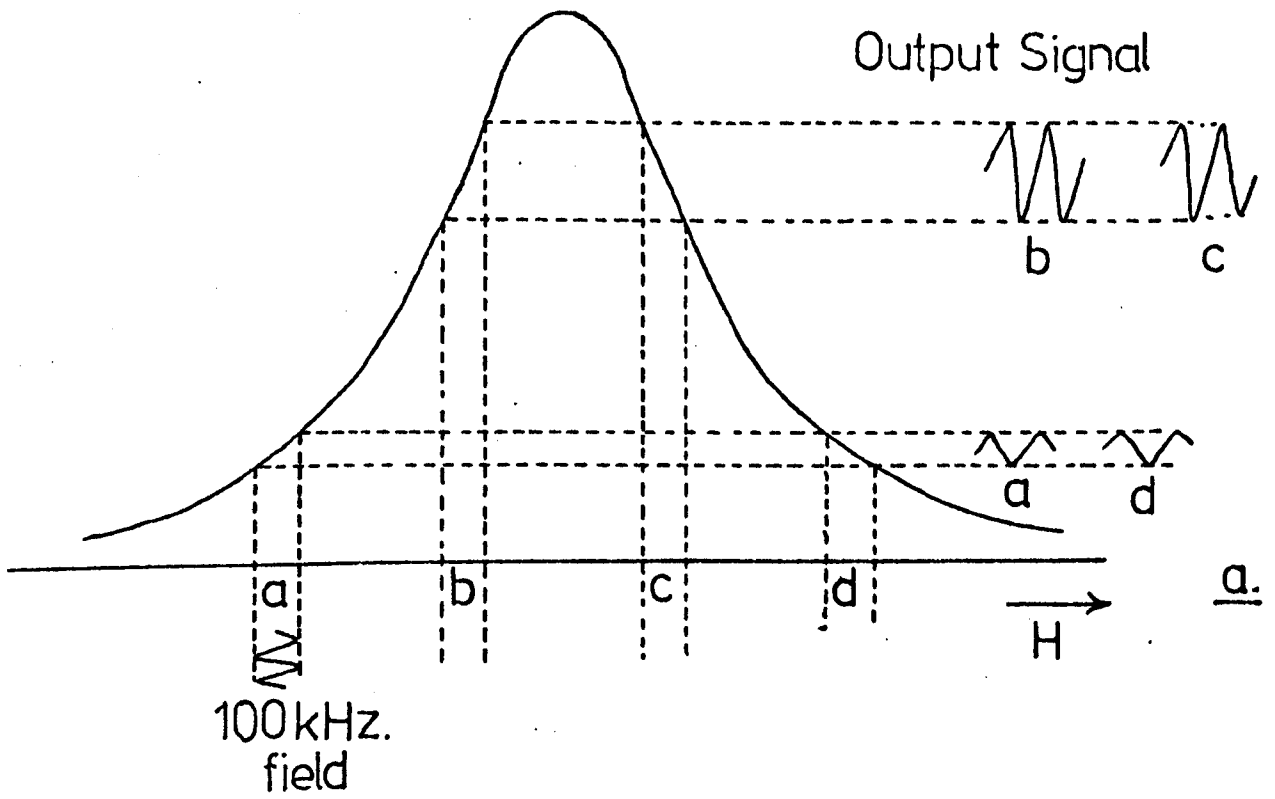


FIGURE 24

as the maximum signal strength is obtained when this ratio is one half, a compromise is imperative.

The advantage of p.s.d. is that coherent signals only are obtained from input signals of exactly the same frequency as the reference, as only these may keep in phase. This will have the effect of minimising noise which tends to be random in phase and amplitude.

To further reduce noise levels longer times of sweeping the absorption peak with corresponding longer time constants for the detection amplifier are used. Care must be taken however that the time constant is not large enough to eliminate the fine splitting as well as the noise.

Use of the electron spin resonance Spectrometer

E.S.R. techniques were reserved, for the purpose of this work, only for obtaining E.S.R. spectra, to be used in the calculation of the electronic make up of the radical, and for the determination of the extinction coefficients of the imidazolyl radicals used in the kinetic studies.

2.3 Recording E.S.R. Spectra

It was found, that the best spectra of benzene solutions of the imidazolyl radicals fluorinated on the 2 ring, were obtained if the following method was observed.

About 2 mls of an almost saturated benzene solution of the dimer was syringed into a silica "Spectrosil" tube of 11 mm external diameter and the solution was degassed under high vacuum (about 10^{-6} mmHg). This was done by freezing down the solution with liquid nitrogen, while at the same time slowly

opening the tap connecting the sample to the vacuum apparatus. The solid solution resulting, was pumped on for about 30 minutes, after which the tap was closed and the solid was allowed to thaw. This permitted the air trapped in solution to bubble off. The process was repeated six times to ensure all the air had been removed, and having done this, the tube, with the sample once more frozen, was sealed off under vacuum at the constriction already drawn in the tube (see Figure 2.5). The tube was then positioned in the cavity so that its base was just in line with the bottom of the irradiation port. The cavity was tuned, and with the R.F. attenuator set at -20dB , the E.S.R. spectrum of the compound was recorded, starting with fast times of sweep, high amplitude of modulation and low time constants, and successively lengthening the time of sweep, with corresponding decreases of amplitude of modulation and increases of time constant until no further resolution of the hyperfine lines was possible. Adjustment of R.F. attenuation from -20dB did not lead to an improvement of spectrum.

2.4 Measurement of Spin Concentration in Solution

Whereas it is impossible to determine exact concentrations of radicals using U.V./Visible spectrophotometry without knowing first the extinction coefficient, it is possible using E.S.R. techniques by employing the fact that the area under the absorption curve is proportional to the number of spins in the sample. Comparison of this area then, with the area under the absorption curve of a standard sample having a known number of spins (and run under the same conditions) will give an exact value of the concentration of radicals in solution. The factors which must be the same to ensure identical conditions of runs are

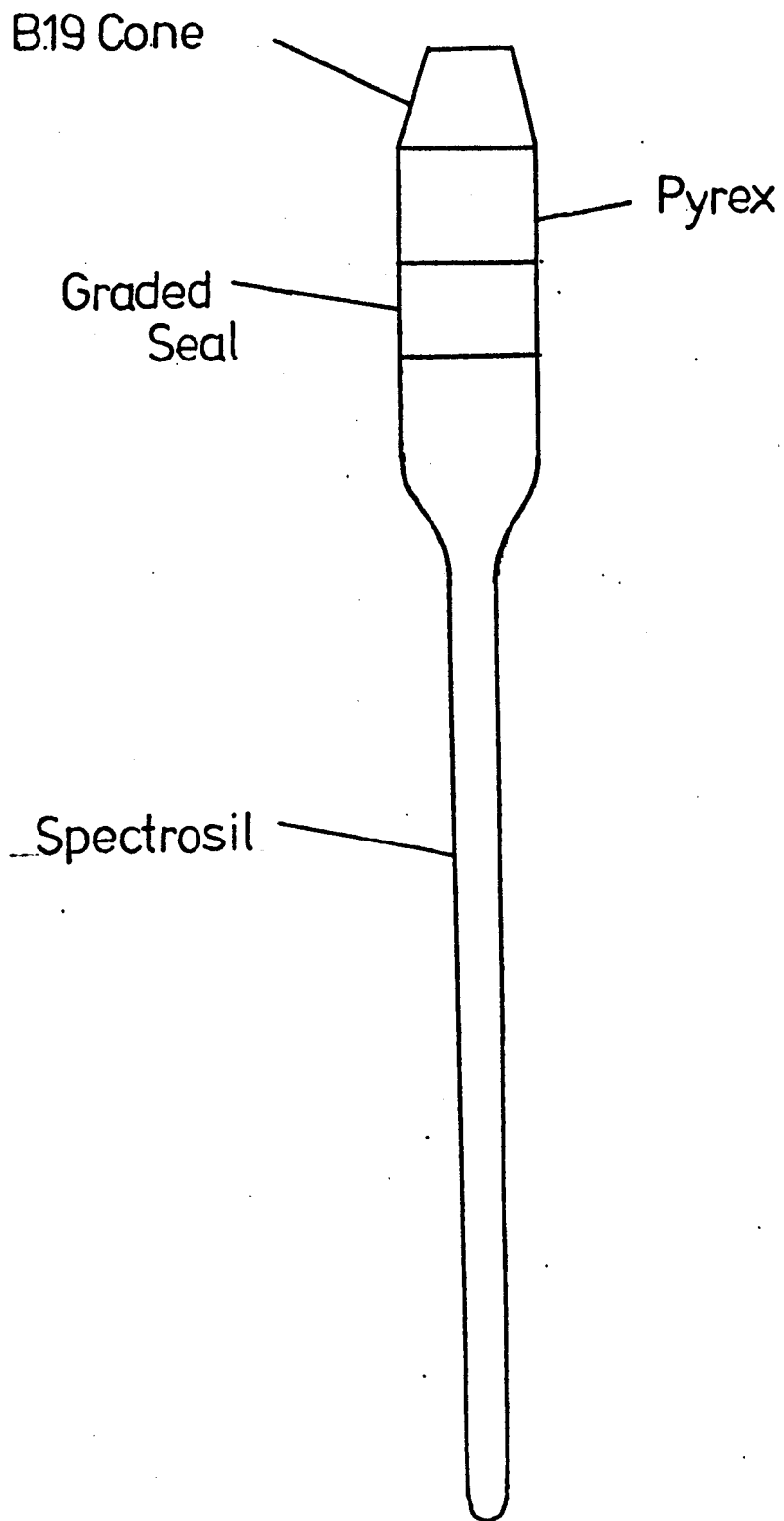


FIGURE 2.5

- i) size and shape of samples and containers
- ii) dielectric properties of the sample
- iii) position of the sample in the cavity
- iv) input microwave power
- v) field scanning rate
- vi) temperature
- vii) modulation amplitude
- viii) amplifier gain

i) will be obeyed if the samples being compared are of the same height in identical "Spectrosil" tubes (4mm external diameter tubing was used therefore throughout the experiments); conditions (iii), (iv), (v), (vii) and (viii) of course will be satisfied if the runs to be compared are carried out using the same spectrometer settings and (vi) is fulfilled by having constant temperature facilities fitted to the E.S.R. spectrometer. (ii) must be assumed to have been satisfied as the phasing of the microwave power, normally sensitive to changes in dielectric constant, never altered by more than a few degrees from sample to sample.

Having taken these precautions then, the relationship between the number of spins for the standard S_s and that of the unknown (S_x) is

$$S_x = S_s \times \frac{A_x}{A_s} \times \frac{Q_s}{Q_x} \quad 2.1.$$

where A_s and A_x are the absorption curve areas of the standard and unknown and Q_s and Q_x are the Q values of the cavity with the respective samples inserted. [A method of measuring the Q

values by calibrated changes of Klystron frequency is given in a booklet issued by Decca Radar Limited, Instrument Division, called "Measurement of Cavity Q and Spin Concentration"]. The inclusion of the Q factor into this expression takes account of any differences of dielectric loss of sample which will also result in changes of signal strength.

The basic standard used in the majority of cases where a sample with a known number of spins is needed, is diphenyl picrylhydrazyl (D.P.P.H.) recrystallized from ether, but this has the disadvantage that its ESR spectrum is made up of five lines, and is thus difficult to integrate. The problem was overcome in this work however, by using a 0.2ml benzene solution of D.P.P.H. (of known concentration) to calibrate a carbon sample, and subsequently using this as a standard for the bimidazolyl solutions.

The carbon, diluted with sodium chloride, was placed in a 4mm "Spectrosil" tube, until the size of the sample was the same as that of the D.P.P.H. solution, and the solid was degassed for about 6 hours at 10^{-6} mm Hg and 100°C and sealed off under vacuum. Spectra of both carbon and D.P.P.H. were run and their absorption curves were constructed by integration of the E.S.R. signals by a method of counting squares. The resulting curves were then traced onto uniform weight card, cut out, and weighed. From these weights the ratio of areas was calculated and using equation 2.1 the number of spins in the carbon sample was estimated.

For a comparison of the absorption curve of the carbon sample to those of the imidazolyl radicals, an easier method, due to Burgess⁴⁶ was employed.

If one considers the derivative curve P' against field H (Figure 2.6A) and the integrated curve P against H (Figure 2.6B) one can see that the area under the latter is given by:

$$(A) = \int_{H_1}^{H_2} P dH$$

Integrating by parts this yields,

$$A = [PH]_{H_1}^{H_2} - \int_{H_1}^{H_2} H P' dH$$

As $P = 0$ at H_1 and H_2

$$A = - \int_{H_1}^{H_2} H P' dH$$

Now if the centre of the profile is H_c ,

$$\begin{aligned} A &= \int_{H_1}^{H_2} (H_c - H) P' dH - \int_{H_1}^{H_2} H_c P' dH \\ &= \int_{H_1}^{H_2} (H_c - H) P' dH \end{aligned}$$

as the integral of P' with respect to H within the limits H_1 and H_2 is zero.

This last expression, is in fact the equation for the first moment of the derivative curve about the midpoint. It follows from this therefore, that the ratio of the first moments of the carbon spectrum and the imidazolyl radical spectrum will also give the ratio of the number of spins in each sample. Burgess has designed a balance especially to determine the first moments of the derivative curves, but it was found as convenient and more accurate to calculate the value from the relationship:

$$\text{First moment of half derivative curve} = m \times r$$

where m is the mass of each half of the derivative signal, and r

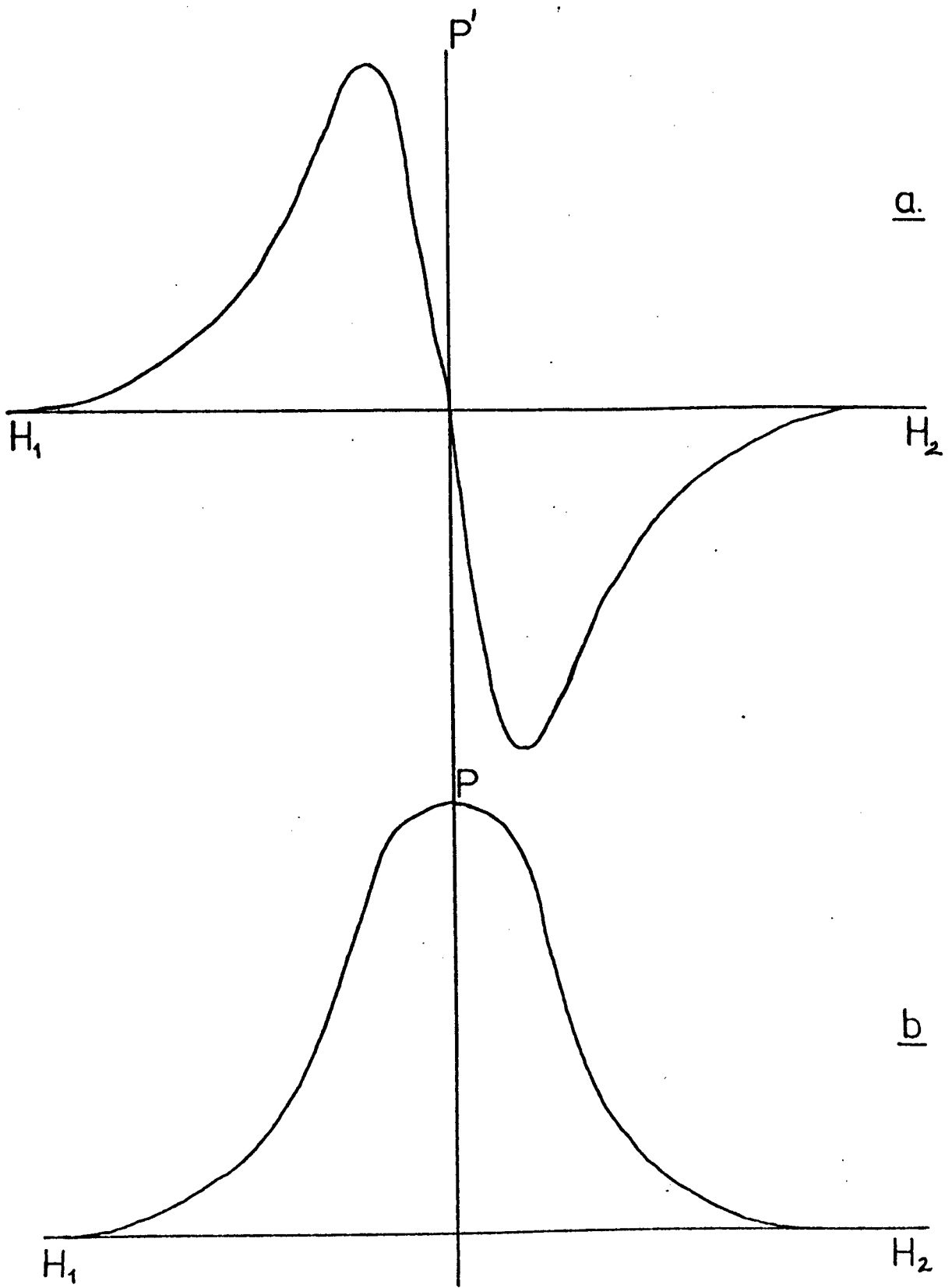


FIGURE 2.6

is the distance of its centre of gravity from the centre point (Figure 2.6). To do this, each half of each derivative curve was traced onto the uniform card, cut out and weighed. The centres of gravity were then ascertained by a plumb line method.

2.5 Determination of Extinction Coefficient.

The extinction coefficient, ϵ , of a substance is given by Beer's law to be

$$\epsilon = \frac{A}{cd}$$

where A is the absorbance or optical density, c is the concentration of the absorbing species and d is the path length in cm.

Using this equation, the values of ϵ for the radicals under investigation were determined by measuring the number of spins in a particular solution at a fixed temperature, in the way described above, and the optical density of the radicals in the same solution and at the same temperature using the Pye Unicam SP800 spectrophotometer. This determination was carried out at several temperatures for each solution. The variation of the cavity temperature was effected using the apparatus shown in Figure 2.7 in which nitrogen gas preheated by an electric coil, was passed through 'Dewar' tubing onto the sample. This was also contained in a 'Dewar' vessel, and to prevent interference with the electronic and magnetic properties of the instrument, the vessel was left unsilvered in the cavity area. The rate of flow of nitrogen was kept constant and in this way the cavity temperature was kept to $\pm 1^\circ\text{C}$ of the required temperature during any measurement.

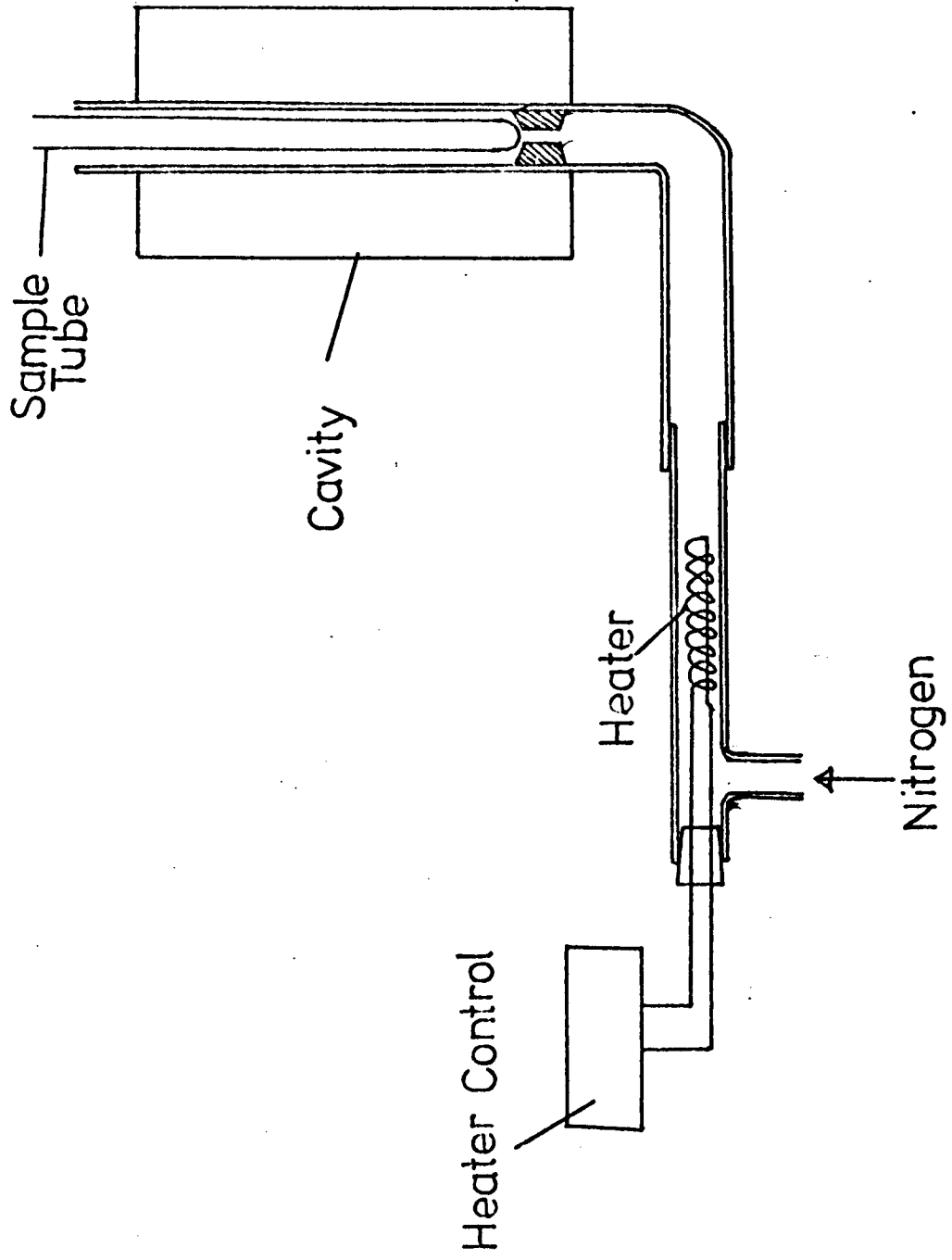


FIGURE 2.7

This method unfortunately, though reasonable for the 2 metafluorophenyl and 2 parafluorophenyl 4,5 diphenyl imidazolyl, and the 2, 4, 5 triphenylimidazolyl radicals, was not sufficiently accurate for the 2 orthofluorophenyl 4,5 diphenyl imidazolyl radicals, which displayed very little thermochromic behaviour. The problem was overcome however by comparing kinetic runs of the decay process, carried out in the E.S.R. apparatus with those carried out on the S.P.800 spectrophotometer, (see Chapter 3).

2.6 Preparation of MaterialsThe imidazoles

To prepare lophine and its fluorinated derivatives the synthesis due to Davidson⁴⁷ was employed. An equimolar solution of benzaldehyde and benzil, were refluxed together in acetic acid for about one hour with the equivalent of eight moles of ammonium acetate. The solution was then poured onto crushed ice, and the precipitate produced was filtered off using a Buchner funnel. The imidazole was recrystallized once from ethanol/water mixture and dried overnight in a vacuum dessicator. The yield obtained was almost quantitative. The imidazoles substituted in the 2-phenyl ring were produced using substituted benzaldehydes (all supplied from Koch Light Ltd.)

The bi-imidazoles⁸

A 1% weight by volume (i.e. 1g per 100 ml.) aqueous solution of potassium ferricyanide (4500ml) was added over a period of several hours to an alcoholic solution (1l.) of lophine (10g) containing potassium hydroxide (120g). During the addition, stirring was maintained and the temperature of the reaction mixture was kept below 5°C. The precipitate produced, was washed many times with water and subsequently was dried under vacuum for several hours. This compound was the piezochromic form of the dimer which when dissolved in warm benzene, formed a deep purple solution. The filtrate of this solution was evaporated to dryness under a reduced pressure using a rotary evaporator, and the photochromic dimer obtained was recrystallized from an ethanol water mixture and dried under vacuum. All the substituted bi-imidazoles were produced in this way. A table of the melting points of the various dimers are given below.

Dimer	Mpt °C
2,2',4,4',5,5' hexaphenyl bi-imidazole	198-201
2,2' orthofluorophenyl 4,4',5,5' tetraphenyl bi-imidazole	206-207.5
2,2' metafluoro " " " "	162.5-163
2,2' parafluoro " " " "	184.5-186

2.7 Purification of Benzene

The purification of benzene was made essential because of the existence of impurities in the solvent, obtained from BDH Laboratory Chemicals Division, which acted as radical traps. The method used was that given by Weissberger ⁴⁸.

A quantity of benzene was shaken for 30 seconds with portions of concentrated sulphuric acid, one quarter of the volume of the benzene, to remove the sulphur compounds. The process was repeated until no darkening of the acid layer was visible. It was found that usually three successive shakings were sufficient. The benzene was then washed with one portion of water, several portions of aqueous sodium hydroxide solution and three more times with water. After drying one night over calcium chloride, and one night over phosphorus pentoxide, the benzene was refluxed over phosphorus pentoxide for about 3 hours on a 3 foot column of clean dry glass helices enclosed in a vacuum jacket. For each litre of benzene being distilled, the first 100ml. were discarded and the next 300ml. were collected (bpt. $80.1 \pm 0.5^{\circ}\text{C}$, 760mm Hg).

CHAPTER 3

RESULTS

3.1 Photochromic Decay Reaction

As mentioned previously, all results from U.V./Visible spectrophotometry were treated by analysing the optical density readings with respect to time. Although this procedure did not directly yield specific reaction rates, it did give an indication of the order of the reaction, and could give specific rates if the extinction coefficient of the radicals concerned was taken into account.

3.1.1 Methods of analysis of results

(i) Integration method

If A_t is the optical density, at time t , of the species involved in the photochromic decay reaction, and if A_∞ is the optical density at infinite time, then by Beer's Law, the concentration of the reacting species at time t , c_t , is given by:

$$c_t = (A_t - A_\infty) / \epsilon \quad (\text{for path length} = 1 \text{ cm}) \quad 3.1$$

Where ϵ is the extinction coefficient.

For a reaction of the n^{th} order, the rate equation will be:

$$\frac{dc_t}{dt} = -Kc_t^n \quad 3.2$$

Integration of this gives

$$\frac{1}{(n-1)c_t^{n-1}} = Kt + \text{const} \quad 3.3$$

$$\text{or } \log_e c_t = -Kt + \text{const}$$

when $n = 1$.

Thus, to test for any order by this method, a plot of t versus the necessary function of optical density must give a straight line.

(ii) Half Period method

The integration method described above, can be further extended so that knowledge of n need not be a prerequisite condition. If limits are set to equation 3.3 above, one obtains:

$$\left[\frac{1}{n-1} c_t^{n-1} \right]_{\frac{c_{t_0}}{2}}^{c_{t_0}} = [Kt]_{t_{\frac{1}{2}}}^{t_0} \quad 3.4$$

where t_0 is the time of start of the reaction and $t_{\frac{1}{2}}$ is the time at which half the radicals have reverted to the dimer. Rearrangement of equation 3.4 then gives

$$-\frac{1}{(n-1) c_{t_0}^{n-1}} + \frac{1}{(n-1) \left(\frac{c_{t_0}}{2}\right)^{n-1}} = +K\tau \quad 3.5$$

(where τ is the half life of the reaction),

$$\text{or} \quad K\tau = \frac{-\frac{1}{2}^{n-1} + 1}{(n-1) \left(\frac{c_{t_0}}{2}\right)^{n-1}}$$

Taking logarithms of both sides:

$$\log K\tau = \log \frac{-\frac{1}{2}^{n-1} + 1}{(n-1)} - (n-1) \log \frac{c_{t_0}}{2} \quad 3.6$$

A plot of $\log \tau$ against $\log c_{t_0}/2$ should therefore give a straight line of gradient $-(n-1)$.

(iii) Gradient method

From the rate equation:

$$\frac{dc_t}{dt} = -Kc_t^n$$

$$\text{one may obtain } \log \frac{-dc_t}{dt} = \log K + n \log c_t \quad 3.7$$

Thus by simply plotting the logarithm of the rate of decay of optical density against the logarithm of the optical density itself, a straightline will be obtained, the gradient of which will be the order of reaction.

3.1.2 Decay kinetics of solid 2,4,5 triphenyl imidazolyl radicals

Using the method described in section 2a, the kinetics of the solid bi-imidazole were followed at various temperatures, ranging from room temperature to about 60°C. A specimen of the type of data received is given in Table 1, and the corresponding graph of optical density against time is shown in Figure 3.1.

TABLE 1

Specimen data for the O.D. decrease with time for lophinyl radicals in the solid state.

Temp = 32°C

Time (Min.)	(O.D. - O.D.)
0	0.1468
20	0.0604
40	0.0422
60	0.0340
80	0.0301
100	0.0270
120	0.0242
140	0.0222
160	0.0208
180	0.0198
200	0.0187
220	0.0178
240	0.0169
260	0.0162
280	0.0156
300	0.0148
320	0.0140
340	0.0130
360	0.0127
380	0.0121
400	0.0115
420	0.0112
440	0.0106
460	0.0101
480	0.0099

Radical Decay in Solid

Temp. = 32°C

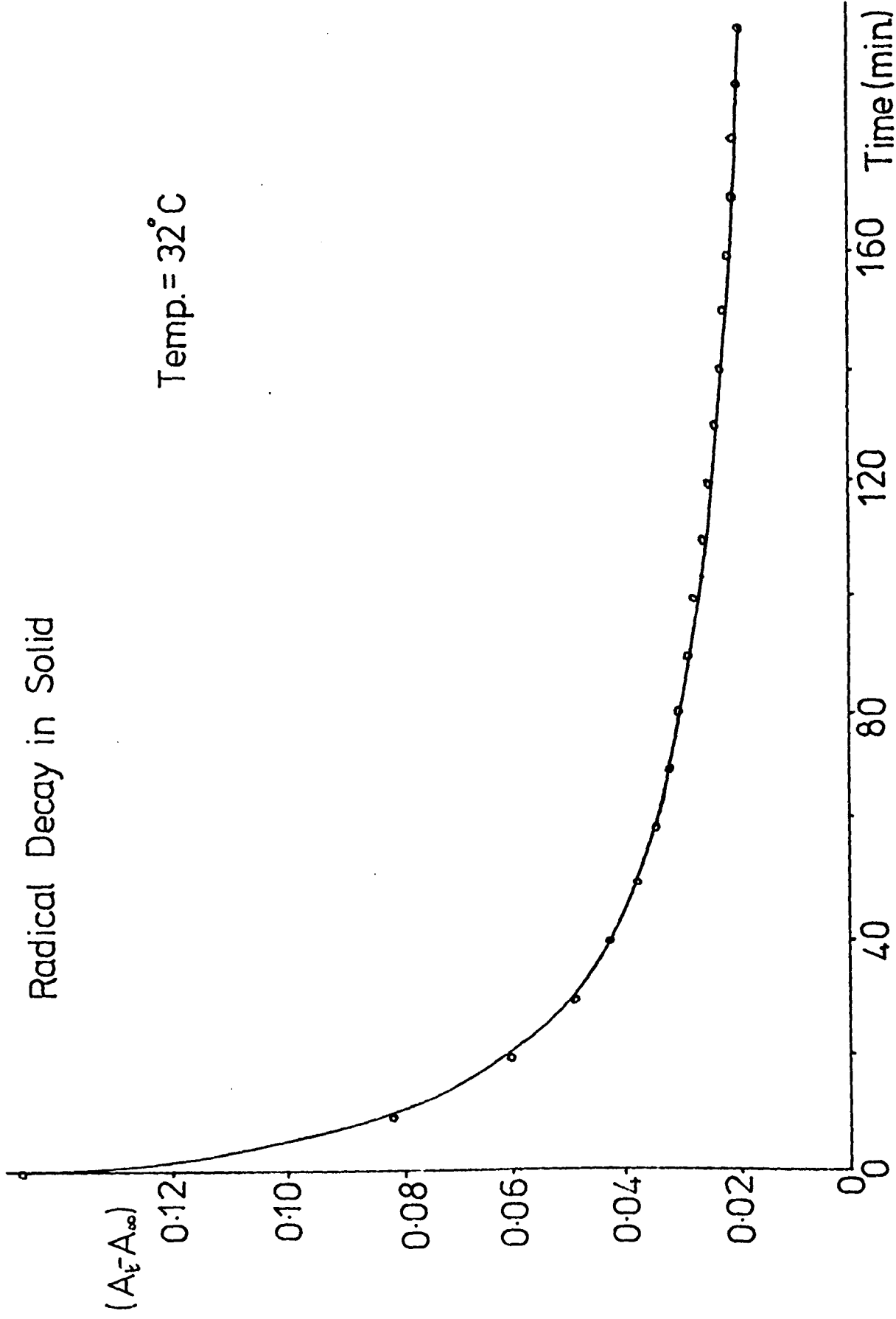


FIGURE 3.1

Conclusions

At temperatures around and slightly above that of room, i.e. in the 18–30°C range), the kinetic plots, obtained from both the integration and gradient methods described above, showed the reaction to be 3rd order with respect to the radical concentration in the initial stages, and 1st order in the later stages (Figures 3.2, 3.3). At slightly higher temperatures (around 40°), the kinetic scheme altered and 3rd order plots no longer gave straight lines. The gradient method of analysis on the beginning of the decay curve however (Figure 3.4) indicated the order to be between 2nd and 3rd and indeed an integrated plot for $n=2.5$ did give a straight line (Figure 3.5). Again 1st order behaviour was observed towards the end of the reaction (Figure 3.6). Around 45°C, the kinetics once again altered, this time to 2nd order falling to first (Figures 3.7 and 3.8). Finally at temperatures of around 55°C a 3/2 order plot gave linearity at the beginning of the reaction, the 1st order part being retained at the end (Figures 3.9 and 3.10). A comparison of temperature of run and reaction orders obtained is given below in Table 2.

TABLE 2

Order of reaction at different temperatures for the decay reaction of the lophinyl radicals in the solid state.

Temperature of Run °C	Apparent Reaction Order	
	At beginning	At end
18	3	—
18	3	1
18	3	—
25	3	—
32	3	1
39	$2\frac{1}{2}$	1
39	$2\frac{1}{2}$	1
44.5	2	1
44.5	2	1
44.5	2	1
52	$1\frac{1}{2}$	1
54	$1\frac{1}{2}$	1

Radical Decay in Solid

Temp. = 32°C

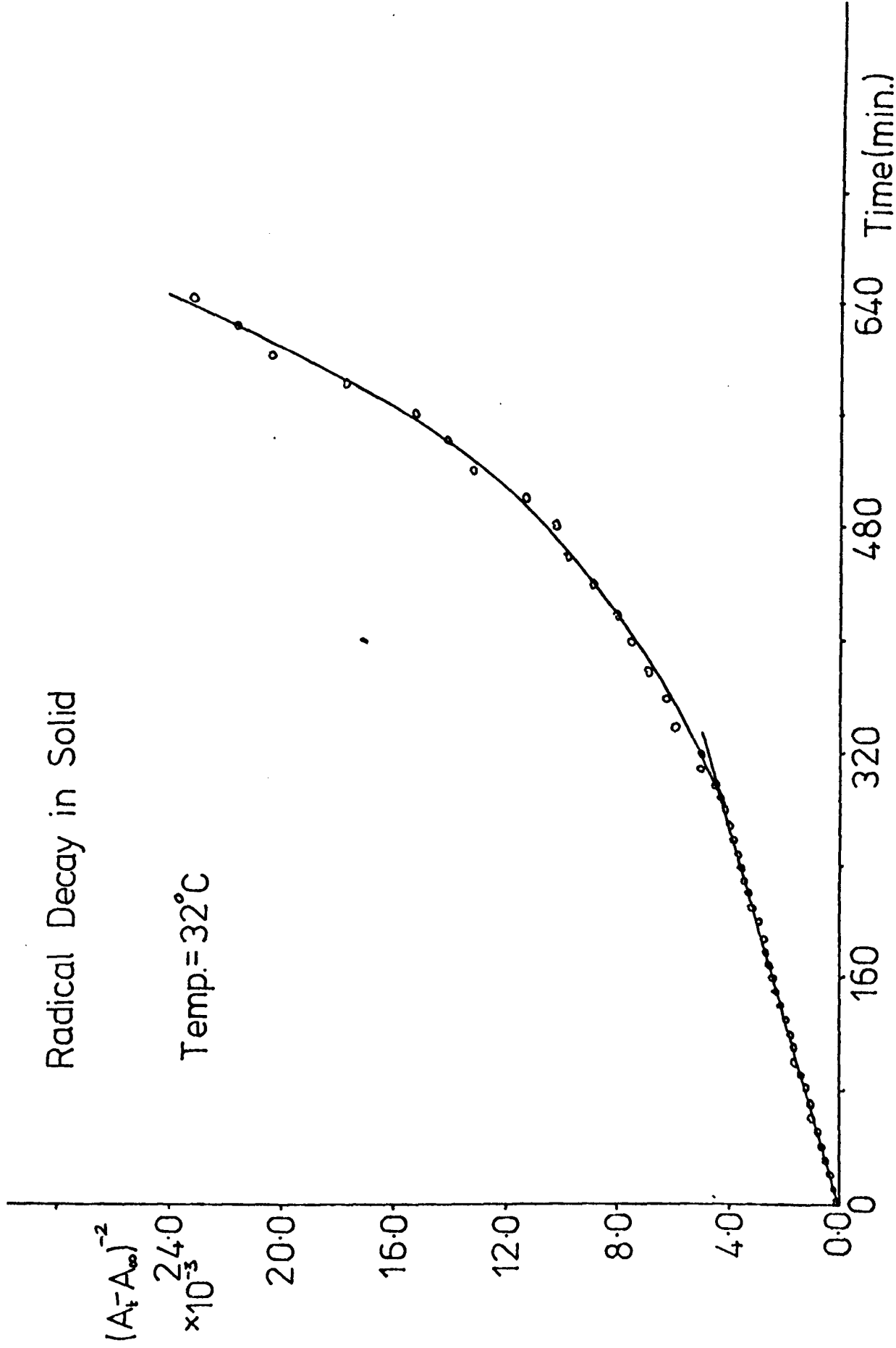


FIGURE 3.2

Radical Decay in Solid

Temp. = 32°C

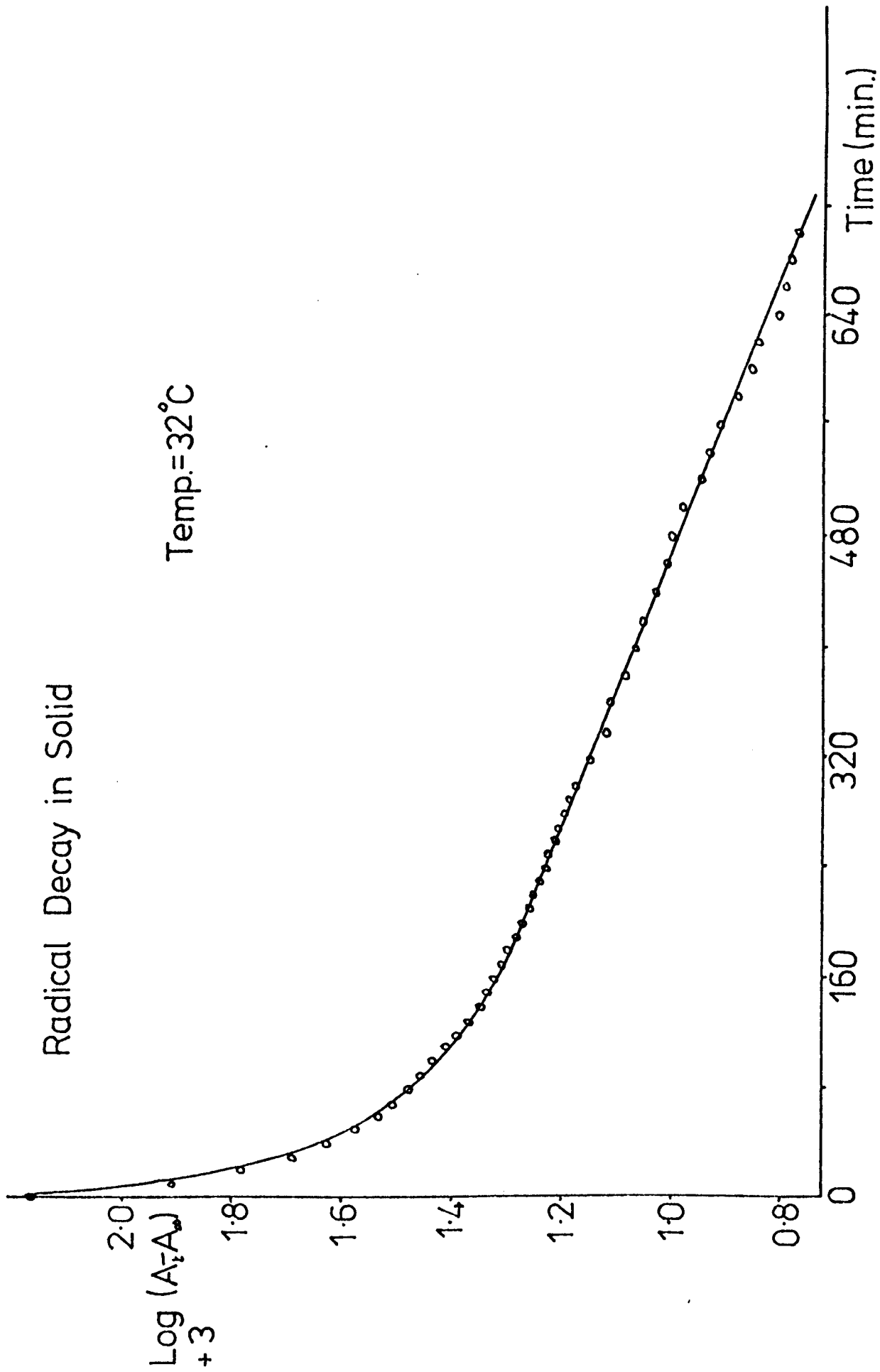


FIGURE 3.3

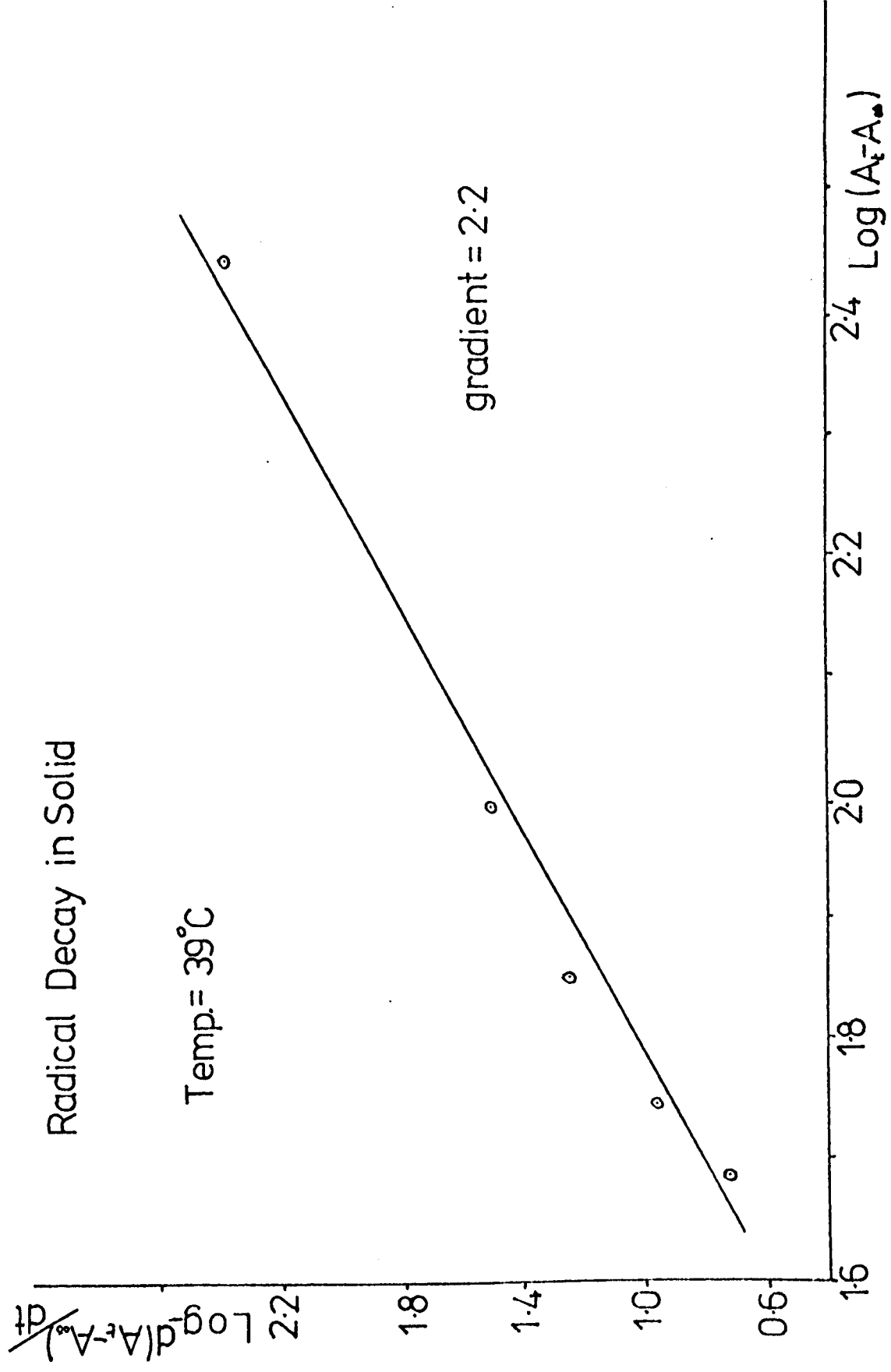


FIGURE 3.4

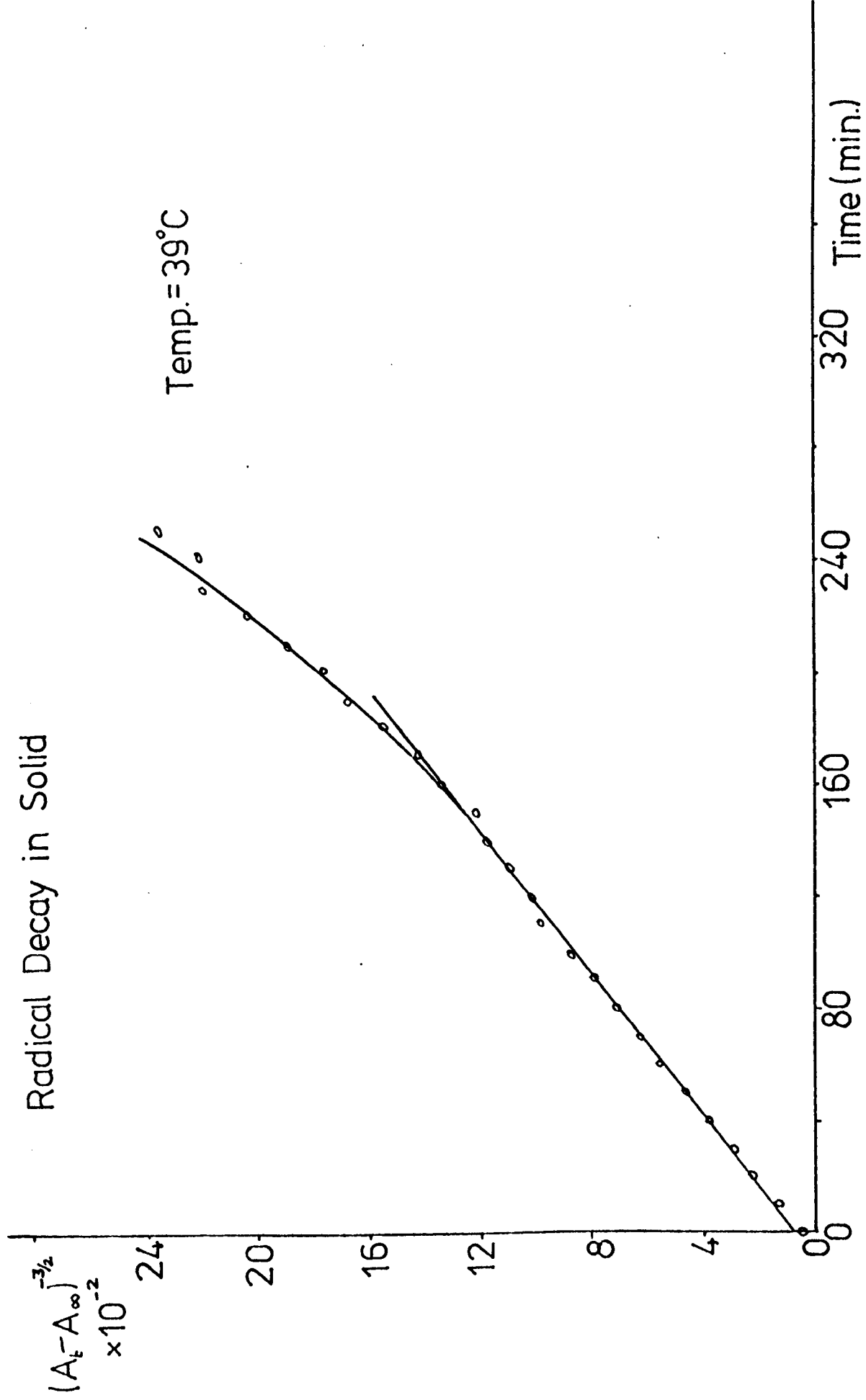


FIGURE 3.5

Radical Decay in Solid

Temp. = 39°C

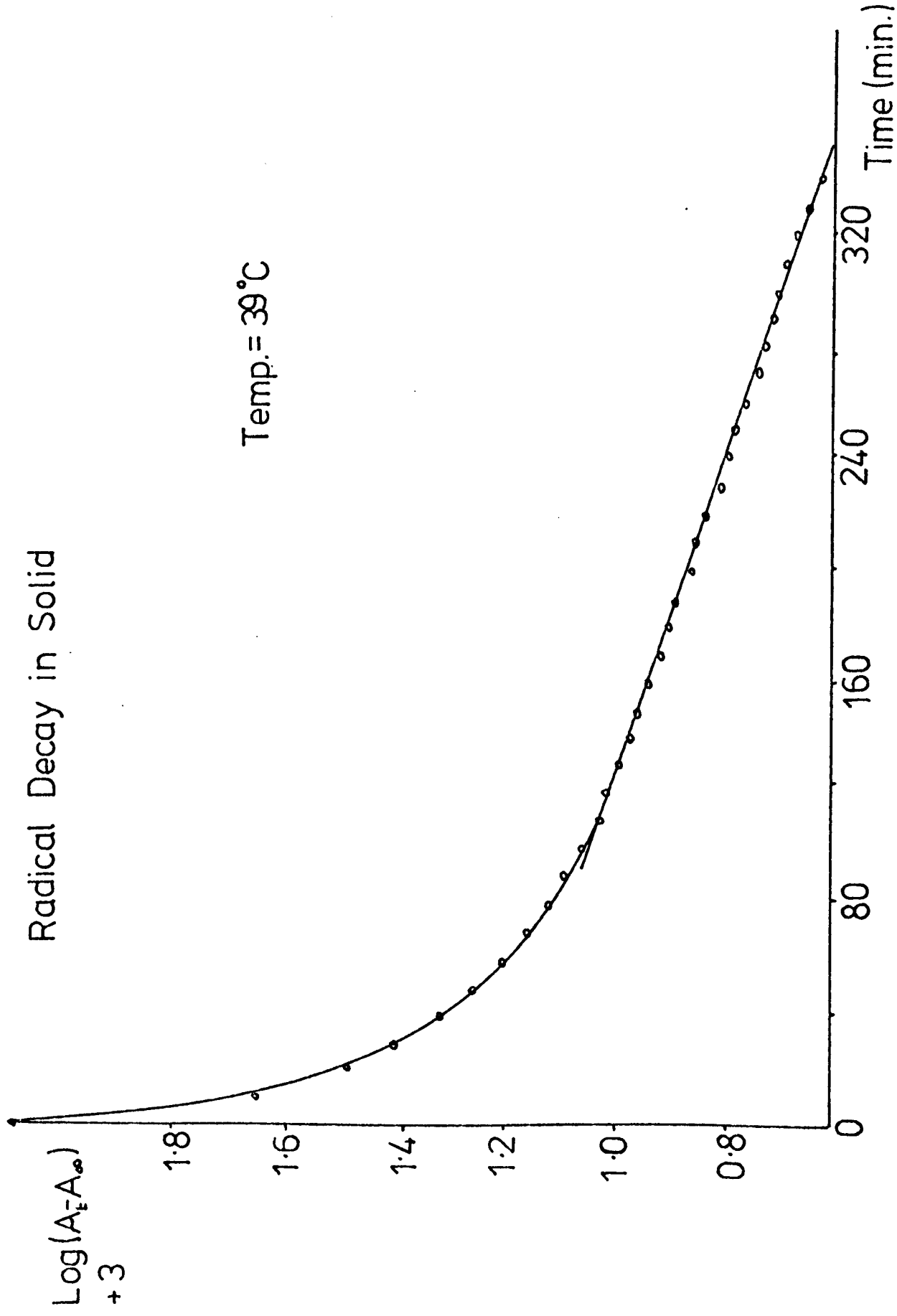


FIGURE 3.6

Radical Decay in Solid

Temp. = 44.5°C

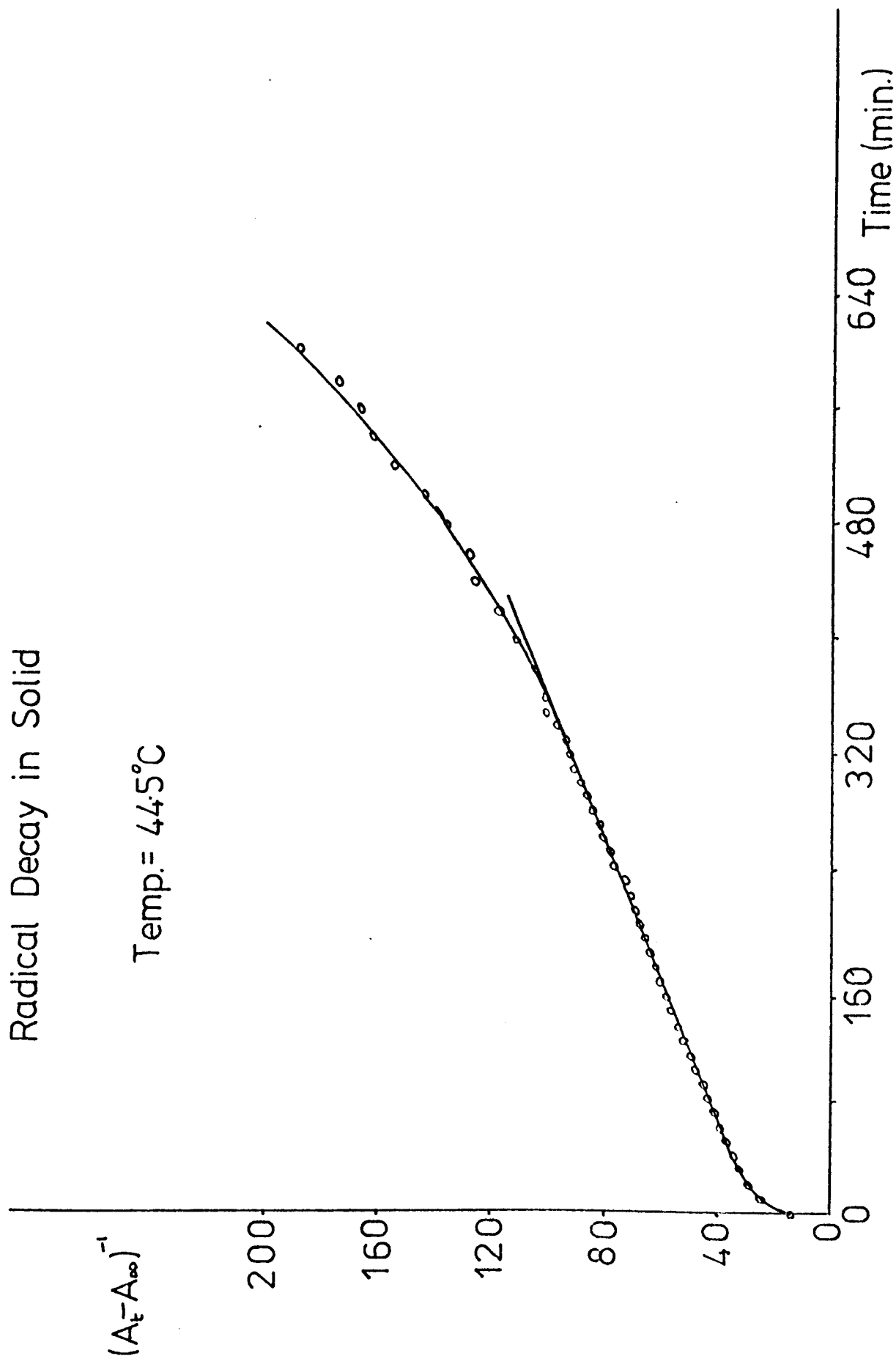


FIGURE 3.7

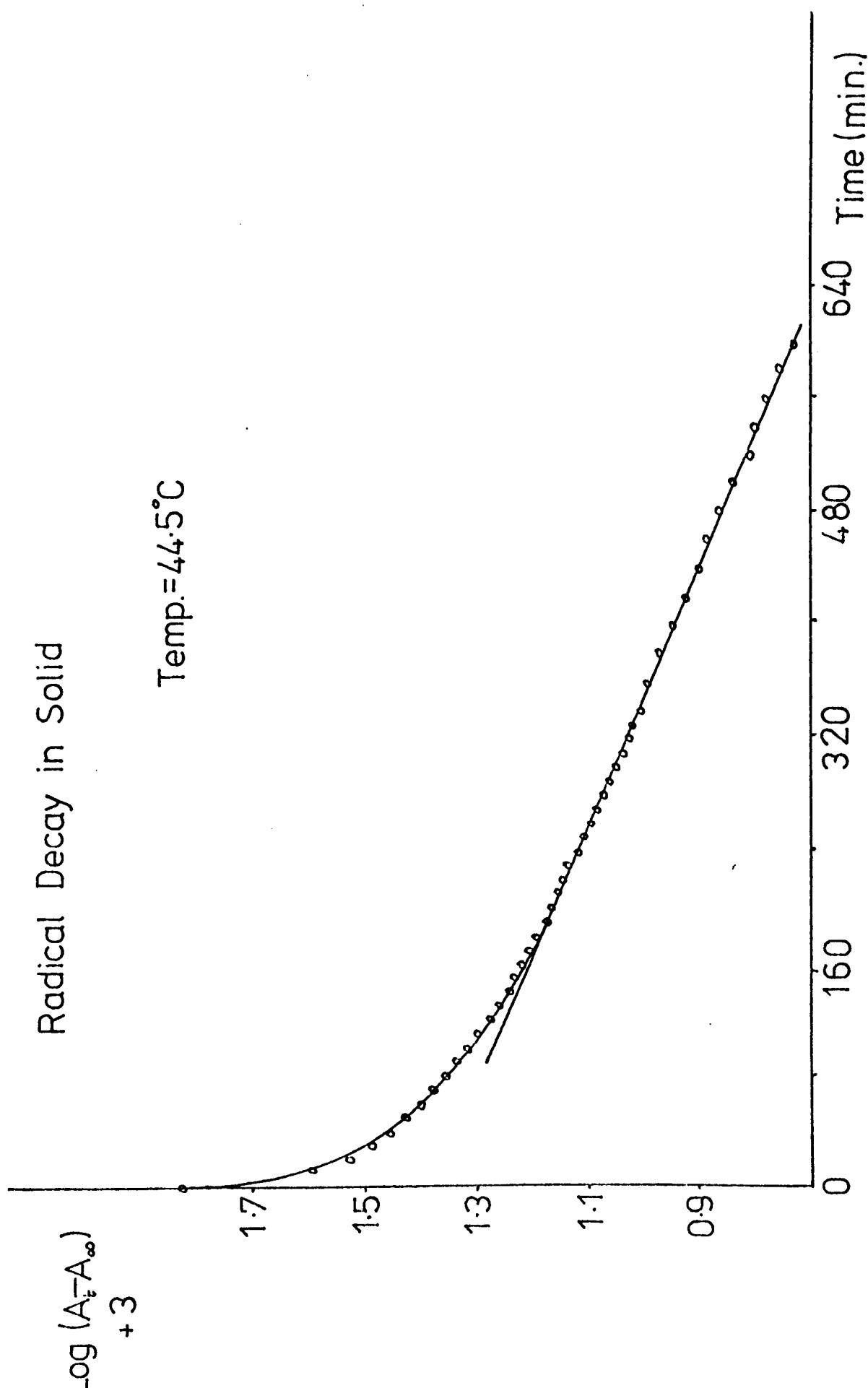


FIGURE 3.8

Radical Decay in Solid

$(A_t - A_\infty)^{-1/2}$ Temp. = 52°C

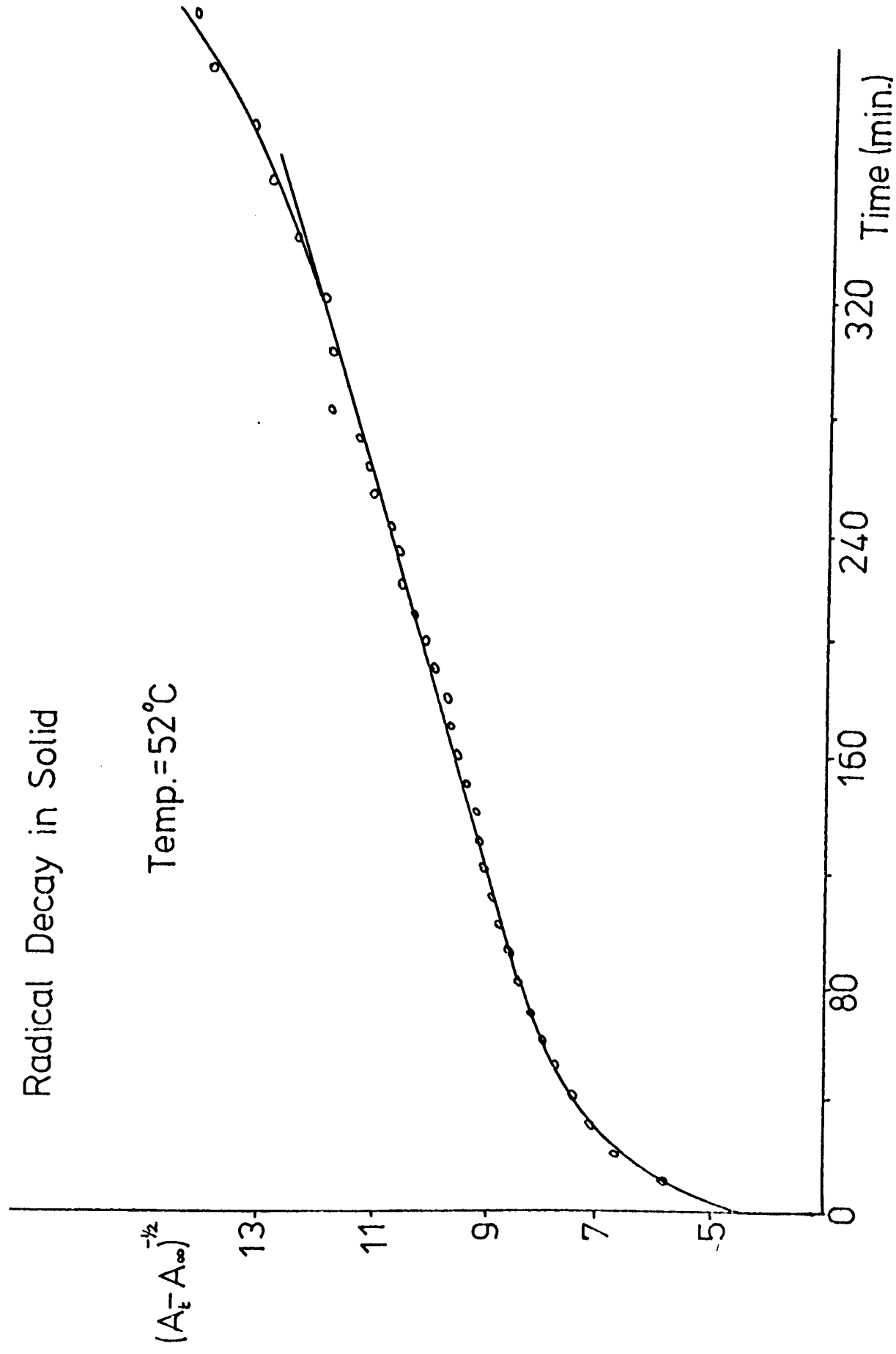


FIGURE 3.9

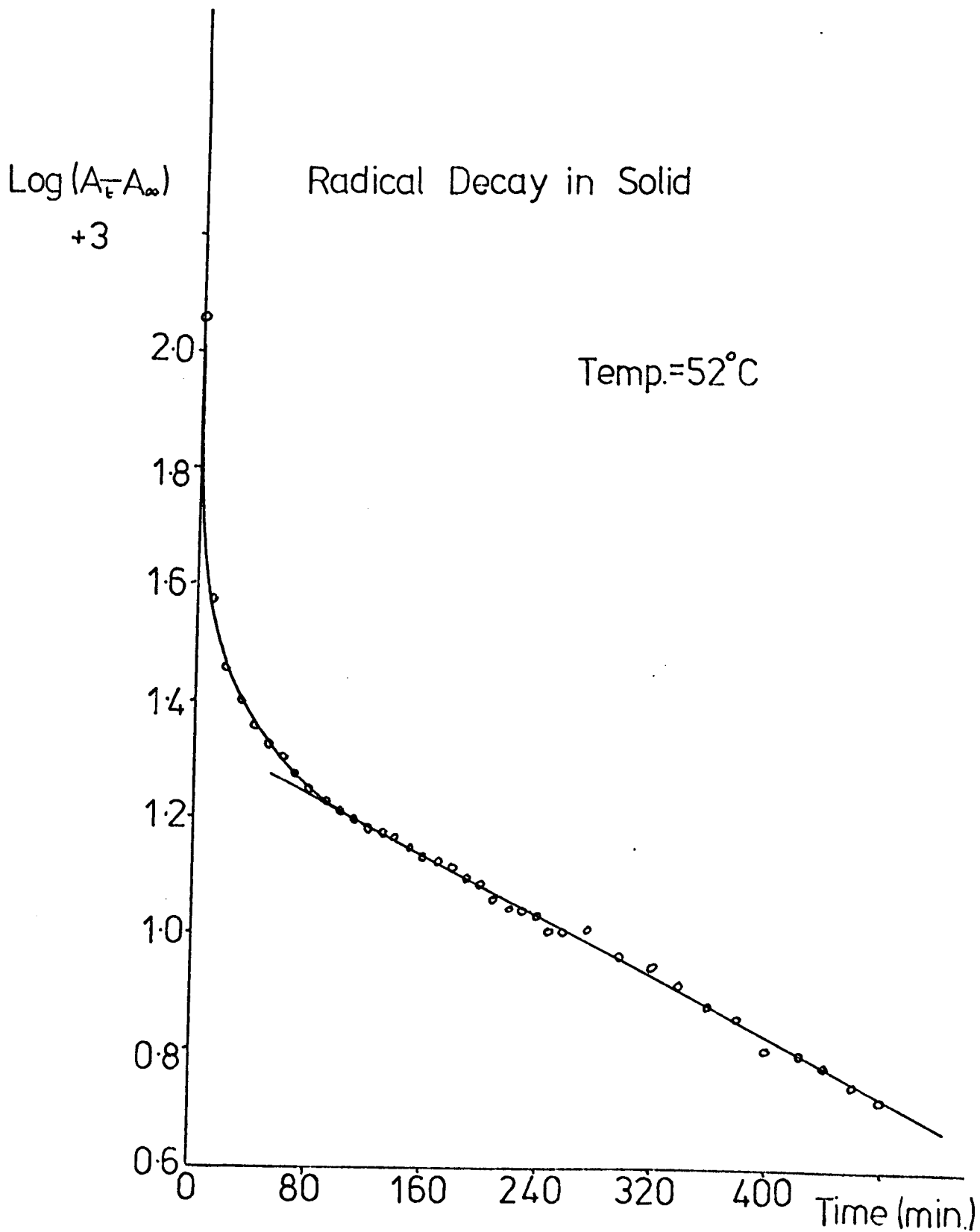


FIGURE 3.10

It must be said, however, that the orders quoted in Table 2 for the first part of the reaction may well only be approximate, as very slight changes to the value of n did not detract from the linearity of the graphs. Also, it may be noticed that in many cases, for the first several minutes of the reaction, the decay is fast and deviates from the suggested order. If the temperature dependent order has any meaning, then, this phenomenon may only be explained by postulation of fast complex surface reactions.

In fact, the significance of a changing order with changing temperature is rather obscure, and a physical interpretation in these terms is difficult to appreciate. The kinetics are thus explained in Chapter 4, by considering the process to be some sort of diffusion controlled reaction.

3.1.3 Decay kinetics of the fluorinated imidazolyl radicals

The decay kinetics of the three fluorinated bi-imidazoles at different concentrations were followed and the results analysed using the integration method.

(a) 2,2', orthofluorophenyl 4,4',5,5' tetraphenyl bi-imidazole

At 10^{-3} M dimer concentration, the orthofluoro radicals underwent recombination to the dimer following second order kinetics. A specimen set of the data is given in Table 3 and a plot of the reciprocal of optical density against time at different temperatures in the 30-60°C range, is shown in Figure 3.11.

Now, the rate constant K , for the reaction is related to the absolute temperature T , by the Arrhenius equation,

$$\log_{10} K = -E_a/RT \times 2.303 + \log_{10} A$$

Table 3

Specimen' data for the decrease of optical density with time for a $10^{-3}M$ solution of the orthofluoro dimer.

Temp = 34.4.°C

Time (min.)	(O.D. - O.D. ∞)	1/(O.D. - O.D. ∞)
0	0.0758	13.19
1	0.0642	15.58
2	0.0561	17.83
3	0.0500	20.00
4	0.0442	22.62
5	0.0404	24.75
6	0.0359	27.86
7	0.0342	29.24
88	0.0321	31.15
9	0.0298	33.56
10	0.0264	37.88
11	0.0255	39.22
12	0.0240	41.67
13	0.0238	42.02
14	0.0220	45.45
15	0.0212	47.17
16	0.0198	50.51
18	0.0181	55.25
20	0.0174	57.47
22	0.0160	62.50
24	0.0146	68.49
26	0.0144	69.44

Orthofluoro Radical Decay (10^{-3} M. Solution)

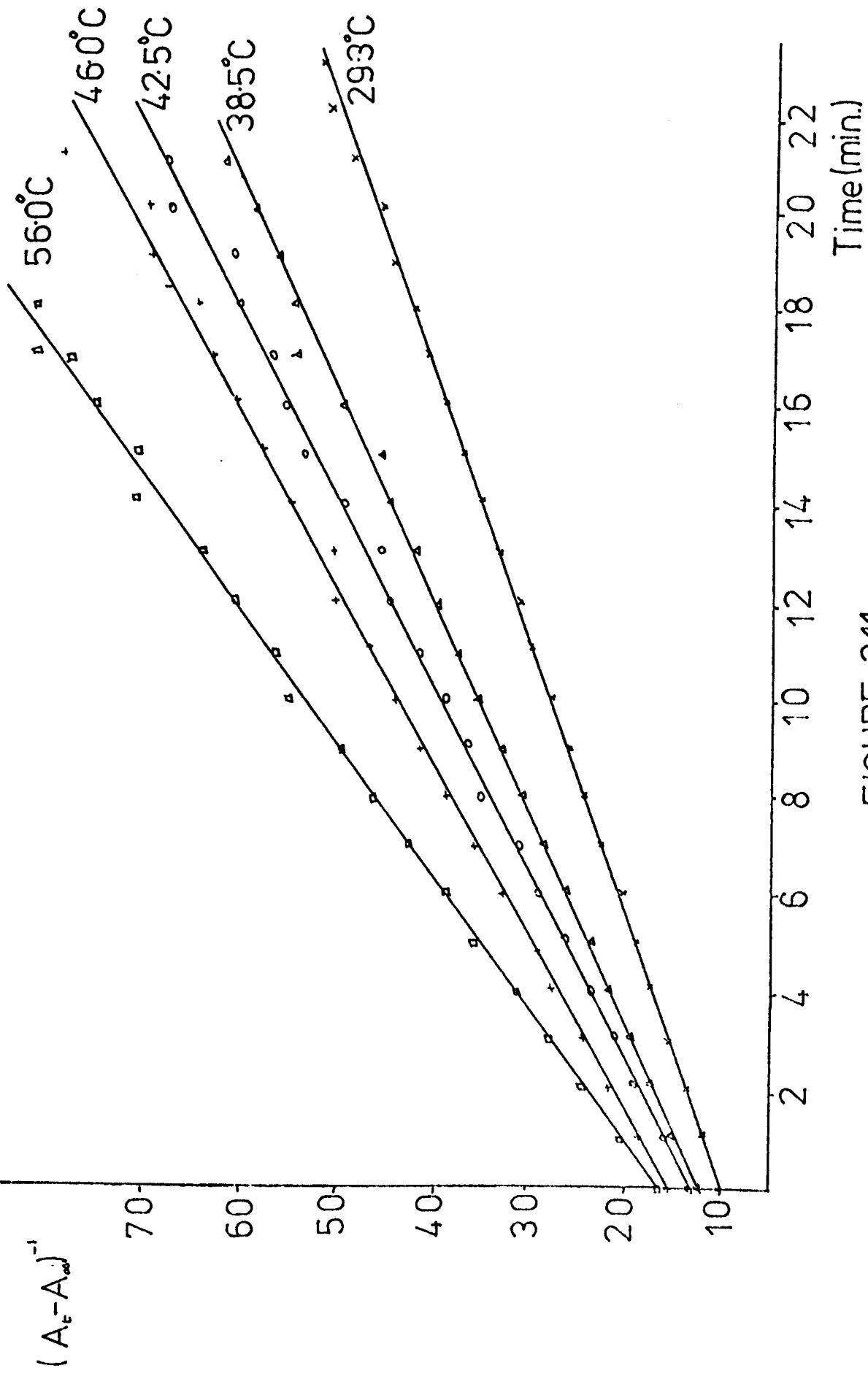


FIGURE 3.11

where E_a is the activation energy of the process, and A is the pre-exponential factor. As the gradient of the second order plot (Table 4), is proportional to K , a graph of the logarithm of G against the reciprocal of the temperature in degrees absolute, should then yield a straight line of gradient $-E_a/R \times 2.303$. This was indeed found to be true, (Figure 3.12) and the activation energy of the recombination process from the plot was calculated to be (26 ± 4) kJoules.

The kinetics of solutions of the orthofluoro compound at dimer concentrations much less than $10^{-3}M$ could not be accurately followed, due to the low quantity of radicals produced by the illumination source, but results at the higher concentration of $5.10^{-3}M$ (e.g. Table 5) showed that the reaction was composed of two separate second orders. This situation is illustrated in Figure 3.13. From the values of the gradients and their behaviour with temperature variation (Table 6) it was concluded that the later second order part of the reaction was the same process as that obtained from the $10^{-3}M$ solution. Indeed, the activation energy for this process (from Figure 3.14) was found to be similar (30 ± 5 kJoules compared to the 26 kJoules for the more dilute solution). The second order process at the beginning was found to have an activation energy of 42 ± 8 kJoules (Figure 3.15).

(b) 2,2', parafluorophenyl 4,4',5,5' tetraphenyl bi-imidazole

Tables 7, 8 and 9 show specimen data for the recombination reaction for the radicals of the parafluoro species at dimer concentrations of $5.10^{-4}M$, $10^{-3}M$ and $5.10^{-3}M$ respectively. Plots of $\frac{1}{\sqrt{O.D.}}$ against time for all three concentrations (Figures 3.16, 3.17 and 3.18). showed

Table 4.

10^{-3} M orthofluoro dimer. Dependence of G_2 upon temperature.

Temp K	Gradient G_2 (min^{-1})	$\log G_2$	$1/T \times 10^3$
302.3	1.88	0.2742	3.308
302.2	1.88	0.2742	3.309
307.0	2.32	0.3655	3.257
307.4	2.28	0.3579	3.253
307.0	2.32	0.3655	3.253
311.5	2.72	0.4346	3.210
311.5	2.52	0.4014	3.210
311.5	2.60	0.4150	3.210
315.5	3.00	0.4771	3.170
315.5	2.98	0.4742	3.170
315.5	3.125	0.4949	3.170
319.6	3.50	0.5441	3.129
319.6	3.38	0.5289	3.129
323.1	3.71	0.5694	3.090
323.1	3.87	0.5888	3.095
323.6	3.675	0.5653	3.095
329.1	4.40	0.6435	3.039
329.0	4.525	0.6551	3.040

Orthofluoro Radical Decay (10^{-3} M. Solution)

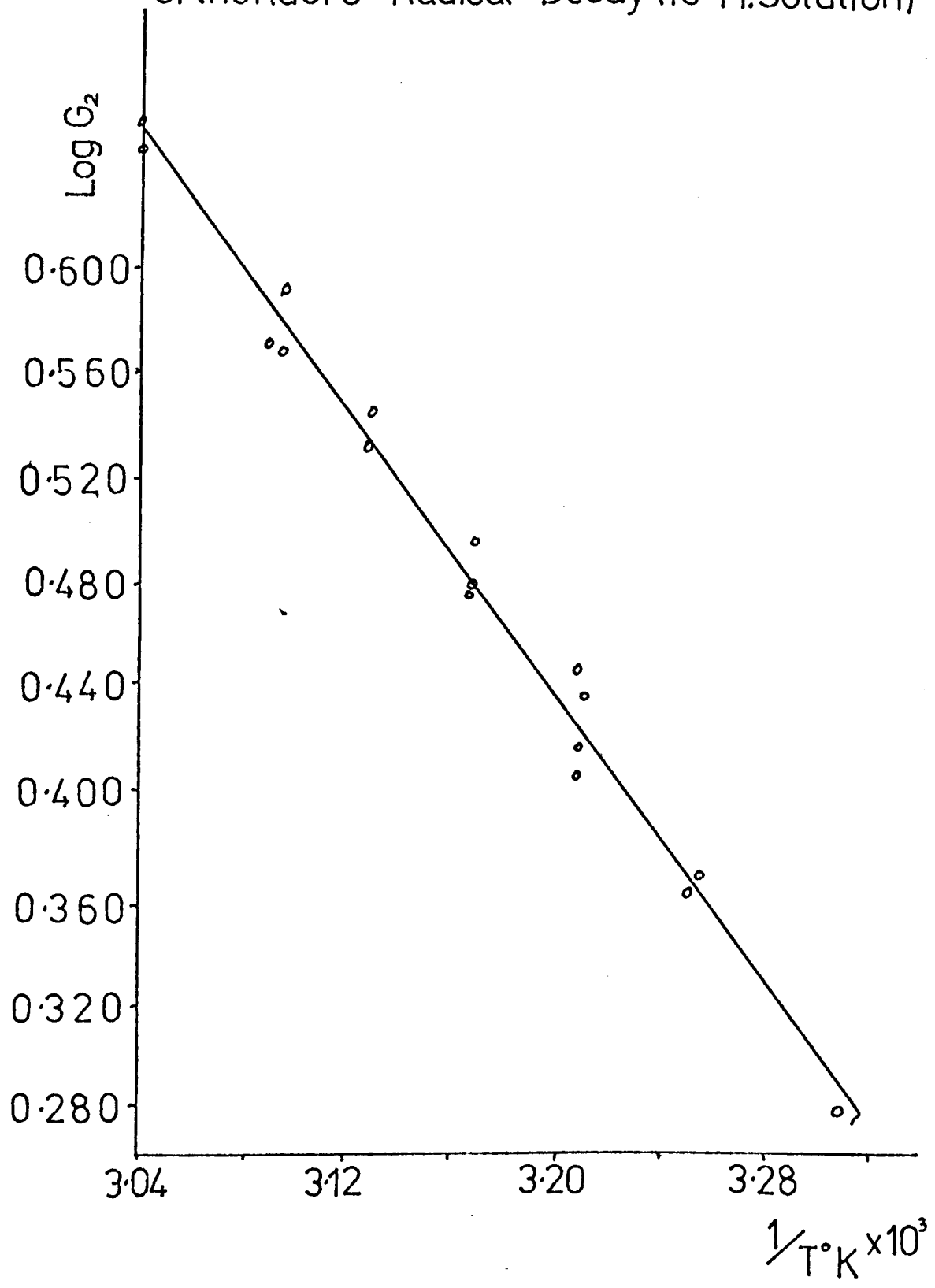


FIGURE 312

Table 5

Specimen data for the O.D. decrease of a $5 \cdot 10^{-3}$ M solution
of the orthofluoro dimer.
Temp = 30.9°C

Time (secs)	(O.D. - O.D. $_{\infty}$)	$1/(O.D. - O.D._{\infty})$
0	0.3036	3.293
20	0.2665	3.752
40	0.2340	4.274
60	0.2084	4.798
80	0.1886	5.302
100	0.1722	5.807
120	0.1580	6.329
140	0.1460	6.849
160	0.1366	7.321
180	0.1276	7.837
200	0.1200	8.333
240	0.1050	9.524
280	0.0946	10.571
320	0.0853	11.723
360	0.0776	12.887
400	0.0719	13.908
440	0.0660	15.152
480	0.0601	16.639
520	0.0560	17.857
560	0.0530	18.868
600	0.0502	19.920
640	0.0480	20.833
700	0.0439	22.779
780	0.0397	25.189
860	0.0362	27.624
920	0.0352	28.409
1000	0.0336	29.762

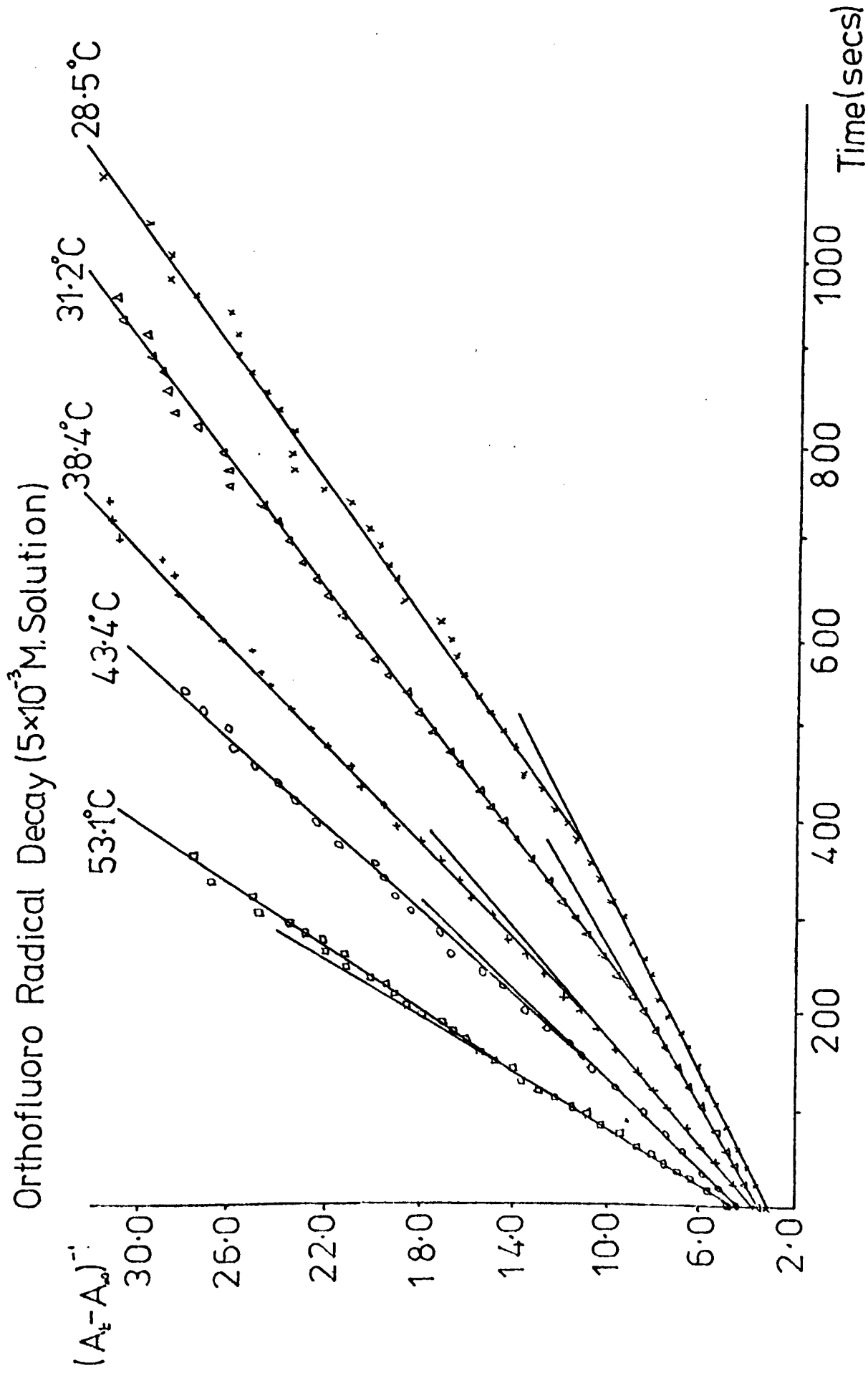


FIGURE 3.13

Table 6 5.10^{-3} M orthofluoro dimerVariation of the gradients $G_2(i)$ and $G_2(ii)$ with temperature.

Temp. K	$G_2(i)$ (min^{-1})	$G_2(ii)$ (min^{-1})	$\log G_2(i)$	$\text{Log } G_2(ii)$	$\frac{1}{T} \times 10^3$
301.5	1.212	1.38	0.0835	0.1399	3.317
301.4	1.220	1.634	0.0864	0.2132	3.318
304.2	1.48	1.900	0.1703	0.2788	3.287
303.9	1.535	1.752	0.1861	0.2435	3.290
311.5	2.014	2.143	0.3040	0.3310	3.210
311.4	1.987	2.326	0.2982	0.3666	3.211
316.4	2.52	2.75	0.4014	0.4393	3.161
316.5	2.69	3.14	0.4298	0.4969	3.160
316.4	2.60	2.60	0.4150	0.4150	3.161
320.2	-	3.425	-	0.5346	3.123
319.6	3.19	3.19	0.5038	0.5038	3.129
321	3.88	3.36	0.5888	0.5232	3.115
326.1	4.224	3.86	0.6257	0.5866	3.066

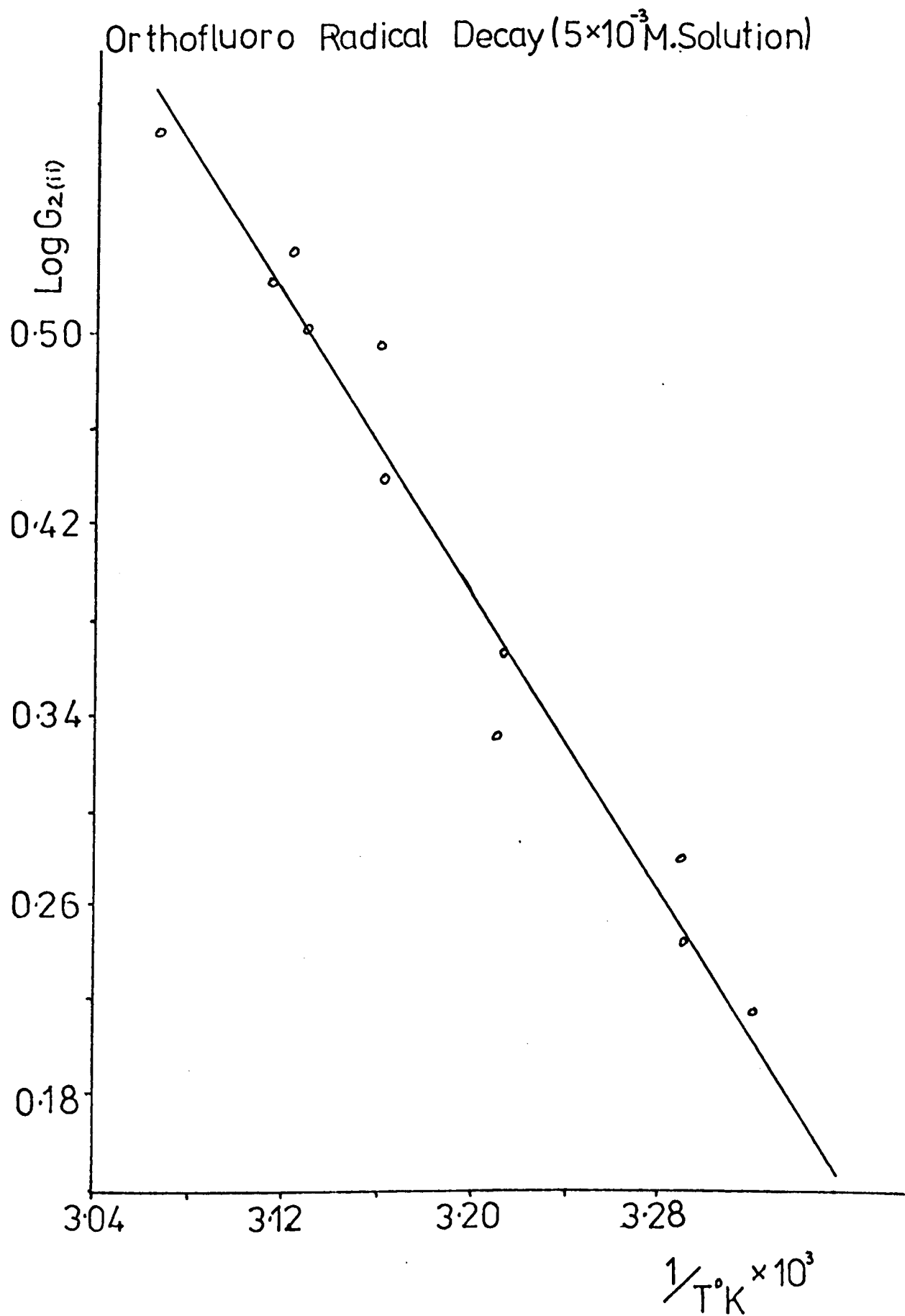


FIGURE 3.14

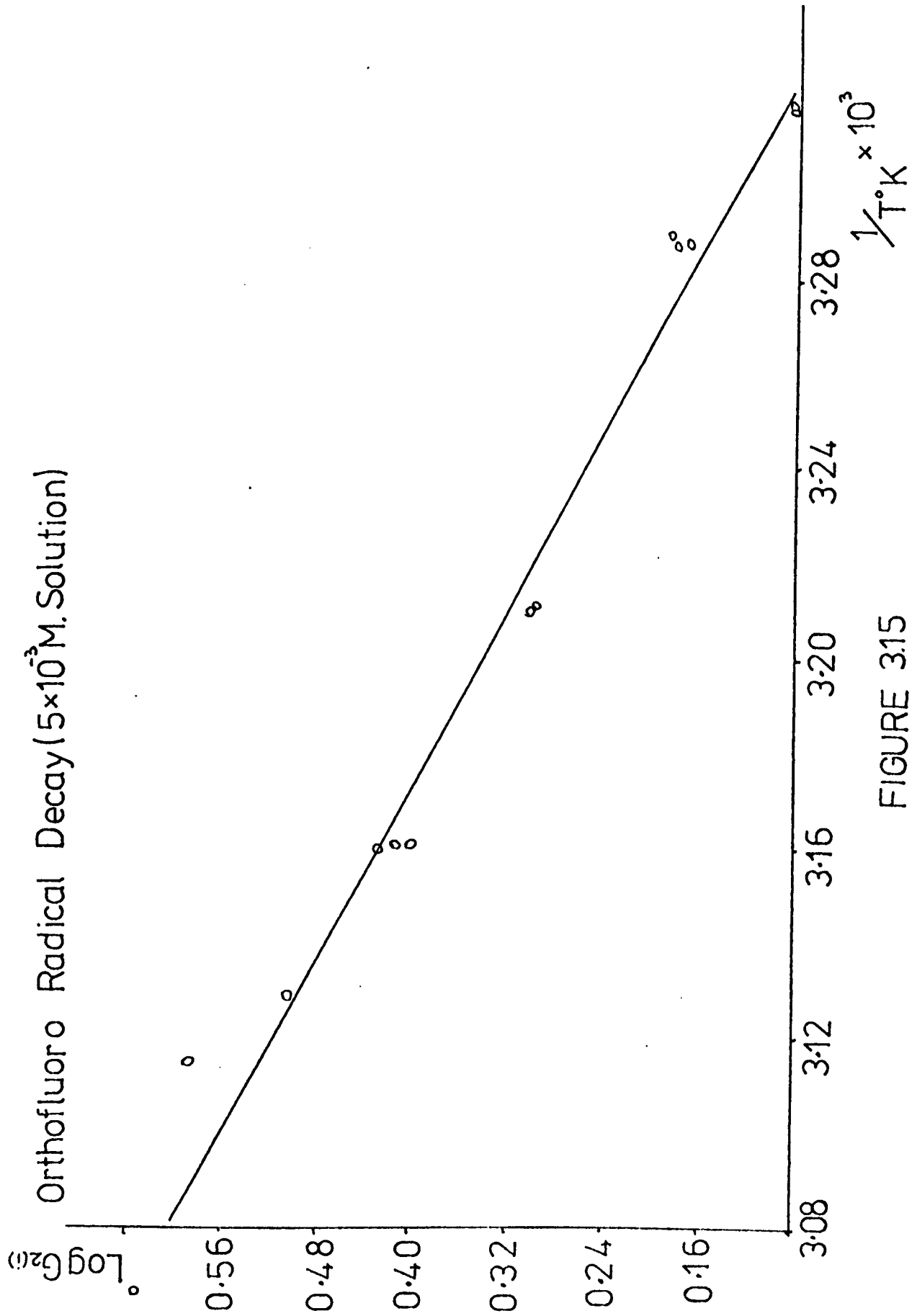


FIGURE 315

Table 7

Specimen data for the O.D. decrease with time for a $5.10^{-4}M$ solution of the parafluoro dimer.

Temp = 31°C

Time (min)	(O.D. - O.D. ∞)	$1/\sqrt{(O.D. - O.D.\infty)}$
0	0.1958	2.259
1	0.1686	2.435
2	0.1498	2.584
3	0.1340	2.732
4	0.1200	2.887
5	0.1078	3.046
6	0.1000	3.162
7	0.0917	3.302
8	0.0836	3.459
9	0.0764	3.618
10	0.0720	3.727
11	0.0662	3.887
12	0.0620	4.016
13	0.0586	4.131
14	0.0560	4.226
16	0.0500	4.472
18	0.0437	4.784
20	0.0400	5.0000
22	0.0346	5.376
24	0.0318	5.608

Table 8

Specimen data for the optical density decrease with time for
a 10^{-3} M solution of the parafluoro dimer

Temp = 32.4°C

Time (min)	(O.D-OD _∞)	$1/\sqrt{(O.D - OD_{\infty})}$
0	0.1966	2.255
1	0.1718	2.412
2	0.1500	2.582
3	0.1322	2.751
4	0.1178	2.914
5	0.1040	3.107
6	0.0940	3.262
7	0.0845	3.439
8	0.0776	3.591
9	0.0701	3.777
10	0.0642	3.947
11	0.0598	4.089
12	0.0555	4.245
13	0.0512	4.419
14	0.0468	4.623
15	0.0436	4.789
16	0.0402	4.988
18	0.0359	5.279
20	0.0320	5.590
22	0.0283	5.944
24	0.0259	6.214
26	0.0222	6.712
28	0.0206	6.969
30	0.0180	7.454

Table 9

Specimen data for the O.D. decrease with time for a $5 \cdot 10^{-3} M$ solution of the parafluoro dimer.

Temp = $30.1^{\circ}C$

Time (sec.)	(O.D. - O.D. _∞)	$1/\sqrt{(O.D. - O.D._{\infty})}$
0	0.6720	1.220
40	0.5840	1.309
80	0.5130	1.396
120	0.4460	1.497
160	0.3940	1.593
200	0.3460	1.700
240	0.3110	1.793
280	0.2800	1.890
320	0.2500	2.000
360	0.2250	2.108
400	0.2050	2.209
440	0.1840	2.331
480	0.1700	2.425
520	0.1550	2.540
560	0.1420	2.654
600	0.1360	2.712
640	0.1210	2.875
680	0.1160	2.936
720	0.1050	3.086
800	0.0960	3.227
880	0.0840	3.450
960	0.0760	3.627
1040	0.0660	3.892

Paraffluoro Radical Decay (5.10^{-4} M. Solution)

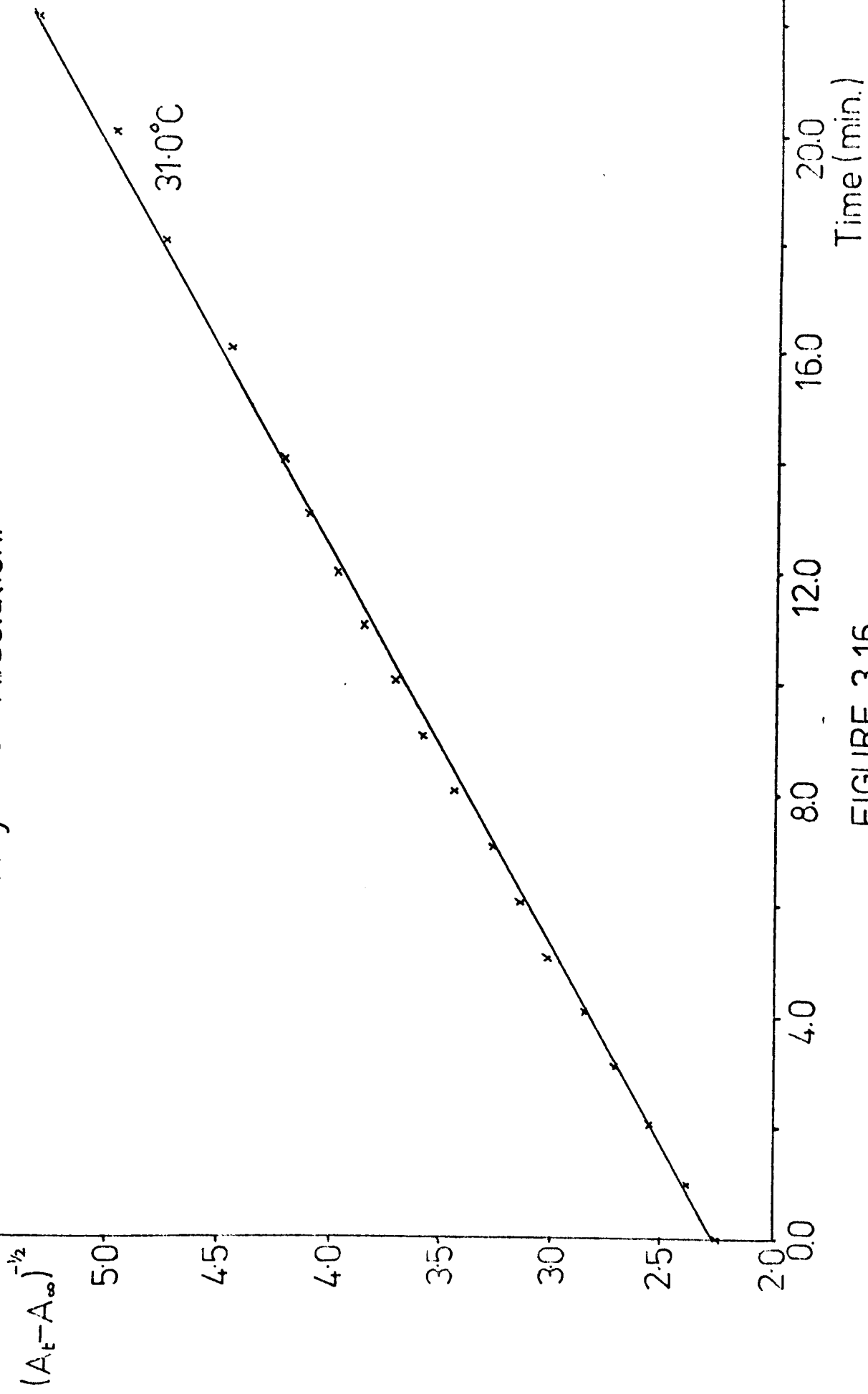


FIGURE 3.16

Parafluoro Radical Decay (10^{-3} M.Solution)

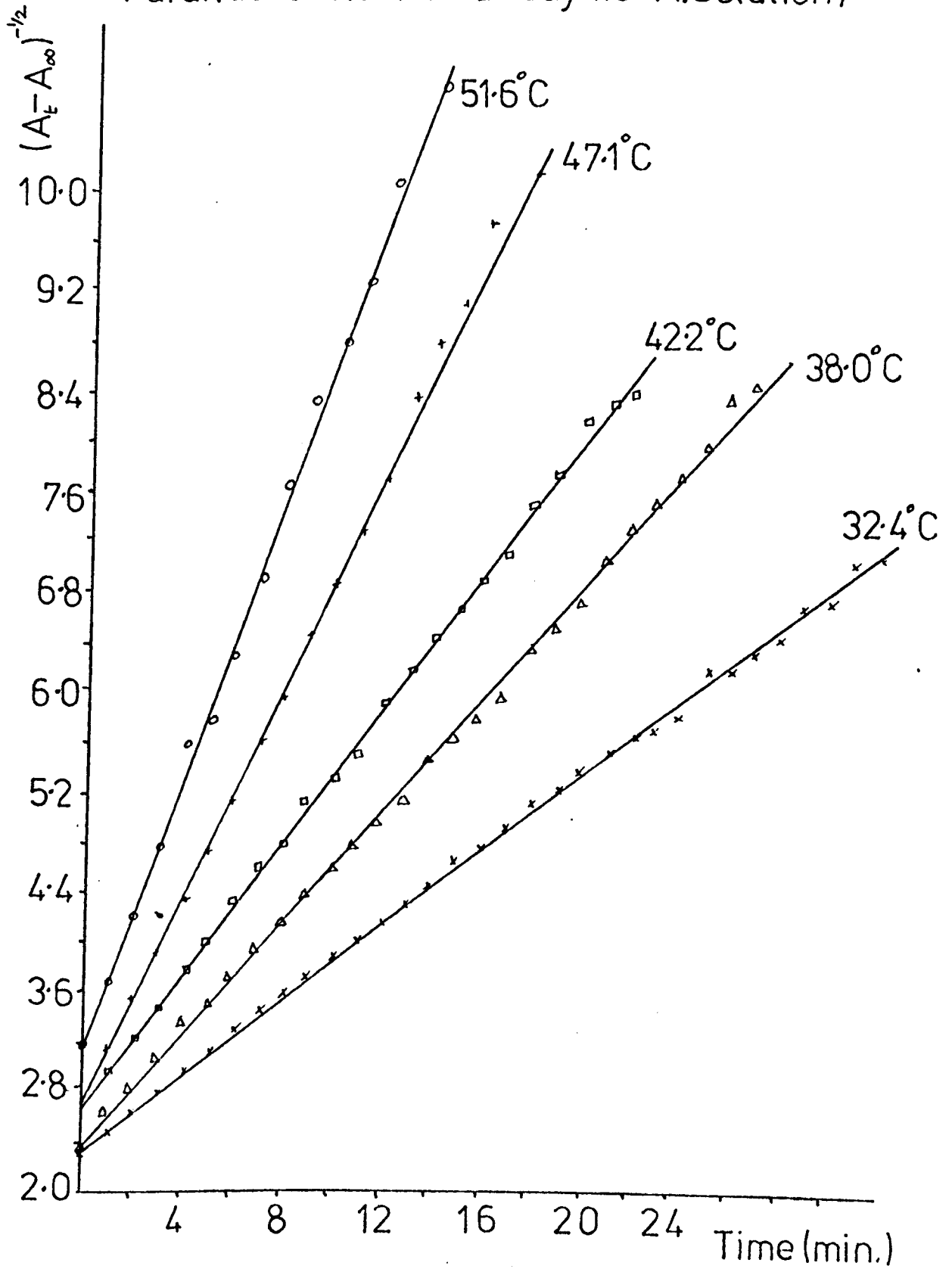


FIGURE 3.17

Paraffluoro Radical Decay ($5 \cdot 10^{-3}$ M. Solution)

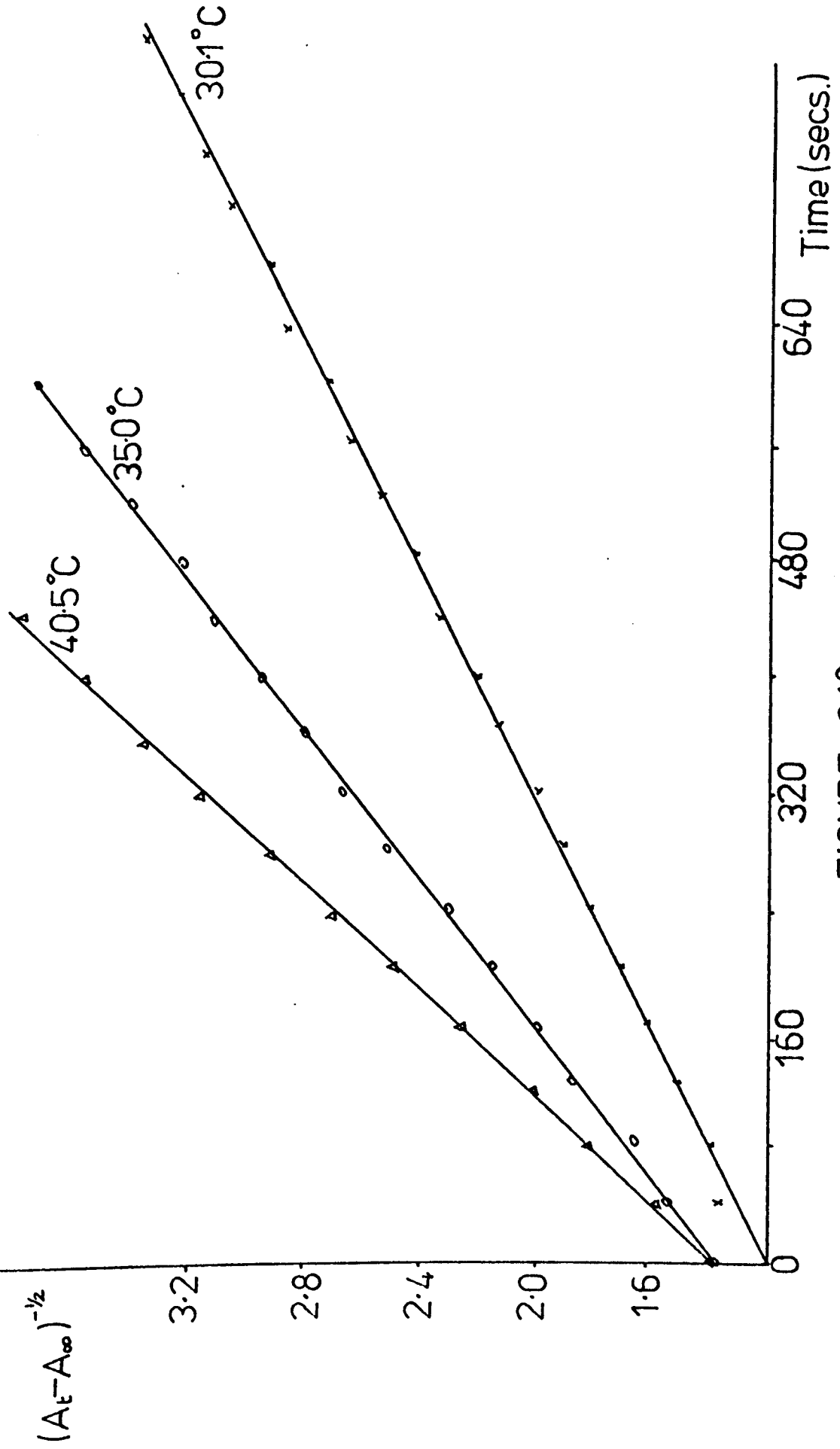


FIGURE 3.18

that the reactions appeared to be $3/2$ order through-out with no change in behaviour for a change in dimer concentration. Table 10 gives the value of the gradient of the $3/2$ order plot (for the $10^{-3}M$ solution) at different temperatures and Figure 3.19 is the corresponding Arrhenius plot. From this graph the activation energy of the process was calculated to be 51 ± 7 k joules.

(c) 2,2' metafluorophenyl 4,4'5,5' tetraphenyl bi-imidazole

Again, specimen data for the reactions in solutions of dimer concentrations $10^{-4}M$, $10^{-3}M$ and $5 \cdot 10^{-3}M$ are given in Tables 11, 12 and 13.

The reaction at $10^{-3}M$, was found to follow the same scheme as that reported for a $10^{-3}M$ solution of 2,2',4,4'5,5' hexaphenyl biimidazole¹⁵, in that an initial recombination following $3/2$ order kinetics, gave way in the later stages to a first order reaction (Figures 3.20 and 3.21). From the Arrhenius plots of both parts (Table 14 and Figures 3.22 and 3.23), the activation energy of the $3/2$ order reaction was found to be 59 ± 3 kjoules and that of the first order was found to be 65 ± 7 kjoules.

At $10^{-4}M$, some similarity to the hexaphenyl system at the same concentration¹⁸ was again seen, some second order behaviour being obtained at the start of the decay reaction (Figure 3.24) followed by a recurrence of the $3/2$ order towards the end (Figure 3.25). Activation energies were found to be 54 ± 6 k joules and 53 ± 9 kjoules, for the second and $3/2$ order reactions respectively (Figures 3.26 and 3.27, Table 15).

The more concentrated solution, $5 \cdot 10^{-3}M$, gave a reaction of which the data were indicative of an order between first and $3/2$. A graph of $\log \tau$ against $\log \frac{(A_t - A_{\infty})}{A_{\infty}}$ (from equation 3.6) pointed to an order of approximately $5/4$ (Figure 3.28) and plots $1/(O.D.)^{1/4}$ and $1/(O.D.)^{1/5}$ against time both gave good straight lines throughout the reaction. For the purpose of the discussion, the order of $6/5$

Table 10

10^{-3} M parafluoro dimer. Dependence of $G_{3/2}$ upon temperature.

Temp K	Gradient (min^{-1}) $G_{3/2} \times 10$	$\log G_{3/2}$ +1	$1/T \times 10^3$
301.5	1.38	0.1399	3.317
302.0	1.33	0.1239	3.311
305.4	1.56	0.1931	3.275
305.4	1.52	0.1818	3.275
304.4	1.56	0.1931	3.285
311.2	2.18	0.3385	3.213
311.1	2.24	0.3502	3.214
311.1	2.20	0.3424	3.214
315.2	2.84	0.4533	3.173
315.0	2.80	0.4472	3.175
315.9	2.84	0.4533	3.166
319.5	3.95	0.5966	3.130
320.2	4.07	0.6096	3.123
320.2	4.00	0.6021	3.123
323.0	4.48	0.6508	3.096
324.8	5.48	0.7384	3.078
324.4	5.43	0.7344	3.082
328.7	5.80	0.7634	3.056
331.5	8.10	0.9085	3.017
331.2	8.95	0.9518	3.019

Parafluoro Radical Decay (10^{-3} M Solution)

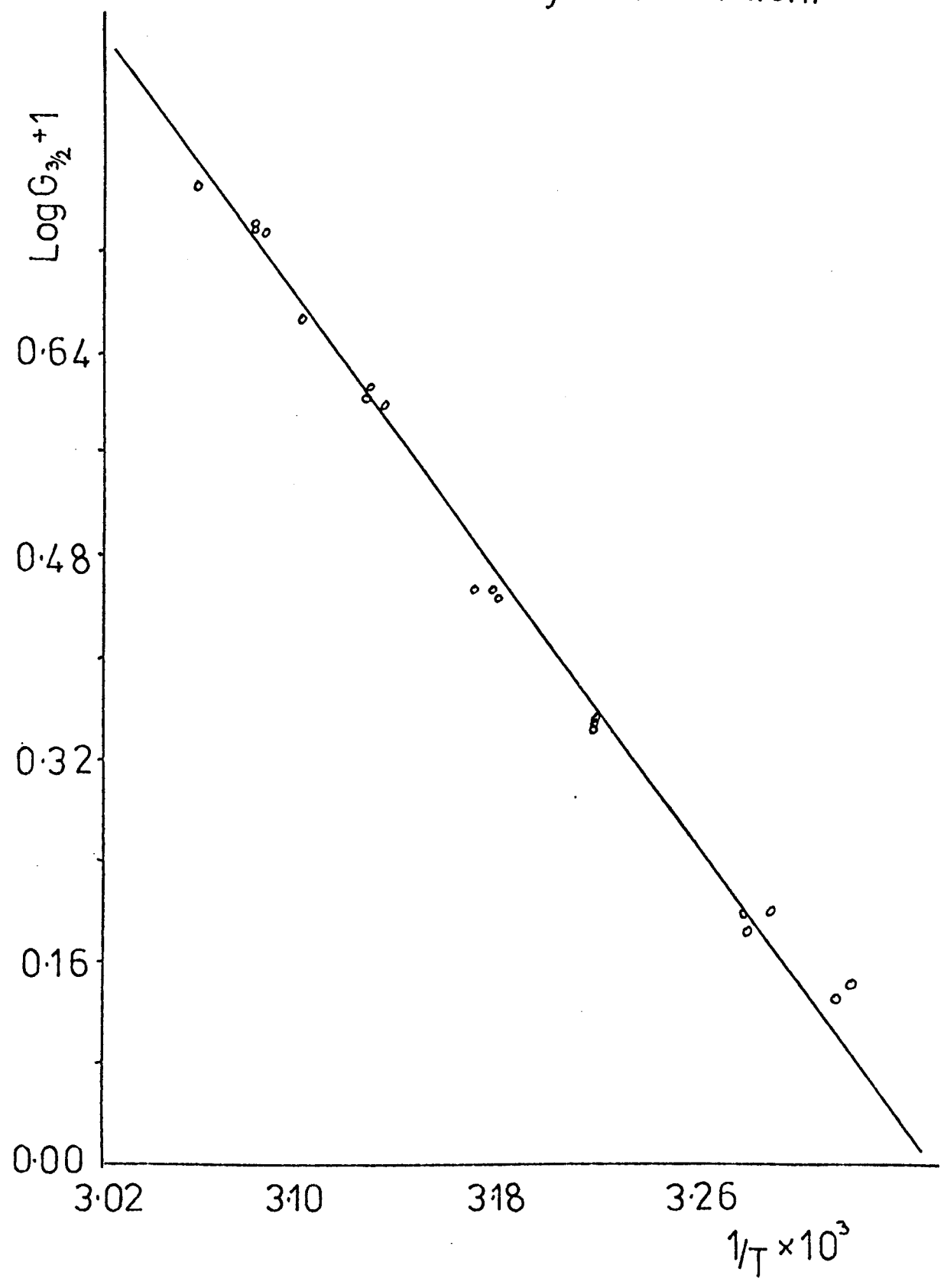


FIGURE 3.19

Table 11

Specimen data for the O.D. decrease with time for a 10^{-4} M solution
for the metafluorodimer.

Temp = 29.8°C.

Time (Secs)	(O.D. - O.D. _∞)	$1/(O.D. - O.D._{\infty})$	$1/\sqrt{(O.D. - O.D._{\infty})}$
0	0.1421	7.037	2.653
40	0.1307	7.651	2.766
80	0.1200	8.333	2.887
120	0.1120	8.929	2.988
160	0.1077	9.285	3.047
200	0.1000	10.000	3.162
240	0.0939	10.650	3.263
280	0.0880	11.364	3.371
320	0.0849	11.779	3.432
360	0.0792	12.626	3.553
400	0.0750	13.333	3.651
480	0.0690	14.493	3.807
560	0.0628	15.924	3.990
640	0.0572	17.483	4.181
720	0.0521	19.194	4.381
800	0.0477	20.964	4.579
880	0.0440	22.727	4.767
960	0.0423	23.641	4.862
1040	0.0398	25.126	5.013
1120	0.0373	26.810	5.178
1200	0.0350	28.571	5.345
1280	0.0322	31.056	5.573
1360	0.0310	32.258	5.680
1440	0.0300	33.333	5.774

Table 12

Specimen data for the O.D. decrease with time for a $10^{-3}M$ solution of the metafluoro dimer.

Temp = 30°C

Time Min.	(O. D. - O. D _∞)	$1/\sqrt{(O. D. - O. D_{\infty})}$	$\log_e(O. D. - O. D_{\infty})$
0	0.3060	1.808	- 1.184
1	0.2640	1.946	1.332
2	0.2226	2.119	1.502
3	0.1936	2.273	1.642
4	0.1679	2.440	1.784
5	0.1498	2.584	1.898
6	0.1216	2.867	2.107
7	0.1158	2.939	2.155
8	0.1033	3.111	2.270
9	0.0907	3.320	2.400
10	0.0820	3.492	2.501
11	0.0738	3.681	2.606
12	0.0660	3.892	2.718
13	0.0602	4.076	2.810
14	0.0542	4.295	2.915
16	0.0460	4.663	3.079
18	0.0380	5.130	3.270
20	0.0318	5.608	3.448
22	0.0274	6.041	3.597
24	0.0240	6.455	3.730
26	0.0199	7.089	3.917
28	0.0178	7.495	4.029
30	0.0162	7.857	4.123
32	0.0140	8.452	4.269
34	0.0122	9.054	4.406

Table 13

Specimen data for the O.D. decrease with time for a $5.10^{-3}M$ solution of the metafluoro dimer.

Temp = $30.6^{\circ}C$

Time (secs)	(O.D. - O.D. $_{\infty}$)	$(1/(O.D. - O.D._{\infty}))^{1/5}$
0	0.6520	1.089
40	0.5735	1.118
80	0.5040	1.147
120	0.4420	1.177
160	0.3880	1.208
200	0.3470	1.236
240	0.3080	1.266
280	0.2710	1.298
320	0.2385	1.332
360	0.2110	1.365
400	0.1885	1.396
440	0.1690	1.427
480	0.1530	1.455
520	0.1400	1.482
560	0.1265	1.512
600	0.1140	1.544
640	0.1030	1.575
680	0.0930	1.608
720	0.0855	1.635
760	0.0775	1.667
800	0.0715	1.695
840	0.0645	1.730
880	0.0595	1.754
920	0.0550	1.786
960	0.0505	1.817

Metafluoro Radical Decay (10^{-3} M. Solution)

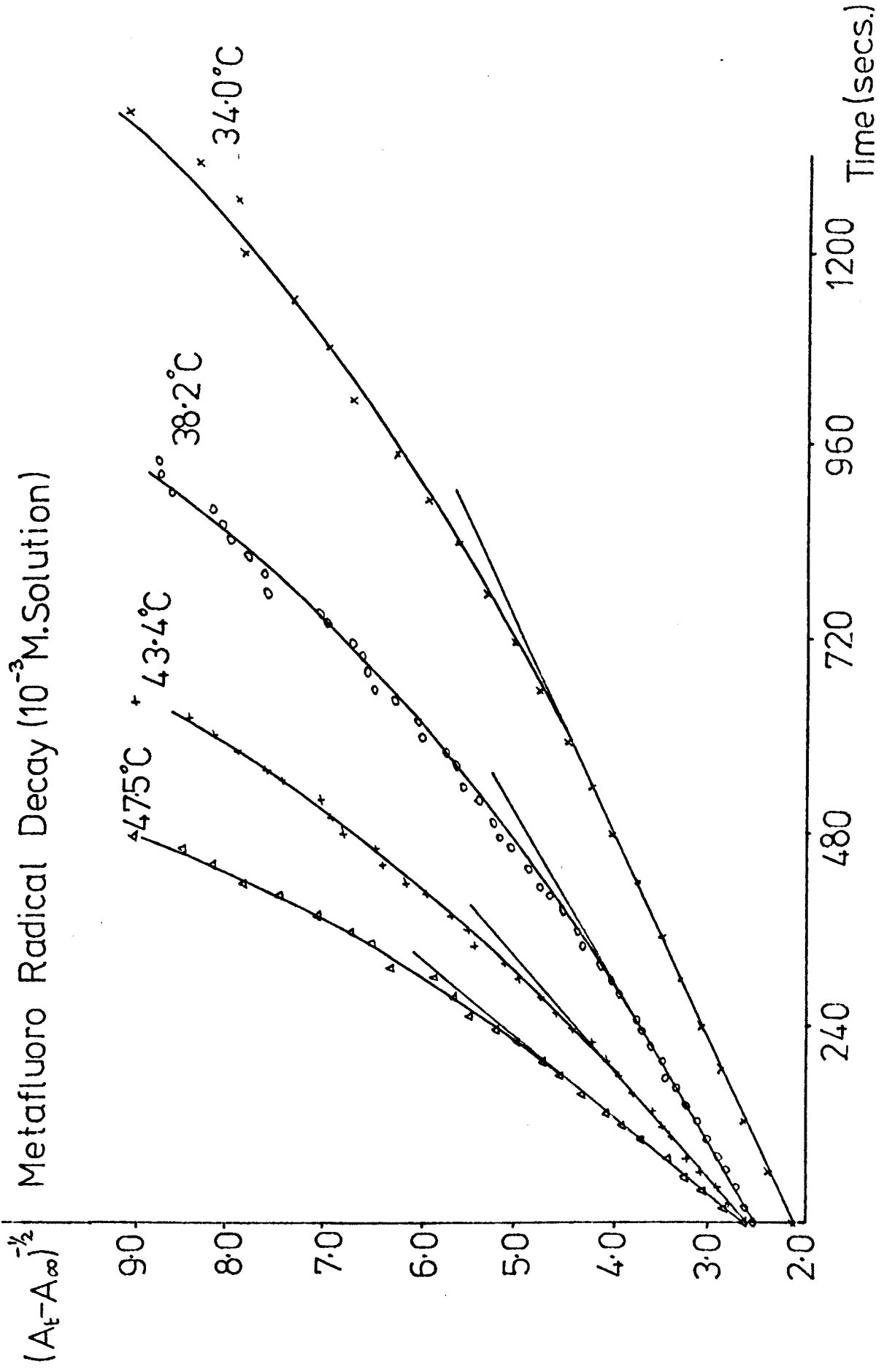


FIGURE 3.20

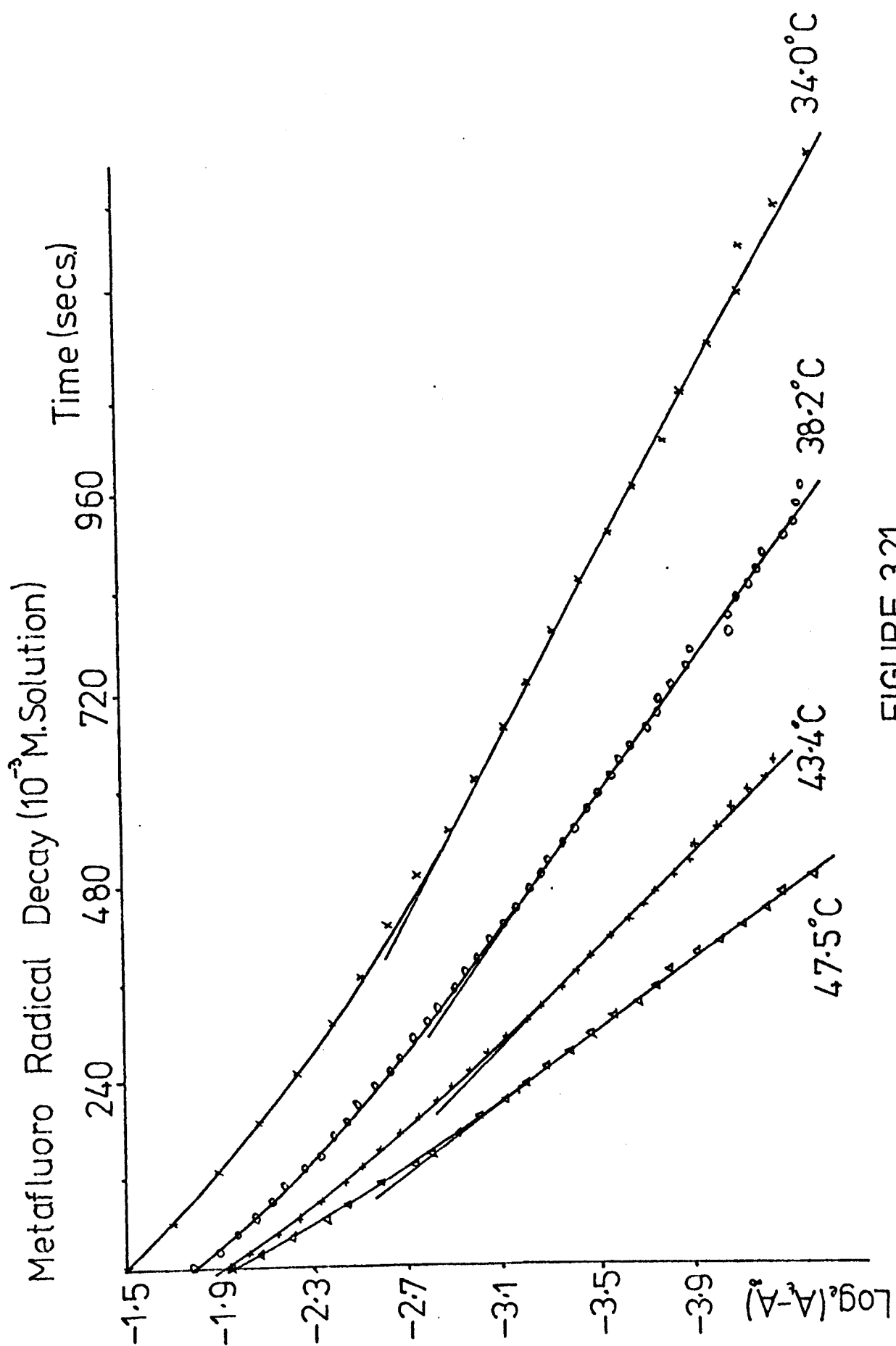


FIGURE 3.21

Table 14

10^{-3} metafluoro dimer. Variation of gradients

$G_{3/2}$ and G_1 with temperature.

Temp K	$G_{3/2}$ (min^{-1}) $\times 10$	G_1 (min^{-1}) $\times 10$	$\log G_{3/2}$ + 1	$\log G_1$ + 2	$1/T \times 10^3$
303.9	1.70	0.708	0.2304	0.8762	3.290
303.5	1.52	0.752	0.1818	0.8500	3.295
307.3	2.30	1.06	0.3617	1.0253	3.254
307.0	2.28	1.02	0.3579	1.0086	3.257
310.7	2.90	1.55	0.4625	1.1903	3.219
311.2	2.925	1.40	0.4653	1.1461	3.213
311.2	3.000	1.48	0.4771	1.1703	3.213
316.4	4.25	1.95	0.6284	1.2900	3.161
316.0	4.25	1.90	0.6284	1.2776	3.165
321.5	6.30	3.30	0.7993	1.5180	3.110
321.2	6.04	-	0.7810	-	3.113
321.3	6.05	3.12	0.7818	1.4942	3.112
327.4	9.06	4.95	0.9571	1.6946	3.054
327.8	9.08	4.73	0.9581	1.6749	3.050
327.8	9.22	4.97	0.9647	1.6964	3.050
331.2	11.45	5.96	1.0589	1.7755	3.019
332.7	12.13	6.70	1.0839	1.8261	3.006

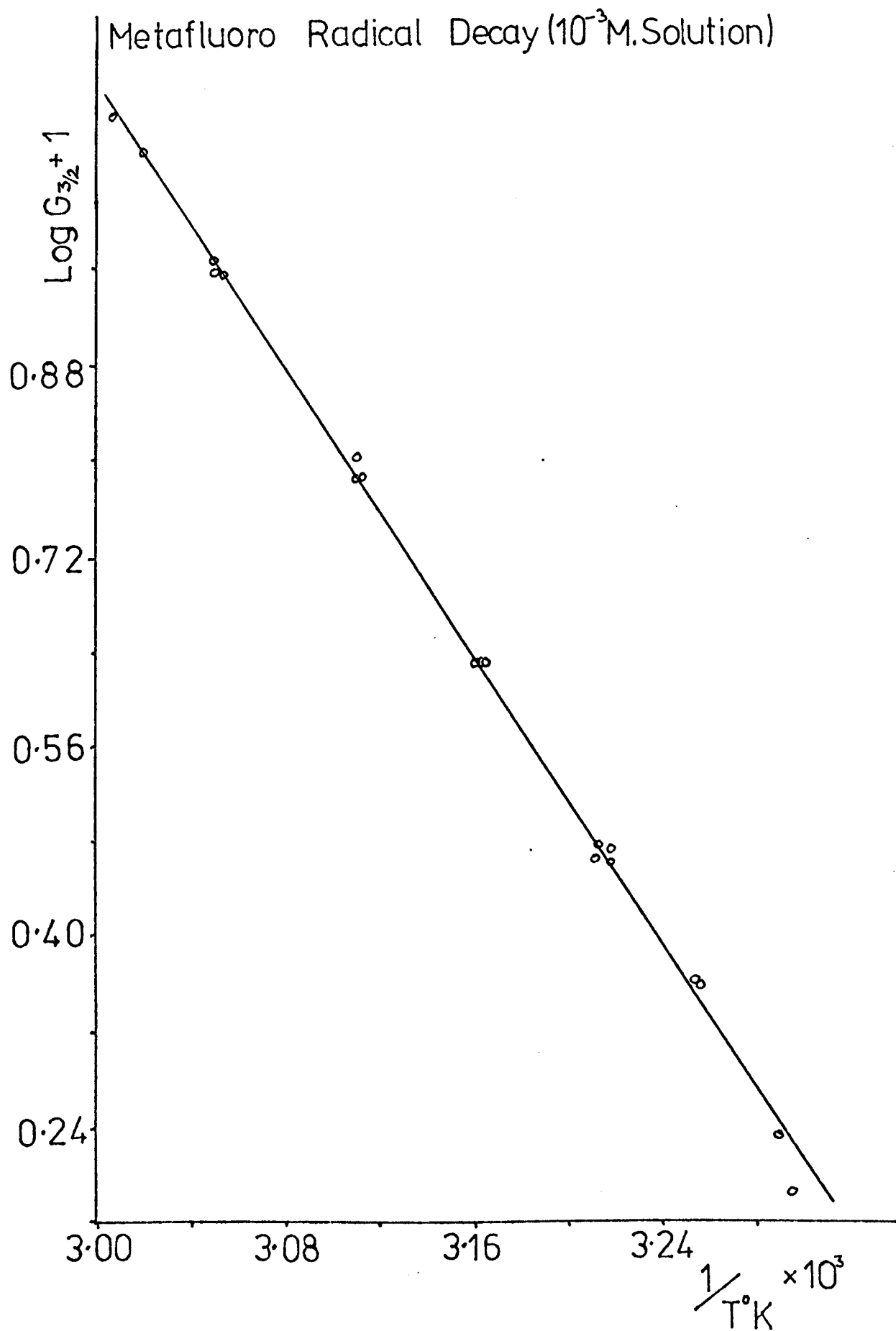


FIGURE 3.22

Metafluoro Radical Decay (10^{-3} M. Solution)

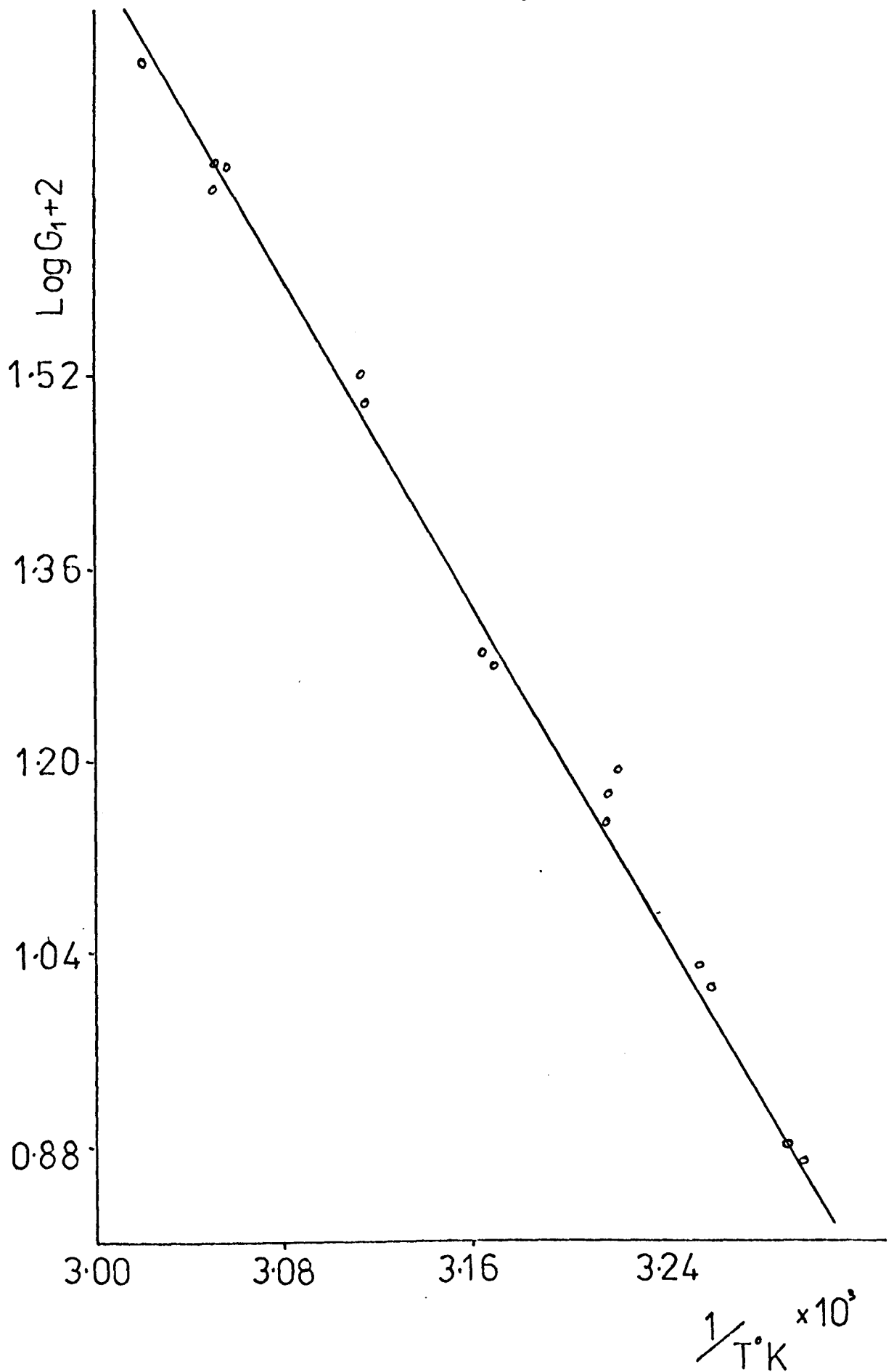


FIGURE 3.23

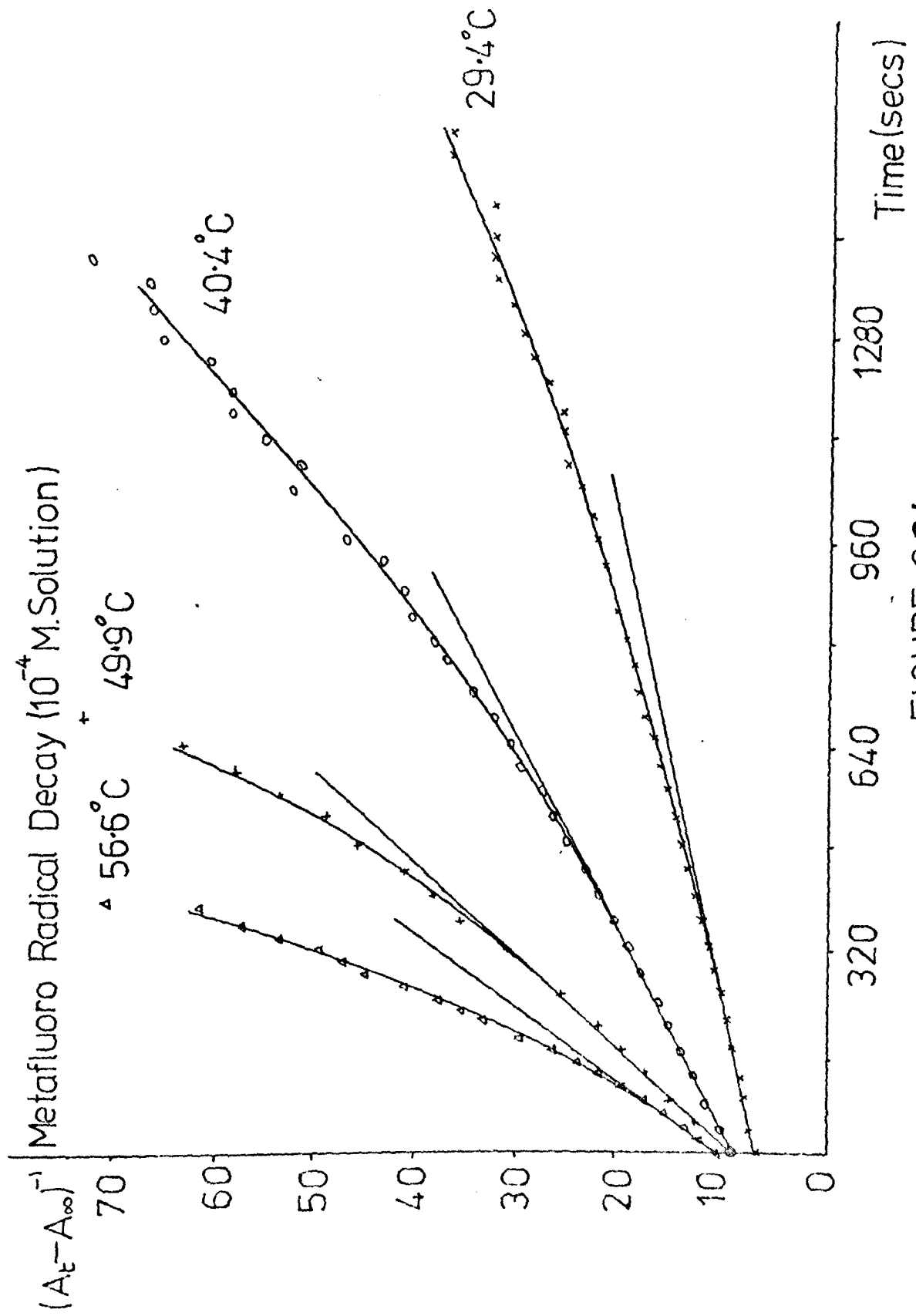


FIGURE 3.24

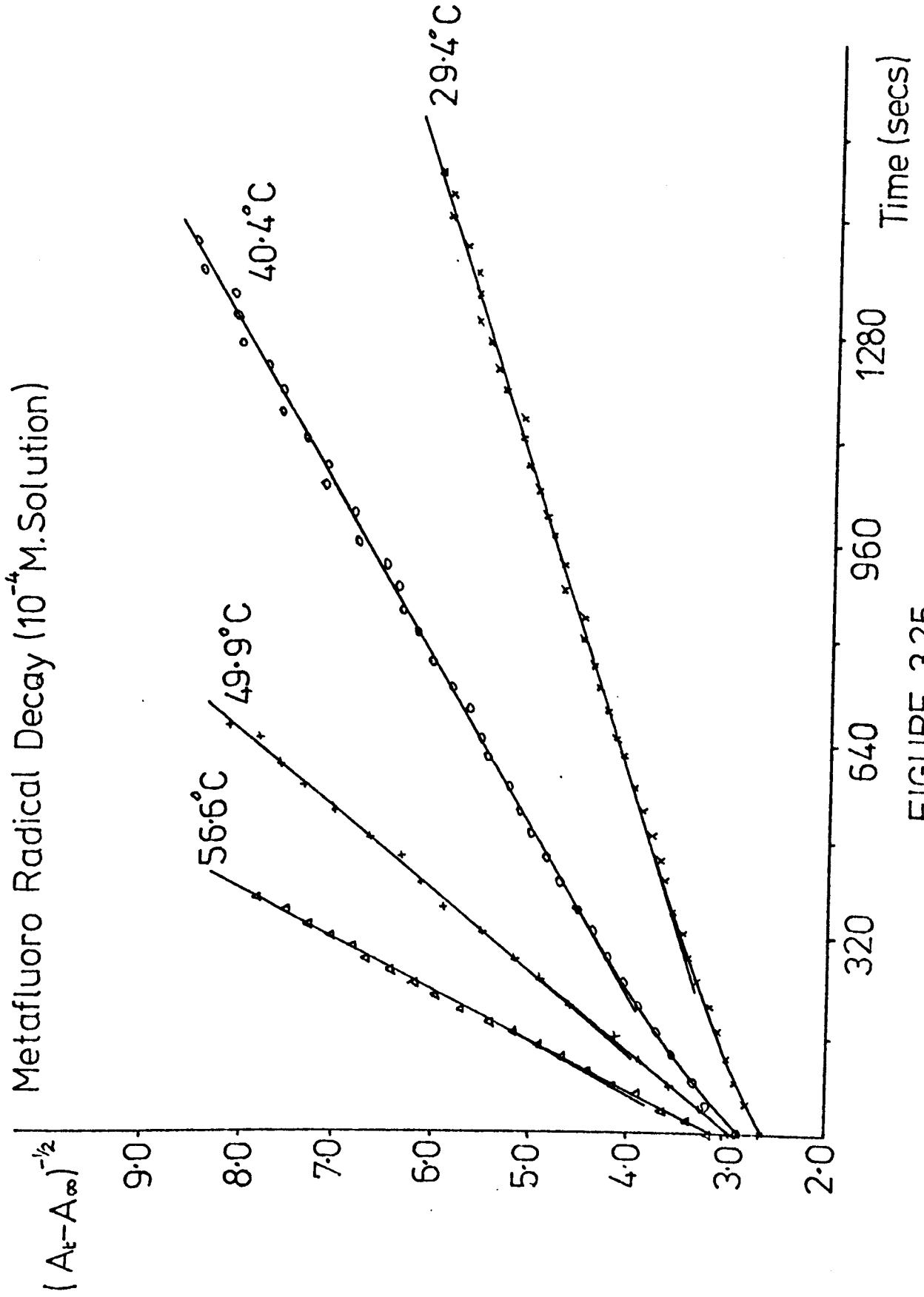


FIGURE 3.25

Table 15

10^{-4} M metafluoro dimer. Variation of gradients G_2 and $G_{3/2}$ with temperature.

Temp. K	G_2 (min^{-1}) $\times 10$	$G_{3/2}$ (min^{-1}) $\times 10$	$\log G_2$ $+ 1$	$\log G_{3/2}$ $+ 1$	$1/T \times 10^3$
302.9	9.40	1.27	0.9731	0.1038	3.301
302.8	9.28	1.30	0.9675	0.1139	3.302
302.8	9.40	1.37	0.9731	0.1367	3.302
309.3	16.2	2.03	1.2094	0.3075	3.233
309.3	15.1	1.96	1.1790	0.2923	3.233
313.6	17.7	2.62	1.2480	0.4183	3.189
311.8	17.8	2.66	1.2504	0.4249	3.201
317.1	26.1	3.33	1.4166	0.5230	3.154
317.2	-	3.78	-	0.5775	3.153
318.0	24.7	3.76	1.3927	0.5752	3.145
322.9	32.7	4.59	1.5145	0.7114	3.097
322.9	33.9	4.64	1.5302	0.7345	3.097
323.1	36.5	4.88	1.5623	0.7499	3.095
323.5	39.9	4.92	1.6010	0.7789	3.091
328.7	46.3	6.85	1.6656	0.8357	3.042
329.6	51.3	7.48	1.7101	0.8739	3.034

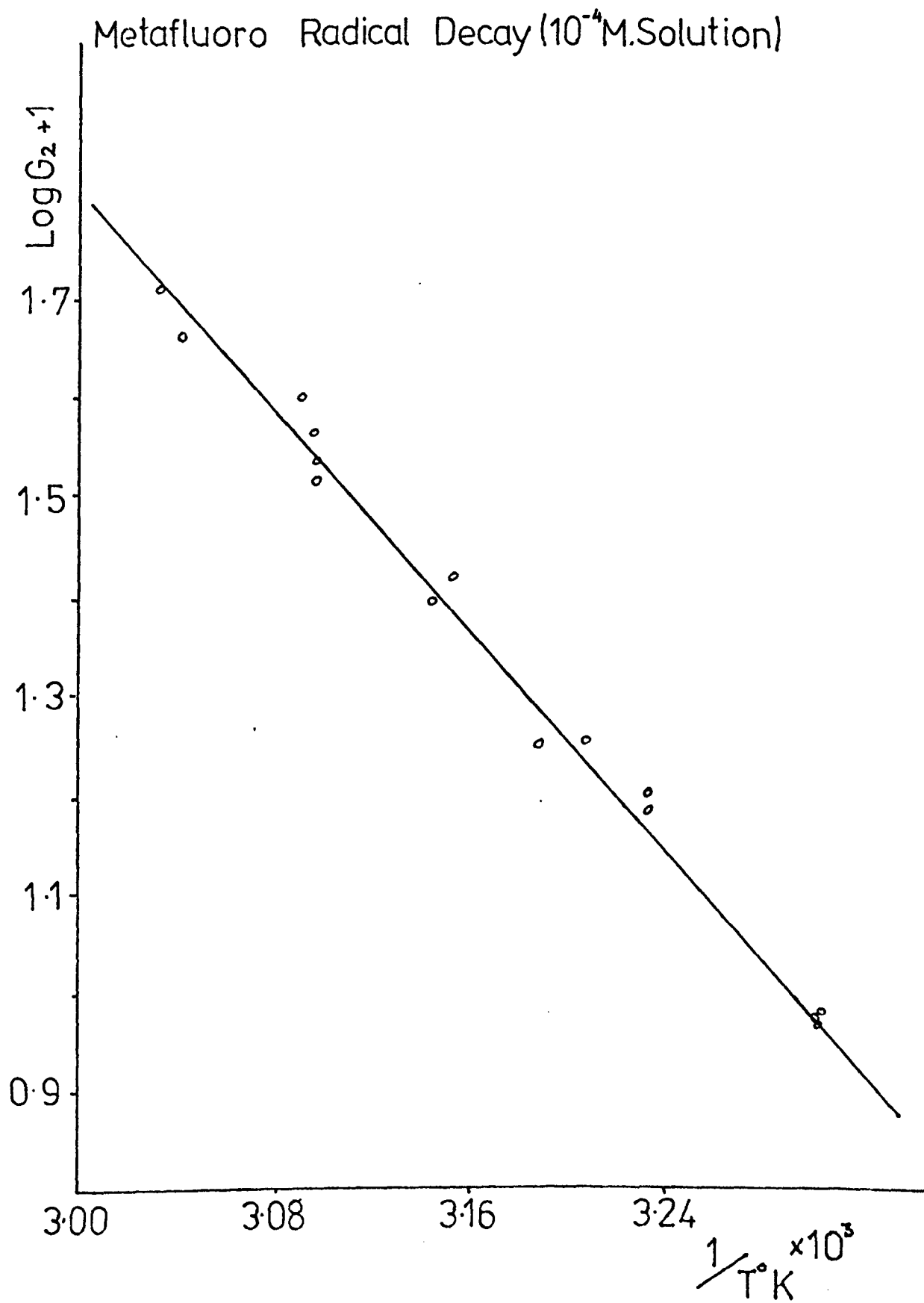


FIGURE 3.26

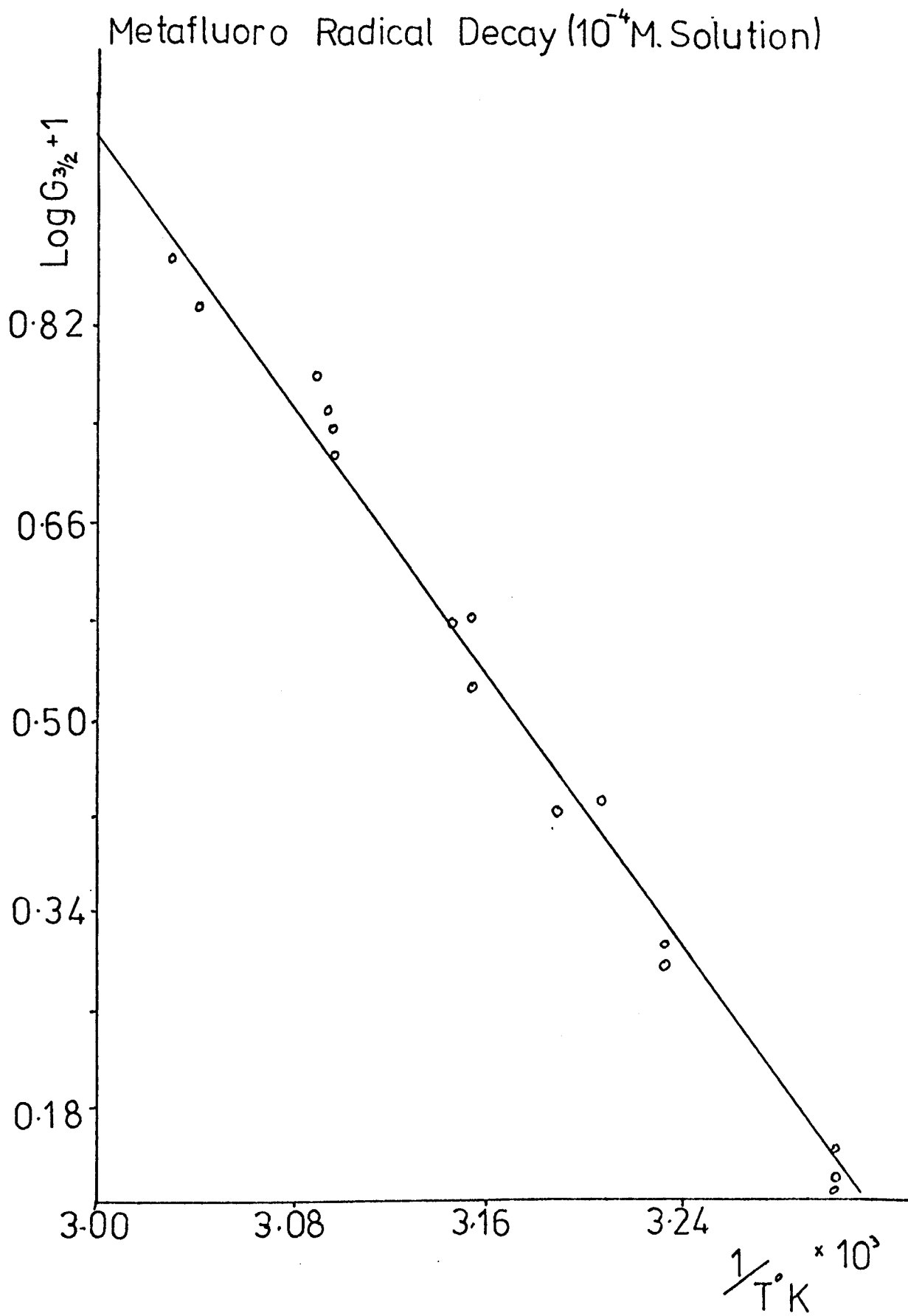


FIGURE 3.27

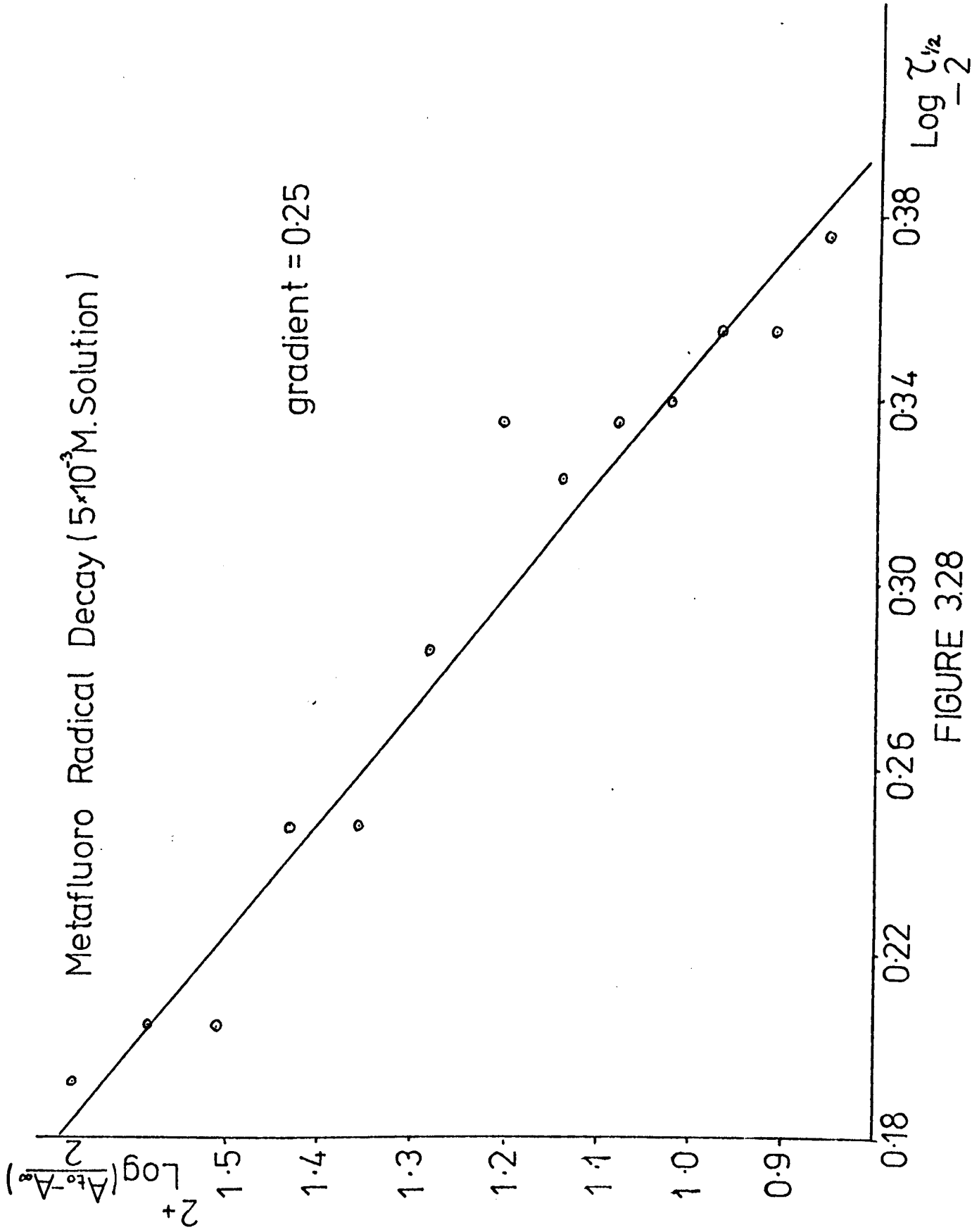


FIGURE 3.28

was adopted (Figure 3.29). The relationship between gradient and temperature, shown in Table 16 and Figure 3.30, gives the activation energy of the process to be 73 ± 5 kJoules.

As the metafluoro compound behaved so much like the parent dimer at all other concentrations, an investigation was carried out to see if a 5.10^{-3} M solution of the hexaphenyl biimidazole also gave a reaction of 6/5 order. An example of the results obtained is shown in Table 17, and Figure 3.31 illustrates the fact that once more the behaviour of both solutions is parallel. The Arrhenius plot (Table 18 and Figure 3.32) gives the activation energy to be 64 ± 7 kJoules.

3.2 Calculation of Rate Constants

The integrated rate equation is given by equation 3.3 as

$$\frac{1}{(n-1)c^t}^{n-1} = Kt + \text{const. for } n \neq 1$$

$$\text{or } \log e c t = -Kt + \text{const. for } n = 1$$

where K is the rate constant of the reaction (of order n)

Substituting $c = A/\epsilon$ from equation 3.1

$$\frac{1}{(n-1)(A/\epsilon)^{n-1}} = Kt + \text{const. for } n \neq 1$$

$$\text{or } \frac{1}{A} n^{-1} = \frac{K(n-1)t}{\epsilon^{n-1}} + \text{const.}$$

Now, if the gradient of the plot of optical density against time is G,

$$K = \frac{\epsilon^{n-1} G}{n-1} \quad 3.8$$

Thus from G and ϵ the rate constant K may be calculated. The problem then lies in finding ϵ .

3.3 Calibration of Spin Content of the Carbon Reference Sample

The card to be used in the determination of spin concentrations (see Chapter 2) was tested for uniformity of area per unit weight, and the results are given in Table 19. Using this card, comparison of the areas under the constructed ESR absorption profiles, obtained from the diphenylpicrylhydrazyl solution, with those from carbon produced under identical conditions was made, and the results along with the Q values for the cavity during each run, are tabulated

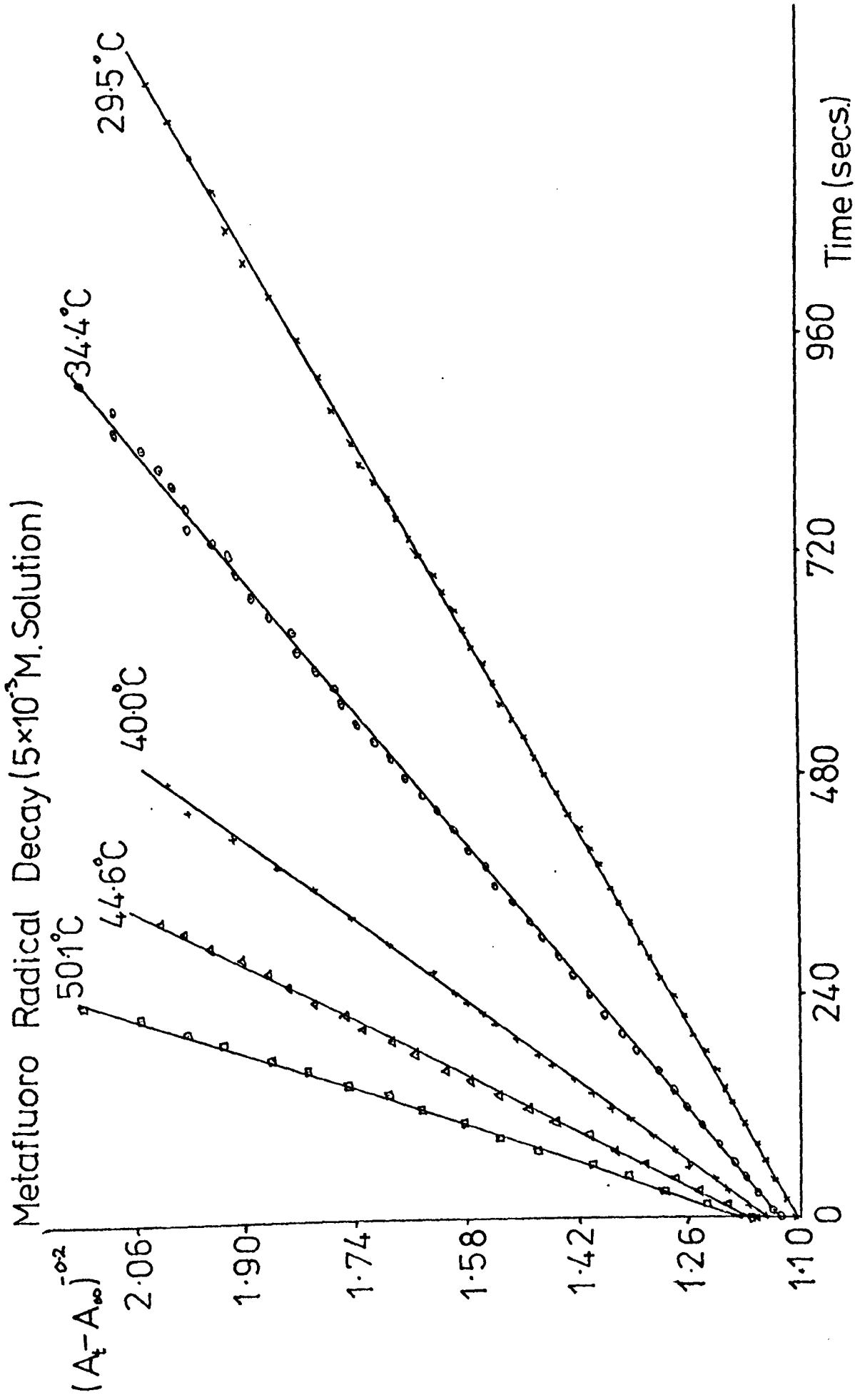


FIGURE 3.29

Table 16

$5 \cdot 10^{-3} \text{M}$, metafluoro dimer. Variation of gradient $G_{6/5}$ with temperature.

Temp K	$G_{6/5}$ (min^{-1})	$\log G_{6/5}$ + 2	$1/T \times 10^3$
302.5	0.046	0.6628	3.306
303.2	0.044	0.6435	3.298
307.4	0.068	0.8325	3.253
307.3	0.066	0.8195	3.254
313.2	0.113	1.0531	3.193
313.0	0.119	1.0755	3.195
317.6	0.170	1.2304	3.149
318.2	0.170	1.2304	3.143
318.1	0.160	1.2041	3.144
322.8	0.254	1.4048	3.098
323.1	0.238	1.3766	3.095
322.6	0.243	1.3856	3.100
327.5	0.360	1.5563	3.053

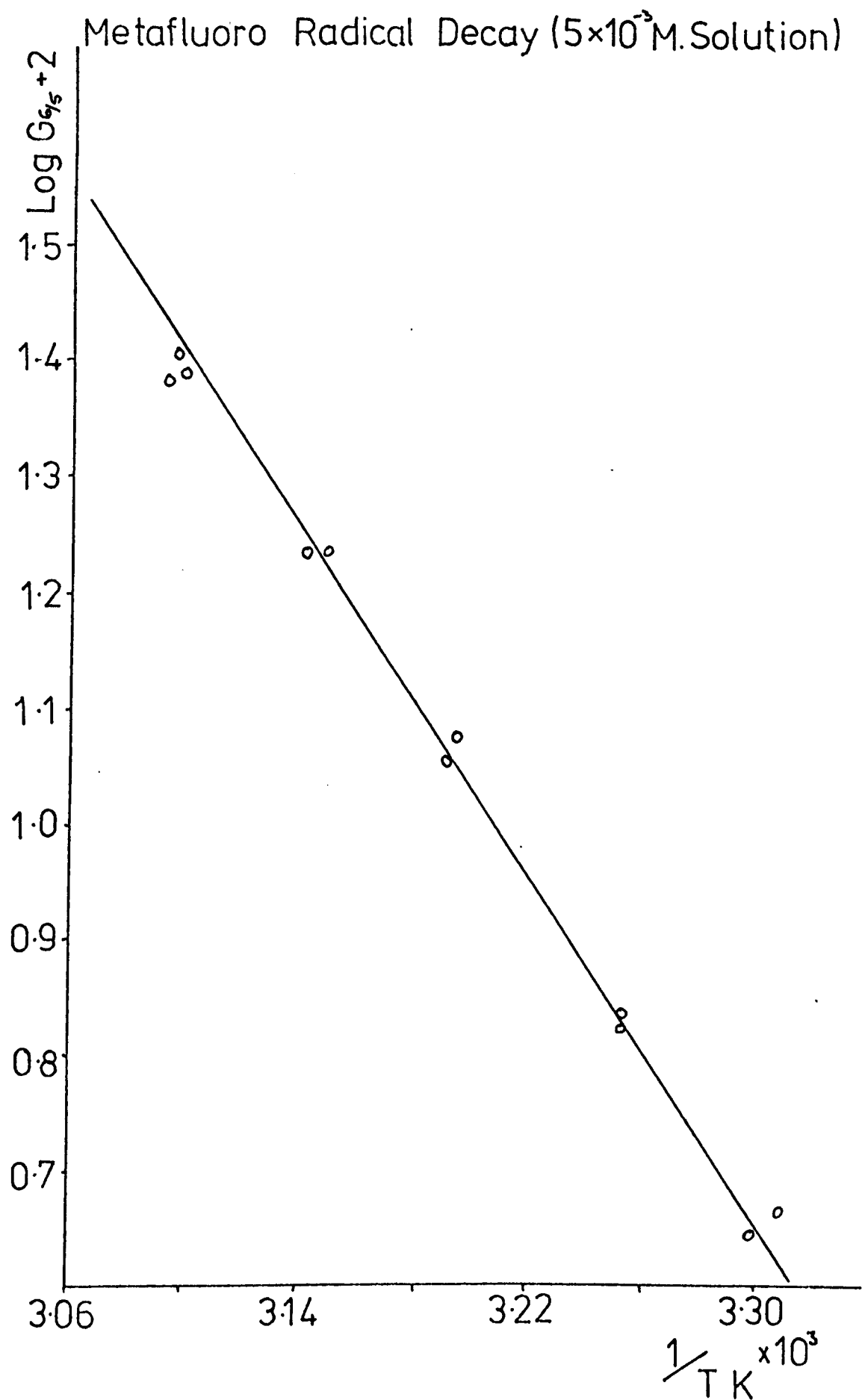


FIGURE 3.30

Table 17

Specimen data for the O.D. decrease with time for a $5.10^{-3}M$ solution of the lophinyl radical dimer.

Temp = $30.2^{\circ}C$

Time (secs)	(O.D. - O.D. $_{\infty}$)	$1/(O.D. - O.D._{\infty})^{1/5}$
0	0.8400	1.0355
40	0.7150	1.0694
80	0.6160	1.1018
120	0.5330	1.1341
160	0.4630	1.1665
200	0.3980	1.2023
240	0.3420	1.2394
280	0.3020	1.2706
320	0.2680	1.3013
360	0.2380	1.3326
400	0.2100	1.3663
440	0.1840	1.4029
480	0.1650	1.4338
520	0.1460	1.4694
560	0.1300	1.5039
600	0.1180	1.5333
640	0.1060	1.5665
680	0.0900	1.6186
720	0.0860	1.6334
760	0.0800	1.6572
800	0.0690	1.7070
840	0.0610	1.7496
880	0.0590	1.7613
920	0.0560	1.7798
960	0.0520	1.8063

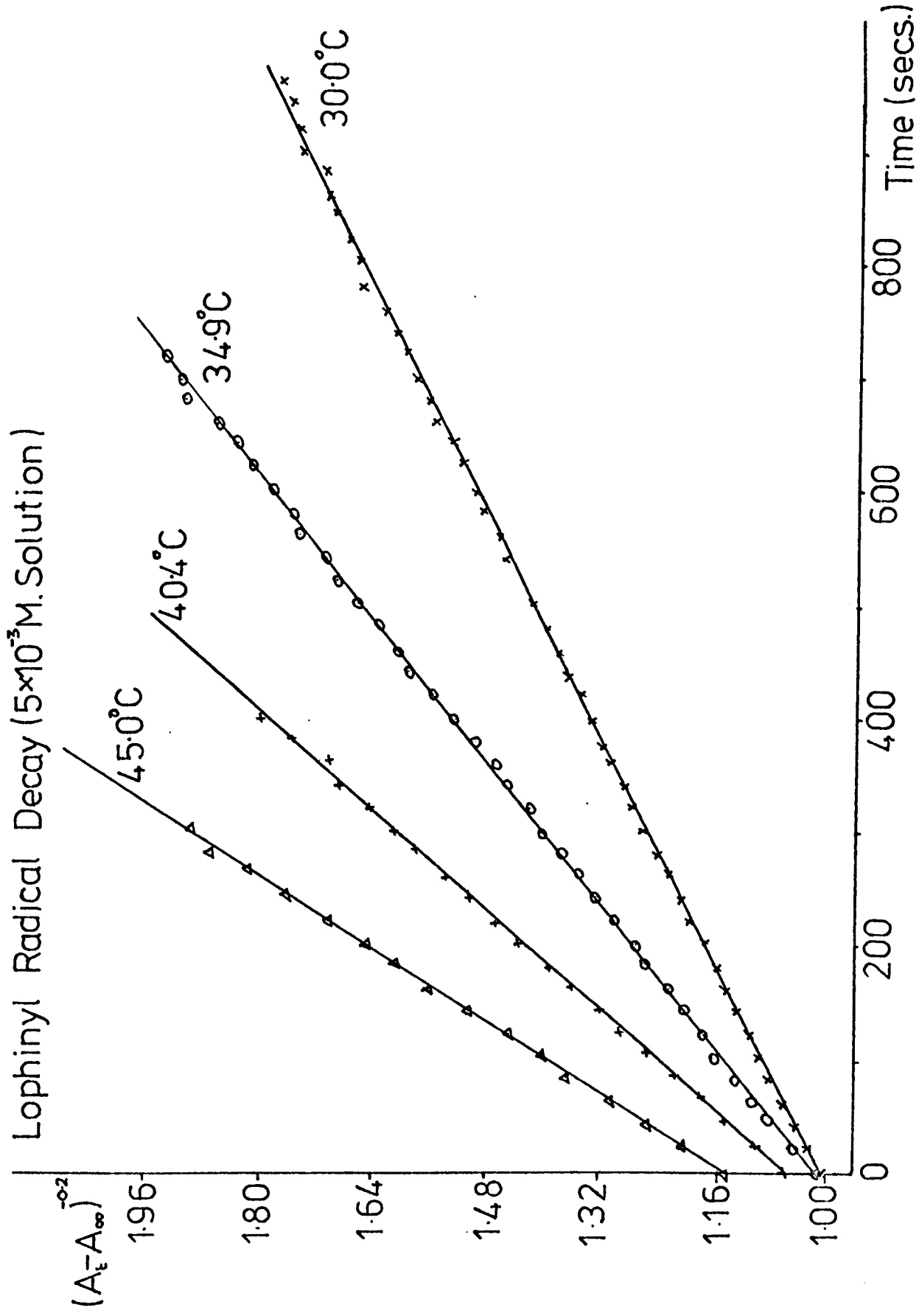


FIGURE 3.31

Table 18

$5 \cdot 10^{-3}$ M lophinyl radical dimer. Variation of gradient $G_{6/5}$ with temperature.

Temp K	$G_{6/5}$ $\text{min}^{-1} \times 10^2$	$\log G_{6/5}$ + 2	$1/T$ $\times 10^3$
303.2	4.90	0.6902	3.296
303.0	4.86	0.6866	3.298
302.1	4.72	0.6739	3.302
307.5	7.61	0.8814	3.250
308.3	7.71	0.8871	3.242
313.4	11.32	1.0539	3.191
312.7	10.62	1.0261	3.196
313.4	10.96	1.0399	3.191
317.1	13.72	1.1373	3.152
318.0	15.80	1.1987	3.143

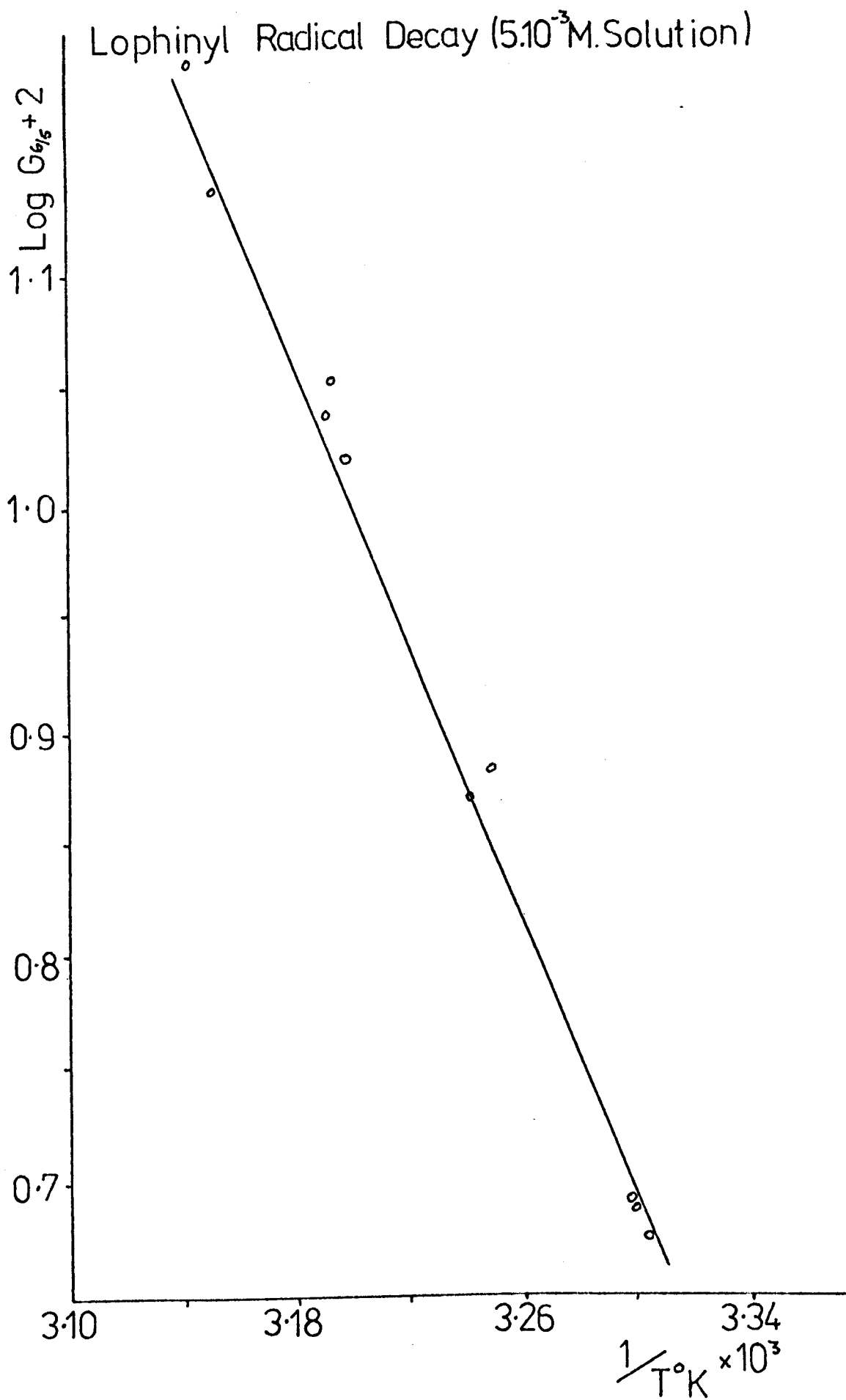


FIGURE 3.32

Table 19

Uniformity of Card

Area (cm ²)	wt (g ⁻¹)	Area per unit weight (cm ² g ⁻¹)
600	19.5920	30.6247
550	17.9268	30.6803
500	16.2950	30.6843
450	14.6223	30.7538
400	13.0009	30.7671
350	11.3889	30.7317

Average area per unit weight = 30.7070 cm²g⁻¹

Standard deviation = 0.0501

= 0.16%

in Table 20. Using equation 2.1, then, the number of spins contained in the carbon sample were calculated (1.70×10^{16} spins).

3.4 Calculation of ϵ for the Radicals

Using the above value for carbon, the number of radicals contained in each of the bi-imidazolyl solutions were then assessed by comparing the first moments of their derivative ESR signals with the carbon, run at the same temperature. Tables 21, 22 and 23 give the number of spins in $5 \cdot 10^{-3} M$ solutions of 2, 2' metafluorophenyl, 2, 2' parafluorophenyl 4,4',5,5' tetraphenyl bi-imidazole, and 2, 2', 4, 4', 5, 5' hexaphenyl bi-imidazole respectively, at various temperatures. As the ESR signal obtained for the carbon showed no temperature variation, averages for its first moment and Q value were taken. (Table 24 shows similar results obtained from an experiment carried out on a $10^{-3} M$ solution of 2, 2', 4, 4', 5, 5' hexaphenyl bi-imidazole). The radical concentrations were then calculated using the relationship

$$c = \frac{Sx}{6.023 \times 10^{23}} \times Vx \quad 3.9$$

where c is the radical concentration in moles per litre, Sx is the number of spins in solution, and Vx is the volume of the solution in litres ($0.2 \times 10^{-3} l$). The values of c for the solutions, together with their optical density obtained at the same temperatures are given in Tables 25, 26 and 27. As the path length used to obtain the optical density was 1 cm, the ratio A/c gives ϵ , the extinction coefficient. Table 28 gives the corresponding result for the $10^{-3} M$ solution of the hexaphenyl biimidazole, and shows that variation of the dimer concentration had no measurable effect on the extinction coefficient.

As mentioned in the experimental section, the extinction coefficient for the 2 ortho-fluorophenyl radical could not be calculated in the same way, owing to the lack of thermochromism of the bi-imidazole. To overcome this problem, a kinetic run was carried out on a $10^{-3} M$ solution of the dimer, using the E.S.R.

Table 20

Calibration of carbon sample

Concentration of d.p.p.h.solution = 1.222×10^{17} spins/0.2 ml.

d.p.p.h.		carbon		No. of spins in carbon $\times 10^{-16}$
Wt. of area under curve	Q value	Wt. of area under curve	Q value	
1.3625	4085	0.1560	3464	1.652
1.3625	4085	0.14806	3492	1.557
1.7764	4080	0.2598	3500	2.099
1.7764	4080	0.2246	3492	1.810
1.1888	4080	0.1238	3500	1.490
1.1888	4080	0.1312	3488	1.580

Average value for carbon sample = 1.70×10^{16}
spins/0.2 ml.

Standard deviation = 0.22

= 13%

Table 21

Spin count for a 0.2 ml. of a $5 \cdot 10^{-3} M$ solution of 2,2' meta-fluorophenyl, 4,4',5,5' tetraphenyl bi-imidazole.

Temp	Bi-imidazole		Carbon		No. of spins in solution $\times 10^{-15}$
$^{\circ}C$	Mr.	Q Value	Mr.	Q Value	
58.1	0.3584	4150			2.950
67	0.5450	4140	1.6659	3500	4.710
63.2	0.4659	4120			4.042
48.9	0.5503	4100			1.919

Table 22

Spin count for 0.2 ml. of a $5 \cdot 10^{-3} M$ solution of 2,2' para-fluorophenyl 4,4',5,5' tetraphenyl bi-imidazole.

Temp	Bi-imidazole		Carbon		No. of spins in solution $\times 10^{-15}$
$^{\circ}C$	Mr.	Q. Value	Mr.	Q Value	
56.4	0.4540	4180	2.7860	3680	2.434
66.4	0.6465	4140			3.508
63.0	0.5295	4180	2.4656	3770	3.300
50.3	0.3750	4180			2.335

Table 23

Spin count for 0.2 ml. of a $5 \cdot 10^{-3}$ M solution of 2,2',4,4',5,5' hexaphenyl bi-imidazole.

Temp	bi-imidazole		Carbon		No. of spins in solution $\times 10^{15}$
$^{\circ}\text{C}$	Mr	Q Value	Mr	Q Value	
40.7	2.062	4300	8.905	3770	3.452
59.9	4.365	4340			7.250
52.9	3.516	4350			5.815
45	2.087	4380			3.434

Table 24

Spin count for a 0.2 ml. of a 10^{-3} M solution of 2,2',4,4',5,5' hexaphenyl bi-imidazole.

Temp	bi-imidazole		Carbon		No. of spins in Solution $\times 10^{15}$
$^{\circ}\text{C}$	Mr	Q Value	Mr	Q Value	
62 $^{\circ}\text{C}$	0.4582	4120	1.3218	3710	2.656

Table 25

Calculation of ϵ for 2 metafluorophenyl 4, 5 diphenyl imidazolyl radical.

Temp °C	Concentration of radicals $c \times 10^5$	O. D. A	$\epsilon = A/c$
58.1	2.452	0.1765	7,215
67.0	3.914	0.2780	7,110
63.2	3.359	0.2268	6,770
48.9	1.574	0.1150	7,315

Average value for $\epsilon = 7,103$

Standard deviation = 237

Standard deviation of the mean = 118

$\epsilon = 7,100 \pm 120$

Table 26

Calculation of ϵ for 2 parafluorophenyl 4,5 diphenylimidazolyl radical

Temp °C	Concentration of radicals $c \times 10^5$	O. D. A	$\epsilon = A/c$
56.4	2.022	0.1700	8,320
66.4	2.918	0.2375	8,140
63.0	2.744	0.2118	7,725
50.3	1.941	0.1316	6,785

Average value for $\epsilon = 7,743$

Standard deviation = 685

Standard deviation of the mean =

343

$\epsilon = 7,740 \pm 340$

Table 27

Calculation of ϵ for 2, 4, 5 triphenyl imidazoly radical

Temp °C	concentration of radicals $c \times 10^5$	O. D. A	$\epsilon = A/c$
40.7	2.865	0.160	5,590
59.9	6.020	0.406	6,740
52.9	4.838	0.306	6,335
45.0	2.852	0.207	7,270

Average value for $\epsilon = 6,484$

standard deviation = 708

standard deviation of the mean = 354

$$\epsilon = 6,480 \pm 350$$

Table 28

Calculation of ϵ for 2, 4, 5 triphenyl imidazoly radical (from a $10^{-3}M$ solution).

Temp °C	concentration of radicals $c \times 10^5$	O. D. A	$\epsilon = A/c$
62	2.656	0.1806	5,730

$$\epsilon = 5730$$

machine, and this was compared to a kinetic run obtained from the same solution at the same temperature using the SP800 spectrophotometer. The relationship, then, between the two runs is given by equation 3.8 as

$$K = \frac{\epsilon^{n-1} G}{n - 1}$$

As $n=2$ for the orthofluoro compound, equation 3.8 may be rearranged to

$$\epsilon = \frac{K_2}{G}$$

where K_2 is the rate constant, and the gradient of the plot of reciprocal of radical concentration against time (from E.S.R.) and G is the gradient of the plot of reciprocal of the optical density against time (from the U.V./Visible spectrometer).

Having already obtained G , Table 4, the reverse photochromic process was followed using the E.S.R. spectrometer by recording a spectrum at certain time intervals (after the period of illumination) as the radicals recombined to form the bi-imidazole. Now, as each derivative curve is of the same spectral line width and shape function, and as experimental conditions were left unaltered for the duration of the run, the relative radical concentration N_1/N_2 for two signals 1 and 2, should be equal to h_1/h_2 the ratio of the peak heights of their derivative curves, i.e. $N_1 \propto h_1$. The constant of proportionality, k , between N_1 and h_1 will be the concentration of spins in a signal of unit height. Now as the reaction had already been found to be second order, a plot of $1/ht$ against t , the time of recording, was expected to give a straight line with gradient equal to $K_2 \times k$. An example of a plot of this kind is shown in Figure 3.33, with the corresponding data in Table 29. A spin concentration determination was carried out on the first three signals of the decay run in the way described above, and from these results an average value for k was calculated (Table 30).

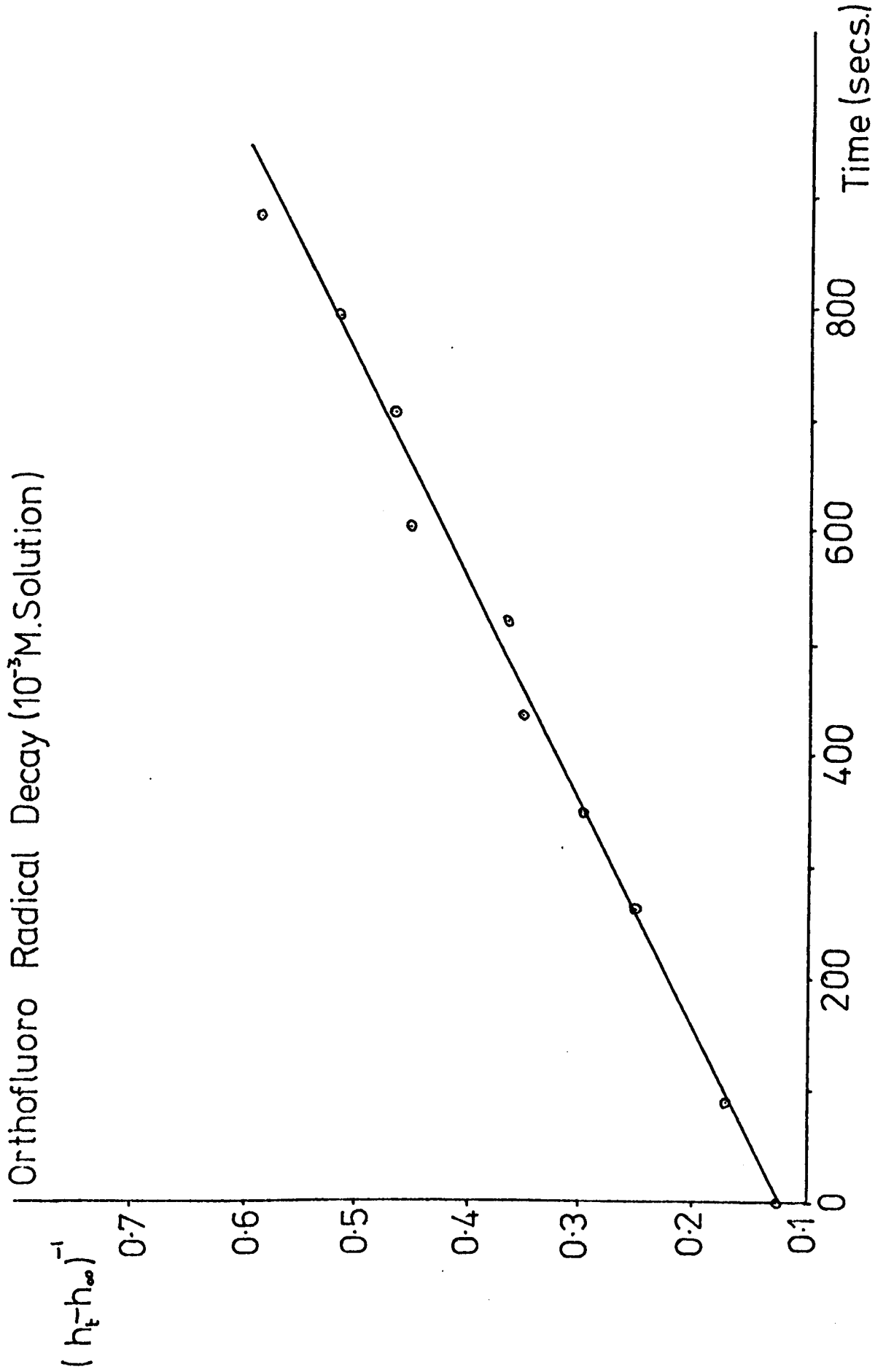


FIGURE 3.33

Table 29

Decrease in height of the E.S.R. signal of a $10^{-3}M$ orthofluoro dimer solution with time, after illumination.

Time (secs)	peak-peak ht. h_t cm.	$h_t - h_{\infty}$	$1/h_t - h_{\infty}$
0	8.28	7.76	0.1289
88.8	6.45	5.93	0.1686
175.4	5.70	5.18	0.1931
263.5	4.49	3.97	0.2519
348.4	3.89	3.37	0.2967
433.1	3.38	2.86	0.3497
519.1	3.26	2.74	0.3650
604.3	2.74	2.22	0.4505
705.6	2.67	2.15	0.4651
793.3	2.46	1.94	0.5155
879.6	2.22	1.70	0.5882
$h_{\infty} = 0.52$ cm.			

Table 30

Spin concentration determination on the first three peaks of the E.S.R. kinetic run, to determine the concentration in moles litre⁻¹ per unit height (k).

$(h_t - h_{\infty})$ cm.	No. of spins in solution	No. of spins per unit height	k $\times 10^6$
7.76	3.135×10^{15}	4.035×10^{14}	3.344
5.93	2.383×10^{15}	4.024×10^{14}	3.340
5.18	2.152×10^{15}	4.160×10^{14}	3.450

Av. k = 3.382×10^{-6}

$$\text{Temp} = 294.5^{\circ}\text{A}$$

$$k = 3.38 \times 10^{-6} \text{ moles l}^{-1}$$

$$K_2 k = 5.04 \times 10^{-4} \text{ sec}^{-1}$$

$$K_2 = 1.487 \times 10^2 \text{ moles}^{-1} \text{ sec}^{-1}$$

$$G = 1.425 \times 10^{-2} \text{ secs}^{-1}$$

$$\epsilon = \underline{10,440}$$

A second run of the same kind gave the following results

$$\text{Temp} = 294.7^{\circ}\text{A}$$

$$k = 2.798 \times 10^{-6} \text{ moles l}^{-1}$$

$$K_2 k = 5.3 \times 10^{-4} \text{ sec}^{-1}$$

$$K_2 = 1.869 \times 10^2 \text{ moles}^{-1} \text{ sec}^{-1}$$

$$G = 1.402 \times 10^{-2} \text{ sec}^{-1}$$

$$\epsilon = \underline{13,330}$$

Average value for $\epsilon = \underline{11890}$

The experimental values for ϵ , for the four types of radical investigated, are tabulated in Table 31 below.

Table 31	
Radical Type	extinction coefficient
2 orthofluorophenyl	11,890
2 metafluorophenyl	7,100
2 parafluorophenyl	7,740
parent imidazolyl radical	6,480

From these values then, it is possible to calculate, using equation 3.8, the rate constants of the various radical recombination processes from the gradients of the plots of the respective functions of optical density against time, G . Indeed, this was done, and Table 32 lists the rate constants for the processes at 303 K.

Table 32

Values of the rate constants for the various reactions.

Radical Type	Dimer conc.	Reaction order	K
Orthofluoro	$10^{-3}M$	2	$2.177 \times 10^4 \text{ moles}^{-1} \text{ min}^{-1} l^{+1}$
"	$5 \cdot 10^{-3}M$	2(i)	$1.458 \times 10^4 \text{ moles}^{-1} \text{ min}^{-1} l^{+1}$
"	"	2(ii)	$1.770 \times 10^4 \text{ moles}^{-1} \text{ min}^{-1} l^{+1}$
parafluoro	10^{-3}	$3/2$	$2.334 \times 10 \text{ moles}^{-\frac{1}{2}} \text{ min}^{-1} l^{+\frac{1}{2}}$
metafluoro	10^{-3}	$3/2$	$2.785 \times 10 \text{ moles}^{-\frac{1}{2}} \text{ min}^{-1} l^{+\frac{1}{2}}$
"	"	1	$7.52 \times 10^{-1} \text{ sec}^{-1}$
"	10^{-4}	2	$6.331 \times 10^3 \text{ mole}^{-1} \text{ min}^{-1} l^{+1}$
"	"	$3/2$	$1.153 \times 10 \text{ moles}^{-\frac{1}{2}} \text{ min}^{-1} l^{+\frac{1}{2}}$
"	$5 \cdot 10^{-3}$	$6/5$	$1.316 \text{ moles}^{-\frac{1}{5}} \text{ min}^{-1} l^{+\frac{1}{5}}$

3.5 Kinetics of the Generation of Radicals in Solution

The generation of radicals in $5 \cdot 10^{-3}$ and 10^{-3} M solutions of the ortho, meta and parafluoro dimers by light of wavelength $27,400 \text{ cm}^{-1}$ were studied as described in Section 2. A typical set of data is shown in Table 33, and an example of the optical density increase with time of illumination, at several temperatures, is given in Figure 3.34.

Ueda ¹⁴ has related the intensity of E.S.R. absorption y , with the time of illumination t of the dimer solution by the equation,

$$y = A(1 - e^{-kt})$$

From earlier discussion, however, it has been seen that the intensity of absorption is proportional to the concentration of radicals C_t , which in turn is proportional to the optical density due to the radicals $(A_t - A_\infty)$. Thus the Ueda equation above, can be rewritten,

$$(A_t - A_\infty) = (A_0 - A_\infty)(1 - e^{-kt}) \quad 3.9$$

where $(A_0 - A_\infty)$ is the optical density of the solution when in the photostationary state. This equation can then be rearranged to

$$\frac{\log (A_0 - A_\infty) - (A_t - A_\infty)}{(A_0 - A_\infty)} = -Kt$$

Figures 3.35 to 3.37 show that for all three 10^{-3} M solutions, the generation of radicals follow this relationship, and what is more, the gradients of the slopes are independent of temperature (Table 34). This seemingly concurs with work carried out by Prochoda and Krongauz ⁴⁹ who have found that the quantum yield of triphenyl imidazolyl radicals in benzene, using light of wavelength 33,000 wavenumbers, was about 1.0 indicating an unactivated process.

Table 33

Specimen data for the O.D. increase with time of illumination
for a 10^{-3} M solution of the parafluoro dimer solution.

Temp = 31.3°C

Time	$(A_t - A_\infty)$	$\frac{(A_0 - A_\infty) - (A_t - A_\infty)}{(A_0 - A_\infty)}$	$\log \frac{(A_0 - A_\infty) - (A_t - A_\infty)}{(A_0 - A_\infty)} + 2$
0	0.000	1.0000	2.0000
30	0.0415	0.8312	1.9197
60	0.0754	0.6932	1.8409
90	0.1064	0.5671	1.7537
120	0.1240	0.4955	1.6951
150	0.1426	0.4199	1.6231
180	0.1564	0.3637	1.5608
210	0.1718	0.3011	1.4786
240	0.1828	0.2563	1.4088
270	0.1904	0.2254	1.3529
300	0.1975	0.1965	1.2934
330	0.2024	0.1766	1.2461
360	0.2060	0.1619	1.2093
390	0.2116	0.1391	1.1434
420	0.2120	0.1375	1.1383
450	0.2150	0.1253	1.0980
480	0.2184	0.1115	1.0472
510	0.2240	0.0887	0.9479
540	0.2222	0.0960	0.9823

$(A_0 - A_\infty) = 0.2458$

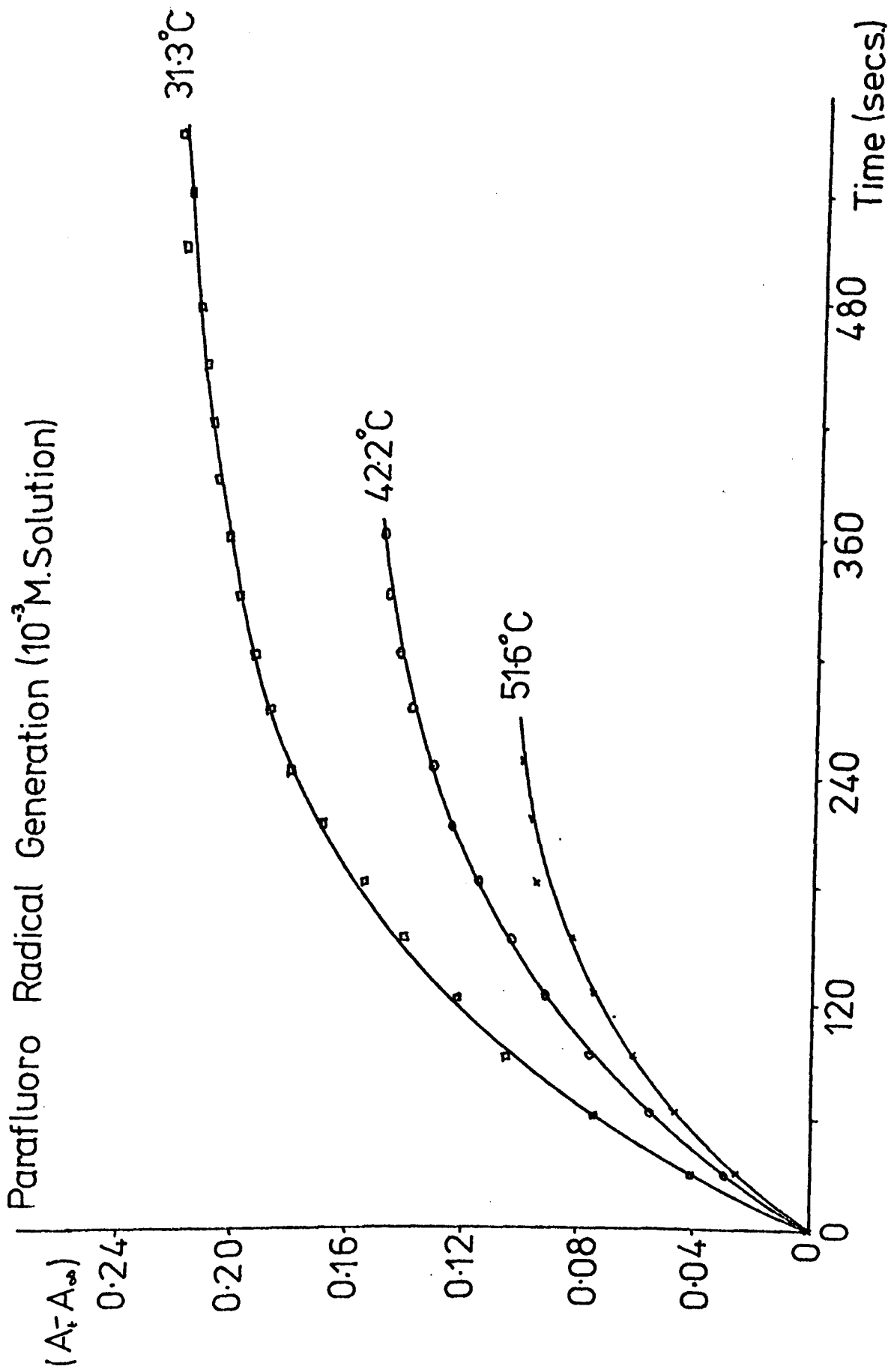


FIGURE 3.34

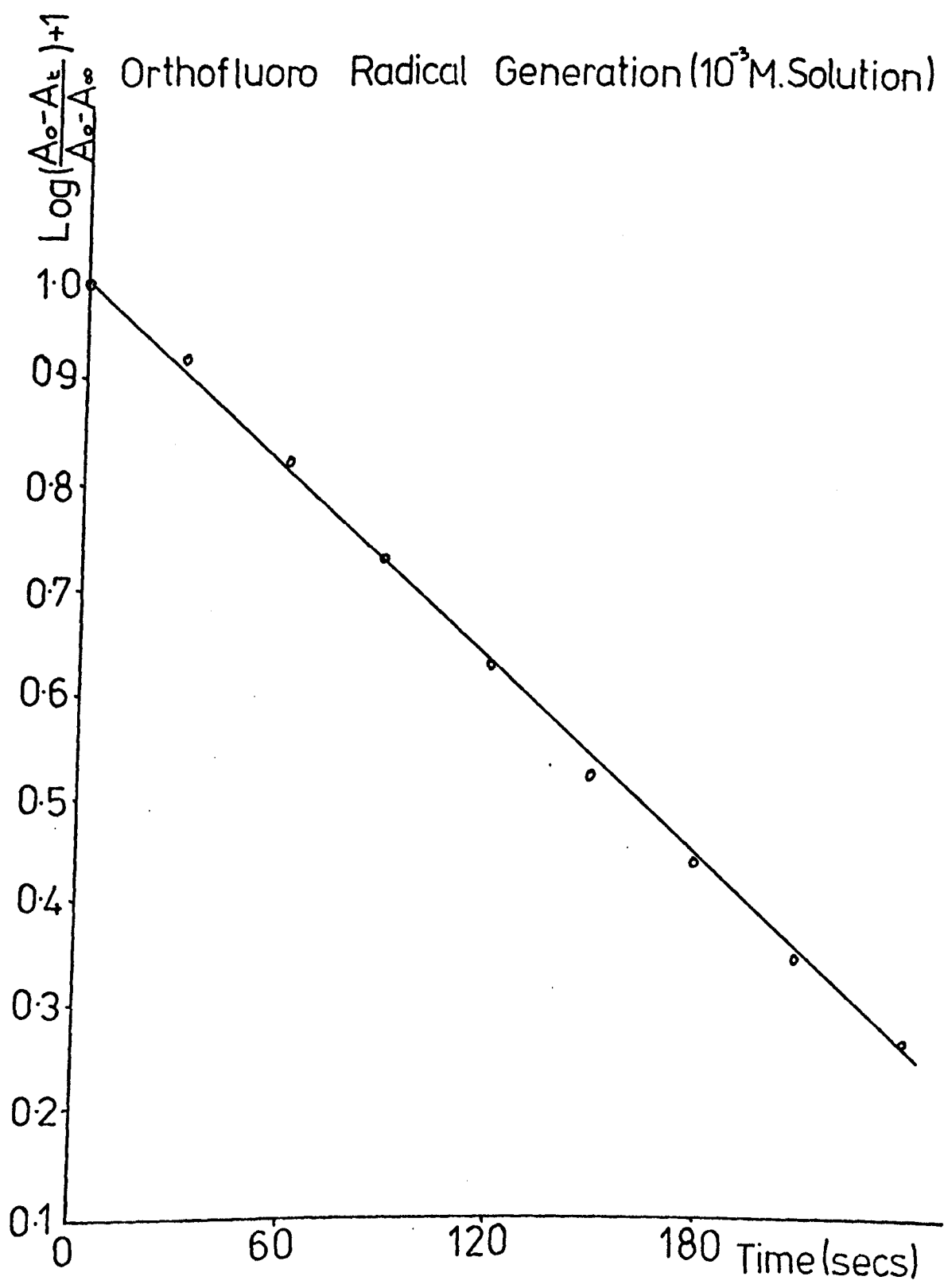


FIGURE 3.35

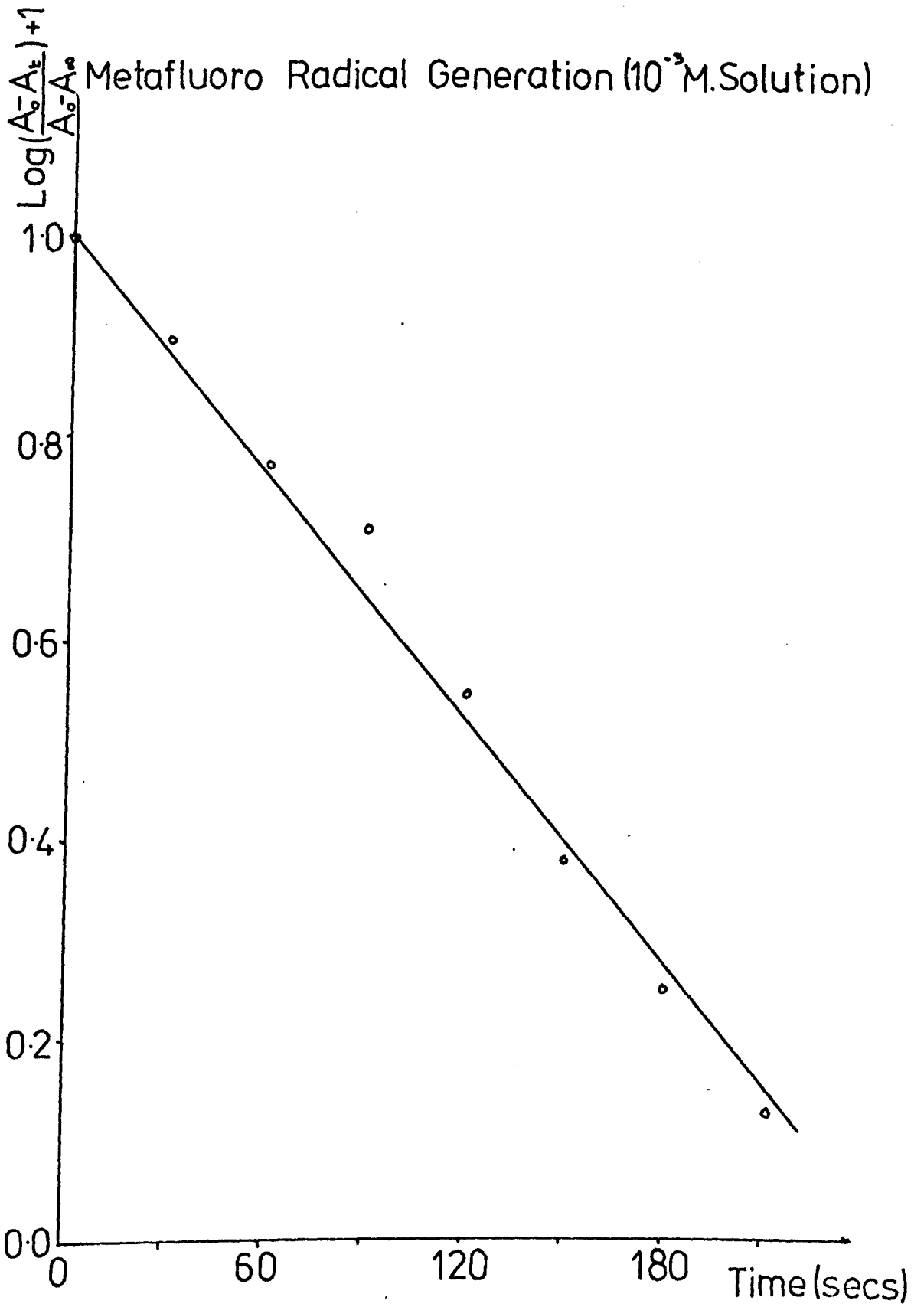


FIGURE 3.36

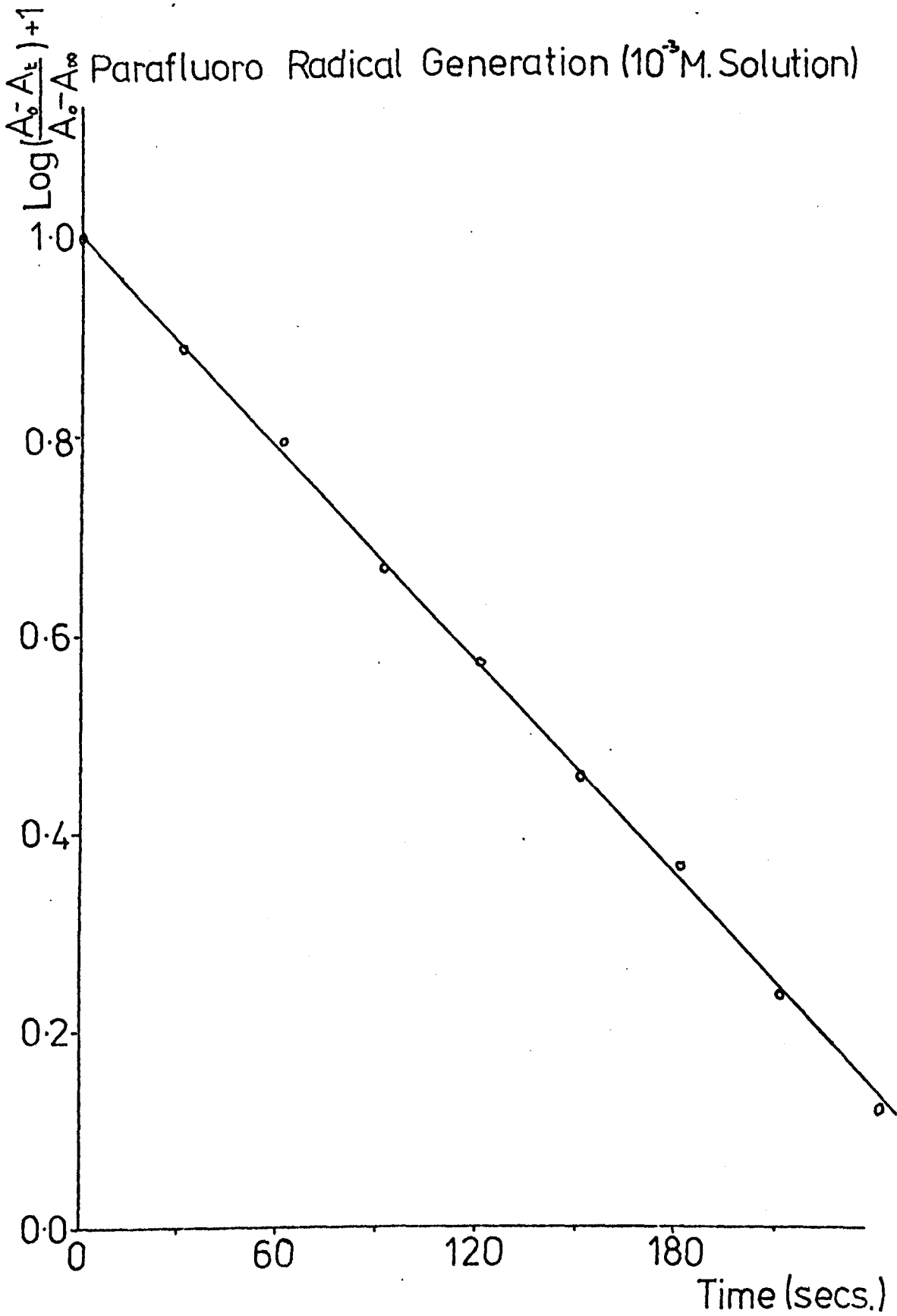


FIGURE 3.37

Table 34

(a) Variation of the gradient of the Ueda plot with temperature for a 10^{-3} M solution of 2,2' orthofluoro phenyl 4,4',5,5' tetraphenyl bi-imidazole.

Temp K	Gradient min^{-1}
302.2	0.244
307.0	0.240
307.4	0.180
311.5	0.180
315.5	0.180
323.6	0.244

(b) Variation of the gradient of the Ueda plot with temperature for a 10^{-3} M solution of 2,2' metafluoro phenyl 4,4',5,5' tetraphenyl bi-imidazole.

Temp K	Gradient min^{-1}
307.0	0.660
307.3	0.512
316.1	0.440
321.2	0.748
327.4	0.580
327.8	0.514

(c) Variation of the gradient of the Ueda plot with temperature for a 10^{-3} M solution of 2,2' parafluoro phenyl 4,4',5',5' tetraphenyl bi-imidazole.

Temp K	Gradient min^{-1}
301.5	0.202
304.3	0.152
305.4	0.208
311.7	0.152
320.2	0.286
324.6	0.242
328.7	0.374

All $5 \cdot 10^{-3} \text{M}$ solutions however, (Figures 3.38 to 3.40) although also obeying the Ueda relationship, do show temperature dependent gradients (Table 35). The plots of logarithm of gradient against temperature of run, for the three systems, are shown in Figures 3.41, 3.42 and 3.43. The reaction has apparently in some way become an activated process.

Orthofluoro Radical Generation (5×10^{-3} M. Solution)

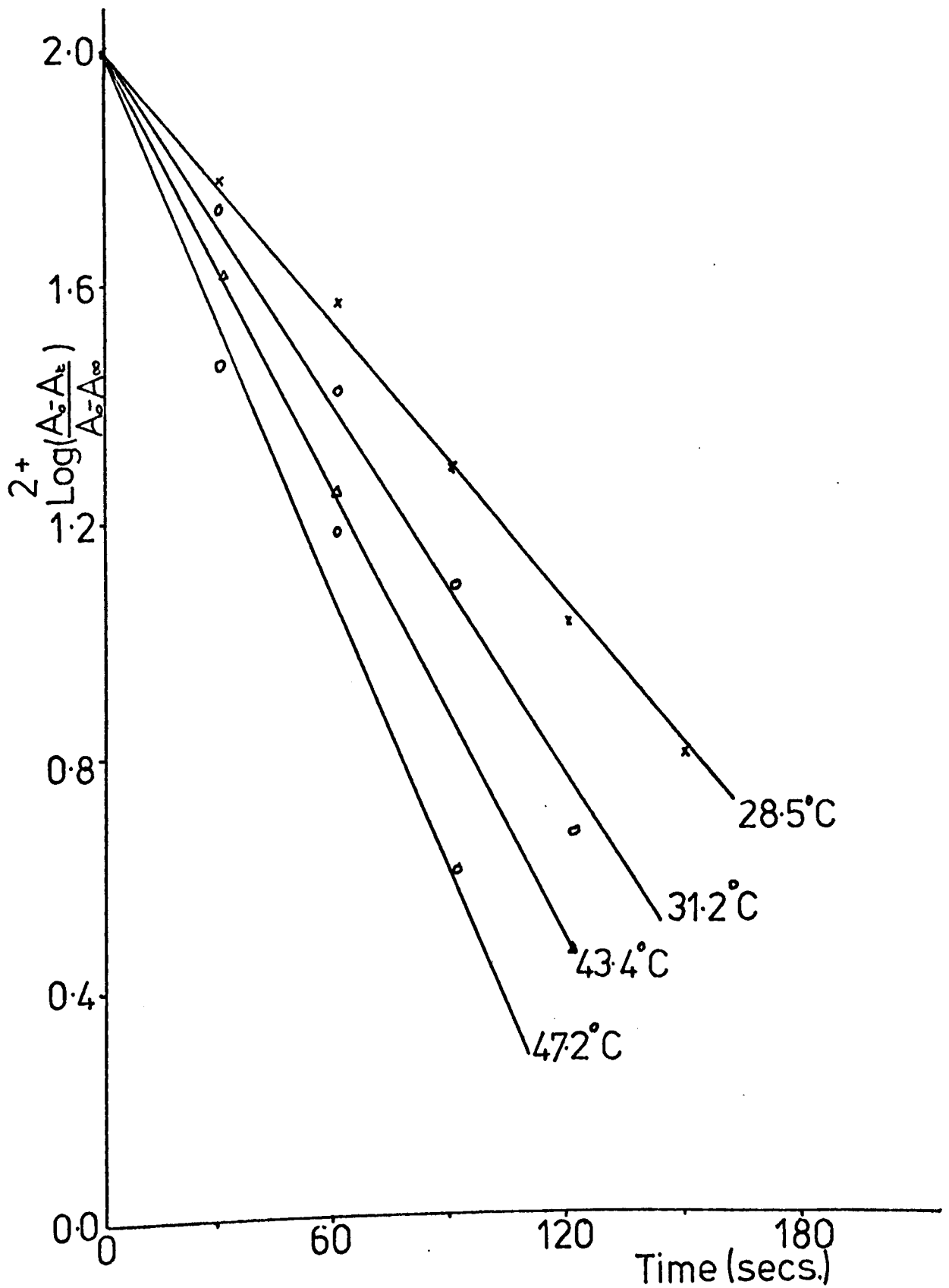


FIGURE 3.38

Metafluoro Radical Generation (5×10^{-3} M. Solution)

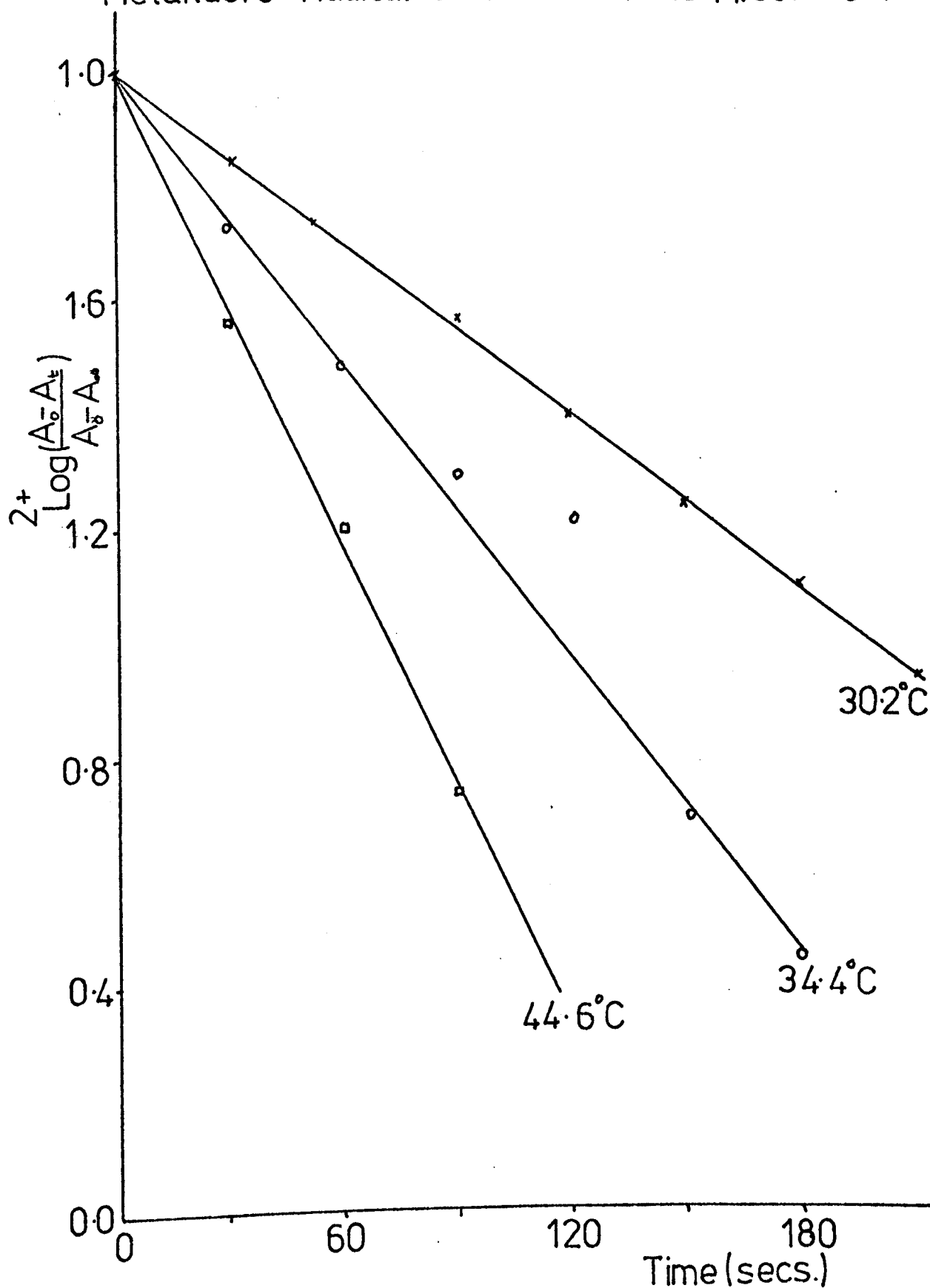


FIGURE 3.39

Parafluoro Radical Generation (5×10^{-3} M. Solution)

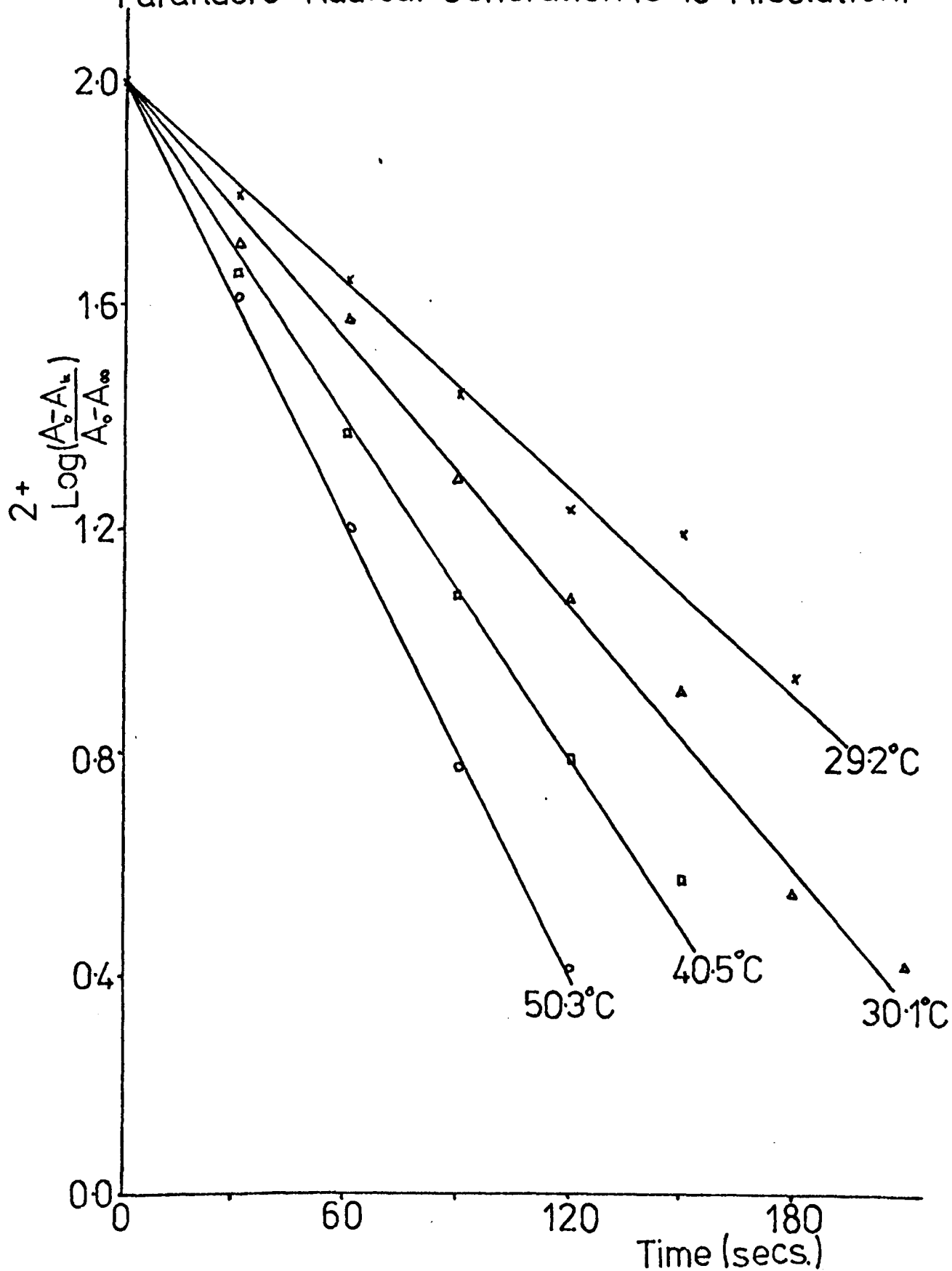


FIGURE 3.40

Table 35

(a) Variation of the gradient of the Ueda plot with temperature for a 5.10^{-3} M solution of 2,2' orthofluoro phenyl 4,4',5,5', tetraphenyl bi-imidazole.

Temp K	Gradient min^{-1}	$\log G$ + 1	$1/T \times 10^3$
301.5	0.488	0.6884	3.317
301.4	0.488	0.6884	3.318
304.2	0.622	0.7938	3.287
303.9	0.540	0.7324	3.290
311.4	0.726	0.8609	3.211
316.4	0.774	0.8887	3.161
320.2	0.932	0.9694	3.123

(b) Variation of the gradient of the Ueda plot with temperature for a 5.10^{-3} M solution of 2,2' metafluoro phenyl 4,4',5,5' tetraphenyl bi-imidazole.

Temp K	Gradient min^{-1}	$\log G$ + 1	$1/T \times 10^3$
303.2	0.308	0.4886	3.298
307.4	0.528	0.7226	3.253
313.2	0.580	0.7634	3.193
317.6	0.848	0.9284	3.149
322.6	1.142	1.0577	3.100

(c) Variation of the gradient of the Ueda plot with temperature for a $5 \cdot 10^{-3} \text{ M}$ solution of 2,2' orthofluorophenyl 4,4',5,5' tetraphenyl bi-imidazole.

Temp °K	Gradient min^{-1}	$\log G$ + 1	$1/T \times 10^3$
303.1	0.496	0.6955	3.299
308.4	0.550	0.7407	3.243
313.5	0.622	0.7938	3.190
318.5	0.642	0.8075	3.140
323.3	0.812	0.9096	3.093

Orthofluoro Radical Generation (5×10^{-3} M. Solution)

Activation Energy = 25.8 kJmol⁻¹

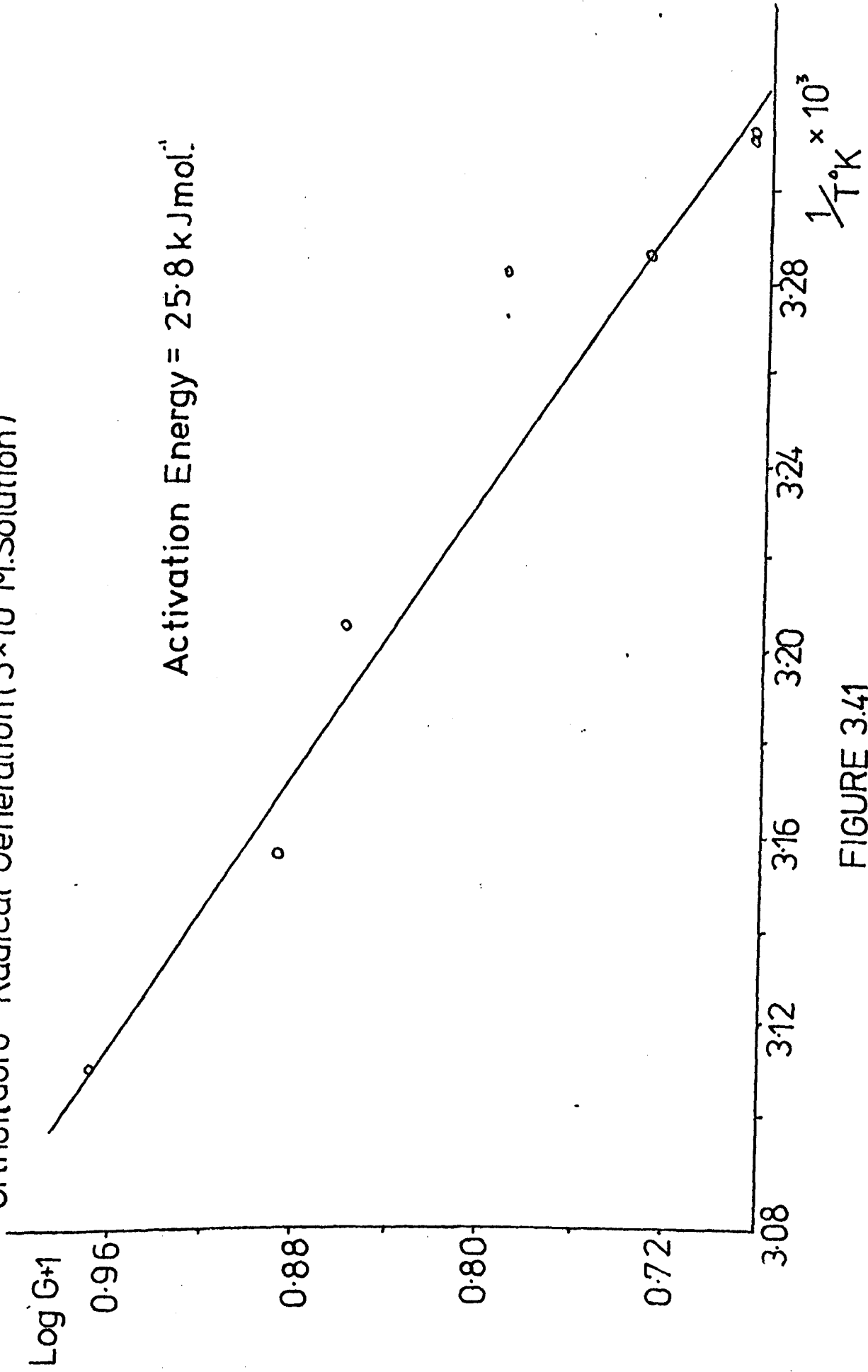


FIGURE 3.41

Metafluoro Radical Generation (5×10^{-3} M. Solution)

Log G₊₁

Activation Energy = 57.4 kJ.mol⁻¹

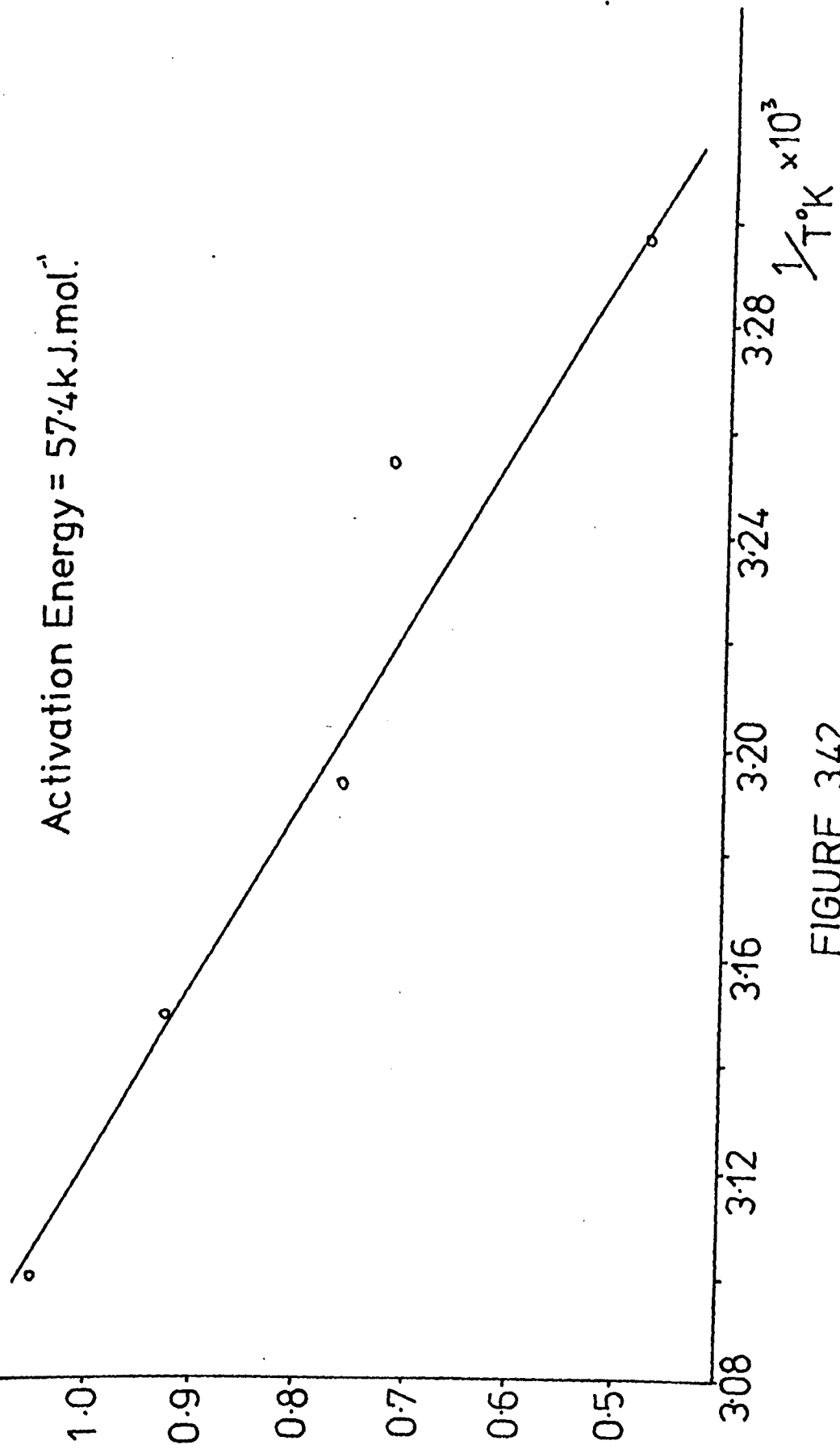


FIGURE 342

Paraffluoro Radical Generation (5×10^{-3} M. Solution)

$\text{Log } G_{+1}$

Activation Energy = 20.4 kJ.mol^{-1}

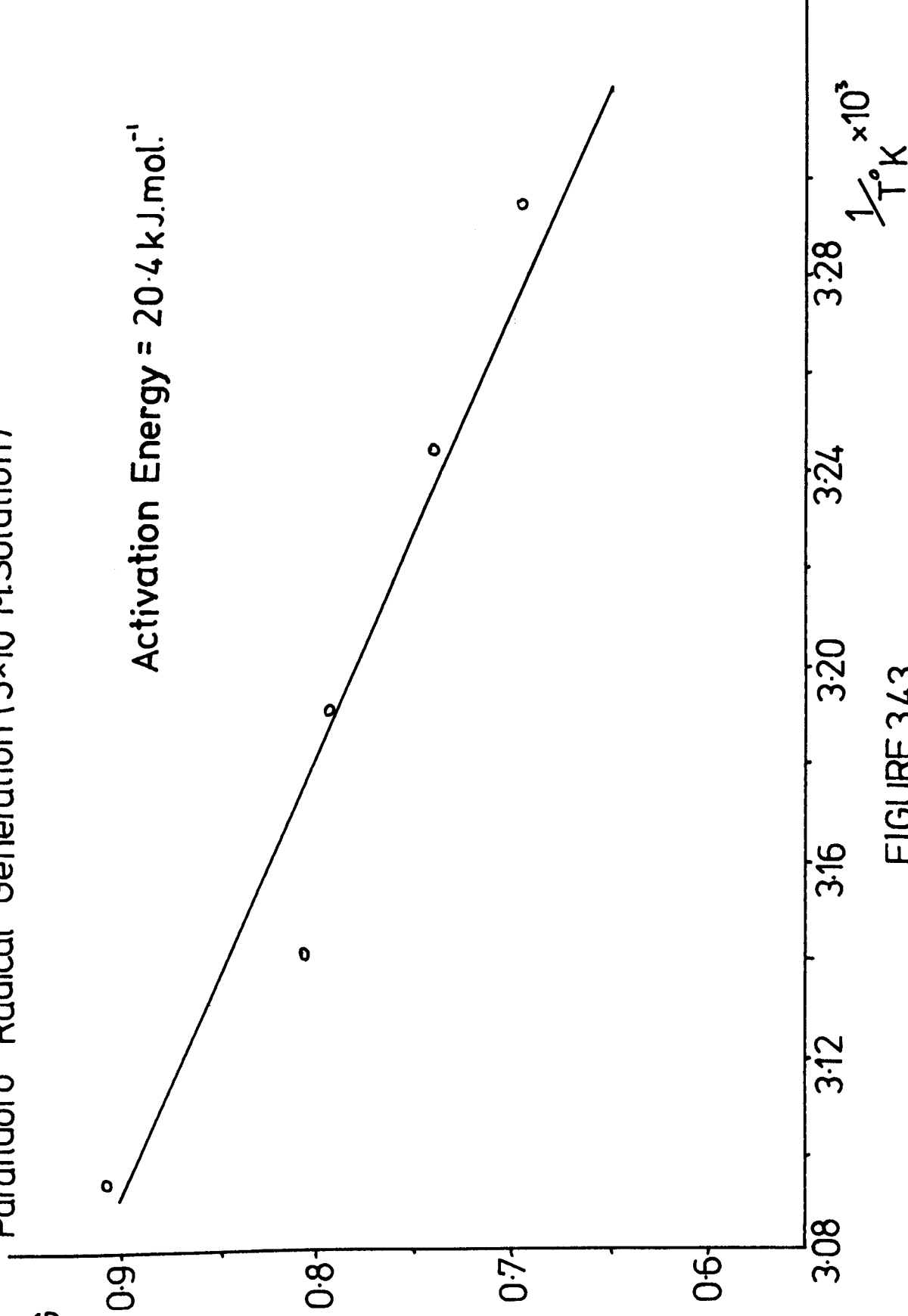


FIGURE 3.43

CHAPTER 4

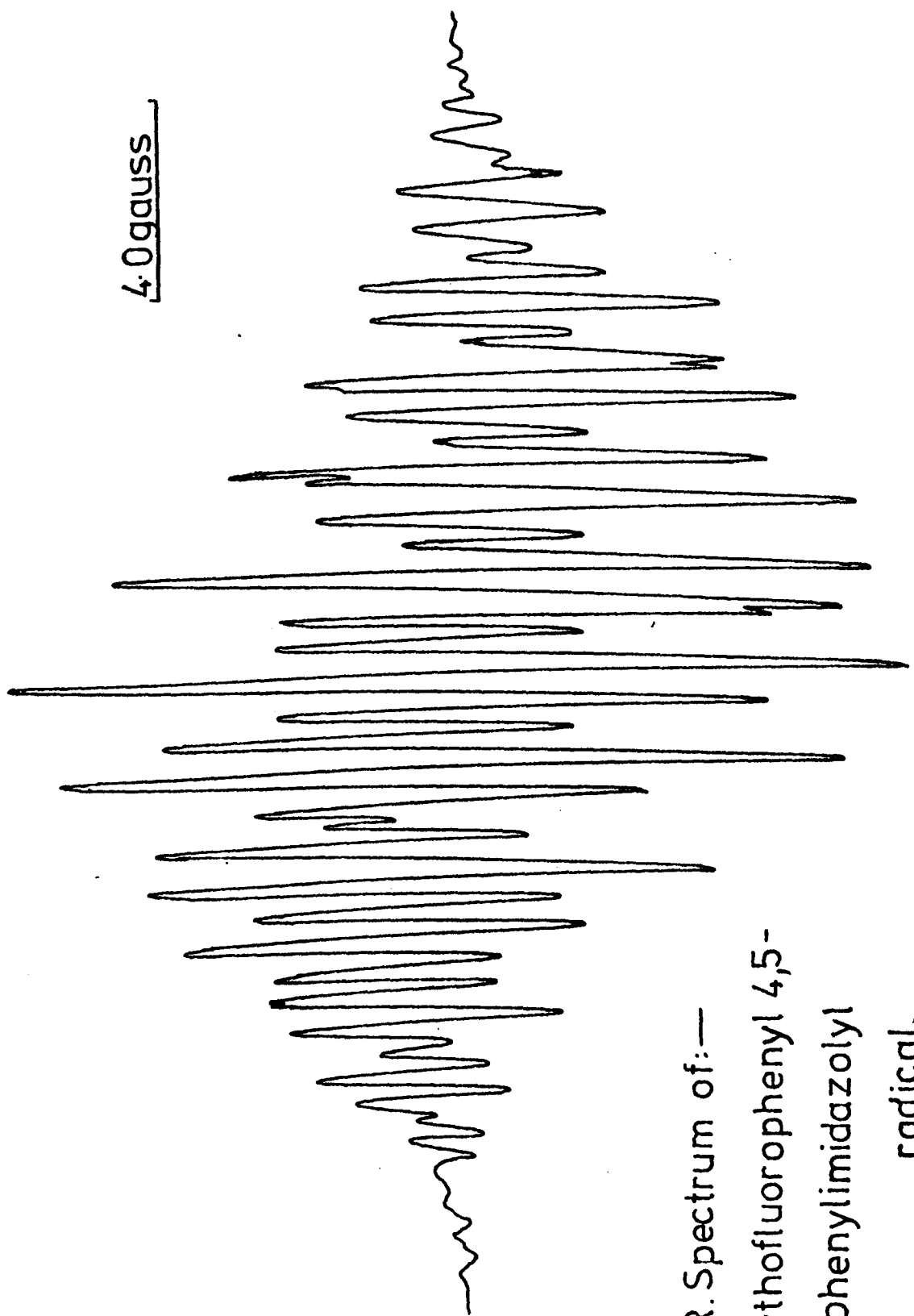
DISCUSSION

4.1 E.S.R. Spectra and Interpretation.

The spectra of the three fluorinated imidazolyl radicals, were recorded under conditions which allowed the best possible resolution, and the results are shown in Figures 4.1, 4.2 and 4.3. Figure 4.4A shows the spectrum obtained from the 2-parafluorophenyl 4,5 diphenyl imidazolyl radical, deuterated on the 4 and 5 rings, used to aid the determination of the splitting due to the fluorine atom. It can be seen from this figure, that the fluorine (spin quantum number of one half) has the effect of splitting the E.S.R. signal into two parts, the separation of which appears to indicate a splitting constant of around 11 gauss. The smaller splitting observed in the spectrum, has been attributed to the nitrogens because of the 5 line pattern of the lines (the ortho and meta hydrogens on the 2 ring should both only give 3 lines), and because of the separation of around 1.4 to 1.5 gauss, similar to the value suggested for nitrogen by Wilks.^{15c}

The only way to check that these values are correct, (as one can never be sure that the splittings indicated by the deuterium spectra are indeed accurate) is to construct in some way, a simulated spectrum from the splitting constants given, and compare this with the experimental result. This simulation was achieved by using a computer program, written by Dr. K. Kuwata of Osaka University and modified by Dr. N. Cyr of Nottingham.

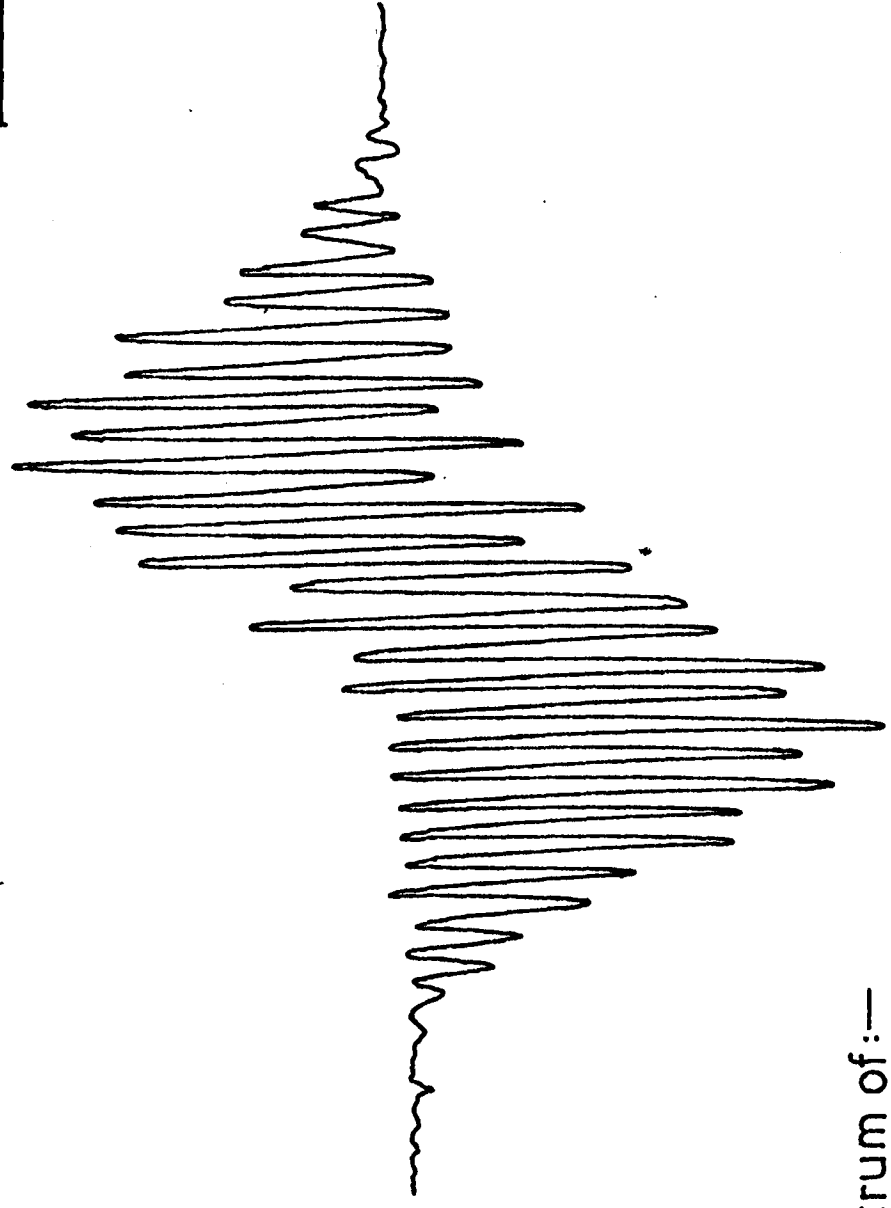
A line shape function of Gaussian or Lorentzian character, in simple terms, is generated by the program, and the half spectrum, after the successive splittings, is calculated according to the assumed splitting constants. The resulting half spectrum of specified line width and length is then drawn out using the computer controlled line plotter. The actual program is shown in Figure 4.5 and the data input is given below.



E.S.R. Spectrum of:—
2-Orthofluorophenyl 4,5-
diphenylimidazolyl
radical.

FIGURE 4.1

4.0 gauss



E.S.R. Spectrum of:—

2-Metafluorophenyl, 4,5- diphenylimidazolyl radical

FIGURE 4.2



E.S.R. Spectrum of:—

2—Parafluorophenyl, 4,5—diphenylimidazolyl radical

FIGURE 4.3

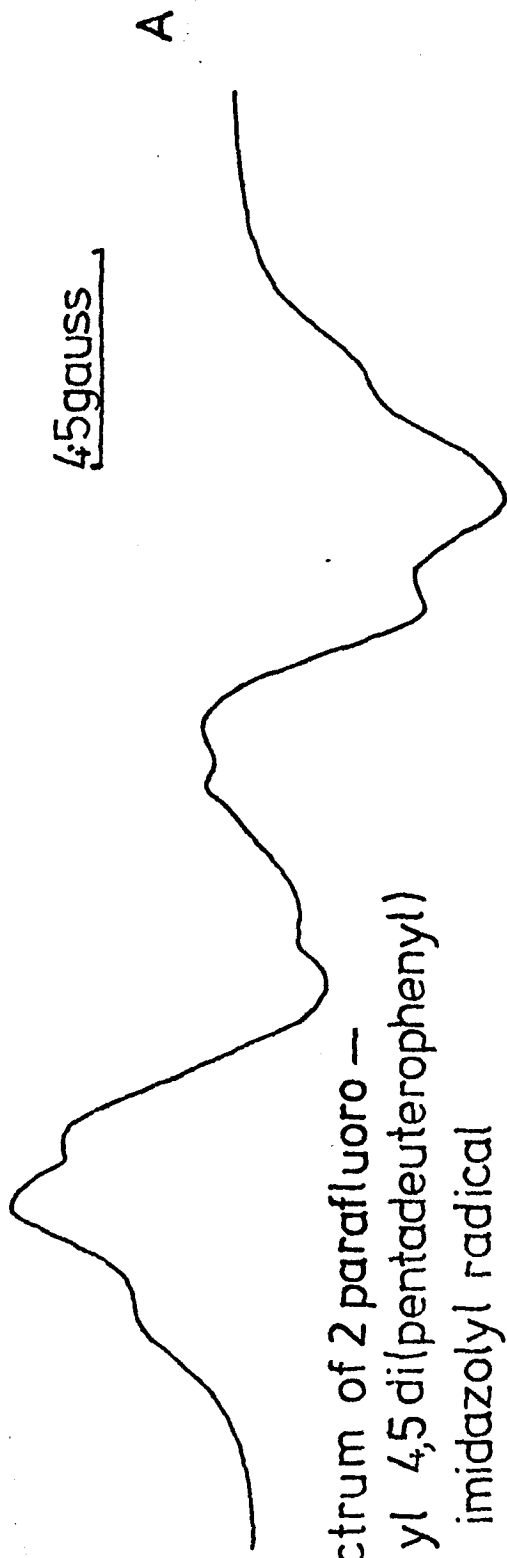
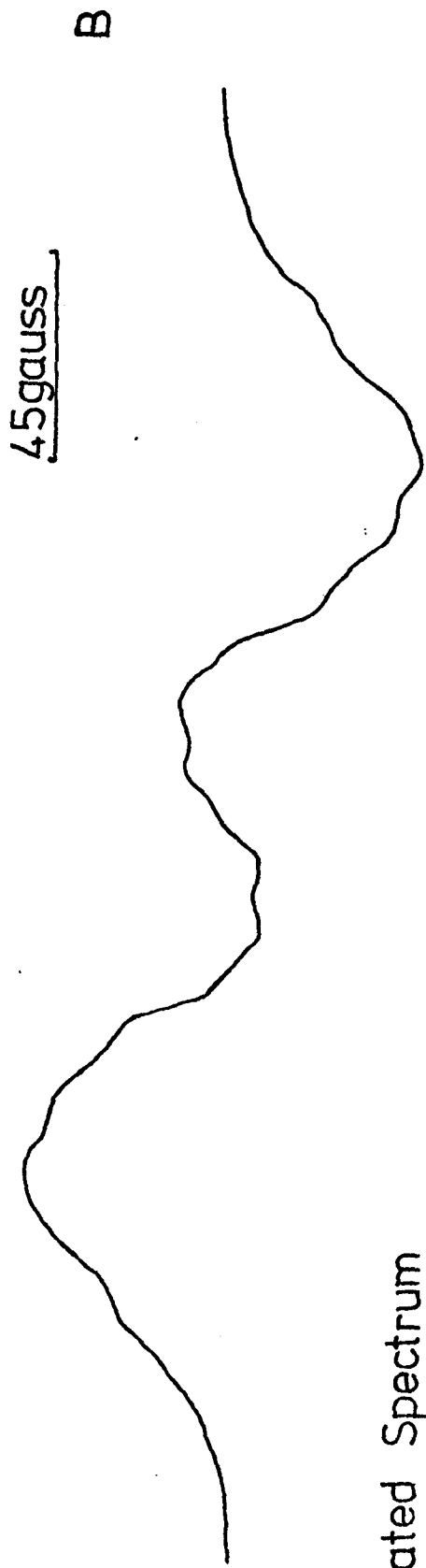


FIGURE 4.4

FIGURE 4.5

*FORTRAN

```
C THIS PROGRAM WAS ORIGINALLY WRITTEN BY DR.K.KUWATA OF OSAKA UNIVERSITY,
C MODIFIED BY N.CYR
      DIMENSION ANAME(12),YA(3,6000),NQA(50),A(50),NQB(50),B(50),NOCHAR(
      15)
2   READ (5,3) (ANAME(I),I = 1,12)
3   FORMAT(12A6)
C NAME OF THE SPECTRUM
      WRITE(6,5) (ANAME(I), I = 1,12)
5   FORMAT (1H1,12A6/)
      READ (5,7) NSPEX,KSHAPE
C NSPEX = NUMBER OF SPECTRA TO OVERLAP,KSHAPE = 0 FOR LORENTZIAN,OTHERS FOR
C GAUSSIAN
7   FORMAT (2I4)
      READ(5,9) WINC,WMAX,WMIN
C WINC = EVERY NUMBER OF GAUSS TO PERFORM CALCULATION
C WMAX = FARTHEST POINT IN GAUSS FROM THE CENTER
C WMIN = NEAREST POINT IN GAUSS FROM THE CENTER
9   FORMAT(4F12.6)
      WRITE(6,11) WINC,WMIN,WMAX
11  FORMAT(10X,12HINCREMENT = ,F12.6,6H GAUSS,/ ,10X,10HRANGE FROM,
      1F12.6,9H GAUSS TO,F12.6,6H GAUSS)
      IF(NSPEX) 2,2,13
13  NSPEC = 0
      NHAFMX = 0
      DO 16 I = 1,6000
16  YA(3,I) = 0.0
      NMIN = WMIN/WINC
      NMAX = WMAX/WINC
19  NSPEC = NSPEC + 1
20  READ (5,3) (ANAME(I),I = 1,12)
C NAME OF THE 1ST SPECIES
      WRITE(6,22) (ANAME(I),I = 1,12)
22  FORMAT(/2X,12A6)
      READ(5,7) NA,NB
C NA = NUMBER OF GROUPS WITH EQUIVALENT SPIN 1/2 FOR THE 1st SPECIES(,LE. 4
C NUCEI IN A GROUP)
C NB = NUMBER OF GROUPS WITH EQUIVALENT SPIN 1 FOR THE 1ST SPECIES(,LE. 3 IN
C A GROUP)
      READ (5,9) WEIGHT,WLINE,PHASE,WSHIFT
C WEIGHT = PART OF THE 1ST SPECIES
C WLINE = LINE WIDTH OF THE 1ST SPECIES IN GAUSS
C PHASE = POSITIVE FOR UP, NEGATIVE FOR DOWN
C WSHIFT = RELATIVE CENTER POSITION IN GAUSS
      IF(NA) 30,30,26
26  READ(5,27) (NQA(I),A(I), I = 1,NA)
C NQA(I) = NUMBER OF SPIN1/2 NUCLEI IN GROUP I, A(I) = HFC OF GROUP I IN GAUSS
27  FORMAT(6(14,F8.3))
      WRITE(6,29) (NQA(I),A(I), I = 1,NA)
29  FORMAT(10X,13,26HEQUIVALENT,I=0.5,WITH A = ,F12.6,6H GAUSS)
30  IF(NB) 34,34,31
31  READ(5,27) (NQB(I),B(I), I = 1,NB)
C NQB(I) = NUMBER OF SPIN 1 NUCLEI IN GROUP I, B(I) = HFC OF GROUP I IN GAUSS
      WRITE(6,33) (NQB(I),B(I), I = 1,NB)
33  FORMAT(10X,13,27H EQUIVALENT,I=1.0,WITH A = , F12.6,6H GAUSS)
```

```

34 WRITE(6,35) WEIGHT,WLINE,WSHIFT
35 FORMAT(10X,17HSPECIES WEIGHT = ,F12.6,/13H,LINWIDTH = ,F12.6,
16H GAUSS,/22HSHIFT OF THE CENTER = ,F12.6,6H GAUSS)
DO 38 I = 1,2
DO 38 J = 1,6000
38 YA(I,J) = 0,0
WID = 0,0
TENS = 1.
IF(NA) 46,46,42
42 DO 45 I = 1,NA
ANQ = NQA(I)
WID = WID + (ANQ*A(I))
45 TENS = TENS*(2,0**ANQ)
46 IF(NB) 51 , 51 , 47
47 DO 50 I = 1,NB
BNQ = NQB(I)
WID = WID + (2,0*BNQ*B(I))
50 TENS = TENS*(3,0**BNQ)
51 PHAF = WID/2.
NI = WLINE/WINC
NSHIFT = WSHIFT/WINC
NGEN = 16*NI
NORG = 8*NI
ORIGIN = WINC*FLOAT(NORG)
PNWID = NGEN + IR(WID/WINC)
PNHAF = NORG + IR(HAF/WINC)
NEN = NSHIFT + NHAF = NMIN
IF(NEN - NMIN) 200,200,61
61 W = WLINE
TENFAC = PHASE*WEIGHT/TENS
IF(KSHAPE) 71,64,71
64 TA = -16,*(W**3)
TB = 3,*(W**2)
DO 69 I = 1,NGEN
XI = I
XA = (XI*WINC) = ORIGIN
69 YA(1,I) = (TENFAC*TA*XA)/((4,*(XA**2)+TB)**2)
GO TO 76
71 TA = -(W**2)/2.
DO 75 I = 1,NGEN
XI = I
XA = (XI*WINC) = ORIGIN
75 YA(1,I) = TENFAC*(XA/TA)*EXP((XA**2)/TA)
76 LENGTH = NGEN
NY = 1
IF(NA) 126,126,79
79 DO 125 K = 1,NA
NEQ = NQA(K)
KUPL = A(K)/WINC
PLENGTH = LENGTH + (NEQ*KUPL)
LENGTH = MINO(LENGTH,NEN,MWID)
84 AK = A(K)
DO 120 I = 1,LENGTH
GO TO (90,89,88,87),NEQ
87 F14 = I - IR(4,*AK/WINC)
88 I3 = I - IR(3,*AK/WINC)
89 I2 = I - IR(2,*AK/WINC)
90 I1 = I - IR(AK/WINC)
YPLUS = 0,0
GO TO (93,96,101,108), NEQ

```

```

93  IF(11) 116,116,97
94  YPLUS = YA(NY,11)
    GO TO 116
96  IF(11) 116,116,94
97  YPLUS = 2.*YA(NY,11)
    IF(12) 116,116,99
99  YPLUS = YPLUS + YA(NY,12)
    GO TO 116
101 IF(11) 116,116,102
102 YPLUS = 3.*YA(NY,11)
    IF(12) 116,116,104
104 YPLUS = YPLUS + 3.*YA(NY,12)
    IF(13) 116,116,106
106 YPLUS = YPLUS + YA(NY,13)
    GO TO 116
108 IF(11) 116,116,109
109 YPLUS = 4.*YA(NY,11)
    IF(12) 116,116,111
111 YPLUS = YPLUS + 6.*YA(NY,12)
    IF(13) 116,116,113
113 YPLUS = YPLUS + 4.*YA(NY,13)
    IF(14) 116,116,115
115 YPLUS = YPLUS + YA(NY,14)
116 GO TO (119,117),NY
117 YA(1,1) = YA(2,1) + YPLUS
    GO TO 120
119 YA(2,1) = YA(1,1) + YPLUS
120 CONTINUE
    GO TO (122,124),NY
122 NY = 2
    GO TO 125
124 NY = 1
125 CONTINUE
126 IF(NB) 179,179,127
127 DO 178 K = 1,NB
    NEQ = NQB(K)
    KUPL = B(K)/WINC
    LENGTH = LENGTH + 2*NEQ*KUPL
    LENGTH = MINO(LENGTH,NEN,NWID)
132 BK = B(K)
    DO 173 I = 1,LENGTH
    GO TO (139,137,135),NEQ
135 I6 = I - IR(6.*BK/WINC)
    I5 = I - IR(5.*BK/WINC)
137 I4 = I - IR(4.*BK/WINC)
    I3 = I - IR(3.*BK/WINC)
139 I2 = I - IR(2.*BK/WINC)
    I1 = I - IR(BK/WINC)
    YPLUS = 0.0
    GO TO (143,148,157),NEQ
143 IF(11) 169,169,144
144 YPLUS = YA(NY,11)
    IF(12) 169,169,146
146 YPLUS = YPLUS + YA(NY,12)
    GO TO 169
148 IF(11) 169,169,149
149 YPLUS = 2.*YA(NY,11)
    IF(12) 169,169,151
151 YPLUS = YPLUS + 3.*YA(NY,12)
    IF(13) 169,169,153
153 YPLUS = YPLUS + 2.*YA(NY,13)
    IF(14) 169,169,155

```

```

155  YPLUS = YPLUS + YA(NY,14)
      GO TO 169
157  IF(11) 169,169,158
158  YPLUS = 3.*YA(NY,11)
      IF(12) 169,169,160
160  YPLUS = YPLUS + 6.*YA(NY,12)
      IF(13) 169,169,162
162  YPLUS = YPLUS + 7.*YA(NY,13)
      IF(14) 169,169,164
164  YPLUS = YPLUS + 6.*YA(NY,14)
      IF(15) 169,169,166
166  YPLUS = YPLUS + 3.*YA(NY,15)
      IF(16),169,169,158
168  YPLUS = YPLUS + YA(NY,16)
169  GO TO (172,170),NY
170  YA(1,1) = YA(2,1) + YPLUS
      GO TO 173
172  YA(2,1) = YA(1,1) + YPLUS
173  CONTINUE
      GO TO (175,177),NY
175  NY = 2
      GO TO 178
177  NY = 1
178  CONTINUE
179  IREAD = NEN + 1
      DO 182 I = 1,NEN
      IREAD = IREAD - 1
182  YA(3,I) = YA(3,I) + YA(NY,IREAD)
      IF(NEN-NHAFMX) 186,186,184
184  NHAFMX = NEN
      IF(NSPEX - NSPEC) 186,186,19
186  YMAX = 0.0
      NMXMN = NMAX - NMIN
      NHAFMX = MINC(NMXMN,NHAFMX)
      WRITE (6,333) NHAFMX
333  FORMAT(27HNUMBER OF POINTS TO PLOT = , 16)
      DO 194 I = 1,NHAFMX
      YY = YA(3,I)
      YY = ABS(YY)
      IF(YY - YMAX) 194,194,193
193  YMAX = YY
194  CONTINUE
      DO 196 I = 1,NHAFMX
196  YA(3,I) = 50.*YA(3,I)/YMAX
      CALL FLABEL(10HLITOBARSKI,10)
197  CALL INCLPT(1)
      CALL CMS
      READ(5,9) DIST
C DIST IS NUMBER OF CENTIMETERS PER GAUSS
      XM = WMAX*DIST
      CALL LIMITS(0.,XM+10.,0.,27)
      CALL REGION(5.,XM+5.,0.,25.)
      CALL MSPACE
      XMAXM = WMAX*100.
      CALL REGION(0.,XMAXM,-100.,100.)
      CALL AXESSI(100.,20.)
      CALL CRSIZE(5.)
      CALL PLOTNC(300.,80.,22)
      CALL JYPENC(19)
      CALL TYPENC(30)
      CALL TYPENC(25)
      CALL PLOTNC(350.,65.,24)
      CALL TYPENC(25)

```

CALL TYPENC (37)

READ(5,350) (NOCHAR(1),I=1,3)

C NOCHAR(1), IS THE IDENTIFIER CHARACTER NUMBER FROM THE NPL CHARACTER SET 5

350 FORMAT(10I4)

DO 351 I = 1,3

351 CALL TYPENC(NO CHAR(I))

CALL POINT(0.,YA(3,1))

DO 352 I = 2,NHAFMX

F1 = FLOAT(I-1)

352 CALL JOIN(F1,YA(3, I))

CALL INCPLT(0)

CALL GREND

READ (5,7) NEXT

C IF THERE IS NO MORE CALCULATION, NEXT = 0

IF (NEXT.EQ.0) GO TO 200

GO TO 2

200 CALL EXIT

END

Data input form.

The brackets following the identifiers contain the format for the reading in of the data.

1. ANAME (I12)

Up to 12 characters identifying the individual programs.

2. NSPEX, KSHAPE (2I4)

Both of these parameters are on the same card. NSPEX defines the number of overlapping spectra, and for all calculations here, NSPEX = 1. KSHAPE controls the character of the line. KSHAPE = 0 for Lorentzian and $\neq 0$ for Gaussian.

3. WINC, WMAX, WMIN (4F12.6)

WINC gives the number of gauss at which each intensity calculation is performed (0.01 gauss), WMAX is the farthest point from the centre of the whole spectrum to which the calculation is made, and WMIN is the nearest point in gauss from the centre (WMIN = 0 in all cases)

4. NA, NB, (2I4)

NA is the number of groups with equivalent spin quantum number $\frac{1}{2}$, (4 equivalent nuclei only being allowed in each group), and NB is the number of groups with equivalent spin 1 (3 equivalent nuclei only being allowed).

5. WEIGHT, WLINE, PHASE, WSHIFT (4F12.6)

WEIGHT is the contribution to the overall spectrum, from each overlapping spectrum. As there is only one species involved here, WEIGHT = 1. WLINE is the line width of the splitting in gauss, and PHASE defines whether the spectrum starts from the centre, with a "down peak" or an "up peak" (=1 for up, -1 for down). This serves to

keep the simulated spectrum in phase with the experimental one.

WSHIFT is the relative centre position of the simulated spectrum (set to 0 in all cases).

6. NQA(I), A(I) (6(I4,F8.3))

NQA(I) defines the number of nuclei (spin $\frac{1}{2}$) in group I, and A(I) is the splitting constant of that group. The order of this data input is, NQA(1), A(1), NQA(2), A(2)...NQA(NA), A(NA).

7. NQB(I),B(I) (6(I4,F8.3))

These are treated in the same way as the above parameters, but represent groups with spin 1.

8. DIST

This parameter governs the scale of the simulated plot, and is in units of centimetres per gauss.

9. NOCHAR (I) (10I4)

NOCHAR is the identifier made up of 3 numbers from the NPL set, used to characterise the spectra obtained from the line plotter.

10. NEXT (I4)

If NEXT \neq 0, the program restarts with a new set of data.

In fact, using the fluorine and nitrogen constants suggested by experimental evidence, and keeping the hydrogen splitting constants the same as those postulated by Dr. N. Cyr⁴⁴, the simulated spectrum of the deuterated parafluoro radical obtained with the above program bore little resemblance to the experimental result. Lowering of the fluorine splitting however improved the correlation and the best fit (Figure 4.4B) was achieved using the following parameters.

1. Linewidth = 1.44 gauss
2. Fluorine splitting = 7.60 Gauss
3. 2 o-protons splitting = 2.40 gauss
4. 2 m-protons splitting = 0.89 gauss
5. Nitrogen splitting = 1.44 gauss

Alteration of the nitrogen and hydrogen splittings from these values made only marginal differences to this simulation. To determine these smaller values, construction of the non deuterated spectrum was necessary but this was found extremely difficult to effect, in that seven splitting parameters needed to be adjusted with no knowledge of the relative magnitude of the perturbation to them caused by the fluorine. Because of this difficulty, it was decided that the best starting point would be a determination of the spin densities on the carbon atoms, from which the hydrogen splitting constants could be estimated. A program based on McLachlan's calculation from Hückel molecular orbitals, shown in Figure 4.6, was thus written in Algol for this purpose. The nature and order of the data input is given below.

1. M, the number of atoms in the molecule involved in the π system
2. G. This parameter indicates whether a second set of calculations with new data is to be undertaken after completion of the first set. (If $G = 1$ the program restarts)
3. A(M,M). This is the matrix related to the Hückel secular determinant, equation 1.19. Each term of the determinant is divided by β_0 and the ratio $\frac{\alpha_0 - \epsilon}{\beta_0}$ is put to zero, leaving only numerical values to put in the matrix e.g. for allyl the matrix becomes,

$$\begin{vmatrix} 0 & 1 & 0 \\ 1 & 0 & 1 \\ 0 & 1 & 0 \end{vmatrix}$$

and for the C-N-C system in which $h\omega = 0.9$ (see equation 1.32), $K_{cx} = 1.0$ (see equation 1.33) and $\delta x = 0.0$ (from equation 1.35) the matrix will be

$$\begin{vmatrix} 0.0 & 1.0 & 0.0 \\ 1.0 & 0.9 & 1.0 \\ 0.0 & 1.0 & 0.0 \end{vmatrix}$$

4. The identifying name of the calculation is read in here, and is of any length providing that it lies between two stars (*). Procedure "copytext" is responsible for this operation.
5. N, is the number of fully filled molecular orbitals.
6. LAMBDA. This parameter is the coefficient λ used in McLachlan's method of determination of spin density (equation 1.39).

The calculation of the molecular orbitals from the secular determinant fed in, is executed by using a KDF9 procedure, "Householder" (line 13 in Figure 4.6), and the eigenvalues and eigenvectors of the wavefunctions so calculated are used to determine the spin density on each atom contributing to the network according to equation 1.39 (lines 30 to 60). Finally, the π bond orders between the atoms are assessed.

The program was checked against the calculations performed on the anthracene cation by McLachlan in his original paper²², using the parameters suggested by him, and the agreement of results is shown below.

Spin Density Program

```

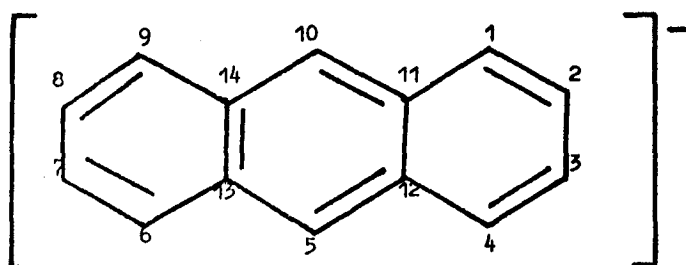
1   'Begin'
    'Real' LAMBDA, T,H;
    'Integer' N,I ,J,S,M,G,K, R;
    Start '.' M = READ;
5   G = READ ;
    'Begin'
    'Array' A,B,C,E,PI (1 '.' M, 1'.' M), W,SUM,TERM (1'.'M);
    'Comment' Huckel Solutions;
    In matr (A,M,M);
10  Rmatpr (A,M,M,1,2);
    Newline (2);
    Matcop (B,A,M,M);
    Househ (B,W,M,1);
    Writetext ((' Huckel '** Molecular '** Orbitals '** For '** );
15  Copytext;
    Newline (5);
    'For' I = 1 'Step' 1 'Until' M'DO'
    'Begin'
    Writetext (('('('CC')' wavefunction '** For '** Energy '**E
    '** = '** Alpha')');
20  Print (W (J),2,6);
    Writetext (('('*'BETA('C')')');
    'For' I = 1 'Step' 1 'Until' M'DO'
    Print (B(J,I) 1,6);
    'End';
25  Newline (5);
    'Comment' Huckel Molecular Orbital calculations complete,
        calculate spin densities
    N = READ;
    LAMBDA = Read;
    Null(PI,M,M)
30  'For' R=1 'Step' 1 'Until' M'DO'
    'Begin'
    'For' S=1 'Step' 1 'Until' M'DO'
    'Begin'
    'For' I = 1 'Step' 1 'Until' N'DO'
35  'For' J = N+1 'Step' 1 'Until' M'DO'
    'Begin'
    T = W(J)-W(I);
    'If' Abs(T) 'LT' 0.00001 'Then' 'Go to' End;
    PI (R,S) = PI(R,S) + (B(I,R) * B(J,S) * B(I,S) * B(J,R));
40  END 'End';
    Start '.' 'End';
    'End';
    Writetext (('('('P')' Mutual '** Polarisability (('C')')');
    'For' I = 1 'Step' 1 'Until' M'DO'
45  'Begin'
    'For' J = 1 'Step' 1 'Until' M'DO'
    PI (I,J) = - 4 PI (I,J);
    'End';
    RMatpr (PI,M,M,1,8);
50  Writetext (('('('P')')');
    'For' R=1 'Step' 1 'Until' M'DO'
    'Begin'
    Sum (R)=0;

```

```

55  'Begin'
    Term (R) = PI (R,S) * B(N+1,S) * B(N+1,S) * LAMBDA:
    SUM(R) = SUM(R) + TERM(R);
    'END'
    WRITEX ( ('('C')' McLachlan '** Spin '** Density '**
                                                    On '** Atom '** Number '));
60  PRINT (R,2,0);
    H = (B(N+1,R)) * (B(N+1,R)) + SUM (R);
    Print (M,1,9);
    'End';
    Writetext (('('P')'));
65  'For' I = 1 "STEP' 1 'UNTIL' M'DO'
    'For' J = 1 'Step' 1 'Until' M 'DO'
    'Begin'
    Writetext (('('C')' Bond '** Order '** For '** Atoms '**));
    Print (I,2,0);
70  Space (2);
    Print (J,2,0);
    C(I,J)=0;
    'For' K = 1 'Step' 1 'Until' N 'DO'
    C(I,J) = C(I,J) + (B(K,I) * B(K,J)) * 2;
75  C(I,J) = C(I,J) + (B(N+1,I) * B(N+1,J));
    Writetext (('('SS')' IS (('SS')'));
    Print (C(I,J), 1, 5);
    Newline (1);
    'End';
80  'End';
    Writetext (('('P')'));
    'If' G 'EQ' 1 'Then' 'Go to' Start;
    'End'
    *Algol*
85  'Procedure' Copytext;
    'Begin'
    'Integer' I;
    L'. Inch (I);
    'If' I 'NE' 13 'Then' 'Go to' L;
90  L1'. Inch I;
    'If' I 'EQ' 13 'Then' 'Go to' End;
    Outch (I);
    'Go to' L1;
    End '. 'End'
95  *Data.

```



Anthracene cation

$$N = 7$$

$$\lambda = 1.14$$

Atom number	1	2	10	11
Spin density (McLachlan)	0.118	0.032	0.256	0.028
Spin density (present work)	0.118	0.032	0.255	0.027

Secondly, the program was used to compute the spin densities on the triphenylimidazolyl radical, for comparison with those values found by Cyr, Wilks and Willis, given in Chapter 1. As the agreement between the two was exact when using the same parameters, the program was assumed to work correctly and was applied to the fluorine substituted radicals.

The values for the various parameters used to construct the secular determinant were kept in the main, the same as those used by Cyr et al to successfully predict the spin densities on the lophinyl radical, with the fluorine being considered to contribute two electrons to the π -molecular framework. I'Haya⁵⁰, in a similar treatment, considered problems involving molecules containing fluorine, and has used a range of values for the correcting factors applied to the Coulombic (h_F) and the resonance (KcF) integrals involving the halogens. He postulated that h_F could vary from 1.5 to 2.1, while KcF was in the range 0.5 to 0.7. The auxiliary inductive parameter δ_F for the adjoining carbon atom, he put to lie between 0.220 and 0.280. With these additions, then, to the secular determinant for the lophinyl radical, the program was run in

conjunction with the simulation program, in an attempt to reproduce theoretically the experimental spectrum of the parafluoro radical. In converting the spin densities to splitting constants for the hydrogens, McConnell's relationship

$$a_H = Q\rho$$

was used, with the value of Q being 30 gauss as suggested by Cyr, Wilks and Willis. The fluorine and nitrogen splittings were kept to the value indicated by the spectrum of the deuterated radical. Again, however, no success was obtained, and using values for the fluorine integrals in and around those given by I'Haya, little similarity between the simulated and experimental spectra was obtained.

The reason for the lack of success, it was thought, was because the Hückel and McLachlan Method of computation of spin density, known to be unreliable for molecules containing heteroatoms, was being taken beyond its limit by the addition of a fluorine atom to the molecular framework, already containing two nitrogens. Because of this, a more sophisticated method was sought.

4.2 Pariser, Pople and Parr Self Consistent Field Molecular Orbital Approach

As has been shown in the preliminary chapter, the P.P.P semi empirical approximation to the self consistent field molecular orbital equations, provides a much more rigorous and satisfactory method of determination of molecular wavefunctions than does Hückel. Indeed, considerable success has already been achieved with the P.P.P. semi-empirical theory, and a large number of calculations for molecules containing hetero atoms have been based on the method. It was thus decided to use it on the imidazolyl radicals, and to this end, a computer program, written in Fortran IV by John Packer and modified by Dr.D. Brailsford, was supplied by the Maths Department of Nottingham University.

The Spin polarised S.C.F. program, with spin projection

The program, shown in Figure 4.7, has been designed basically for treatment of open shell systems (molecules in which not all electrons are paired), in that it calculates the S.C.F. spin polarised wavefunctions (discussed in Chapter 1) for half closed shell states, i.e. it considers the α and β spin electrons separately.

Despite the rather complex computing techniques involved, the program is relatively simple to use because of the simplicity of the data input. In the following description of the form of this, all matrices have their size specified in brackets e.g. $H(N,N)$ and all formats are indicated for individual and variable lists. Where the variable list is enclosed in slashes, a sequence of cards of identical format, one card for each element in the matrix, is indicated, e.g. $/H(N,N)/$. Also, in reading in all symmetrical doubly dimensioned matrices, only the upper triangles are used.

Data input form.

N33, ICV, ICON, (3I3)

All three are read in on the same card. N33 controls the use of the spin polarising routine PURV, which is only called if $N33=5$. The subroutine is used to obtain spin polarised ground states, by alternating the α and β spin density. For non ground states $N33 \neq 5$.

ICV, controls the subroutine VSORT, which is used for making treatment of states with unusual configuration possible. It is only used when $ICV \neq 1$.

ICON, is used to decide whether the simple spin projection routine due to Amos and Hall, or the full projection operation, given in Chapter 1, are employed. When $ICON = 2$ only the simple operator is used, but when $ICON = 3$, the more accurate projection is carried out.

Title card (Free format)

This simply allows a program title to be read in.

FIGURE 4.7

```

0007         MASTER FRED
0008         DIMENSION A1(30),E(30),Z(30),ANA(30),ANB(30),BETA(30,30),
0009         1 GAMA(30,30),ENA(30),PA(30,30),PB(30,30),FA(30,30),
0010         2 FB(30,30),QA(30,30),QB(30,30),C(30,30),H(30,30),
0011         3 CH(30,30),CA(30,30),CB(30,30),X(30,30),CF(30,30),D(30)
0012 C         MOLECULE OPEN SHELL LCAO,MO,SCF,
0013         208 READ(5,984)N33,ICV,ICON
0014         984 FORMAT(3I3)
0015 C         N33 LABELS TITLE REQUIRED
0016         CALL RITE(N33)
0017         500 READ(5,1)N
0018 C         N GIVES THE NUMBER OF ATOMS IN THE MOLECULE
0019         1 FORMAT(I3)
0020         READ(5,1)NIT
0021         READ(5,900)GN,CONVG,DVC
0022         900 FORMAT(3F20.8)
0023         N5=1
0024         DO 2 I=1,N
0025         DO 2 J=1,N
0026         READ(5,3) PA(I,J)
0027         2 PA(J,I)=PA(I,J)
0028         3 FORMAT(F20.8)
0029         READ(5,3) (A1(I),I=1,N)
0030         READ(5,3) (E(I),I=1,N)
0031         READ(5,3) (Z(I),I=1,N)
0032         DO 9 I=1,N
0033         DO 9 J=1,N
0034         READ(5,3) H(I,J)
0035         BETA(I,J)=H(I,J)
0036         BETA(J,I)=H(I,J)
0037         9 H(J,I)=H(I,J)
0038 C         READ THE HUCKEL MATRIX
0039 C         RESONANCE INTEGRAL MATRIX
0040         DO 10 I=1,N
0041         10 BETA(I,I)=0.0
0042         WRITE(6,23)
0043         23 FORMAT(14H HUCKEL MATRIX,/)
0044         DO 24 I=1,N
0045         24 WRITE(6,301) (H(I,J),J=1,N)
0046         301 FORMAT(12F8.3)
0047         WRITE(6,51)
0048         51 FORMAT(1H,///,21H IONIZATION POTENTIAL,/)
0049         WRITE(6,301) (A1(I),I=1,N)
0050         WRITE(6,52)
0051         52 FORMAT(1H,///,18H ELECTRON AFFINITY,/)
0052         WRITE(6,301) (E(I),I=1,N)
0053         WRITE(6,56)
0054         56 FORMAT(1H,///,14H R(I,J) MATRIX,/)
0055         DO 57 I=1,N
0056         57 WRITE(6,301) (PA(I,J),J=1,N)
0057         WRITE(6,58)
0058         58 FORMAT(1H,///,17H RESONANCE MATRIX,/)
0059         DO 59 I=1,N
0060         59 WRITE(6,301) (BETA(I,J),J=1,N)
0061         WRITE(6,53)
0062         53 FORMAT(1H,///,23H NUMBER OF PI ELECTRONS,/)
0063         WRITE(6,301) (Z(I),I=1,N)
0064         CALL COUL(A1,E,PA,GAMA,N)
0065         DO 753 I=1,N

```

```

0066          DO 753 J=1,N
0067          753 GAMA(I,J)=GN*GAMA(I,J)
0068          WRITE(6,754) GN
0069          754 FORMAT(1H,///,13H GAMA FACTOR=,F6.3,/)
0070          C      GAMA(I,J) MATRIX
0071          800 READ(5,3) (ANA(I),I=1,N)
0072          READ(5,3) (ANB(I),I=1,N)
0073          WRITE(6,54)
0074          54 FORMAT(1H,///,17H ALPHA OCCUPATION,/)
0075          WRITE(6,301) (ANA(I),I=1,N)
0076          WRITE(6,55)
0077          55 FORMAT(1H,///,16H BETA OCCUPATION,/)
0078          WRITE(6,301) (ANB(I),I=1,N)
0079          WRITE(6,901)
0080          901 FORMAT(1H,///,31H CLOSED SHELL SCF APPROXIMATION,/)
0081          IF(N5,NE,1) CALL PUTIN(CH,PA,PB,ANA,ANB,N)
0082          IF(N5,NE,1) GO TO 581
0083          CALL SCFCS(H,BETA,GAMA,AI,E,Z,FA,CA,CB,PA,PB,ANA,ANB,ENA,D,N)
0084          IF(N33.EQ,5) CALL PURV(PA,PB,N)
0085          DO 902 I=1,N
0086          DO 902 J=1,N
0087          902 CH(I,J)=CA(I,J)
0088          581 WRITE(6,60)
0089          60 FORMAT(1H,///,10H PA MATRIX,/)
0090          DO 61 I=1,N
0091          61 WRITE(6,302) (PA(I,J),J=1,N)
0092          302 FORMAT(1H,10F10.5)
0093          WRITE(6,62)
0094          62 FORMAT(1H,///,10H PB MATRIX,/)
0095          DO 63 I=1,N
0096          63 WRITE(6,302) (PB(I,J),J=1,N)
0097          WRITE(6,903)
0098          903 FORMAT(1H,///,19H SPIN POLARIZED SCF,/)
0099          DO 11 L=1,NIT
0100          VC=1.0-DVC*FLOAT(L)
0101          IF(VC.LT.0.0)VC=0.0
0102          VCM=1.0-VC
0103          CONV=VC*CONVG
0104          CALL FMAT (AI,E,PA,PB,Z,GAMA,BETA,N,FA,FB)
0105          C      F MATRICES ALPHA AND BETA
0106          CALL RECAL(FA,QA,ANA,N,CA,X,CF,D,ICV)
0107          CALL RECAL(FB,QB,ANB,N,CB,X,CF,D,ICV)
0108          C      RECALCULATES P MATRICES AS QA AND QB
0109          PEN=POLEN(FA,FB,QA,QB,AI,BETA,Z,GAMA,N)
0110          WRITE(6,757)PEN
0111          757 FORMAT(1H,///,17H TOTAL PI ENERGY=,F10.4,/)
0112          IF(L.EQ,NIT) GO TO 81
0113          DO 13 I=1,N
0114          DO 13 J=1,N
0115          13 IF(ABS(PA(I,J)-QA(I,J)).GT,CONV,OR,
0116             1  ABS(PB(I,J)-QB(I,J)).GT,CONV) GO TO 91
0117          WRITE(6,904) CONV
0118          904 FORMAT(1H,///,28H METHOD HAS CONVERGED, CONV=F8.5,/)
0119          81 WRITE(6,31) L
0120          31 FORMAT(1H,///,22H NUMBER OF ITERATIONS=,13,/)
0121          WRITE(6,16)
0122          15 FORMAT(16H FINAL PA MATRIX,/)
0123          DO 64 I=1,N
0124          64 WRITE(6,302) (QA(I,J),J=1,N)
0125          WRITE(6,17)
0126          17 FORMAT(1H,///,16H FINAL PB MATRIX,/)
0127          DO 65 I=1,N
0128          65 WRITE(6,302) (QB(I,J),J=1,N)

```

```

0129          WRITE(6,905)
0130          905 FORMAT(1H ,///,29H CHARGE AND BOND-ORDER MATRIX,/)
0131          DO 906 I=1,N
0132          DO 906 J=1,N
0133          906 C(I,J)=QA(I,J)+QB(I,J)
0134          DO 907 I=1,N
0135          907 WRITE(6,302) (C(I,J),J=1,N)
0136          WRITE(6,908)
0137          908 FORMAT(1H ,///,5H ATOM,10X,13H SPIN DENSITY,10X,
0138          115H CHARGE DENSITY,/)
0139          DO 909 I=1,N
0140          X(1,I)=QA(I,I)-QB(I,I)
0141          WRITE(6,755) I,X(1,I),C(I,I)
0142          755 FORMAT(1H ,13,14X,F8.5,14X,F8.5,/)
0143          909 CONTINUE
0144          CALL QLRV(FA,C,ENA,D,N,IFAIL)
0145          IF(IFAIL.EQ.1) CALL ABORT
0146          CALL VSORT(C,CA,X,CF,ENA,N,ICV)
0147          WRITE(6,69)
0148          69 FORMAT(1H,///,18H ALPHA EIGENVALUES,/)
0149          WRITE(6,302) (ENA(I),I=1,N)
0150          WRITE(6,70)
0151          70 FORMAT(1H ,///,19H ALPHA EIGENVECTORS,/)
0152          DO 71 I=1,N
0153          71 WRITE(6,302) (C(I,J),J=1,N)
0154          CALL QLRV(FB,C,ENA,D,N,IFAIL)
0155          IF(IFAIL.EQ.1) CALL ABORT
0156          CALL VSORT(C,CB,X,CF,ENA,N,ICV)
0157          WRITE(6,72)
0158          72 FORMAT(1H ,///,17H BETA EIGENVALUES,/)
0159          WRITE(6,302) (ENA(I),I=1,N)
0160          WRITE(6,73)
0161          73 FORMAT(1H ,///,18H BETA EIGENVECTORS,/)
0162          DO 74 I=1,N
0163          74 WRITE(6,302) (C(I,J),J=1,N)
0164          CALL SPIN(QA,QB,PA,PB,FA,FB,CA,CB,C,CF,H,X,BETA,A1,E,Z,GAMA,
0165          1N,ICON,ANA,A1B)
0166          GO TO 205
0167          91 DO 32 I=1,N
0168          DO 32 J=1,N
0169          PA(I,J)=VC*PA(I,J)+VCM*QA(I,J)
0170          32 PB(I,J)=VC*PB(I,J)+VCM*QB(I,J)
0171          11 CONTINUE
0172          205 READ(5,1) N5
0173          IF(N5.EQ.5) GO TO 208
0174          IF(N5.EQ.1) GO TO 751
0175          WRITE(6,752)
0176          752 FORMAT(1H ,///,14H EXCITED STATE,/)
0177          GO TO 800
0178          751 STOP
0179          END

```

END OF SEGMENT, LENGTH 1445, NAME FRED

```

0180
0181 SUBROUTINE SPIN(QA,CB,FA,PB,FA,FB,CA,CB,C,CF,H,X,BETA,AI,E,Z,
0182 1 GAMA,N,ICON,ANA,ANB)
0183 DIMENSION QA(30,30),QB(30,30),PA(30,30),PB(30,30),FA(30,30),
0184 1 FB(30,30),CA(30,30),CB(30,30),C(30,30),CF(30,30),H(30,30),
0185 1 X(30,30),BETA(30,30),AI(30),E(30),Z(30),GAMA(30,30)
0186 1 ,ANA(30),ANB(30)
0187 Q=0.0
0188 P=0.0
0189 DO 1 I=1,N
0190 P=P+ANA(I)
0191 1 Q=Q+ANB(I)
0192 PPQ=P+Q
0193 PMQ=ABS(P-Q)
0194 SZ=PMQ*0.5
0195 SM=SZ*(SZ+1.0)
0196 I=IFIX(PMQ)+1
0197 WRITE(6,2)
0198 2 FORMAT(1H ,///,31H****SPIN PROJECTION ROUTINE****,/)
0199 WRITE(6,3) I,SZ,SM
0200 3 FORMAT(23H MULTIPLICITY OF STATE=,12,10X,18H Z-SPIN COMPONENT=,
0201 1F5.2,/,25H SPIN OF PURE STATE,(S2)=,F5.2,/)
0202 CALL AMAT(CA,QB,FA,N)
0203 C STORES(PQ) IN FA
0204 T=SECTR(FA,N)
0205 C T=TRACE(PQ)
0206 SM=0.25*PMQ +0.5*PPQ-T
0207 WRITE(6,4) SM
0208 4 FORMAT(23H UNPROJECTED SPIN,(S2)=,F9.6,/)
0209 WRITE(6,5)
0210 5 FORMAT(27H SIMPLIFIED SPIN PROJECTION,/)
0211 DO 6 I=1,N
0212 DO 6 J=1,N
0213 6 X(I,J)=FA(I,J)
0214 CALL AMAT(FA,X,FB,N)
0215 C STORES(PQPQ) IN FB
0216 T2=SECTR(FB,N)
0217 C T2=TRACE(PQPQ)
0218 X(1,1)=(SZ+1.0)*(SZ+2.0)-SM
0219 SM=SM-((P-T)*(Q-T)+2.0*(T-T2))/X(1,1)
0220 WRITE(6,7) SM
0221 7 FORMAT(23H AFTER PROJECTION,(S2)=,F9.6,/)
0222 CALL AMAT(FA,QA,CA,N)
0223 CALL AMAT(QB,FA,CB,N)
0224 CALL AMAT(QB,QA,CF,N)
0225 C CA=(PQP) CB=(QPQ) CF=(QP)
0226 DO 8 I=1,N
0227 DO 8 J=1,N
0228 PA(I,J)=QA(I,J)-(CA(I,J)-0.5*(FA(I,J)+CF(I,J)))/X(1,1)
0229 PA(J,I)=PA(I,J)
0230 PB(I,J)=QB(I,J)-(CB(I,J)-0.5*(FA(I,J)+CF(I,J)))/X(1,1)
0231 8 PB(J,I)=PB(I,J)
0232 C PA AND PB ARE NEW SPIN PROJECTED MATRICES
0233 WRITE(6,9)
0234 9 FORMAT(29H SPIN PROJECTED BOND MATRICES,/)
0235 WRITE(6,10)
0236 10 FORMAT(11H ALPHA SPIN,/)
0237 DO 11 I=1,N
0238 11 WRITE(6,12) (PA(I,J),J=1,N)
0239 12 FORMAT(10F10.6)
0240 WRITE(6,13)
0241 13 FORMAT(1H ,///,10H BETA SPIN,/)
0242 DO 14 I=1,N
0243 14 WRITE(6,12) (PB(I,J),J=1,N)

```

```

0244          DO 15 I=1,N
0245          DO 15 J=1,N
0246          H(I,J)=PA(I,J)+PB(I,J)
0247          15 H(J,I)=H(I,J)
0248          WRITE(6,16)
0249          16 FORMAT(1H //,18H TOTAL BAND MATRIX,/)
0250          DO 17 I=1,N
0251          17 WRITE(6,12) (H(I,J),J=1,N)
0252          CALL SPWRT(PA,PB,H,X,N)
0253          CALL PROJEN(BETA,A1,E,Z,GAMA,QA,QB,FA,PA,PB,X,H,C,N)
0254          IF(ICON,EQ,2) GO TO 26
0255          WRITE(6,18)
0256          18 FORMAT(37H****MORE ACCURATE SPIN PROJECTION****,/)
0257          X(1,2)=P
0258          IF(P,GT,Q) X(1,2)=Q
0259          X(1,2)=X(1,2)+SZ*(SZ+1,0)
0260          C X(1,2)=A
0261          X(1,3)=X(1,2)*X(1,2)
0262          C X(1,3)=A*A
0263          T3=TRACE(FB,FA,N)
0264          C T3=TRACE(PQPQPQ)
0265          X(1,4)=X(1,2)-T
0266          C X(1,4)=S*S
0267          X(1,5)=X(1,3)+P*Q+2,0*(T*T-T2)-T*(2,0*X(1,2)+PPQ-2,0)
0268          C X(1,5)=S*S*S*S
0269          X(1,6)=X(1,3)*X(1,2)+X(1,2)*P*Q+P*Q*(2,0*X(1,2) +PPQ-2,0)
0270          X(1,6)=X(1,6)-T*(3,0*X(1,3)+3,0*X(1,2)*(PPQ-2,0)+(PPQ-2,0)*
0271          1 (PPQ-2,0)+P*Q+4,0*(P-1,0)*(Q-1,0))
0272          X(1,6)=X(1,6)+2,0*(3,0*X(1,2)+3,0*PPQ-10,0)*(T*T-T2)
0273          X(1,6)=X(1,6)-6,0*(T*T*T-3,0*T2*T+2,0*T3)
0274          C X(1,6)=S*S*S*S*S*S
0275          X(1,7)=(SZ+1,0)*(SZ+2,0)
0276          X(1,8)=X(1,7)*X(1,7)
0277          SM=X(1,6)-2,0*X(1,7)*X(1,5)+X(1,8)*X(1,4)
0278          SM=SM/(X(1,5)-2,0*X(1,7)*X(1,4)+X(1,8))
0279          WRITE(6,19) SM
0280          19 FORMAT(23H AFTER PROJECTION,(S2)=,F9,6,/)
0281          CALL AMAT(QB,CA,H,N)
0282          CALL AMAT(FB,QA,C,N)
0283          CALL AMAT(H,QB,PB,N)
0284          C H=(QPQP) C=(PQPQP) PB=(QPQPQ)
0285          X(1,2)=X(1,2)-SZ*(SZ+1,0)-2,0*(SZ+1,0)
0286          X(1,3)=X(1,2)*X(1,2)
0287          C NEW A AND A*A VALUES
0288          X(2,1)=X(1,3)+P*Q+T*(3,0+2,0*T-2,0*X(1,2)-PPQ)
0289          C X(2,1)=A*A+PQ+TRACE(PQ)(3-2TRACE(PQ)-2A-N)
0290          X(2,2)=PPQ-4,0*T-3,0+2,0*X(1,2)
0291          C X(2,2)=N-4TRACE(PQ)-3+2A
0292          X(2,3)=2,0*T+1,0-X(1,2)
0293          C X(2,3)=2TRACE(PQ)+1,0A
0294          X(2,4)=X(1,3)+P*Q+T*(2,0+2,0*T-2,0*X(1,2)-PPQ)
0295          C X(2,4)=A*A+PQ+TRACE(PQ)(2+2TRACE(PQ)-2A-N)
0296          T3=SECTR(H,N)
0297          C T3=TRACE(QPQPQ)
0298          DO 21 I=1,N
0299          DO 21 J=1,N
0300          C(I,J)=4,0*(I,J)+QA(I,J)*(X(2,1)-Q-2,0*T2)
0301          C(I,J)=C(I,J)+(P-T)*QB(I,J)+CB(I,J)
0302          C(I,J)=C(I,J)+X(2,2)*CA(I,J)+(FA(I,J)+CF(I,J))*(X(2,3)-P)
0303          C(I,J)=C(I,J)-2,0*(FB(I,J)*H(I,J))
0304          C(I,J)=C(I,J)/(X(2,4)-2,0*T2)
0305          C(J,I)=C(I,J)
0306          PR(I,J)=4,0*PR(I,J)+QB(I,J)*(X(2,1)-P-2,0*T3)

```

```

0307          PB(I,J)=PB(I,J)+(Q-T)*QA(I,J)+CA(I,J)
0308          PB(I,J)=PB(I,J)+X(2,2)*CB(I,J)+(FA(I,J)+CF(I,J))*(X(2,3)-Q)
0309          PB(I,J)=PB(I,J)-2.0*(H(I,J)+FB(I,J))
0310          PB(I,J)=PB(I,J)/(X(2,4)-T3*2.0)
0311          PB(J,I)=PB(I,J)
0312          21 CONTINUE
0313          C      C AND PB ARE NEW DENSITY MATRICES
0314          WRITE (6,9)
0315          WRITE (6,10)
0316          DO 22 I=1,N
0317          22 WRITE(6,12) (C(I,J),J=1,N)
0318          WRITE(6,13)
0319          DO 23 I=1,N
0320          23 WRITE(6,12) (PB(I,J),J=1,N)
0321          DO 24 I=1,N
0322          DO 24 J=1,N
0323          PA(I,J)=C(I,J)+PB(I,J)
0324          24 PA(J,I)=PA(I,J)
0325          WRITE(6,16)
0326          DO 25 I=1,N
0327          25 WRITE (6,12) (PA(I,J),J=1,N)
0328          CALL SPWRT(C,PB,PA,X,N)
0329          CALL PROJEN(BETA,AI,E,Z,GAMA,QA,QB,FA,C,PB,X,PA,H,N)
0330          26 RETURN
0331          END

```

END OF SEGMENT, LENGTH 1859, NAME SPIN

```

0332
0333         SUBROUTINE SPWRT(PA,PB,H,X,N)
0334 C PRINTS OUT RESULTS FROM SPINPOL
0335         DIMENSION PA(30,30),PB(30,30),X(30,30),H(30,30)
0336         WRITE (6,1)
0337 1  FORMAT(1H ,//,5H ATOM,10X,13H SPIN DENSITY,10X,
0338 1  15H CHARGE DENSITY,/)
0339         DO 2 I=1,N
0340         X(1,2)=PA(1,1)-PB(1,1)
0341         WRITE (6,3) I,X(1,2),H(1,1)
0342 2  CONTINUE
0343 3  FORMAT(1H ,13,14X,F8.5,14X,F8.5,/)
0344         RETURN
0345         END

```

END OF SEGMENT, LENGTH 100, NAME SPWRT

```
0346
0347     SUBROUTINE AMAT(A,B,C,N)
0348     DIMENSION A(30,30),B(30,30),C(30,30)
0349     DO 1 I=1,N
0350     DO 1 J=1,N
0351     C(I,J)=0.0
0352     DO 1 K=1,N
0353     1 C(I,J)=C(I,J)+A(I,K)+B(K,J)
0354     RETURN
0355     END
```

END OF SEGMENT, LENGTH 106, NAME AMAT

```
0356  
0357     REAL FUNCTION TRACE (A,B,N)  
0358     DIMENSION A(30,30),B(30,30)  
0359     TRACE=0.0  
0360     DO 1 I=1,N  
0361     DO 1 J=1,N  
0362     1  TRACE=TRACE+A(I,J)*B(J,I)  
0363     RETURN  
0364     END
```

END OF SEGMENT, LENGTH 74, NAME TRACE

```

0365
0366      SUBROUTINE HUCK(H,NF,CA,ENA,PA,D,N)
0367 C HUCKEL APPROXIMATION
0368      DIMENSION H(30,30),CA(30,30),ENA(30),PA(30,30),D(30)
0369      CALL QLRV(H,CA,ENA,D,N,IFAIL)
0370      IF(IFAIL.EQ.1) CALL ABORT
0371      DO 1 I=1,N
0372      DO 1 J=1,N
0373      PA(I,J)=0.0
0374      DO 1 K=1,NF
0375      1 PA(I,J)=PA(I,J)+CA(K,I)*CA(K,J)*2.0
0376      RETURN
0377      END

```

END OF SEGMENT, LENGTH 141, NAME HUCK

```

0378
0379      SUBROUTINE COUL(A1,E,R,GAMA,N)
0380      C EVALUATES COULOMB INTEGRALS
0381      DIMENSION A1(30),E(30),R(30,30),GAMA(30,30)
0382      C EQUATION 8 , MONOMER , OPEN SHELL
0383      DO 1 I=1,N
0384      DO 1 J=1,N
0385      1 GAMA(I,J)=1 0/((R(I,J)/14.41)+(2.0/(A1(I)-E(I)+A1(J)
0386      1-E(J))))
0387      RETURN
0388      END

```

END OF SEGMENT, LENGTH 103, NAME COUL

```

0389
0390      SUBROUTINE PUTIN(CH,PA,PB,ANA,ANB,N)
0391      DIMENSION CH(30,30),PA(30,30),PB(30,30),ANA(30),ANB(30)
0392      DO 1 I=1,N
0393      DO 1 J=1,N
0394      PA(I,J)=0.0
0395      PB(I,J)=0.0
0396      DO1 K=1,N
0397      PA(I,J)=PA(I,J)+CH(K,I)*CH(K,J)*ANA(K)
0398      1 PB(I,J)=PB(I,J)+CH(K,I)*CH(K,J)*ANB(K)
0399      RETURN
0400      END

```

END OF SEGMENT, LENGTH 162, NAME PUTIN

```

0401
0402      SUBROUTINE FMAT(AI,E,PA,PB,Z,GAMA,BETA,N,FA,FB)
0403      C SETS UP F MATRIX
0404      DIMENSION AI(30),E(30),PA(30,30),PB(30,30),Z(30),
0405      1GAMA (30,30),BETA(30,30),FA(30,30),FB(30,30)
0406      C EQUATION 3 AND 4 ,OPEN SHELL MOLECULE
0407      DO 2 I=1,N
0408      FA(I,I)=0.0
0409      FB(I,I)=0.0
0410      DO 1 J=1,N
0411      IF(I.EQ.J) GO TO 1
0412      -FA(I,J)=BETA(I,J)-PA(I,J)*GAMA(I,J)
0413      FB(I,J)=BETA(I,J)-PB(I,J)*GAMA(I,J)
0414      FA(I,I)=FA(I,I)+GAMA(I,J)*(PA(J,J)+PB(J,J)-Z(J))
0415      FB(I,I)=FB(I,I)+GAMA(I,J)*(PB(J,J)+PA(J,J)-Z(J))
0416      1 CONTINUE
0417      FA(I,I)=FA(I,I)-AI(I)*PB(I,I)*(AI(I)-E(I))
0418      2 FB(I,I)=FB(I,I)-AI(I)+PA(I,I)*(AI(I)-E(I))
0419      RETURN
0420      END

```

END OF SEGMENT, LENGTH 331, NAME FMAT

```

0421     REAL FUNCTION POLEN(FA,FB,PA,PB,AI,BETA,Z,GAMA,N)
0422     C CALCULATES TOTAL ENERGY
0423     DIMENSION FA(30,30),FB(30,30),PA(30,30),PB(30,30),AI(30),
0424     1 Z(30),BETA(30,30),GAMA(30,30)
0425     POLEN=0,0
0426     DO 1 I=1,N
0427     X=0,0
0428     DO 2 J=1,N
0429     IF(I.EQ.J) GO TO 2
0430     POLEN=POLEN+PA(J,I)*(FA(I,J)+BETA(I,J))+PB(J,I)*(FB(I,J)+
0431     1 BETA(I,J))
0432     X=X+Z(J)*GAMA(J,I)
0433     2 CONTINUE
0434     1 POLEN=POLEN+PA(I,I)*(FA(I,I)-X-AI(I))+PB(I,I)*(FB(I,I)-X-
0435     1 AI(I))
0436     POLEN=0,5*POLEN
0437     RETURN
0438     END
0439

```

END OF SEGMENT, LENGTH 211, NAME POLEN

```
0440          SUBROUTINE PURV(PA,PB,N)
0441          C PERFORMS ALTERNATION ON BOND ORDER MATRICES FOR CLOSED SHELL STATES.
0442          DIMENSION PA(30,30),PB(30,30)
0443          WRITE (6,1)
0444          1  FORMAT(1H ,//,26H PA AND PB ANTISYMMETRIZED,/)
0445          DO 2  I=1,N,2
0446             PA(I,I)=PA(I,I)*1.3
0447          2  PB(I,I)=PB(I,I)*0.7
0448          DO 3  I=2,N,2
0449             PB(I,I)=PB(I,I)*1.3
0450          3  PA(I,I)=PA(I,I)*0.7
0451          RETURN
0452          END
0453
```

END OF SEGMENT, LENGTH 120, NAME PURV

```
0454
0455     SUBROUTINE RITE(N)
0456     DIMENSION CHAR(12)
0457     READ(5,1) (CHAR(I),I=1,12)
0458     1  FORMAT(12A 6)
0459     WRITE(6,2) (CHAR(I),I=1,12)
0460     2  FORMAT(1H1,1H ,12A6,///)
0461     RETURN
0462     END
```

END OF SEGMENT, LENGTH 56, NAME RITE

```
0463
0464     REAL FUNCTION SECTR(A,N)
0465     DIMENSION A(30,30)
0466     SECTR=0.0
0467     DO 1 I=1,N
0468 1 SECTR=SECTR+A(I,I)
0469     RETURN
0470     END
```

END OF SEGMENT, LENGTH 51, NAME SECTR

```

0471          SUBROUTINE PROJEN(BETA,AI,E,Z,GAMA,QA,QB,FA,PA,PB,X,H,C,N)
0472          C CALCULATES TOTAL ENERGY AFTER PROJECTION
0473          DIMENSION BETA(30,30),AI(30  ),E(30),Z(30),GAMA(30,30),QA(30,30),
0474          1 QB(30,30),FA(30,30),PA(30,30),PB(30,30),X(30,30),H(30,30),
0475          2 C(30,30)
0476          DO 1 I=1,N
0477          C(I,I)=0.0
0478          DO 2 J=1,N
0479          IF (I.EQ.J) GO TO 2
0480          C(I,I)=C(I,I)-Z(J)*GAMA(I,J)
0481          C(I,J)=BETA(I,J)
0482          2 CONTINUE
0483          1 C(I,I)=C(I,I)-AI(I)
0484          X(1,3)=TRACE(H,C,N)
0485          DO 3 I=1,N
0486          H(I,I)=0.0
0487          C(I,I)=0.0
0488          DO 4 J=1,N
0489          IF(I.EQ.J) GO TO 4
0490          C(I,I)=C(I,I)+(QA(J,J)+QB(J,J))*GAMA(I,J)
0491          C(I,J)=-QB(I,J)*GAMA(I,J)
0492          H(I,J)=-QA(I,J)*GAMA(I,J)
0493          4 CONTINUE
0494          H(I,I)=C(I,I)+QB(I,I)*(AI(I)-E(I))
0495          3 C(I,I)=C(I,I)+QA(I,I)*(AI(I)-E(I))
0496          X(1,3)=X(1,3)+0.5*(TRACE(PA,H,N)+ TRACE(PB,C,N))
0497          X(1,4)=0.0
0498          DO 5 I=1,N
0499          DO 6 J=1,N
0500          IF(I.EQ.J) GO TO 6
0501          X(1,4)=X(1,4)+(QA(I,J)-FA(I,J))*(FA(J,I)-QB(J,I))*GAMA(I,J)
0502          6 CONTINUE
0503          5 X(1,4)=X(1,4)+(QA(I,I)-FA(I,I))*(FA(I,I)-QB(I,I))*(AI(I)-E(I))
0504          X(1,4)=0.5*X(1,4)/X(1,1)
0505          WRITE (6,7) X(1,4)
0506          7 FORMAT (1H ,//,17H CORRECTION TERM=,F10,6,/)
0507          X(1,3)=X(1,3)-X(1,4)
0508          WRITE (6,8) X(1,3)
0509          8 FORMAT(34H TOTAL ENERGY WITH SPIN PROJECTED=,F12,6,/)
0510          RETURN
0511          END
0512

```

END OF SEGMENT, LENGTH 637, NAME PROJEN

```

0513          SUBROUTINE RECAL(F,Q,AN,N,CH,X,CF,D,ICV)
0514          DIMENSION F(30,30),Q(30,30),AN(30),ENA(30),C(30,30),CH(30,30)
0515          1 ,X(30,30),CF(30,30),D(30)
0516          C RECALCULATES P FROM F EIGENVECTORS RETURNS AS Q
0517          CALL QLRV(F,C,ENA,D,N,IFAIL)
0518          IF (IFAIL.EQ.1) CALL ABORT
0519          CALL VSORT(C,CH,X,CF,ENA,N,ICV)
0520          DO 2 I=1,N
0521          DO 2 J=1,N
0522          Q(I,J)=0.0
0523          - DO 2 K=1,N
0524          2 Q(I,J)=Q(I,J)+AN(K)*C(K,I)*C(K,J)
0525          DO 3 I=1,N
0526          DO 3 J=1,N
0527          3 CH(I,J)=C(I,J)
0528          RETURN
0529          END
0530

```

END OF SEGMENT, LENGTH 202, NAME RECAL

```

0531
0532      SUBROUTINE SCFCS(H,BETA,GAMA,AI,E,Z,FA,CA,CB,PA,PB,ANA
0533      1ANB,ENA,D,N)
0534      DIMENSION H(30,30),BETA(30,30),GAMA(30,30),AI(30),E(30),
0535      1 FA(30,30),CA(30,30),CB(30,30),PA(30,30),PB(30,30),Z(30
0536      2 ANA(30),ANB(30),ENA(30),D(30)
0537      NIT=5
0538      W=0.0
0539      DO 1 I=1,N
0540      1 W=W+ANA(I)+ANB(I)
0541      W=W*0.5
0542      NF=IFIX(W)
0543      DO 24 I=1,N
0544      24 WRITE(6,301) (H(I,J), J=1,N)
0545      301 FORMAT(12F8.3)
0546      CALL HUCK(H,NF,CA,ENA,PA,D,N)
0547      DO 3 L=1,NIT
0548      DO 4 I=1,N
0549      FA(I,I)=0.0
0550      DO 5 J=1,N
0551      IF(I.EQ.J) GO TO 5
0552      FA(I,J)=BETA(I,J)-0.5*PA(I,J)*GAMA(I,J)
0553      FA(I,I)=PA(I,I)+(PA(J,J)-Z(J))*GAMA(I,J)
0554      5 CONTINUE
0555      4 FA(I,I)=FA(I,I)-AI(I)+0.5*PA(I,I)*(AI(I)-E(I))
0556      IF(L.EQ.NIT) NF=N
0557      CALL QLRV(FA,CA,ENA,D,N,IFAIL)
0558      IF(IFAIL.EQ.1) CALL ABORT
0559      IF(L.EQ.NIT) GO TO 7
0560      DO 6 I=1,N
0561      DO 6 J=1,N
0562      PA(I,J)=0.0
0563      DO 6 K=1,NF
0564      6 PA(I,J)=PA(I,J)+CA(K,I)*CA(K,J)*2.0
0565      3 CONTINUE
0566      7 DO 8 I=1,N
0567      DO 8 J=1,N
0568      CB(I,J)=CA(I,J)
0569      PA(I,J)=0.0
0570      PB(I,J)=0.0
0571      DO 8 K=1,N
0572      PA(I,J)=PA(I,J)+CA(K,I)*CA(K,J)*ANA(K)
0573      8 PB(I,J)=PB(I,J)+CA(K,I)*CA(K,J)*ANB(K)
0574      RETURN
0575      END
0576

```

END OF SEGMENT, LENGTH 583, NAME SCFCS

```

0577          SUBROUTINE VSORT(C,CH,X,CF,ENA,N,ICV)
0578          C SORTS EIGENVECTORS TO ENSURE THAT THE ELECTRONS ARE ASSIGNED TO THE
0579          C INTENDED ORBITALS EVEN IF THEY CHANGE TO BECOME ENERGETICALLY
0580          C UNFAVOURABLE DURING THE COURSE OF THE SCF ITERATIONS
0581          DIMENSION C(30,30),CH(30,30),X(30,30),CF(30,30),
0582          1 ENA(30),ENAF(30),IM(30)
0583          IF(ICV.EQ.1) GO TO 18
0584          DO 1 M=1,N
0585          DO 1 I=1,N
0586          X(M,I)=0.0
0587          DO 1 J=1,N
0588          1 X(M,I)=X(M,I)+CH(I,J)*C(M,J)
0589          DO 2 M=1,N
0590          IM(M)=1
0591          DO 2 J=2,N
0592          IF(X(M,J).LE.X(M,1)) GO TO 2
0593          X(M,1)=X(M,J)
0594          IM(M)=J
0595          2 CONTINUE
0596          IY=0
0597          DO 3 I=1,N
0598          3 IY=IY+IM(I)
0599          IZ=N*(N+1)/2
0600          IF(IY.EQ.IZ) GO TO 15
0601          NM1=N-1
0602          DO 10 I=1,NM1
0603          IP1=I+1
0604          DO 10 J=IP1,N
0605          IF(IM(I).EQ.IM(J)) GO TO 11
0606          10 CONTINUE
0607          11 IF(X(I,1).GE.X(J,1)) GO TO 12
0608          IM(I)=IZ-IY+IM(I)
0609          GO TO 13
0610          12 IM(J)=IZ-IY+IM(J)
0611          13 IY=0
0612          DO 14 I=1,N
0613          14 IY=IY+IM(I)
0614          IF(IY.EQ.IZ) GO TO 15
0615          WRITE(6,16)
0616          16 FORMAT(13H DOUBLE DEGEN,/)
0617          15 DO 6 I=1,N
0618          K = IM(I)
0619          ENAF(K)=ENA(I)
0620          DO 6 J=1,N
0621          6 CF(K,J)=C(I,J)
0622          DO 7 I=1,N
0623          ENA(I)=ENAF(I)
0624          DO 7 J=1,N
0625          7 C(I,J)=CF(I,J)
0626          18 RETURN
0627          END
0628

```

END OF SEGMENT, LENGTH 505, NAME VSORT

```

0629          SUBROUTINE QLRV(A,Z,D,E,N,IFAIL)
0630          DIMENSION A(30,30),D(30),Z(30,30),E(30)
0631          IFAIL=0
0632          TOL=1.46E-28
0633          DO 1 I=1,N
0634          DO 1 J=1,I
0635          1 Z(I,J)=A(I,J)
0636          DO 2 I1=2,N
0637          I=N+2-I1
0638          L=I-2
0639          F=Z(I,I-1)
0640          G=0.0
0641          IF(L.EQ.0) GO TO 3
0642          DO 4 K= 1,L
0643          B=Z(I,K)
0644          4 G=G+B*B
0645          3 H=G+F*F
0646          IF(G.GT.TOL) GO TO 5
0647          E(I)=F
0648          H=0.0
0649          GO TO 2
0650          5 L=L+1
0651          G,E(I)=-SIGN(SQRT(H),F)
0652          H=H-F*G
0653          Z(I,I-1)=F-G
0654          F=0.0
0655          DO 7 J=1,L
0656          Z(J,I)=Z(I,J)/H
0657          G=0.0
0658
0659          DO 8 K=1,J
0660          8 G=G+Z(J,K)*Z(I,K)
0661          M=J+1
0662          IF(M.G.L) GO TO 9
0663          DO 10 K=M,L
0664          10 G=G+Z(K,J)*Z(I,K)
0665          9 E(J)=G/H
0666          7 F=F+G*Z(J,I)
0667          HH=F/(2.0*H)
0668          DO 11 J=1,L
0669          F=Z(I,J)
0670          G,E(J)=E(J)-HH*F
0671          DO 11 K=1,J
0672          11 Z(J,K)=Z(J,K)-F*E(K)-G*Z(I,K)
0673          2 D(I)=H
0674          D(1),E(1)=0.0
0675          DO 12 I=1,N
0676          L=I-1
0677          IF(D1).EQ.0.0) GO TO 13
0678          IF(L.EQ.0) GO TO 13
0679          DO 14 J=1, L
0680          G=0.0
0681          DO 15 K=1,L
0682          15 G=G+Z(I,K)*Z(K,J)
0683          DO 14 K=1,L
0684          14 Z(K,J)=Z(K,J)-G*Z(K,I)
0685          13 D(I)=Z(I,I)
0686          Z(I,I)=1.0
0687          IF(L.EQ.0) GO TO 12
0688          DO 16 J=1,L
0689          16 Z(I,J),Z(J,I)=0.0
0690          12 CONTINUE
0691          ACHEPS=0.0000000001
0692          DO 17 I=2,N

```

```

0693      17 E(I-1)=E(I)
0694          E(N),B,F=0.0
0695          DO 21 L=1,N
0696              J=0
0697              H=ACHEPS*(ABS(D(L))+ABS(E(L)))
0698              B=AMAX1(B,H)
0699              DO 19 M=L,N
0700                  IF(ABS(E(M)).LE.B) GO TO 20
0701      19 CONTINUE
0702      20 IF(M,EQ,L) GO TO 21
0703      18 IF(J,EQ,30) GO TO 22
0704          J=J+1
0705          P=(D(L+1)-D(L))/(2.0*E(L))
0706          R=SQRT(P*P+1.0)
0707          IF(P.LT.TOL) GO TO 80
0708          H=D(L)-(E(L)/(P+SIGN(1.0,P)*R))
0709          GO TO 81
0710      80 H=D(L)-E(L)
0711      81 CONTINUE
0712          DO 23 I=L,N
0713      23 D(I)=D(I)-H
0714          F=F+H
0715          P=D(M)
0716          C=1.0
0717          S=0.0
0718          MM=M-1
0719          IF(MM.LT.L) GO TO 24
0720          DO 28 I=L,MM
0721              I=MM+L-I
0722              G=C*E(I)
0723              H=C*R
0724              IF(ABS(P).LT.ABS(E(I))) GO TO 26
0725              C=E(I)/P
0726              R=SQRT(C*C+1.0)
0727              E(I+1)=S*P*R
0728              S=C/R
0729              C=1.0/R
0730              GO TO 27
0731      26 C=P/E(I)
0732              R=SQRT(C*C+1.0)
0733              E(I+1)=S*E(I)*R
0734              S=1.0/R
0735              C=C/R
0736      27 P=C*D(I)-S*G
0737              D(I+1)=H+S*(C*G+S*D(I))
0738              DO 28 K=1,N
0739                  H=Z(K,I+1)
0740                  Z(K,I+1)=S*Z(K,I)+C*H
0741      28 Z(K,I)=C*Z(K,I)-S*H
0742      24 E(L)=S*P
0743          D(L)=C*P
0744          IF(ABS(E(L)).GT.B) GO TO 18
0745      21 D(L)=D(L)+F
0746          DO 29 I=1,N
0747              K=I
0748              P=D(I)
0749              IF(I.EQ.N) GO TO 30
0750              IT=I*I
0751              DO 31 J=I+1,N
0752                  IF(D(J).GE.P) GO TO 31
0753                  K=J
0754                  P=D(J)

```

```
0755          31 CONTINUE
0756          30 IF(K.EQ.1) GO TO 29
0757             D(K)=D(1)
0758             D(1)=P
0759             DO 32 J=1,N
0760             P=Z(J,1)
0761             Z(J,1)=Z(J,K)
0762          32 Z(J,K)=P
0763          29 CONTINUE
0764             CALL ROWS(Z,N)
0765             RETURN
0766          22 IFAIL=1
0767             RETURN
0768             END
```

END OF SEGMENT, LENGTH 1370, NAME QLRV

```
0769
0770          SUBROUTINE ROWS(Z,N)
0771          DIMENSION Z(30,30),E(30,30)
0772          DO 40 ISOD=1,N
0773          DO 40 JSOD=1,N
0774          40 E(ISOD,JSOD)=Z(JSOD,ISOD)
0775          CONTINUE
0776          DO 41 ISOD=1,N
0777          DO 41 JSOD=1,N
0778          41 Z(ISOD,JSOD)=E(ISOD,JSOD)
0779          RETURN
0780          END
```

END OF SEGMENT, LENGTH 101, NAME ROWS

```
0781          SUBROUTINE ABORT
0782          WRITE (6,99)
0783          99  FORMAT (///, 'QR FAILS')
0784          STOP
0785          END
```

END OF SEGMENT, LENGTH 21, NAME ABORT

```
0786          SUBROUTINE WRITE(A,N,S)
0787          DIMENSION A(30,30),S(2)
0788          WRITE(6,1) S
0789          DO 3 I=1,N
0790          3 WRITE(6,2) (A(I,J), J=1,N)
0791          RETURN
0792          1 FORMAT(2X,2A8)
0793          2 FORMAT(10(1X,F10.5))
0794          END
```

END OF SEGMENT, LENGTH 71, NAME WRITE

N (I3)

N is the number of donating atoms in the molecule ≤ 30 .

NIT (I3)

This represents the maximum number of iterations, ≤ 50 .

GN, CONVG, DVC (3F20.8)

Again, all three parameters are fed in on the same card.

GN is the constant by which the Mataga, Nishimoto approximation for the Coulomb integrals is multiplied. Normally this is set to 1.

CONVG is the convergence criterion, which sets the degree of consistency to which the bond order matrices must converge. Usually CONVG = 0.001.

DVC is a parameter used to control a feedback routine for successive bond matrices. This technique, which involves mixing some of the previous bond order with the new one calculated after each iteration, is normally essential to help the results converge. A typical value for the DVC would be 0.3.

/R(N,N)/ (F20.8)

This represents the geometric matrix R, in which all interatomic distances within the molecule are specified. As it is a symmetrical matrix, only the upper triangle is fed in i.e. the matrix is presented as R_{11} , R_{12} , R_{13} ... R_{1N} , R_{22} ... R_{2N} , R_{33} etc.

/AI(N)/ (F20.8)

This matrix contains the ionization potential of each atom contributing to the molecular system.

/E(N)/ (F20.8)

E(I) is the electron affinity of atom I.

/Z(N)/ (F20.8)

Z(I) is the virtual charge of atom I, and is equal to the number of electrons atom I contributes to the system.

/H(N,N)/ (F20.8)

H(N,N) is the matrix for the core resonance integrals $\beta_{\mu\nu}$.

Like the distance matrix, it is symmetrical and only the top triangle is needed.

/ANA(N)/ (F20.8)

This matrix specifies the α orbital occupation, counting from the lowest occupied orbital upwards. ANA(I) = 1 for an occupied orbital, otherwise it is zero.

/ANB(N)/ (F20.8)

The similar matrix for the β occupation.

N5 (I3)

If N5 = 5, the program restarts. If N5 = 1 however, the program stops.

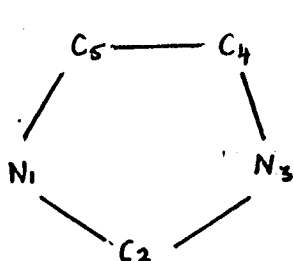
In all cases, both the accurate and simple spin projection routines were employed, and the spin and charge densities were written out at the conclusion of each step.

The program was first tried out on the parent lophinyl radical, with the preliminary objective being to ascertain reasonable assignments for the stereochemistry and the other parameters needed for the P.P.P. calculation of the spin densities. This involved choosing an initial set of data, shown below, and making then, reasonable adjustment to it, until the spin densities obtained were in close agreement to those given by Cyr Wilks and Willis.⁴⁴

(i) Distance matrix.

To construct the distance matrix, crystallographic data was essential, but unfortunately, this was not available for the triphenyl imidazolyl radical and a compromise was thus used in its construction.

The distance between the adjacent carbon atoms in the three pendant rings were taken as equal to that distance in a benzene molecule⁵¹, i.e. 1.39\AA . The interatomic distances between the atoms in the imidazolyl ring were based upon the crystallographic evidence obtained from other molecules containing nitrogen, especially pyrimidine⁵², and the angles within the five membered ring, were estimated by considering the data for pyrrole⁵³, and imidazole⁵⁴. As a result, the distances in this were put as follows



$$N_1 - C_2 = N_3 - C_2 = 1.33\text{\AA}$$

$$N_1 - C_5 = N_3 - C_4 = 1.35\text{\AA}$$

$$C_5 - C_4 = 1.39\text{\AA}$$

$$\angle N_1 C_2 N_3 = 113^\circ$$

$$\angle C_2 N_1 C_5 = 106^\circ$$

Finally, the separation between the phenyl rings and the five membered imidazolyl ring were needed. The C2 - C18 distance (see Figure 1.11) was calculated simply from its bond order (given by the Hückel method) using the relationship of bond order with distance given by Roberts⁵⁵, while the C4 - C12 and C5 - C6 distances were estimated by considering the data given for diphenyl and its halo-derivatives⁵⁶. This parallel would seem quite reasonable, as both the rings (with respect to each other) in the diphenyl compound, and the 4 and 5 phenyl rings (with respect to the imidazolyl ring) in the triphenyl imidazolyl radical (see below) are considered to be twisted at about the same angle i.e. 45° . Using these approximations then,

$$C_2 - C_{18} = 1.44\text{\AA}$$

$$C_4 - C_{12} = C_5 - C_6 = 1.48 - 1.54\text{\AA}$$

After a number of trials with the program, a C4 - C12 and C5 - C6 distance of 1.51\AA was decided upon.

Having calculated the individual distances between adjacent atoms, the whole molecule was drawn out accurately, bearing in mind the angle of twist of the 4 and 5 phenyl rings, and the whole distance matrix was constructed.

(ii) Hückel matrix

From the completed distance matrix, then, the core resonance integrals (for neighbouring atoms μ, ν) $\beta_{\mu\nu}$ could be calculated using the equation (1.66) given by Stout and Bell.

$$\beta_{\mu\nu} = -2524 \left\{ -5.047 \left(\frac{Z_{\mu} + Z_{\nu}}{Z_c} - 2 \right)^2 - 5r_{\mu\nu} \right\}$$

where $Z_N = 2.318$ and $Z_c = 2.095$

In fact, graphs illustrating the variation of $\beta_{\mu\nu}$ with $r_{\mu\nu}$ for carbon - carbon bonds and for carbon nitrogen bonds are shown in Figures 4.8 and 4.9 respectively. Now Cyr, Wilks and Willis ; in their discussion of the ESR spectrum of the radical, have suggested that the 4 and 5 rings must be twisted to some degree out of plane to avoid steric clashing, and have suggested that this angle would be about 40° . Indeed, models show this estimate to be reasonable, and accordingly, the resonance integrals for the 4-12 and 5-6 bonds were multiplied by the cosine of the angle of twist, a relationship often used in Hückel calculations.

(iii) Valence state electron affinity and ionization potential.

There exist two common sets of valence state ionization potentials and electron affinities for carbon and nitrogen atoms, the first being due to Pritchard and Skinner,⁵⁷ and the other due to Hinze and Jaffé³².

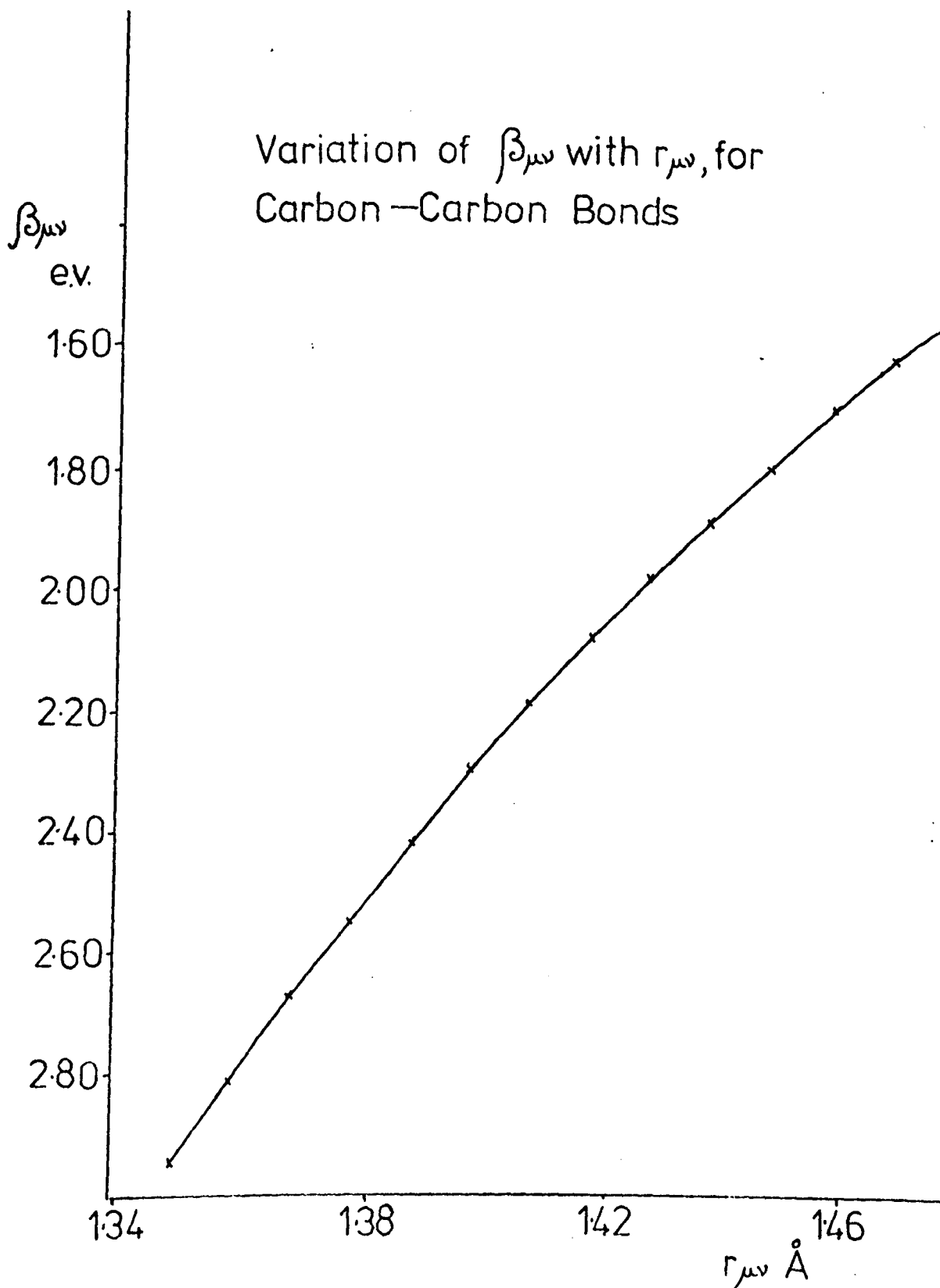


FIGURE 4.8

Variation of $\beta_{\mu\nu}$ with $r_{\mu\nu}$, for
Carbon — Nitrogen Bonds

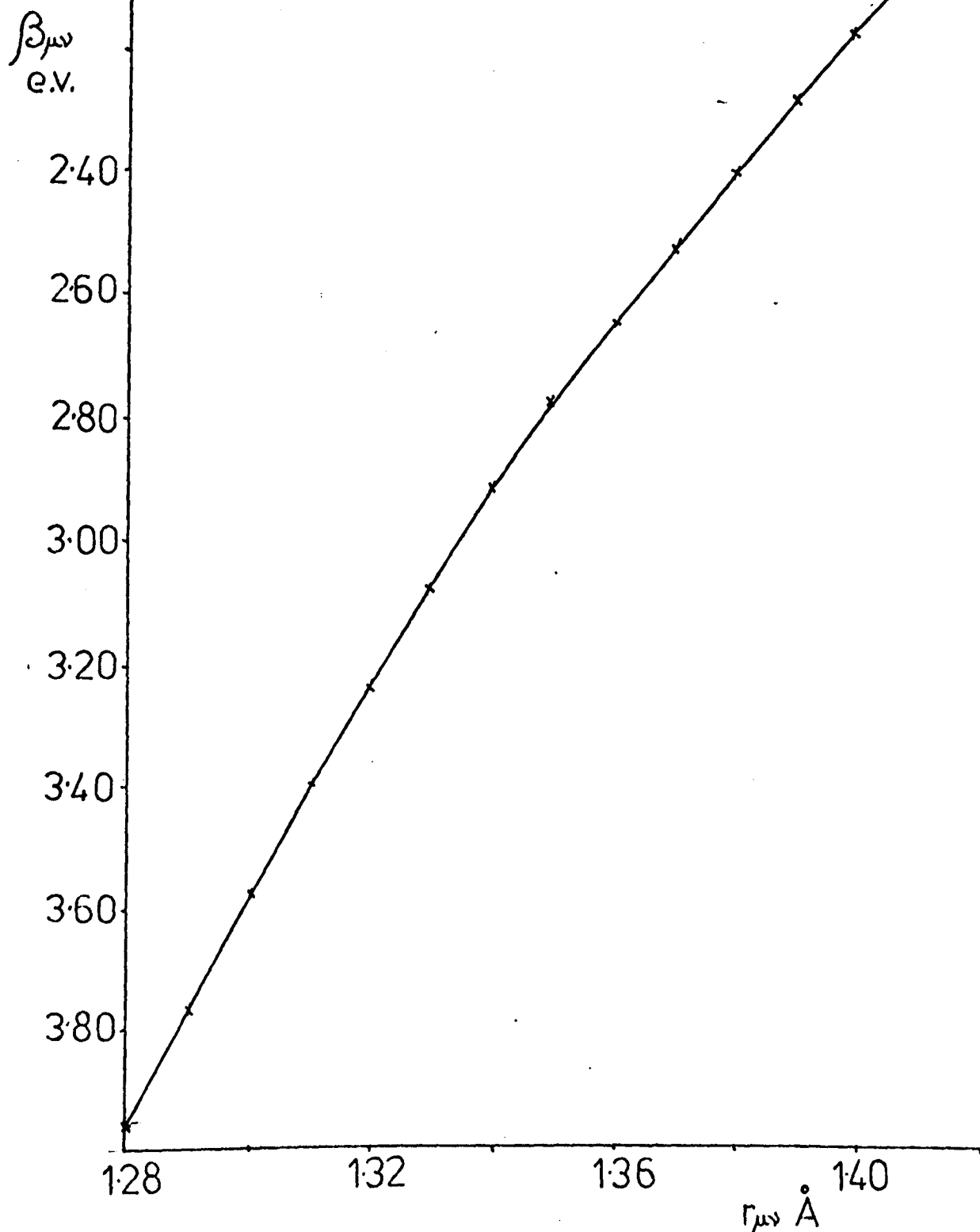


FIGURE 4.9

These are:-

Atom	(Pritchard and Skinner)		(Hinze and Jaffe)	
	V.S.I.P.	V.S.E.A.	V.S.I.P.	V.S.E.A.
C	11.22	0.62	11.16	0.03
N as in -N=	14.51	1.20	14.12	1.58

It can be seen, that there is a very large discrepancy between both sets of electron affinities, and which set is used would seem to be dependent upon the property under investigation i.e. it has been shown that different electron affinities and ionization potentials are required for correlation of different ground state properties with experiment. As little work has been done to evaluate their relative merits, each set was taken in turn as a starting point for the calculations of the spin densities on the lophinyl radical. Using both sets however, no reasonable amount of alteration of the distance or core resonance integral matrices, could bring good agreement between these values and those given by Cyr, Wilks and Willis.

Adjustment of the electron affinities and ionization potentials did lead to better results, and eventually reasonable agreement was reached for the ortho and para positions of the 3 phenyl rings with the electron affinities for carbon and nitrogen of 0.600 and 1.80, and their ionization potentials of 11.16 and 14.12 respectively. The spin densities on the meta positions on the other hand, were still many times too great.

It was at first thought, that there was an inherent fault in the spin polarising routine of the program, resulting in negative spin densities becoming larger than expected. However, Tiño⁵⁸ has shown that the value for Q as given in the relationship

$$a_H \approx Q\rho$$

is not constant as assumed by Cyr et al, but is strongly dependent upon a) the sign of the spin density and b) upon the method used to calculate them. Considering a number of radicals, Tiño has compared the spin densities obtained for each, from various molecular orbital methods with experimental splitting constants, and has made statistical conclusions about the results. For instance the Unrestricted Hartree Fock method due to Berthier⁵⁹ and Pople and Nesbet⁶⁰, gives spin densities which must have the following values of Q

- a) positions with negative spin densities = 11.40
- b) positions with positive spin densities = 20.50
- c) positions having one carbon bonded to central sp^2 = 24.46

Thus, if one assumes that the splitting constants of Cyr et al, are correct, and that these values of Q are applicable to the results from the spin polarising program given in this thesis, then the spin densities now required, are as follows.

position	o	m	p	o'	m'	p'
spin density	0.0624	-0.0439	0.0659	0.1020	-0.0697	0.1039

One may see, that the value for the meta positions is much higher than previously thought, and the program now appeared to be giving reasonable results. Table 35 shows the spin densities obtained using the data given in Figure 4.10

Table 35

position	o	m	p	o'	m'	p'
spin density	0.0621	-0.0452	0.0593	0.0897	-0.0610	0.0856

N33=2.0 ICV=1.0 ICON=3.0

N=23.0

NIT=50.0

GN=1.0 CONVG=0.001 DVC=0.3

N	1	2	3	4	5	6	7	8	9	10	11	12	13	14	15	16	17	18	19	20	21	22	23
AI	14.12	11.16	14.12	11.16	11.16	11.16	11.16	11.16	11.16	11.16	11.16	11.16	11.16	11.16	11.16	11.16	11.16	11.16	11.16	11.16	11.16	11.16	11.16

N	1	2	3	4	5	6	7	8	9	10	11	12	13	14	15	16	17	18	19	20	21	22	23
E	2.0	0.7	2.0	0.7	0.7	0.7	0.7	0.7	0.7	0.7	0.7	0.7	0.7	0.7	0.7	0.7	0.7	0.7	0.7	0.7	0.7	0.7	0.7

N	1	2	3	4	5	6	7	8	9	10	11	12	13	14	15	16	17	18	19	20	21	22	23
Z	1.0	1.0	1.0	1.0	1.0	1.0	1.0	1.0	1.0	1.0	1.0	1.0	1.0	1.0	1.0	1.0	1.0	1.0	1.0	1.0	1.0	1.0	1.0

N	1	2	3	4	5	6	7	8	9	10	11	12	13	14	15	16	17	18	19	20	21	22	23
ANP	1.0	1.0	1.0	1.0	1.0	1.0	1.0	1.0	1.0	1.0	1.0	1.0	0.0	0.0	0.0	0.0	0.0	0.0	0.0	0.0	0.0	0.0	0.0

N	1	2	3	4	5	6	7	8	9	10	11	12	13	14	15	16	17	18	19	20	21	22	23
ANB	1.0	1.0	1.0	1.0	1.0	1.0	1.0	1.0	1.0	1.0	1.0	0.0	0.0	0.0	0.0	0.0	0.0	0.0	0.0	0.0	0.0	0.0	0.0

FIGURE 4.10

R(N,N) Matrix

	1	2	3	4	5	6	7	8	9	10	11	12	13	14	15	16	17	18	19	20	21	22	23
1	0.0	1.32	2.19	2.19	1.35	2.49	3.66	4.83	5.15	4.43	3.09	3.60	4.49	5.89	6.36	5.65	4.30	2.45	2.87	4.24	5.09	4.64	3.71
2	1.32	0.0	1.32	2.16	2.16	3.55	4.57	5.86	4.68	5.69	4.32	3.55	4.32	5.69	6.31	5.86	4.57	1.44	2.43	3.68	4.22	3.68	2.43
3	2.19	1.32	0.0	1.35	2.19	3.60	4.30	5.65	6.36	5.89	4.49	2.49	3.09	4.43	5.15	4.83	3.66	2.45	3.71	4.64	5.09	4.24	2.87
4	2.19	2.16	1.35	0.0	1.39	2.50	3.08	4.42	5.15	4.90	3.70	1.51	2.49	3.77	4.25	3.74	2.48	3.54	4.53	5.85	6.28	5.58	4.20
5	1.35	2.16	2.19	1.39	0.0	1.51	2.48	3.74	4.25	3.77	2.49	2.50	3.70	4.90	5.15	4.42	3.08	3.54	4.20	5.58	6.28	5.83	4.53
6	2.49	3.55	3.60	2.50	1.51	0.0	1.39	2.39	2.81	2.39	1.39	3.04	4.28	5.21	5.19	4.23	3.00	4.88	5.32	6.69	7.56	7.25	6.00
7	3.66	4.57	4.30	3.08	2.48	1.39	0.0	1.39	2.44	2.81	2.45	3.00	3.99	4.66	4.51	3.71	2.86	5.90	6.47	7.82	8.62	8.23	6.92
8	4.83	5.86	5.65	4.42	3.74	2.39	1.39	0.0	1.39	2.45	2.82	4.23	5.13	5.56	5.13	4.23	3.71	7.18	7.60	8.97	9.34	9.52	8.24
9	5.15	4.68	6.36	5.15	4.25	2.81	2.44	1.39	0.0	1.39	2.43	5.17	6.25	6.74	6.25	5.13	4.53	7.59	7.81	9.15	10.18	10.00	8.75
10	4.43	5.69	5.89	4.90	3.77	2.39	2.81	2.45	1.39	0.0	1.39	5.21	6.45	7.12	6.74	5.56	4.66	8.83	6.92	8.20	7.98	7.87	6.70
11	3.09	4.32	4.49	3.70	2.49	1.39	2.45	2.82	2.43	1.39	0.0	4.28	5.88	6.45	6.28	5.13	3.99	5.48	5.62	6.87	7.98	7.87	6.70
12	3.60	3.55	2.49	1.51	2.50	3.04	3.00	4.23	5.17	5.21	4.28	0.0	1.39	2.39	2.81	2.39	1.39	4.88	6.00	7.25	7.56	6.69	5.32
13	4.49	4.32	3.09	2.49	3.70	4.28	3.99	5.13	6.25	6.45	5.88	1.39	0.0	1.39	2.44	2.81	2.45	5.48	6.70	7.87	7.98	6.87	5.62
14	5.89	5.69	4.43	3.77	4.90	5.21	4.66	5.56	6.74	7.12	6.45	2.39	1.39	0.0	1.39	2.45	2.82	6.83	8.08	9.23	9.28	8.20	6.92
15	6.36	6.31	5.15	4.25	5.15	5.19	4.51	5.13	6.25	6.74	6.25	2.81	2.44	1.39	0.0	1.39	2.43	7.59	8.75	10.00	10.18	9.15	7.81
16	5.65	5.86	4.83	3.74	4.42	4.23	3.71	4.23	5.13	5.56	5.13	2.39	2.81	2.45	1.39	0.0	1.39	7.18	8.24	9.52	9.34	8.97	7.60
17	4.30	4.57	3.66	2.48	3.08	3.00	2.85	3.71	4.53	4.66	5.13	1.39	2.45	2.82	2.43	1.39	0.0	5.90	6.92	8.23	8.62	7.82	6.47
18	2.45	1.44	2.45	3.54	3.54	4.88	5.90	7.18	7.59	6.83	5.48	4.88	5.48	6.83	7.59	7.18	5.90	0.0	1.39	2.39	2.81	2.39	1.39
19	2.87	2.43	3.71	4.53	4.20	5.32	6.47	7.60	7.81	6.92	5.62	6.00	6.70	8.08	8.75	8.24	6.92	1.39	0.0	1.39	2.43	2.83	2.45
20	4.24	3.68	4.64	5.85	5.58	6.69	7.82	8.97	9.15	8.20	6.87	7.25	7.87	9.23	10.00	9.52	8.23	2.39	1.39	0.0	1.39	2.45	2.81
21	5.09	4.22	5.09	6.28	6.20	7.56	8.62	9.34	10.18	9.28	7.98	7.56	7.98	9.28	10.18	9.34	8.62	2.81	2.43	1.39	0.0	1.39	2.43
22	4.64	3.68	4.24	5.58	5.83	7.25	8.23	9.52	10.00	9.23	7.87	6.69	6.87	8.20	9.15	8.97	7.82	2.39	2.83	2.45	1.39	0.0	1.39
23	3.71	2.43	2.87	4.20	4.53	6.00	6.92	8.24	8.75	8.08	6.70	5.32	5.62	6.92	7.81	7.60	6.47	1.39	2.45	2.81	2.43	1.39	0.0

FIGURE 4.10

H(N,N) Matrix

1	1	2	3	4	5	6	7	8	9	10	11	12	13	14	15	16	17	18	19	20	21	22	23
1	0.0	-3.25	0.0	0.0	-2.79	0.0	0.0	0.0	0.0	0.0	0.0	0.0	0.0	0.0	0.0	0.0	0.0	0.0	0.0	0.0	0.0	0.0	0.0
2	-3.25	0.0	-3.25	0.0	0.0	0.0	0.0	0.0	0.0	0.0	0.0	0.0	0.0	0.0	0.0	0.0	0.0	-1.79	0.0	0.0	0.0	0.0	0.0
3	0.0	-3.25	0.0	-2.79	0.0	0.0	0.0	0.0	0.0	0.0	0.0	0.0	0.0	0.0	0.0	0.0	0.0	0.0	0.0	0.0	0.0	0.0	0.0
4	0.0	0.0	-2.79	0.0	-2.38	0.0	0.0	0.0	0.0	0.0	-1.22	0.0	0.0	0.0	0.0	0.0	0.0	0.0	0.0	0.0	0.0	0.0	0.0
5	-2.79	0.0	0.0	-2.38	0.0	-1.22	0.0	0.0	0.0	0.0	0.0	0.0	0.0	0.0	0.0	0.0	0.0	0.0	0.0	0.0	0.0	0.0	0.0
6	0.0	0.0	0.0	0.0	-1.22	0.0	-2.38	0.0	0.0	-2.38	0.0	0.0	0.0	0.0	0.0	0.0	0.0	0.0	0.0	0.0	0.0	0.0	0.0
7	0.0	0.0	0.0	0.0	0.0	-2.38	0.0	-2.38	0.0	0.0	0.0	0.0	0.0	0.0	0.0	0.0	0.0	0.0	0.0	0.0	0.0	0.0	0.0
8	0.0	0.0	0.0	0.0	0.0	0.0	-2.38	0.0	-2.38	0.0	0.0	0.0	0.0	0.0	0.0	0.0	0.0	0.0	0.0	0.0	0.0	0.0	0.0
9	0.0	0.0	0.0	0.0	0.0	0.0	0.0	-2.38	0.0	-2.38	0.0	0.0	0.0	0.0	0.0	0.0	0.0	0.0	0.0	0.0	0.0	0.0	0.0
10	0.0	0.0	0.0	0.0	0.0	0.0	0.0	0.0	-2.38	0.0	-2.38	0.0	0.0	0.0	0.0	0.0	0.0	0.0	0.0	0.0	0.0	0.0	0.0
11	0.0	0.0	0.0	0.0	0.0	-2.38	0.0	0.0	0.0	-2.38	0.0	0.0	0.0	0.0	0.0	0.0	0.0	0.0	0.0	0.0	0.0	0.0	0.0
12	0.0	0.0	0.0	-1.22	0.0	0.0	0.0	0.0	0.0	0.0	0.0	0.0	-2.38	0.0	0.0	0.0	0.0	0.0	0.0	0.0	0.0	0.0	0.0
13	0.0	0.0	0.0	0.0	0.0	0.0	0.0	0.0	0.0	0.0	0.0	0.0	0.0	-2.38	0.0	0.0	0.0	0.0	0.0	0.0	0.0	0.0	0.0
14	0.0	0.0	0.0	0.0	0.0	0.0	0.0	0.0	0.0	0.0	0.0	0.0	0.0	0.0	-2.38	0.0	0.0	0.0	0.0	0.0	0.0	0.0	0.0
15	0.0	0.0	0.0	0.0	0.0	0.0	0.0	0.0	0.0	0.0	0.0	0.0	0.0	0.0	0.0	-2.38	0.0	0.0	0.0	0.0	0.0	0.0	0.0
16	0.0	0.0	0.0	0.0	0.0	0.0	0.0	0.0	0.0	0.0	0.0	0.0	0.0	0.0	0.0	0.0	-2.38	0.0	0.0	0.0	0.0	0.0	0.0
17	0.0	0.0	0.0	0.0	0.0	0.0	0.0	0.0	0.0	0.0	0.0	-2.38	0.0	0.0	0.0	0.0	0.0	0.0	0.0	0.0	0.0	0.0	0.0
18	0.0	-1.79	0.0	0.0	0.0	0.0	0.0	0.0	0.0	0.0	0.0	0.0	0.0	0.0	0.0	0.0	0.0	0.0	0.0	0.0	0.0	0.0	0.0
19	0.0	0.0	0.0	0.0	0.0	0.0	0.0	0.0	0.0	0.0	0.0	0.0	0.0	0.0	0.0	0.0	0.0	-2.38	0.0	-2.38	0.0	0.0	0.0
20	0.0	0.0	0.0	0.0	0.0	0.0	0.0	0.0	0.0	0.0	0.0	0.0	0.0	0.0	0.0	0.0	0.0	0.0	0.0	-2.38	0.0	0.0	0.0
21	0.0	0.0	0.0	0.0	0.0	0.0	0.0	0.0	0.0	0.0	0.0	0.0	0.0	0.0	0.0	0.0	0.0	0.0	0.0	0.0	-2.38	0.0	0.0
22	0.0	0.0	0.0	0.0	0.0	0.0	0.0	0.0	0.0	0.0	0.0	0.0	0.0	0.0	0.0	0.0	0.0	0.0	0.0	0.0	0.0	-2.38	0.0
23	0.0	0.0	0.0	0.0	0.0	0.0	0.0	0.0	0.0	0.0	0.0	0.0	0.0	0.0	0.0	0.0	0.0	0.0	0.0	0.0	0.0	0.0	-2.38

FIGURE 4.10

It is suggested, then, as Tiño has indicated that the value for Q is strongly dependent upon the method of calculation, that the next logical step would be to "calibrate" the spin polarising program with well documented radicals in a similar way to Tiño. Having then obtained the "best" factors, it may be easier to explain the lophinyl splittings and from these to interpret the E.S.R. spectra of the fluorinated radicals.

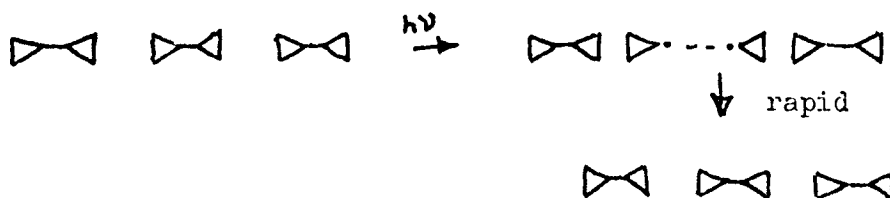
4.3 The Photochromic Process in the Solid.

The kinetic data in chapter 3, has shown that the decay reaction in the solid is influenced to a large extent by temperature, in that the apparent order decreases as the temperature increases. An explanation of this behaviour in terms of normal chemical kinetics is difficult to imagine, and it would thus seem, that the nature of the reaction in solid is fundamentally different to that in solution.

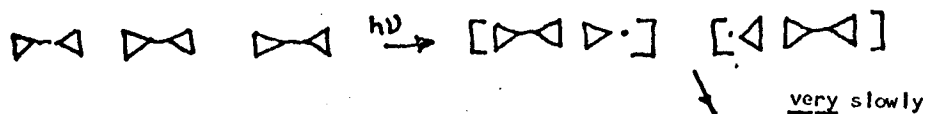
Nature of radical decay in solid.

It is envisaged, that during the generation process in the solid, two species which contribute to the photochromic colour are formed, the first being the simple radical (shown in the schemes below as $\triangleright\cdot$) and the second being the radical-dimer complex ($\triangleright\blacktriangleleft\triangleright\cdot$),¹⁵ postulated by Wilks in 1966 to provide an explanation for the decay kinetics of the triphenyl imidazolyl radicals in solution. It must be noted, that as yet no indication as to the exact form of this complexation has been found, but it seems reasonable to assume that π overlap is responsible for the bonding between the two parts.

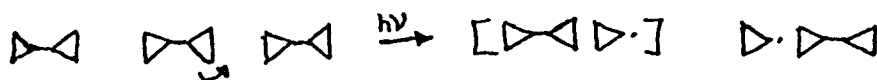
Interaction of a photon with the dimer molecules ($\triangleright\blacktriangleleft$), then, may have one of several effects. It could for instance, lead to the formation of a pair of radicals only, which because of the cage effect, would tend to recombine very rapidly according to second order kinetics.



On the other hand, it is also possible that a pair of complex species would be formed, and these because of their size and lack of mobility would be relatively inactive.



A third possibility, and because of the rates of the previous recombination processes, an important one, is that the light is of sufficient energy, not only to cause dissociation of the dimer, but also to bring about rotation of one of the radicals formed, leaving the situation as



In order then, to recombine, the free radical must undergo rotational diffusion. If it is assumed that this process is the rate determining step, and that recombination once the reactants are in the correct configuration is instantaneous, the reaction may be treated as being diffusion controlled.

Waite⁶¹, has considered the irregular motion of reacting particles with initial random distribution, and has solved the differential equation for the rate. Although the general form of this solution is complicated in its full form, it may be simplified by considering the limiting case for which diffusion is the rate determining step. In such a case, for a reaction $A + B \rightarrow AB$, the equation becomes

$$-\frac{dA}{dt} = -\frac{dB}{dt} = 4\pi r_0 (D_A + D_B) \left[1 + \frac{r_0}{(\pi(D_A + D_B)t)^{1/2}} \right] [A][B] \quad 4.1$$

where D_A and D_B are the diffusion coefficients for species A and B respectively and r_0 is the capture radius of the two reactants. Figure 4.11 the type of curve obtained for the decay of radicals in solid, illustrates the fact that the pre-illumination value for the optical density (taken as the arbitrary zero), is slightly less than that used for the infinity reading. The difference between the two, A_{∞} , represents the excess of the comparatively unreactive radical-dimer complex, left after all the free radicals have reacted. Presumably, these species will eventually recombine to give the dimer, but no noticeable change in the infinity reading was observed even after a period of several days. As the reaction involves the disappearance of both radical and complex at the same rate i.e.

$$L \cdot + L_2L \cdot \rightarrow 2L_2, \text{ one may write:}$$

$$[L_2L \cdot]_t \propto \frac{A_t - A_{\infty}}{2} + A_{\infty}$$

$$[L \cdot]_t \propto \frac{A_t - A_{\infty}}{2}$$

where A_t is the optical density at time t , taking the pre-illumination value as zero. Substitution of these values into equation 4.1 then, will give

$$\frac{dL \cdot}{dt} = \frac{dL_2L \cdot}{dt} = k \left(1 + \frac{c}{\sqrt{t}}\right) \left(\frac{A_t - A_{\infty}}{2}\right) \left(\frac{A_t - A_{\infty}}{2} + A_{\infty}\right)$$

$$\text{Where } k = 4\pi r_0 (D_L + D_{L_2L \cdot})$$

$$\text{and } c = \frac{r_0}{(\pi (D_L + D_{L_2L \cdot}))^{1/2}}$$

$$\text{or, as } \frac{dA_t}{dt} = \frac{dL \cdot}{dt} + \frac{dL_2L \cdot}{dt}$$

$$\frac{dA_t}{dt} = 2k \left(1 + \frac{c}{\sqrt{t}}\right) \left(\frac{A_t - A_{\infty}}{2}\right) \left(\frac{A_t - A_{\infty}}{2} + A_{\infty}\right)$$

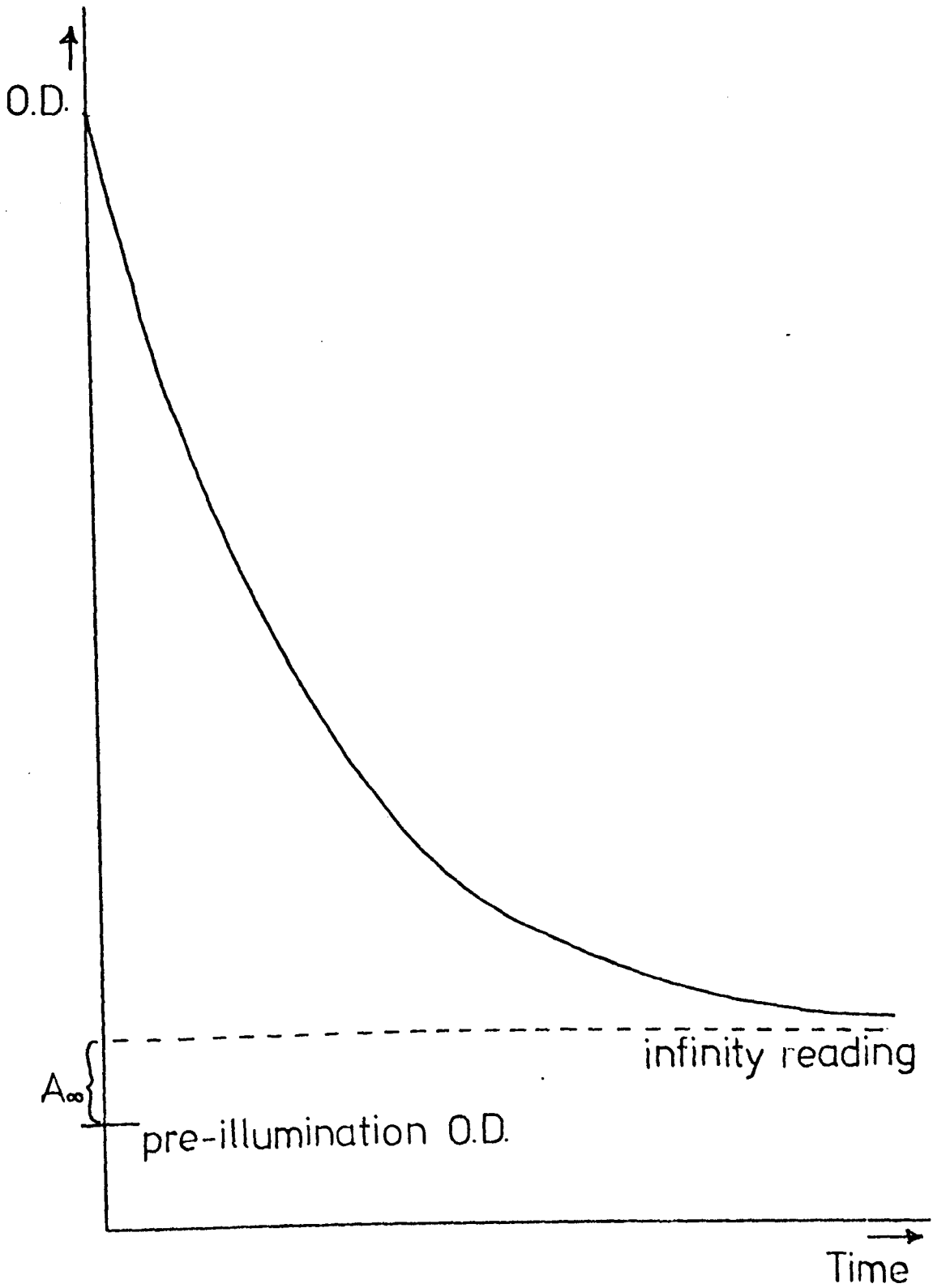


FIGURE 4.11

Now, at low values, it is expected that the factor c/\sqrt{t} will be greater than 1, and the value of $A_t - A_\infty$ will be much larger than A_∞ , so that the above equation will approximate to

$$\frac{dA_t}{dt} = K' \frac{c}{\sqrt{t}} (A_t - A_\infty)^2$$

This, on integration yields,

$$\frac{1}{(A_t - A_\infty)} \propto \sqrt{t}$$

At long times, however, the opposite situation must exist, in that c/\sqrt{t} becomes smaller than 1, and A_∞ becomes larger than $A_t - A_\infty$. This means that equation 4.1 rearranges to:

$$\begin{aligned} \frac{dA_t}{dt} &= K' \frac{(A_t - A_\infty)(A_\infty)}{2} \\ &= K'' \frac{(A_t - A_\infty)}{2} \end{aligned}$$

If indeed diffusion is the important step in the reaction, one should obtain, according to the above considerations, two distinct parts for the kinetic behaviour. The first part, at short time, will obey equation 4.1, and a plot of $1/A_t - A_\infty$ against \sqrt{t} for the first few minutes of the reaction should give a straight line. This was in fact proved to be so, and such plots for several temperatures are shown in Figures 4.12 to 4.15. The second part, at longer times, should according to equation 4.1 follow first order kinetics. As this has already been shown to be true in Chapter 3, it would appear that the postulate of the reaction in solid being diffusion controlled, is a reasonable one.

Arrhenius plots for both parts of the reaction scheme were constructed, but unfortunately neither yielded a straight line. It is thought that this deviation could well be caused by either non-uniform generation of radicals on the surface, quite possible due to the polycrystalline nature of the sample, or by a permanent degradation of the photochromic

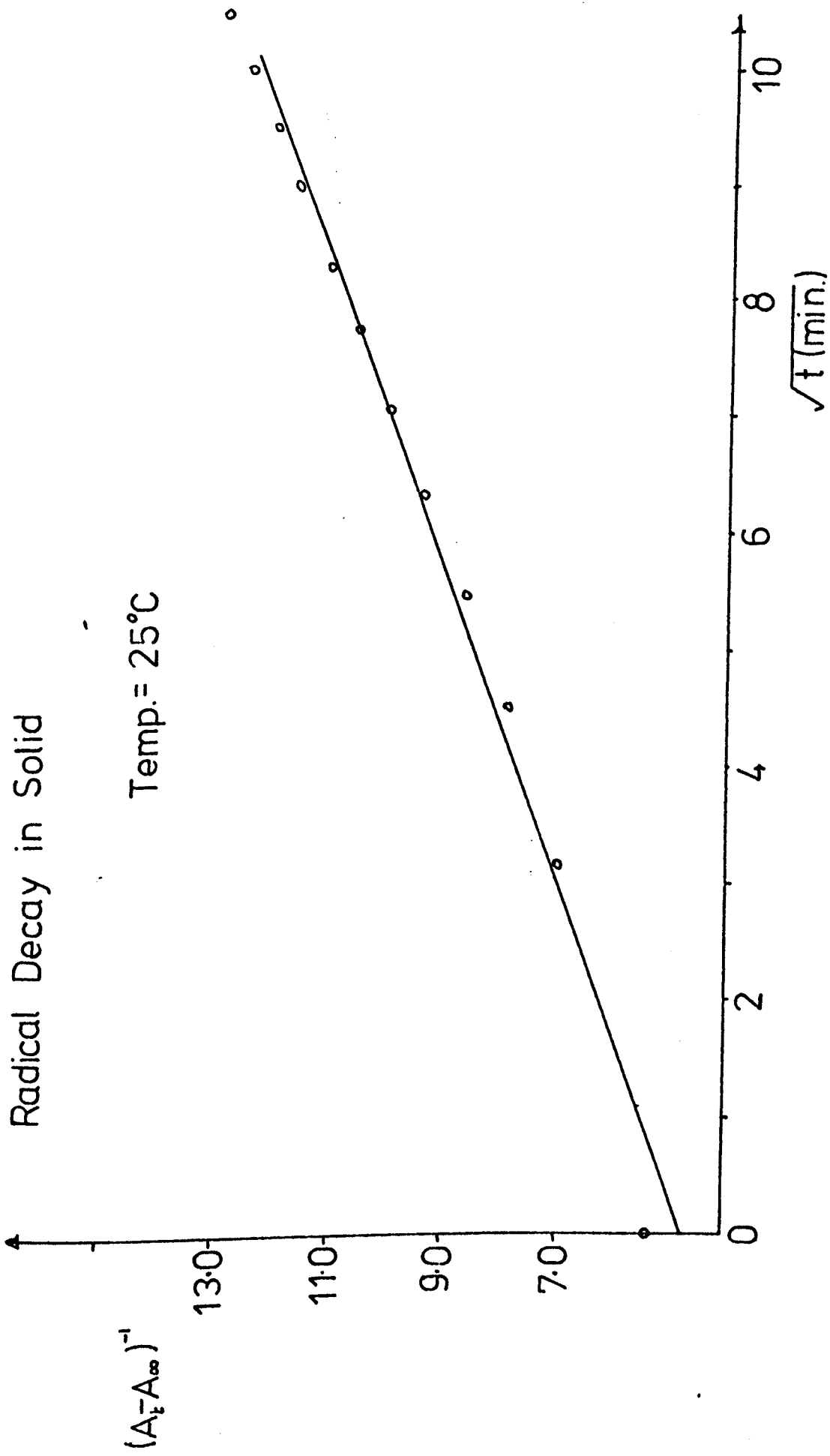


FIGURE 4.12

Radical Decay in Solid

Temp. = 35°C

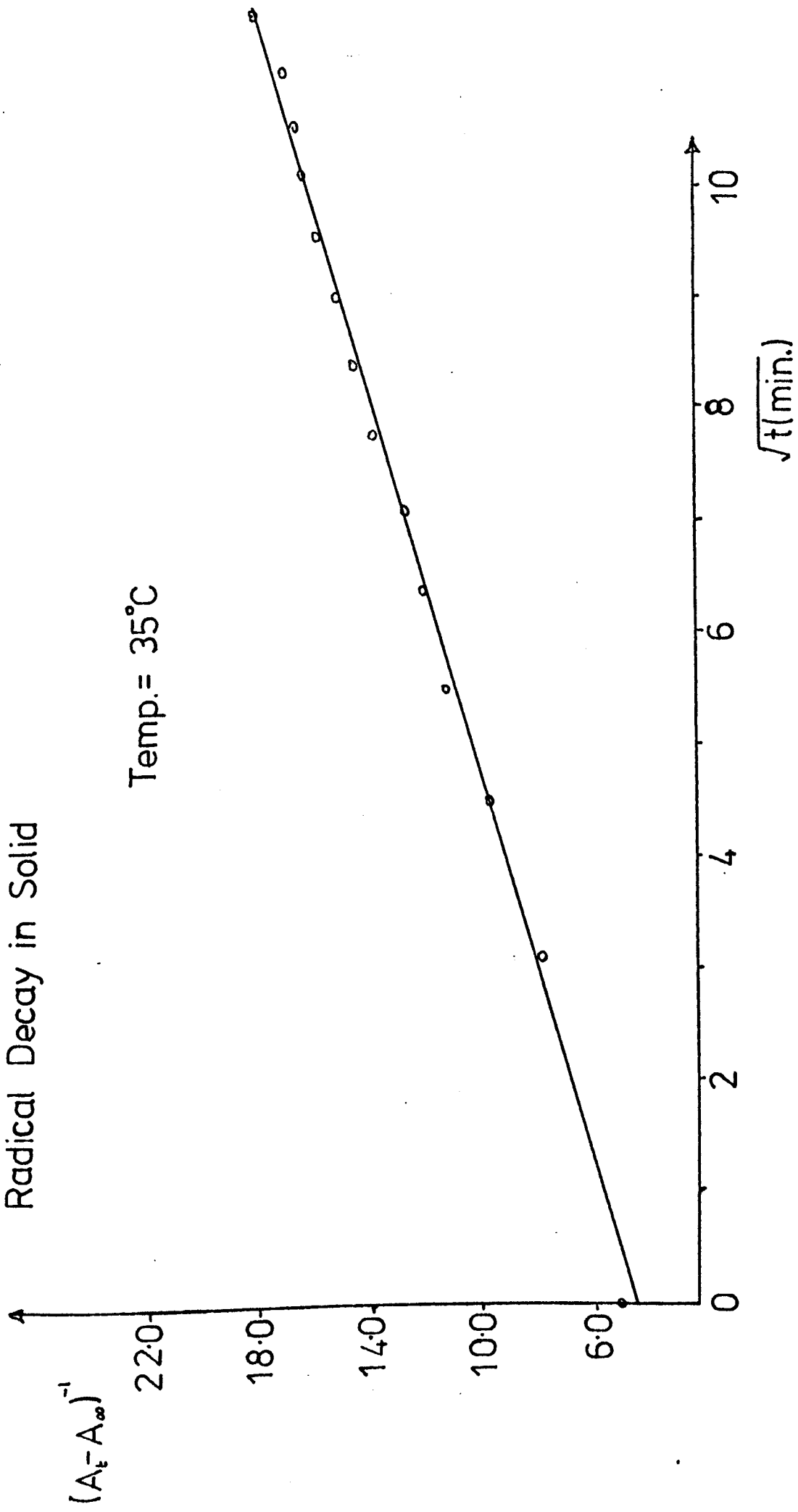


FIGURE 4.13

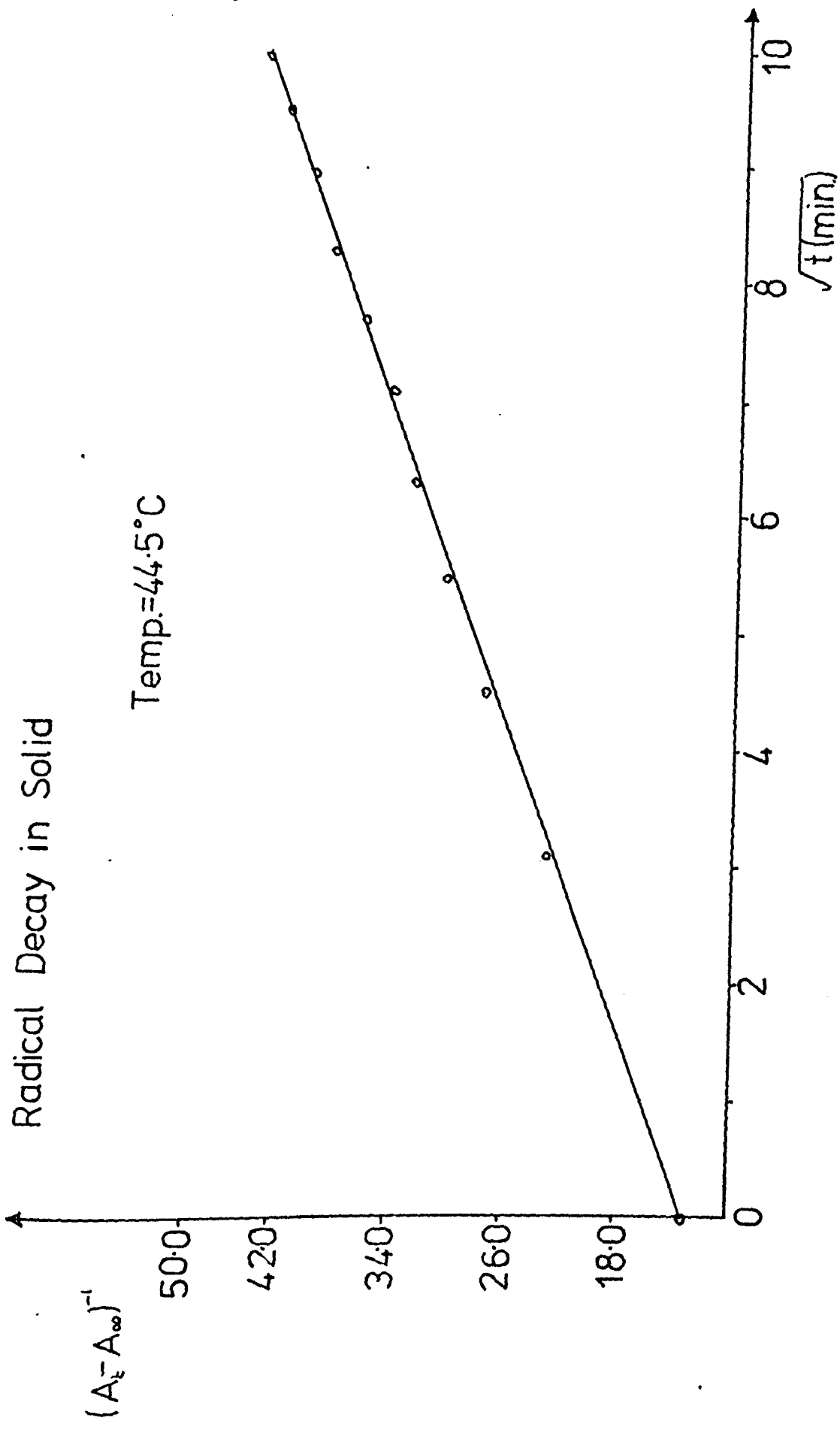


FIGURE 4.14

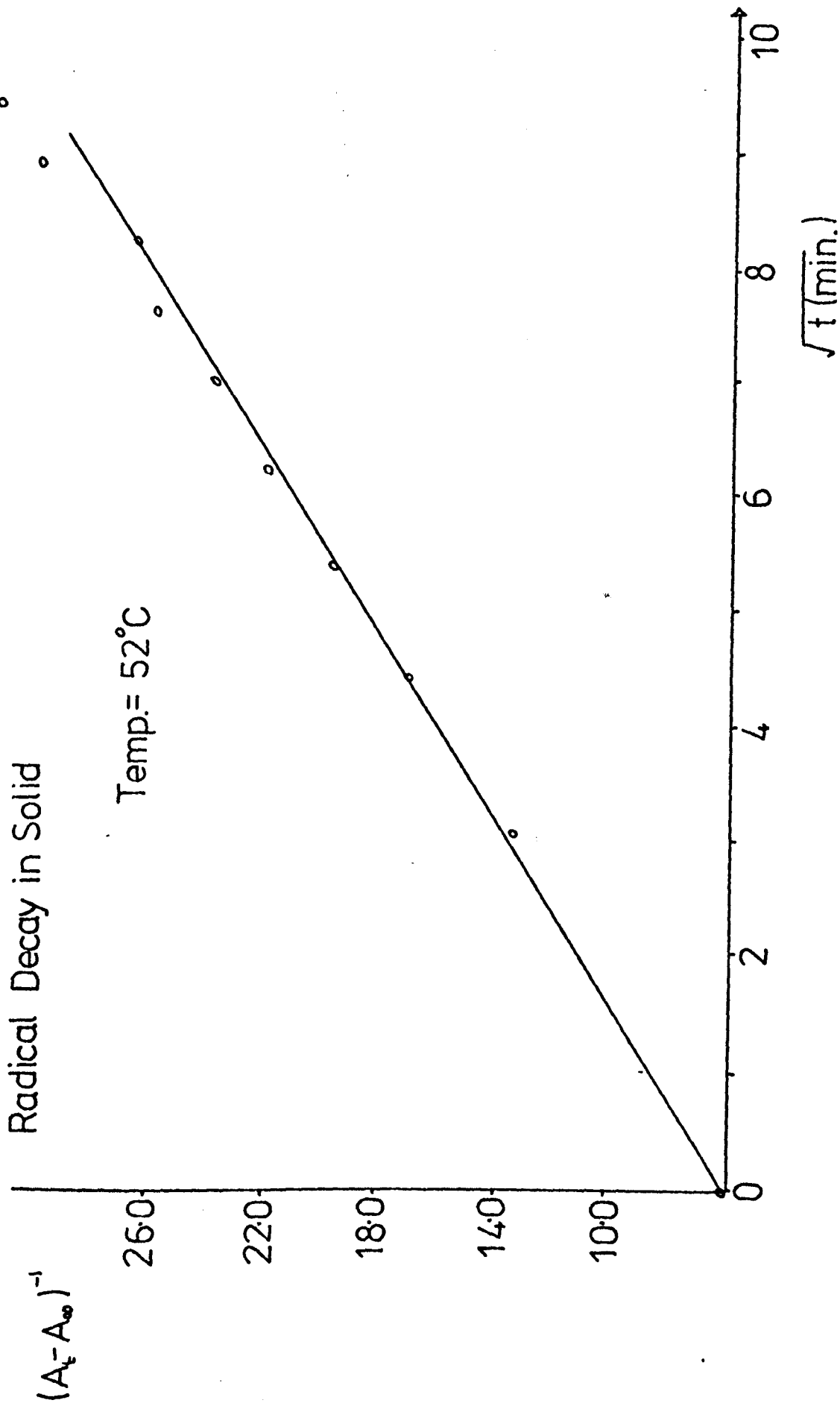


FIGURE 4.15

dimer, confusing the radical decay data. The latter reason is supported by the fact that a completely new sample could not be used for each kinetic run (because of the quantity of material needed), and often only the surface layer of the sample could be removed after a decay. This was indeed reflected by a gradual reduction in the initial radical concentration obtained at the beginning of subsequent decays run on the same sample.

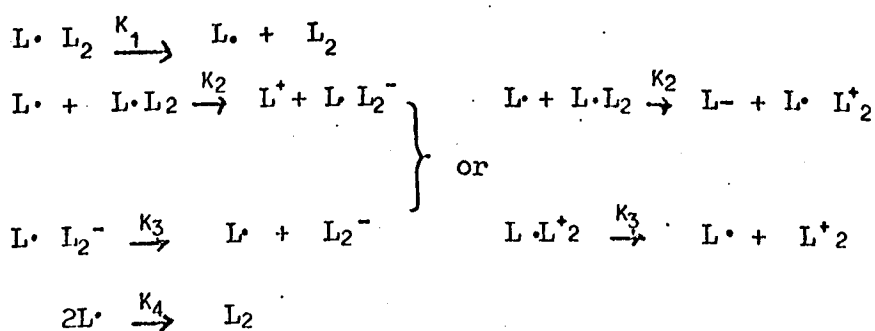
4.4 The Photochromic Processes in Solution

Decay kinetics in solution

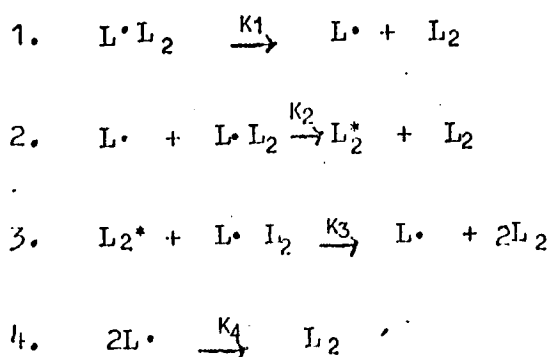
The decay kinetics of the imidazolyl radicals have been shown in Chapter 3, to be dependent to a great extent upon the concentration of the dimer solution. The only reasonable explanation to this behaviour would seem to be based upon the postulate, of Wilks and Willis¹⁵, of the existence of some sort of radical-dimer complex. The recombination of the fluorinated imidazolyl radicals in benzene solutions have thus been interpreted in these terms.

4.4.1 Decay of 2 metafluorophenyl 4, 5 diphenylimidazolyl radicals

It has been shown, that radicals generated from a 10^{-3} M. dimer solution, recombine in a similar way to the parent lophinyl radicals, in that the decay obeys $3/2$ order kinetics at the beginning and 1st order kinetics in the later stages. Wilks and Willis, as mentioned in Chapter 1, have suggested a mechanism to explain this behaviour, in which they postulate the existence of not only the radical-dimer complex, but also of ionic species i.e



Now, the existence of ionic species in low polar media such as benzene does not seem favourable, and for this reason, the following similar scheme is suggested as an alternative:-



Again the existence of the complex species $L \cdot L_2$ is assumed, but it is suggested that instead of the interaction of $L \cdot L_2$ with the simple radical $L \cdot$ giving an ionic species, the stereochemistry of the complex will result in $L \cdot$ attacking in such a way that the piezochromic dimer L_2^* must be formed. This is then considered to be long lived enough to react with the complex species.

If one then assumes that the back reactions of the above scheme are much slower than the forward reactions, and this assumption seems quite reasonable as the readings of optical density taken during a kinetic run were significantly greater than the equilibrium readings, and if it is also assumed that the loss of $L \cdot L_2$ is responsible for the disappearance of the photochromic colour, a steady state treatment on $L \cdot$ and L_2^* will give the following result

$$\begin{aligned}
 -\frac{d[L \cdot]}{dt} &= \frac{d[L_2^*]}{dt} = 0 \\
 \frac{d[L_2^*]}{dt} &= K_2 [L \cdot] [L_2 \cdot L \cdot] - K_3 [L_2^*] [L \cdot L_2] = 0 \\
 \therefore K_2 [L \cdot] [L_2 \cdot L \cdot] &= K_3 [L_2^*] [L \cdot L_2] \\
 -\frac{d[L \cdot]}{dt} &= -K_1 [L \cdot L_2] + K_2 [L \cdot] [L \cdot L_2] - K_3 [L_2^*] [L \cdot L_2] \\
 &\quad + K_4 [L \cdot]^2 = 0 \\
 \therefore K_4 [L \cdot]^2 &= K_1 [L \cdot L_2]
 \end{aligned}$$

Considering the disappearance of $[L \cdot L_2]$ with time, one obtains:

$$-\frac{d[L \cdot L_2]}{dt} = K_1 [L \cdot L_2] + K_2 [L \cdot] [L \cdot L_2] + K_3 [L_2^*] [L \cdot L_2]$$

which from the above considerations becomes

$$-\frac{d[L.L_2]}{dt} = K_1 [L.L_2] + 2K_2 (K_1/K_4)^{\frac{1}{2}} [L.L_2]^{\frac{3}{2}}$$

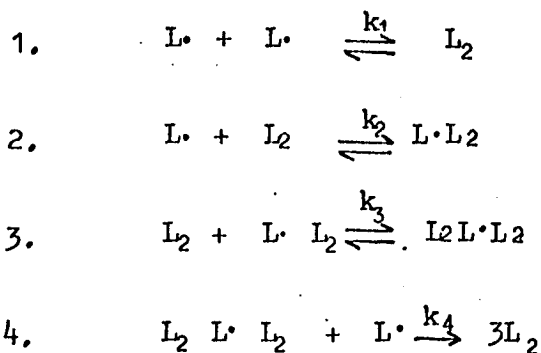
Thus, if $2K_2 (K_1/K_4)^{\frac{1}{2}}$ is greater than K_1 the reaction will appear to follow the observed kinetic scheme of $\frac{3}{2}$ order, falling to first order when the concentration of $L.L_2$ becomes small.

On altering the dimer concentration from 10^{-3} M to 10^{-4} M, the kinetic scheme changes from being $\frac{3}{2}$ falling to first, to being 2nd order falling to $\frac{3}{2}$. Again this behaviour has been exhibited by the imidazolyl radicals and the second order part has been interpreted¹⁸ as being due to the straight radical recombination ($L \cdot + L \cdot \rightarrow L_2$). This is thought to be an acceptable postulate in that the low concentration of the dimer at the beginning of the reaction, means that the concentration of $L.L_2$ will be low compared to that of the radical. As the reaction proceeds however, the free radicals will be consumed, and the concentration of the complex will become relatively more significant, so that the reaction reverts to that given for the 10^{-3} M solution.

At dimer concentrations of 5×10^{-3} M, the kinetics change completely, and the decay appears to follow an order of approximately $1\frac{1}{4}$ throughout. This complicated reaction order once again must suggest that dimer-radical complexes are involved.

In fact, no scheme similar to that postulated for the more dilute solutions could be found to fit the data, and the only explanation of the behaviour that could be found, involves the formulation of an order of 1.2, and the postulate that the reaction is comprised of a series of equilibria with one rate determining step in which a new

complex $L_2 L \cdot L_2$ is featured:



Considering the equilibria:

$$\text{from } 1 \quad [L \cdot]^2 = k_1 [L_2]$$

$$\text{from } 2 \quad [L \cdot][L_2] = k_2 [L \cdot L_2]$$

$$\text{or } [L \cdot]^3 = k_1 k_2 [L \cdot L_2]$$

$$\text{from } 3 \quad [L_2][L \cdot L_2] = k_3 [L_2 L \cdot L_2]$$

$$\begin{aligned}
 \text{or } [L \cdot]^5 &= k_1^2 k_2 k_3 [L_2 L \cdot L_2] \\
 &= K' [L_2 L \cdot L_2]
 \end{aligned}$$

If then the species $L_2 L \cdot L_2$ is responsible for the colour of the photochromic solution, the kinetics may be represented by:

$$\begin{aligned}
 - \frac{d[L_2 L \cdot L_2]}{dt} &= k_4 [L \cdot][L_2 L \cdot L_2] \\
 &= k_4 (K')^{1/5} [L_2 L \cdot L_2]^{6/5}
 \end{aligned}$$

Although this scheme may not appear entirely satisfactory, in that it requires a completely new kinetic scheme, it does explain an order which fits the data, and at the same time, does not introduce any species too far removed from any already encountered. Indeed, as the existence of a complex $L \cdot L_2$ has already been suggested, it seems quite plausible, that in a more concentrated solution, in which many more dimer molecules are present, a species such as $L_2 L \cdot L_2$ could be formed.

As expected the unsubstituted imidazolyl radicals once more gave parallel results.

The similarity between the behaviour of the two species of radicals discussed above is not too difficult to understand, as a fluorine substituted into the meta position of the 2 phenyl ring of the triphenyl imidazolyl radical, would not be expected to make any major difference to either the electronic or steric properties of the compound.

4.4.2 Decay of 2 - parafluorophenyl 4, 5 diphenyl imidazolyl radicals.

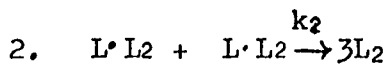
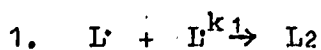
The kinetics of decay of the parafluoro radicals may be explained in a similar way to the scheme given above for the decay of the meta fluoro radicals in a 10^{-3} M dimer solution, with the additional postulate that K_1 becomes so small that the first order part of the reaction becomes lost in the noise at the end of the decay.

Second order behaviour was not observed for the parafluoro radical, but as it was very difficult to follow the reaction at dimer concentrations much lower than 10^{-3} M, no conclusions may be drawn from this fact. Similarly no $\frac{6}{5}$ order was found for the parafluoro radical decay. This could possibly be due to the unfavourability of the existence of the $L_2L'L_2$ complex, but without information as to the exact nature of that complex, this remains as an hypothesis.

4.4.3 Decay of the 2 - orthofluorophenyl 4, 5 diphenyl imidazolyl radicals

The decay kinetics of the orthofluoro radicals in solution have shown that two separate second orders exist, one taking place in both 10^{-3} M and $5 \cdot 10^{-3}$ M. dimer solutions, the other being found only at $5 \cdot 10^{-3}$ M. Interpretation of this behaviour can only be made by suggesting that two straight recombination

processes are taking place i.e.



If (1) is considered to be the reaction occurring at both concentrations, which seems reasonable, as one would expect the reaction involving the radical-dimer complex to occur at the higher dimer concentration, then the results indicate k_2 to be greater than k_1 .

Since the complex $L \cdot L_2$ is present in solution, one would think, that the reaction scheme for the metafluoro, parafluoro and lophinyl radicals would also be applicable to the orthofluoro compound i.e. one would expect to find an order of $\frac{3}{2}$ at some stage. The fact that no indication of this was found, led to the belief that the piezochromic dimer of the orthofluoro radical was a highly unstable entity. Indeed, it was found upon investigation that oxidation of 2 orthofluoro 4, 5 diphenyl imidazole with potassium ferricyanide did not give the piezochromic dimer as experienced with the other imidazoles, but resulted rather in the formation of the photochromic dimer. This evidence thus, not only gave an explanation for the different behaviour of the orthofluoro radical, but also supported the postulation of the participation of the piezochromic dimer in the reactions of the other compounds. Again, as with the parafluoro compound, no $\frac{6}{5}$ order was found.

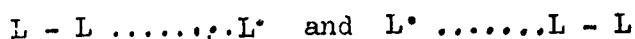
4.4.4 The nature of the radical-dimer complex

It has been seen, that the kinetic studies in both the solution and the solid state, have strongly suggested the existence of some kind of radical-dimer complex, but unfortunately, no evidence as to the exact nature of the interaction between the species is

available. Such interactions, however, are not unknown and Lyons and Watson⁶² have observed conglomeration between free radicals and solvent molecules, but have drawn no conclusion as to the way in which the two interact. In the bi-imidazolyl system, there would appear to be three possible ways in which interaction could occur. They are:

(i) Delocalisation of the unpaired electron

This interaction involves the delocalisation of the radical's unpaired electron over the whole structure of the L_2L complex leading to subsequent stabilisation of the free radical with contributions from the resonance structures



Because of the delocalisation of the electron, it might be expected that the E.S.R. spectrum of the radical, would be greatly affected by such an interaction, but as yet, no such effect has been observed. Possibly, this may be due to the fact that the interaction may be too small to obtain noticeable splittings from the protons of the dimer.

(ii) Dipolar interactions.

The asymmetric structure of the bi-imidazole dimer, should lead to a significant dipole in the compound, which could well further induce a dipole into the highly polarizable radical. Indeed J.N. Murrell and V.M.S. Gill⁶³ have provided strong evidence, using n.m.r., for self association in solutions of heterocyclic aromatics such as pyridine.

(iii) Solvation at polar centres.

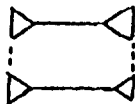
Studies of solvent shifts by n.m.r. have suggested that aromatic solvents such as benzene can solvate polar centres in other molecules⁶⁴. It may then be quite possible, that a similar type of interaction will take place between, say, the pendant phenyl rings of the radical and the nitrogens of the dimer.

Although all three types of interaction exist as strong possibilities, in the absence of definitive experimental information, no further speculation as to the exact nature and geometry of the complex may be made.

4.4.5 Generation kinetics in solution

In Chapter 3, it was shown, that although for 10^3 M dimer solutions the generation of radicals is an unactivated process, an increase in dimer concentration leads to a temperature dependent rate. The way in which this process has become activated, is thought to involve a sort of cage effect.

In dilute solutions, the dimer molecules will exist as separate entities, and with the wavelength of light used, the absorption of a photon will give immediate dissociation. In more concentrated solutions, however, it is envisaged, that the dimer molecules form small aggregates e.g.



Absorption of a photon still results in the dissociation of the molecule, but the cage effect means that the two radicals formed, will be so close that they will dimerize at once. As the temperature is increased, then, the thermal energy will tend to break up these groups leading to a faster yield of photochromic radicals.

The activation energies quoted for these processes in Chapter 3, give an idea of the forces involved in the dimer association.

4.5 Suggestions for Further Work

It has already been indicated that further work, probably along the lines suggested in Chapter 4, will be necessary if the P.P.P. molecular orbital program is to be used to draw up reasonable electronic pictures of the lophinyl radical and its three fluorinated derivatives. The completion of accurate molecular orbital calculations are not only essential to enable theoretical reproductions of the experimental electron spin resonance spectra to be made, but may also prove to be useful in obtaining some proof of existence of the species and schemes postulated for the decay kinetics by giving one an idea of the energies involved in the reactions.

At the same time, definite experimental evidence is required if one is to prove the existence of the complex species invoked for the schemes. Preliminary investigations using E.S.R. and molecular weight methods have been carried out, but have given no suggestion of complexation. This does not mean, however, that more accurate experiments using these methods and others including boiling point elevation, freezing point depression, viscosity etc., will not furnish the proof needed. Certainly, until some positive indication as to the feasibility of these complex species is obtained, the kinetic schemes given in this thesis can only remain as postulates.

References.

General References and Text-Books

- B1 J. Calvert and J. Pitts, "Photochemistry", Wiley, New York (1966).
- B2 P.D.Ayscough, "Electron Spin Resonance in Chemistry", Methuen London, 1967.
- B3 F. Gerson, High Resolution E.S.R. Spectroscopy, John Wiley and Sons Ltd., 1960.
- B4 A. Streitwieser, Jr., "Molecular Orbital Theory for Organic Chemists", Wiley, New York, 1961.
- B5 W. Wendlant and H.G. Hecht, Reflectance, Spectroscopy, Interscience 1966.

Specific References and Papers.

1. A. Bertrand, Revue de l'Institut Francais du Petrole et Annales de Combustibles Liquides XXI, 1009 (1966).
2. R. Dessauer and J.P.Paris, Advances in Photochemistry, 1, 275 (1963).
3. E. ter Meer, Ann. Chem., 181, 1 (1976).
4. Glenn H. Brown, "Photochromism", Techniques of Chemistry Vol. 3, Wiley-Interscience, New York (1971) p.49.
5. G.S. Hartley, Nature, 140, 281 (1937)
6. J.A.Chopoorian, K.O. Loeffler, W.F. Marzluff and G.H. Dorian, Nature, 204, 180 (1964).
7. W.R. Dawson and M.W. Windsor, Appl. Opt., 8, 1045 (1969).
8. T. Hayashi, K. Maeda, S. Shida and K. Nakada, J. Chem. Phys., 32 1568 (1960).
9. T.Hayashi, K. Maeda, Bull. Chem. Soc. Japan., 33, 555 (1960).
- 10 a) T. Hayashi, K. Maeda, M. Morinaga, Bull. Chem. Soc., Japan, 37 1563 (1964).
- b) T: Hayashi, K. Maeda and Takuchi, Bull. Chem. Soc. Japan, 37, 1717 (1964).

11. D.M.White and J. Sonnenberg, *J. Amer. Chem.Soc.*, 88, 3825 (1966).
12. T. Hayashi and K. Maeda, *Bull, Chem. Soc. Japan*, 36, 1052 (1963).
13. T. Hayashi and K. Maeda, *Bull. Chem. Soc. Japan*, 42, 3509 (1969).
14. a) H. Ueda, *J. Phys. Chem.*, 68, 1304 (1964).
b) H. Ueda, *J. Phys. Chem.*, 70, 3349 (1966).
15. a) M.A.J. Wilks, M.R.Willis, *Nature*, 212, 500 (1966).
b) M.A.J. Wilks, M.R.Willis, *J. Chem. Soc.*, 1526 (1968).
c) M.A.J. Wilks (Ph.D. Thesis, Nottingham, 1968).
16. H. Baumgärtel and H. Zimmermann, *Z. Naturforschg.*, 186, 406 (1963).
17. J.G.Kirkwood, *J. Chem. Phys.*, 2, 351 (1934).
18. A.L. Prochoda, V.A. Krongauz, *Khim.Vys. Energ.*, Vol. 4, No. 2, 1970, p176.
19. T. Hayashi and K. Maeda, *Bull. Chem. Soc. Japan*, 38, 685 (1965).
20. T. Hayashi, K. Maeda, *Bull. Chem. Soc. Japan*, 38, 857 (1965).
21. M.J.S. Dewar, *J. Chem. Soc.*, 463. (1949).
22. A. D. McLachlan, *Mol. Phys.*, 3, 233 (1960).
23. J. A. Pople and R. K. Nesbet, *J.Chem.Phys.*, 22, 571 (1954).
24. J. A. Pople, *Trans. Faraday Soc.* 49, 1375 (1953).
25. J. E. Lennard-Jones, *Proc.Roy.Soc. (London) A* 198 1,14 (1949).
26. G. G. Hall, *Proc. Roy. Soc. (London) A* 205, 541, (1951).
27. C.C.J. Rootham, *Rev. Mod. Phys.*, 23, 69 (1951).
28. M. Goepfert-Mayer and A.L. Sklor, *J. Chem. Phys.*, 6, 645 (1938).
29. J. N. Murrel, A. J. Margett, *Semi-Empirical Self Consistent Field Molecular Orbital Theory of Molecules*, Wiley, New York, 1972, pp. 11-31.
30. P. O. Lowdin, *J. Chem. Phys.*, 18, 365 (1950).
31. T. Loopman, *Physica*, 1, 104 (1933).
32. J. Hinze and H. H. Jaffe, *J. Amer. Chem. Soc.*, 84, 540,(1962).
33. R.L. Flurry, E.W. Stout and J.J. Bell, *Theoret.Chim.Acta*, 8, 203, (1967).

34. J.C. Slater, Phys. Rev., 36, 57 (1930).
35. R. Pariser, J. Chem. Phys., 21, 568 (1953).
36. N. Mataga and K. Nishimoto, Z. Physik. Chem.(Frankfurt), 12
335; 13, 140 (1957).
37. J.A. Pople and R.K. Nesbet, J. Chem. Phys., 22, 571 (1954).
38. A. Brickstock, and J.A. Pople, Trans.Faraday Soc., 50, 901 (1954).
39. P.O. Lowdin, Phys. Rev., 97, 1509 (1953).
40. A.T. Amos, G.G. Hall, Proc. Phys. Soc., A 263, 483 (1961).
41. A.T. Amos, G.G. Hall, "Advances in Atomic and Molecular Physics",
Vol 1, 1964.
42. A. Carrington, Quart. Rev., 17, 67 (1963).
43. H.M. McConnell, J. Chem. Phys., 24, 764 (1956).
44. N. Cyr, M.A.J. Wilks and M.R. Willis, J.Chem.Soc. (B) 404 (1971).
45. A. Hands, M.W. Litobarski and M.R. Willis, "Spectrovision",
Pye Unicam, Vol. 24 (1970).
46. V. Burgess, J. Sci. Instr., 38, 98 (1961).
47. D. Davidson, J. Org. Chem., 2, 319 (1938).
48. A. Weissberger, "Technique of Organic Chemistry", Interscience,
New York, 1955 (2nd ed.) Vol. VII.
49. A.L. Prochoda, V.A. Krongauz, Khim.Viz. Energ., Vol. 3, No.6,
1969, p495.
50. I'Haya, J. Am. Chem. Soc., 81, 6120 (1959).
51. I.L. Karle, J. Chem. Phys., 20, 65 (1952).
52. C.J.B. Clews and W.Cochran, Acta. Cryst. 1, 4 (1948).
53. B. Bak, D. Christensen, L. Hansen and J. Rastrup-Andersen, J.
Chem. Phys. 24, 720 (1956).
54. G. Will, Z. Kryst, 129, 211 (1969).
55. O. Bastiansen, Acta.Chemica Scandanavika, 3, 408 (1949).
56. J.D. Roberts, "Notes on Molecular Orbital Calculations",
W.A. Benjamin Inc., New York, 1962.

57. H.O. Pritchard and M.A. Skinner, *J. Inorg. Nucl. Chem.*, 24, 937 (1967).
58. J. Tino, *Theoret. Chim. Acta*, 18 (2), 119 (1970).
59. a) G. Berthier, *Compt. Rend. Acad. Sci.*, 238, 91 (1954).
b) G. Berthier, *J. Chim. Physique*, 51 363 (1954).
60. J.A. Pople and R.K. Nesbet, *J. Chem. Phys.*, 22, 571 (1954).
61. a) T.R. Waite, *J. Chem. Phys.*, 28, 103 (1958).
b) T.R. Waite, *Phys. Rev.*, 107, 463 (1957).
62. Lyons and Watson, *J. Polymer Sci.*, 18, 141 (1955).
63. J.N. Murrell, V.M.S. Gill, *T.F.S.*, 61, 402 (1965).
64. J. Ronayne, D.M. Williams, *Chem. Consns.*, 20, 712 (1966).